Universidad Miguel Hernández

Doctorado en Tecnologías Industriales y de Telecomunicación

Nuevos paradigmas para el estudio de artefactos y mecanismos cognitivos relacionados con la marcha a partir de señales EEG

Tesis que presenta:

Álvaro Costa García

Directores de tesis:

José María Azorín Poveda

Eduardo Iáñez Martínez

Elche, Alicante, España *Mayo, 2015*

UNIVERSITAS
Miguel
Hernández

AUTORIZACIÓN DE PRESENTACIÓN DE TESIS DOCTORAL

Directores: Dr. José María Azorín Poveda, Profesor Titular de Universidad, y el Dr. Eduardo Iáñez Martínez, Profesor Asociado, ambos del Departamento de Ingeniería de Sistemas y Automática de la Universidad Miguel Hernández de Elche

Título de la tesis: Nuevos paradigmas para el estudio de artefactos y mecanismos cognitivos relacionados con la marcha a partir de señales EEG.

Autor: Álvaro Costa García

Los directores de la tesis reseñada certifican que ha sido realizada bajo su dirección por D. Álvaro Costa García en el Departamento de Ingeniería de Sistemas y Automática de la Universidad Miguel Hernández y autorizan su presentación de acuerdo con lo dispuesto en el R.D. 99/2011, de 28 de enero, por el que se regula el tercer ciclo de estudios universitarios.

Elche, a , de de 2016

Firmado: José María Azorín Firmado: Eduardo Iáñez Martínez

UNIVERSITAS
Miguel
Hernández

Dr. D. Ignacio Moreno Soriano, Coordinador del Programa de Doctorado en Tecnologías Industriales y de Telecomunicación de la Universidad Miguel Hernández de Elche,

Hace constar

Que el trabajo realizado por D. Álvaro Costa García titulado "Nuevos paradigmas para el estudio de artefactos y mecanismos cognitivos relacionados con la marcha a partir de señales EEG.", ha sido dirigido por el Dr. D. José María Azorín Poveda y el Dr. D. Eduardo Iáñez Martínez dentro del Programa de Doctorado en Tecnologías Industriales y de Telecomunicación, y se encuentra en condiciones de ser leído y defendido como Tesis Doctoral ante el correspondiente tribunal en la Universidad Miguel Hernández de Elche. Lo que firmo para los efectos oportunos,

Elche, a , de de 2016.

Fdo. Ignacio Moreno Soriano
Coordinador del Programa de Doctorado en
Tecnologías Industriales y de Telecomunicación

DEPARTAMENTO DE CIENCIA DE MATERIALES, ÓPTICA Y TECNOLOGÍA ELECTRÓNICA
Campus de Elche. Avda. de la Universidad s/n – 03202 ELCHE
Tel.: 96 665 84 98

UNIVERSITAS
Miguel
Hernández

“かいぞくおうにおれはなる”
“Kaisoku ou ni ore wa naru!"
“¡Yo seré el próximo rey de los piratas!”

MONKEY D. LUFFY, Eichiro Oda

UNIVERSITAS
Miguel
Hernández

Agradecimientos

Siempre he considerado la sección de agradecimientos como aquella en la existe una mayor libertad literaria. Aunque lo común es que ocupe alrededor de una única página, no he encontrado normativas ni razones para no extenderla más allá de lo habitualmente establecido. Por este motivo me dispongo a agradecer de forma extensa y detallada a todas aquellas personas que, desde mi nacimiento, me han hecho llegar hasta donde estoy. De esta forma doy por avisados a los posibles lectores apasionados de las interfaces cerebro-máquina de que la fiesta, para ellos, no comenzará hasta dentro de un buen rato. Para el resto, os invito a que disfrutéis leyendo esta sección tanto como yo he disfrutado escribiéndola.

Si comenzamos por el principio, me toca adentrarme en los primeros años de mi vida, muy borrosos en mi memoria salvo por algunos detalles. Aun siendo yo el más sorprendido por lo que estoy a punto de decir, quiero agradecer a 3 compañeros de parvularios, Miguel Ángel, Manolo y Begoña. De ellos solo tengo leves recuerdos, todos ellos traumáticos, negativos y ya superados hace muchos años. Aun con esas, sin ellos seguramente no habría sido consciente de lo agradecido que se debe estar por tener buenos amigos.

Durante el colegio y el bachiller forjé muchas amistades y, al no provenir todas del ámbito escolar, se me hace complicado ordenar mis ideas para no dejarme a nadie en el tintero, sin embargo voy a intentarlo. Ángel fue una de las primeras amistades que establecí al comenzar el colegio, aunque hace mucho que perdimos el contacto, todavía le recuerdo con una sonrisa. Por supuesto no puedo olvidar a ese grupo de grandes personas que conocí durante la ESO y que sigo considerando grandes amigos. Johan, Xixo, Dani, Nico, Manu y Ryan muchas gracias por esos años de tolerar e incluso diría que, en ocasiones, admirar mis rarezas. Sobre todo teniendo en cuenta lo convulsos que pueden ser los años de instituto para un chaval al que abiertamente no le gustaba el futbol ni salir de fiesta. EN SERIO, vuestra amistad fue para mí más importante de lo que os podéis imaginar. De la misma forma tengo que agradecer a todos mis profesores durante esta

etapa. No sé si soy capaz de recordarlos a todos pero de nuevo voy a hacer el esfuerzo ya que me gustaría que sus nombres quedasen reflejados: Encarna, Joaquín, Gloria, Pepe, Paco, Rosa, Inma, Carmen, Nieves, Encarnita, Sorsona, Luis, Berná, Carmina, Raquel, Derek, Mercedes, Zapata, Conesa, Gamuz, Amalia, Mario y Felipe. Como en todas partes, hay profesores buenos, profesores malos y una amplia gama de grados intermedios. En mi caso, debo agradecer a todos por igual, a los mejores por todo lo que me enseñaron y a los peores porque gracias a ellos aprendí a lidiar con las pequeñas injusticias que todos nos encontramos a lo largo de la vida.

En paralelo, no puedo olvidarme de toda la gente que conocí en la academia de inglés en la que ingresé a los 8 años. En especial debo mencionar a Jesús, con quien compartía colegio. Gracias a él conocí a gente como Álvaro, Pablo y Niti, con quienes disfrute muchos y muchos recreos. También agradecer al resto de compañeros de la academia con quienes pasé muchas tardes de risas mientras aprendíamos inglés: Mario, Carmen, Maria José, Ainara y Mere. Y por supuesto nuestro maravilloso profesor James. Yo comencé a estudiar inglés con él a los 8 años y concluí al cumplir los 18, por lo que James me vio pasar de la niñez hasta casi la adultez. Pero dado que cuando conocí a James, él era un inglés soltero en España y cuando terminé mis estudios, él estaba casado, tenía un niño y estaba esperando gemelas, se puede decir que yo también lo vi crecer. Sin sus clases de inglés, que para mí eran más divertidas que quedarme en casa, no habría llegado a donde estoy actualmente.

Por último, y para cerrar esta etapa, debo mencionar a Rubén, con quien pasé casi todas las tardes de vacaciones y fines de semana de entre los 8 y los 14 años. Gracias a él conocí a personas relevantes en mi adolescencia como Carlos, Abraham, Sandra y Milagros pero sobre todo me permitió conocer a un par de personas muy importantes en mi vida, Clara y Jose, a quienes me reservo para más adelante ;).

Y comenzaron los años de universidad. De nuevo en esta etapa conocí a mucha gente que influyó de forma muy relevante en mi. Agradecer a todos los que

algunas vez han sido compañeros de carrera: Arturo, Juanjo, Tomás, Pepe, Juanma, Siso, Robert, Chema, Jaime, Belén, Ana, María, Tonet, José Manuel, Joaquín, a todos los erasmus y todos los séneca. Análogamente, agradezco a todo el profesorado, gracias a ellos he ido superándome continuamente. En este caso, no los listaré porque además de ser demasiados, de la mayoría solo recuerdo el mote que, religiosamente, Juanjo les ponía. Debo agradecer también a toda la gente que, en diferentes momentos, han sido fieles compañeros de tren: María José y Juanjo por sus IN-CREIBLES anécdotas, Josam por sus movidas como comercial de Jazztel, Álvaro por sus magníficas experiencias en Everis (nunca me convenciste para unirme a vuestra bella familia laboral :D) y por supuesto a Xixo por todos aquellos minijuegos Android que alguna vez provocaron que acabásemos en Torrellano. Gracias a todos, no sé si podría haber aguantado hora y media de tren diaria durante 8 años sin vosotros.

Debo hacer un pequeño paréntesis para referirme a ese grupillo que se formó durante segundo de carrera formado por Siso, Pepe, Marta, Elena y José Manuel. Juegos de Rol, quedadas en Torrevieja, aventuras y desventuras, amor y desamor. Supuso una etapa muy intensa de mi vida y me quedo con toda ella, lo bueno y lo malo, gracias chic@s!

Y para cerrar esta etapa debo hablar de las personas que, desde mi punto de vista, fueron el mayor apoyo en el día a día. Por supuesto me refiero a Xixo y a Pepe, a quienes ya he mencionado previamente, pero esto es lo que tiene la vida, los buenos amigos pueden provenir de muy diversos sitios. ¿Cuantas horas habremos pasado juntos en la universidad? No compartíamos clases, casi ni compartíamos asignaturas, pero si tuviese que elegir a alguien para pasarme el resto de mis días estudiando, no elegiría a nadie más que a ellos. Esas horas de comer en la Galia y en Altabix, las reservas de aula en la hemeroteca, todos las escenas y personajes que creábamos en nuestra imaginación, todas las bromas de grupo, todas las cosas que conseguimos gratis en las máquinas expendedoras, todas las horas de Minecraft y Counter De verdad, con ellos, la universidad no fue nada. Las asignaturas, los exámenes, las horas de estudio, todo ello pudo suponer un

90 % de mis días, pero yo lo único que recuerdo es ese 10 % de bromas y tonterías que dejaban al otro 90 % como un pequeño mal que se sufría con mucho gusto. Muchas gracias a ambos por todos los años de universidad y por todo lo demás.

Y sin mayor ceremonia, comencé a trabajar en un laboratorio de investigación. Llegados a este punto, la primera persona a la que debo agradecer es a mi director de PFC y de Tesis, José María Azorín. Él supo ver mis inquietudes e hizo factible mi entrada al fantástico mundo de la investigación. Su experiencia en la investigación y su capacidad para lidiar con los problemas han sido una inspiración para mi durante estos casi 3 años de Tesis Doctoral. Debo agradecer también a todas las personas que he conocido durante los viajes que he realizado en esta etapa, que no son pocas. A toda la gente del Summer School de Baiona 2014, especialmente a Amelric, Daegun, Adam y Ana. A toda la gente del Hospital de Toledo: Esther, Elisa, Fernando, Antonio, Ana, Enrique, Diego, Vicente, Antonio y Ángel. Al resto de integrantes del proyecto Biomot: Elena, Mónica, Luca, Marta, Tomislav, Dirk, Mari Carmen, Fran, José, Juan y Jose Luis. Además, quiero hacer una mención especial a Guillermo, quizás la persona que más ha currado a lo largo de este proyecto y mi compañero de locuras por Japón. Gracias también a todos los integrantes de RIKEN (Okajima, Matti, Fady, Alejandro, Nagai, Matsui y Shingo) por hacer mi estancia en Japón tan enriquecedora. Gracias a Aki, Chiaki, Akari y a todos aquellos japoneses y japonesas anónimos que nos echaron una mano mientras sobrevivíamos en sus hospitalarias tierras. Gracias a todos los compañeros de laboratorio, cuyo número crece y crece cada día: Javi, Jorge, Arturo, Chemas, Luisda, Juan, Antonio, Ángel, Enrique, Carlos, Irene, Andrea, Santi, Yalena, Samara, Jose Antonioy que leches, también a Ricardo. Sin vosotros, estos tres años habrían sido mucho más duros. Y claro, me he dejado para el final a todos aquellos que han formado parte del BMI Systems Lab. Al chiflado de Dani (y su mujer y esposa Mar) a quienes no puedo nombrar por separado, porque sería como decir Epi y no decir Blas. A Enrique, quizás la persona con más amigos que he conocido en mi vida (tiene el record Guinness de cumpleaños asistidos en un mes). A Andrés, mi único y verdadero amor, aunque lo nuestro sea imposible por aquello de ser archienemigos. A Edu, que le dejo que se crea mi codirector

para que me deje trabajar tranquilo. A Rocío, aquella chica que viajó a las colonias en busca de oro, fama y poder y a quien sus compañeros esperan en la patria gachupina. A Marisol, que está loca, y es mejor agradecerle para que no me mate. Y por supuesto a Nayeli y Nadia, las recientes incorporaciones del grupo con quienes aún no tengo confianza suficiente como para insultar públicamente, pero tranquilas chicas, todo se andará.

Y aunque con esto se cierran las 3 etapas de mi vida hasta la actualidad, existen una serie de personas que han sido constantes durante todas ellas y por lo tanto se merecen menciones especiales. A Johan, Xixo, Pepe, Lucía, Jesús, Viti y Pap. Gracias por vuestra amistad y por formar parte de esas personas que han dado estabilidad a mi vida. A Jose y a Clara. Bueno que decir sobre ellos podría llenar páginas y páginas si me pusiese. Sinceramente no estoy seguro de que ellos alcancen a comprender lo importantes que son para mí. Son las primeras referencias que tuve de VERDADERA amistad. Por algún motivo, recuerdo perfectamente el momento en que cada uno de ellos me invitó a su cumpleaños por primera vez, por allá cuando yo tenía unos 9-10 años?. Recuerdo lo que sentí, son esas cosas que solo se pueden sentir una vez en la vida. Para que algunos me entendáises algo así como la felicidad que se siente la primera vez que el profesor Oak me pregunta tu nombre y te presenta a mi rival. Creo que es un ejemplo que lo define bastante bien. Chicos, sin vosotros, yo no sería yo, sería otra cosa diferente a mí, y por ello, os estaré siempre agradecido.

Y finalmente, que mayor constante en la vida que la familia. Debo agradecer a mis abuelos Pepe, Asunción, Manolo y Concha por ser referentes de futuro en mi vida. A mis tios, tias, primos y primas Maria Dolores, Inma, Mari Carmen, Pablo, Jose Antonio, Paco, Alejandro, Mario, Inmaculada, Francisco y Juan por todos los buenos momentos en familia. Y claro, como no, a mis Padres y a mi Hermana, cuyos nombres no son en absoluto importantes. Da igual como pudiesen llamarse porque seguirían siendo ellos. Siempre han estado ahí, compartiendo las alegrías y sufrimientos, ayudando y protegiendo. Me han dado todo lo que tengo y me habría sido imposible llegar hasta aquí sin ellos. Supongo que todo el mundo

quiere mucho a sus padres y hermanos, pero yo sinceramente, creo haber tenido una suerte especial con ellos. Sin importar los problemas que pueda sufrir o la distancia que exista entre nosotros, siempre formarán parte de mí. Gracias.

¿Creíais que había acabado? No, no, aún no. No me gustan los finales emotivos en exceso. Dan la sensación de que no hay nada más después de ellos. Por eso, me he dejado a la última incorporación de mi familia para el final. Gracias a nuestro perro Mushu, por ser el ser (valga la redundancia) más feliz del universo y transmitirnos cada dia su emoción incondicional hacia la totalidad de lo que le rodea.

Índice general

Índice de figuras

Índice de tablas

Glosario

Acrónimo	Descripción en castellano	Descripción en inglés
AEP	Potencial Evocado Auditivo	*Auditory Evoked Potential*
AMLR	Potencial Auditivo de Latencia Media	*Auditory Middle Latency Response*
API	Interfaz de programación de aplicación	*Application Programming Interface*
AR	Auto Regresivo	*Auto-Regressive*
ASSR	Respuesta Auditiva de Estado Estacionaria	*Auditory Steady-State Response*
BCI	Interfaz Cerebro-Computador	*Brain-Computer Interface*
CAR	Referencia Media Común	*Common Average Reference*
CNV	Variación de Contingencia Negativa	*Contingent Negative Variation*
CSIC	Consejo Superior de Investigaciones Científicas	*Spanish National Research Council*
CSP	Patrones Espaciales Comunes	*Common Spatial Patterns*
DTL	Aprendizaje por Árbol de Decisión	*Desicion Tree Learning*
ECoG	Electrocorticografía	*Electrocorticography*
EEG	Electroencefalografía	*Electroencefalography*
EMG	Electromyografía	*Electromyography*
EOG	Electrooculografía	*Electrooculography*
ERD	Event-Related Desynchronization	*Desincronización Relacionada a Evento*
ERP	Potencial Relacionado a Evento	*Event-Related Potential*
ErrP	Potencial Relacionado a Error	*Error-Related Potential*
fMRI	Imagen por Resonancia Magnética Funcional	*Functional Magnetic Resonance Imaging*
FPR	Tasa de Falsos Positivos	*False Positive Rate*
HA	Amplitud Alta	*High Amplitude*

Acrónimo	Descripción en castellano	Descripción en inglés
ICA	Analisis de Componentes Independientes	*Independent Component Analysis*
IMU	Unidades de Medición Inercial	*Inertial Measurement Unit*
KNN	K-vecinos más cercanos	*K-Nearest Neighbors*
LDA	Análisis de Discriminación Lineal	*Linear Discriminant Analysis*
MEG	Magnetoencefalografía	*Magnetoencefalography*
MEM	Método de Máxima Entropía	*Maximum Entropy Method*
NB	Classificador Bayes Ingenuo	*Naive Bayes*
NIH	Instituto Nacional de la Salud	*National Institute of Health*
PSD	Densidad de Potencia Espectral	*Power Spectral Density*
QDA	Análisis de Discriminación Lineal	*Quadratic Discriminant Analysis*
REST	Técnica de Estandarización de Electrodo de Referencia	*Reference Electrode Standarization Technique*
ROC	Característica Receptor-Operador	*Receiver-Operating Characteristic*
SA	Amplitud Repentina	*Sudden Amplitude*
SCP	Potencial Cortical Lento	*Slow Cortical Potential*
SMA	Media de Máximos por Segmento	*Segment Maximum Average*
SMR	Ritmos Sensitivo-Motrices	*Sensorimotor rhythms*
TPR	Tasa de Verdaderos Positivos	*True Positive Rate*
VEP	Potencial Evocado Visual	*Visual Evoked Potential*
WHO	Organización Mundial de la Salud	*World Health Organization*

Resumen

En este trabajo se pretende evaluar los mecanismos cognitivos que experimenta el ser humano durante el proceso de la marcha partir de las señales electroencefalográficas (EEG). Uno de los principales objetivos es el desarrollo de interfaces cerebro-máquina que permitan determinar el estado cognitivo de un usuario de forma que se pueda utilizar dicha información con fines de asistencia y rehabilitación.

El registro de señales corticales durante la marcha es un campo poco explorado en la actualidad y dado que estas señales tienen una relación señal a ruido muy pobre, es necesario realizar una evaluación y validación de las mismas durante la marcha humana. Para ello, esta Tesis Doctoral comienza realizando una evaluación de artefactos corticales producidos principalmente por presiones mandibulares que, en última instancia, permiten el desarrollo de dos sistemas de control bidimensional basados en los mismos: uno donde se controla un cursor por pantalla y otro donde se controla un brazo robótico. Ambos demuestran una gran eficiencia en el alcance de objetivos pudiendo ser de gran ayuda como sistemas de asistencia para personas con movilidad reducida.

Con los conocimientos sobre artefactos adquiridos con el trabajo anterior se realizan mediciones EEG durante la marcha humana y se comparan con mediciones realizadas durante experimentos en reposo. De esta comparación se descubren dos fuentes de ruido que afectan a las señales corticales relacionadas con fallos de conductividad entre el cuero cabelludo y los electrodos utilizados para realizar las mediciones. Su evaluación permite el desarrollo de protocolos de experimentación que reduzcan la influencia de artefactos durante pruebas en movimiento. Estos protocolos son utilizados posteriormente para realizar una experimentación en la que se evalúan mecanismos cognitivos experimentados por humanos durante la marcha.

En este estudio se evalúa el nivel de atención que una persona presta a la marcha humana. Se realiza un barrido frequencial de las señales registradas para discernir a qué frecuencia se produce el fenómeno buscado. Los resultados muestran una desincronización en la banda gamma (30-90 Hz) relacionada con

mecanismos de atención selectiva. Las clasificaciones realizadas proporcionan resultados muy prometedores de cara a la implementación de sistemas en tiempo real.

En el futuro se pretende diseñar sistemas que permitan obtener estos parámetros en tiempo real para utilizarlos como realimentación en terapias de rehabilitación de miembro inferior. Estudios recientes sugieren que este tipo de trabajos incrementa el grado de involucración de los pacientes en sus terapias, potenciando la plasticidad cerebral y, en última instancia, los resultados de la rehabilitación.

Abstract

This thesis is focused on the evaluation of electroencephalographic (EEG) signals in order to improve current understanding of cognitive processes experienced by humans during ambulation. The main goal is to set the basis of brain-machine interfaces (BMIs) development that provide information about the user cognitive state during walking. This information could be used as feedback for assistive and rehabilitation technologies.

Currently, recording of cortical activity during ambulation has not been widely explored. EEG potentials have a poor signal to noise ratio which makes their recording difficult during movement. It is necessary to develop protocols that asses the validity of these signals during walking. Therefore, the thesis starts with the evaluation of cortical artifacts produced by jaw clenches. This first study was used to develop a system to control a cursor and a robotic arm in a two-dimensional workspace through jaw clenches. Both systems show promising results in the field of assistive technologies oriented to physically impaired people.

In a second study, cortical signals were measured both during ambulation and movement-free conditions. Both conditions were compared to find unexpected behaviors during walking. After this comparison, two types of noise were found in the signals with higher influence on ambulation recordings. Results suggest that it can be the result of conductivity changes between the scalp and the electrodes during movement. The evaluation of these noises would allow the development of protocols for recording valid EEG signals during ambulation. These protocols were used to evaluate cognitive mechanisms.

The mechanism evaluated is related to the level of attention paid by humans in gait process. This work evaluates the whole EEG bandwidth to find evidence of classifiable cortical information related to this phenomenon. Results show a desynchronization in the gamma band (30-90 Hz) associated to selective attention mechanisms. Performed offline classifications provide promising results that could be implemented as a real time system.

This study showed promising results in detection of cognitive mechanisms during ambulation. Taken together, these findings could be applied in future

brain-machine interfaces for rehabilitation. This kind of interface would provide, in real time, several parameters related to cognitive state of patients. These parameters could be used during the rehabilitation strategy to adapt therapies to patients' mental state. This would provide patients a way to be involved with their rehabilitation.

Capítulo 1

INTRODUCCIÓN

En este capítulo se presentan las motivaciones que han llevado al desarrollo de esta Tesis Doctoral, partiendo de la problemática social de la cual provienen. Se especifican los objetivos perseguidos a lo largo de las investigaciones realizadas y cómo permiten abordar el problema planteado. Por último, se muestran todos los trabajos realizados dentro del marco de investigación de la Tesis Doctoral. En este aspecto se destactan las contribuciones en revista y congresos nacionales e internacionales, los capítulos de libros escritos y los proyectos final de carrera codirigidos.

1.1. Motivaciones

En el año 1970, la organización mundial de la salud (WHO del inglés *World Health Organization*) estimó que el 2011 un 10 % de la población mundial sufriría algún tipo de discapacidad. Sin embargo, el informe de 2011 mostraba que un 15 % de la población la padecía [1]. De estas personas, entre un 2 % y un 4 % experimentan grandes dificultades a la hora de llevar una vida normal. De estos datos de discapacidad crecientes ha surgido una preocupación social centrada en el desarrollo de investigaciones y dispositivos que permitan mejorar las condiciones de vida de estas personas y que contribuyan a la reducción de casos que deriven en discapacidad.

Una de las principales causas de discapacidad severa son las lesiones de médu-

la espinal [2]. Estas lesiones se producen generalmente por causas traumáticas que afectan a la médula y que bloquean los caminos de comunicación nerviosos entre el cerebro y los músculos. Al contrario que con otras lesiones y enfermedades, uno de los sectores de población con más riesgo de sufrir lesiones de médula espinal es el de los jóvenes de entre 15 y 30 años. Las personas con estas lesiones tienen entre 2 y 5 veces más posibilidades de sufrir una muerte prematura, siendo el riesgo muy elevado en el primer año de lesión. Las personas que sufren de estas enfermedades son más propensas a sufrir problemas de salud secundarios como espasmos musculares, infecciones del tracto urinario, dolor crónico y problemas respiratorios. Todo esto conlleva un incremento del gasto económico en terapia y medicaciones por lo que se consideran un factor de empobrecimiento de la población. Por otro lado, puesto que afecta principalmente a un sector joven de la población, tiene consecuencias sociales en términos de rendimiento escolar y desarrollo social.

Al sufrir estas lesiones, se pierde o se ve reducida la comunicación entre zonas del cerebro y grupos musculares. Sin embargo, el cerebro es un órgano plástico que tiene la capacidad de generar nuevas conexiones neuronales y reestablecer, en cierta medida, el control sobre las zonas perdidas [3]. Este proceso se potencia con la rehabilitación física y cognitiva del paciente, lo que hace de la rehabilitación una de las etapas más críticas tras la lesión de médula espinal. Se ha demostrado que las mejoras más significativas que se producen en pacientes que sufren estas lesiones se dan durante los 6 primeros meses de recuperación [4]. Por otro lado, los efectos de estas lesiones en cada paciente son muy variables y, por lo tanto, es necesario que la rehabilitación sea diseñada con un alto grado de especificidad [5]. Disponer de poco tiempo y tener que evaluar las condiciones específicas de cada paciente ha hecho que la rehabilitación se convierta en un campo de gran interés para la ciencia.

Muchas investigaciones se centran en el desarrollo de técnicas y dispositivos que permitan mejorar las terapias de rehabilitación incrementando el grado de mejora sobre los pacientes y reduciendo el tiempo exigido por las terapias [6, 7]. En este aspecto, el campo de la robótica ha desarrollado multitud de dispositivos orientados a mejorar la rehabilitación [8, 9]. Concretamente el uso de exoesquele-

tos que se acoplan a las extremidades de un pacientes y lo asisten en el movimiento se ha vuelto muy popular en estas terapias [10, 11]. En relación con este campo, encontramos las interfaces cerebro-máquina (BMI del inglés *Brain-Machine Interface*), que tratan de estudiar las formas de utilizar las ondas cerebrales de las personas para generar comandos para controlar dispositivos externos. Estas interfaces han sido propuestas dentro de la comunidad científica como forma de incrementar el grado de involucración de un paciente en su terapia [12, 13]. Se ha podido comprobar que, de esta forma, se fomenta la plasticidad cerebral y, en última instancia, los resultados de la rehabilitación.

Actualmente se están comenzando a usar interfaces cerebro-máquina no invasivas en combinación con dispositivos robóticos orientados a la rehabilitación de miembro inferior [14, 15]. Las lesiones de miembro inferior son una de las principales consecuencias de las lesiones de médula espinal y suponen una gran limitación física a la hora de llevar una vida normal. Sin embargo, la medición de señales corticales no invasivas durante la marcha resulta muy delicada debido a la pobre relación señal a ruido de estos potenciales [16]. Por este motivo, en la actualidad se está intentando abordar esta problemática de forma que sea posible la medición de parámetros cognitivos durante el movimiento [17]. Esto permitirá ajustar las terapias de rehabilitación al estado mental del paciente de forma que se fomente su involucración y que, consecuentemente, mejoren los resultados finales de su rehabilitación.

1.2. Objetivos de la Tesis Doctoral

Bajo este contexto social y científico, el objetivo de esta Tesis Doctoral consiste en desarrollar interfaces cerebro-máquina que proporcionen información del estado congnitivo de un usuario durante la marcha humana a partir de sus señales EEG. Para ello será necesario un estudio que permita validar las señales corticales registradas bajo estas condiciones y, posteriormente, estudiar los mecanismos corticales cognitivos. Con este trabajo se pretenden cumplir los siguientes objetivos:

- Evaluar las fuentes de ruido que se producen en las señales corticales prestando especial atención a las que se producen de forma específica durante la marcha humana.

- Implementación de protocolos que nos permitan registrar señales corticales durante la marcha de forma que sea posible la evaluación de estas ondas durante el movimiento.

- Estudio de las ondas corticales orientado a la extracción de información cognitiva que nos permita aproximar el estado cognitivo de un usuario.

- Aplicación de los resultados obtenidos a lo largo de la Tesis Doctoral al desarrollo de sistemas de asistencia y rehabilitación que permitan mejorar la vida de personas con movilidad reducida, centrándose en especial en los lesionados incompletos de médula espinal.

Esta Tesis Doctoral se encuentra dentro del marco del proyecto BioMot - Smart Wearable Robots with Bioinspired Sensory-Motor Skills (con el acuerdo de subvención número IFP7-ICT-2013-10-611695) financiado por la Comisión de la Unión Europea. El objetivo de este proyecto es el desarrollo de un exoesqueleto de miembro inferior orientado a la rehabilitación de lesionados de médula espinal cuyo funcionamiento venga definido por el contexto físico y mental del paciente a través de una realimentación electrofisiológica. Este proyecto tiene una duración de 3 aos (del 1 de Octubre de 2013 al 30 de Septiembre del 2016). En el participan cinco grupos de investigación europeos (Universidad Miguel Hernández de Elche, Agencia del Consejo Superior de Investigaciones Científicas, Hospital Nacional de Paraplégicos de Toledo, Vrije Universiteit Brussel y Universit degli Studi di Padova), un grupo de investigación japonés (RIKEN) y dos empresas (Technaid S.L. y Ossur hf). El proyecto está dirigido por Juan C. Moreno, perteneciente al Instituto Cajal del Consejo Superior de Investigaciones Científicas de Madrid (CSIC).

1.3. Trabajos publicados

Esta Tesis Doctoral consta de una serie de publicaciones divididas en dos grupos:

- *Publicaciones en revistas impactadas.* Se presentan tres trabajos que conforman la línea de investigación seguida durante la Tesis Doctoral. Dos de ellas están clasificadas en el primer cuartil (Q1) del ranking JCR por índice de impacto mientras que la tercera está clasificadas dentro del segundo cuartil (Q2).
- *Contribuciones en congresos.* Se incluye una publicación perteneciente a una contribucion en congreso internacional que apoya el trabajo realizado.

Además, durante la realización de esta Tesis Doctoral se realizaron otros trabajos que se vieron representados con contribuciones a congresos nacionales e internacionales, capítulos de libro y proyectos final de carrera codirigidos.

1.3.1. Publicaciones en revistas impactadas

Autores: *Á. Costa*, E. Iáñez, A. Úbeda, E. Hortal, D. Planelles, J. M. Azorín
Título: Supplementary System of a Brain-Machine Interface based on jaw artifacts for bidimensional control of a robotic arm.
Ref. revista / Libro: Plos One
ISSN: 1932-6203
DOI : 10.1371/journal.pone.0112352
Índice de impacto (JCR 2014): 3.234
Lugar que ocupa en el área de *MULTIDISCIPLINARY SCIENCES*: 7/56 (Q1)
Clave: A Volumen(número): 9(11) Páginas: 1-13
Fecha de publicación: 12 Noviembre 2014
Editorial: PUBLIC LIBRARY SCIENCE
Lugar de publicación: Estados Unidos

Autores: *Á. Costa*, R. Salazar-Varas, A. Úbeda, J. M. Azorín

Título: Characterization of Artifacts Produced by Gel Displacement on Non-invasive Brain-Machine Interfaces during Ambulation

Ref. revista / Libro: Frontiers in Neuroscience

ISSN: 1662-453X

DOI : 10.3389/fnins.2016.00060

Índice de impacto (JCR 2014): 3.656

Lugar que ocupa en el área de *NEUROSCIENCES*: 82/252 (Q2)

Clave: A Volumen(número): 10(60) Páginas: 1-14

Fecha de publicación: 25 Febrero 2016

Editorial: FRONTIERS RESEARCH FOUNDATION

Lugar de publicación: Suiza

Autores: *Á. Costa*, E. Iáñez, A. Úbeda, E. Hortal, A. Del-Ama, Ángel Gil-Agudo J. M. Azorín

Título: Decoding the attentional demands of gait through EEG gamma band features

Ref. revista / Libro: Plos One

ISSN: 1932-6203

DOI : 10.1371/journal.pone.0154136

Índice de impacto (JCR 2014): 3.234

Lugar que ocupa en el área de *MULTIDISCIPLINARY SCIENCES* : 9/57 (Q1)

Clave: A Volumen(número): 11(4) Páginas: 1-21

Fecha de publicación: 26 Abril 2016

Editorial: PUBLIC LIBRARY SCIENCE

Lugar de publicación: Estados Unidos

1.3.2. Contribuciones en congresos

Autores: *Á. Costa*, E. Iáñez, A. Úbeda, D. Planelles, E. Hortal, J.M. Azorín
Título: Experimental Setup and First Results of a BCI System for Attention Levels Classification During Gait
Ref. revista / Libro: 2014 International Conference on Autonomous Intelligent Systems (IAS-13). Workshops Proceedings. Workshop on Neuro-Robotics for Patient-Specific Rehabilitation.
ISBN: 978-88-95872-06-3
Clave: CL Páginas: 470-473 Fecha: 15-19 de Julio 2014
Congreso: Internacional
Editorial: Padova University
Lugar de publicación: Padova, Italia

1.3.3. Otras contribuciones en congresos

Se incluye el resto de contribuciones a congresos publicadas durante el desarrollo de la presente Tesis Doctoral:

- *Á. Costa*, R. Salazar-Varas, E. Iáñez, A. Úbeda, E. Hortal, J.M. Azorín. *Studying cognitive attention mechanisms during walking from EEG signals*. IEEE International Conference on Systems, Man, and Cybernetics (SMC 2015), Special Session on *Robotic Exoskeletons with Bioinspired Skills* Hong Kong, 9-12 Oct 2015. Páginas: 882-886. ISBN: 978-1-4799-8697-2. 9-12 Octubre 2015.

- *Á. Costa*, G. Asín-Prieto, S. Shimoda, E. Iáñez, J.C. Moreno, J.L Pons, J.M. Azorín. *Integración de interfaz cerebro-computador y exoesqueleto de miembro inferior orientado a la rehabilitación*. Actas de las XXXVI Jornadas de Automática, Bilbao, España, Páginas: 766-772. 2 4 Septiembre, 2015.

- *Á. Costa*, E. Iáñez, A. Úbeda, Daniel Planelles, E. Hortal and J.M. Azorín. *Frequency and Number of Neighbors Study for Attention Level Classification Using EEG Signals*. International Workshop on Wearable Robotics (WeRob 2014),

Baiona, Spain, Páginas: 14-19 Septiembre 2014.

- *Á. Costa*, E. Iáñez, A. Úbeda, D. Planelles, E. Hortal and J.M. Azorín. *Experimental Setup and First Results of a BCI System for Attention Levels Classification During Gait*. NeuroRob-2014, Padova, Italia, 18 Julio 2014.

- *Á. Costa*, D. Planelles, A. Úbeda, E. Iáñez and J.M. Azorín. *Arquitectura para el análisis de los estados cognitivos relacionados con la marcha*. Cognitive Area Networks, proceedings of 6 Simposio CEA Bioingeniería, Granada, España. Vol. 1, Páginas: 19-24. ISSN: 2341-4243. 12-13 Junio, 2014.

- *Á. Costa*, E. Iáñez, E. Hortal, J. M. Azorín, A. Rodríguez, D. Tornero, J.A Berná, J.M. Cano. *Movimiento bidimensional de un cursor mediante el uso de artefactos en señales electroencefalográficas*. Actas de las XXXIV Jornadas de Automática. Terrassa, España, Páginas: 108-114. ISBN: 978-84-616-5063-7, 4-6 Septiembre 2013.

1.3.4. Capítulos de libro

En el marco de esta Tesis Doctoral se ha publicado un capítulo de libro relacionado con la misma temática:

- I.N. Angulo-Sherman, *Á.Costa-García*, E. Monge-Pereira, R. Salazar-Varas, R.Zerafa, *BCI Applied to Neurorehabilitation*. Book: Emerging Therapies in Neurorehabilitation II, 169-196 (27 páginas). Springer International Publishing Suiza, 10 Diciembre 2015. ISBN 978-3-319-24899-8. dx.doi.org/10.1007/978-3-319-24901-8

1.3.5. Proyectos final de carrera codirigidos

Por último, se ha codirigido el siguiente proyecto final de carrera durante la realización de la presente Tesis Doctoral:

Título: Control de un brazo robot en 3D a partir de artefactos en señales EEG
Alumno: Javier Alarcón Domínguez
Tutores: José María Azorín Poveda, Álvaro Costa García
Titulación: Ingeniero Industrial
Universidad: Miguel Hernández de Elche
Calificación: 9
Lugar y Fecha: 5 de Septiembre de 2014

UNIVERSITAS
Miguel
Hernández

Capítulo 2

ANTECEDENTES

En esta sección se describen todos aquellos términos de relevancia dentro del marco conceptual de la presente Tesis Doctoral. Su comprensión facilitará el seguimiento de las investigaciones descritas. Se especifican, en mayor detalle, las preocupaciones sociales y científicas que motivan el desarrollo de esta línea de investigación, principalmente las lesiones que producen movilidad reducida y sus consecuencias. Se describen las bases de los sistemas de adquisición de señales corticales más usados, centrando la atención en la electroencefalografía. Además, se abordaran las ventajas de estas tecnologías en el campo de la rehabilitación y su combinación con otros dispositivos como brazos robots y exoesqueletos. Finalmente se describen los desafíos a los que se enfrenta en la actualidad la ciencia, en relación a estos sistemas.

2.1. Lesiones que producen movilidad reducida

Las lesiones que afectan a alguna de las partes del sistema nervioso reducen, en mayor o menor medida, la capacidad de movimiento de una persona. El sistema nervioso puede dividirse en sistema nervioso central y periférico. El sistema nervioso central está formado por el cerebro, encargado de la toma de decisiones, y la médula espinal, que transmite los comandos del cerebro a los nervios del resto del cuerpo. El sistema nervioso periférico, por su lado, está formado por las terminaciones nerviosas finales que reciben los impulsos nerviosos y provocan los movimientos musculares. Es posible clasificar las lesiones que causan movi-

lidad reducida en función de la parte del sistema nervioso a la que afectan. En este aspecto podemos diferenciar entre lesiones nerviosas periféricas, lesiones de médula espinal y accidentes cerebrovasculares.

2.2. Lesiones nerviosas periféricas

Estas lesiones afectan a las terminacones del sistema nervioso periférico. En función de su severidad se pueden dividir en 3 tipos de acuerdo con el sistema de clasificación de Seddon [18]:

- *Neuropraxia (leve)*: consiste en una interrupción temporal de la conducción eléctrica de un nervio sin que se haya producido una rotura en las conexiones nerviosas. Su principal causa son los golpes sobre fibras musculares y fibras óseas nerviosas que, a su vez, provocan una presión prolongada sobre un nervio. Esta lesión causa parálisis completa o parcial del segmento del cuerpo que el nervio afectado controla. Por lo general, el paciente recupera la movilidad en un corto periodo de tiempo tras el tratamiento médico de la lesión que haya causado la presión nerviosa [19].

- *Axonotmesis (intermedia)*: consiste en la degeneración de las vainas mielínicas y los axones sin la pérdida de continuidad en el nervio. Su causa suelen ser golpes o contusiones de mayor grado que en la neuropraxia. El nervio no llega a romperse pero los tejidos internos se dañan. De nuevo, se manifiesta como parálisis total o parcial de la zona del cuerpo controlada por el nervio afectado. Los casos más leves permiten una recuperación completa tras varios meses de regeneración nerviosa. Otro casos, sin embargo, requieren de cirugías de reconstrucción y, en última instancia, el uso de dispositivos de asistencia para compensar la pérdida de movilidad [20].

- *Neurotmesis (grave)*: consiste en la rotura total o parcial de un nervio tras un traumatismo severo. Entre sus efectos está el dolor intenso, la disestesia, y la pérdida completa de funciones motoras y sensoriales de la zona afectada. El principal tratamiento es el uso de medicamentos para reducir el dolor. En algunos casos es posible reparar la lesión mediante cirugía, bien uniendo

los extremos nerviosos dañados o transfiriendo nervios de otras parte del cuerpo [21].

2.3. Lesiones de médula espinal

Se trata de una lesión en el sistema nervioso central, concretamente en la médula espinal (SCI del inglés *Spinal Cord Injury*). Estas lesiones se registran principalmente en personas jóvenes y sanas como resultado de algún traumatismo provocado por un accidente. Su tasa de mortalidad tiende a ser mayor en los niños pequeños con lesiones de columna [22].

2.3.1. Causas de lesión de la médula espinal

Las lesiones de médula espinal pueden estar causadas por traumatismos físicos asociados con impactos y agitaciones bruscas de la columna vertebral [23]. Las principales causas son los accidentes de tráfico, las lesiones deportivas, las agresiones físicas, las caídas y las heridas de bala [24]. También pueden producirse por negligencias médicas como inyecciones mal realizadas en la médula espinal [25]. Estas lesiones también pueden tener un origen no traumático. Entre el 30 % y el 80 % de lesiones de médula espinal tienen orígenes no traumáticos dependiendo en gran medida de la zona del mundo en la que nos fijemos [26]. En los países desarrollados tienen mayores porcentajes de lesiones medulares debido a enfermedades degenerativas y tumores [27]. En países en vías de desarrollo es más común que estas lesiones se originen por infecciones como el virus de la inmunodeficiencia humana (VIH), la tuberculosis o la poliomielitis [24]. También puede estar causada por enfermedades que afecten a la columna vertebral (hernias) o al sistema vascular, bloqueando la llegada de sangre a zonas de la médula espinal [28].

2.3.2. Efectos de la lesión de médula espinal

El efecto principal de la lesión de médula espinal es la pérdida total o parcial de movilidad y sensibilidad por debajo de la zona lesionada de la médula. En

función de este factor se considera la lesión completa o incompleta, respectivamente. Las áreas de afectación y otros efectos dependerán en gran medida de la zona de la columna vertebral donde se haya producido la lesión (ver figura 2.1):

- *Zona lumbar y sacra*: se reduce la movilidad de una o ambas piernas y la cadera. Además es común la pérdida del control sobre los músculos que controlan los intestinos y la vejiga [29].

- *Zona torácica*: desaparece la movilidad y sensibilidad en piernas y cadera (paraplejia). Presenta diferentes grados de severidad en función del punto torácico afectado. Las lesiones entre las vértebras T9 y T12 mantienen el control sobre los músculos torácicos. Sin embargo, esto no es así en las que se producen entre T1 y T8, haciendo difícil o imposible el control del tronco [30].

- *Zona cervical*: estas lesiones suelen resultar en tetraplejia total o parcial dependiendo de la zona donde se produzcan. Las lesiones entre C7 y T1 permiten mantener un control parcial de los brazos aunque el control de las manos es muy reducido. Entre C4 y C6, el control sobre los brazos se reduce drásticamente, manteniendo algún débil control sobre muñecas, bíceps y hombros (según el nivel de afectación). Por último, las lesiones sobre C3 y superiores, producen una pérdida en la función del diafragma. Esto provoca la incapacidad de respirar por voluntad propia y la necesidad de un ventilador mecánico [31].

Existen otras afectaciones como el síndrome del cordón central (parálisis sobre brazos y manos) [32], síndrome del cordón posterior (pérdida de la capacidad propioceptiva) [33], síndrome de Brown-Sequard (parálisis de un lado del cuerpo) [34], esclerosis y mielitis transversa.

2.3.3. Tratamiento de la lesión de médula espinal

Los pacientes requieren de rehabilitaciones especializadas en función del grado de la lesión y de las zonas más afectadas. La fase de recuperación en el hospital suele durar entre 8 y 12 semanas, tras lo que comienza la fase de rehabilitación

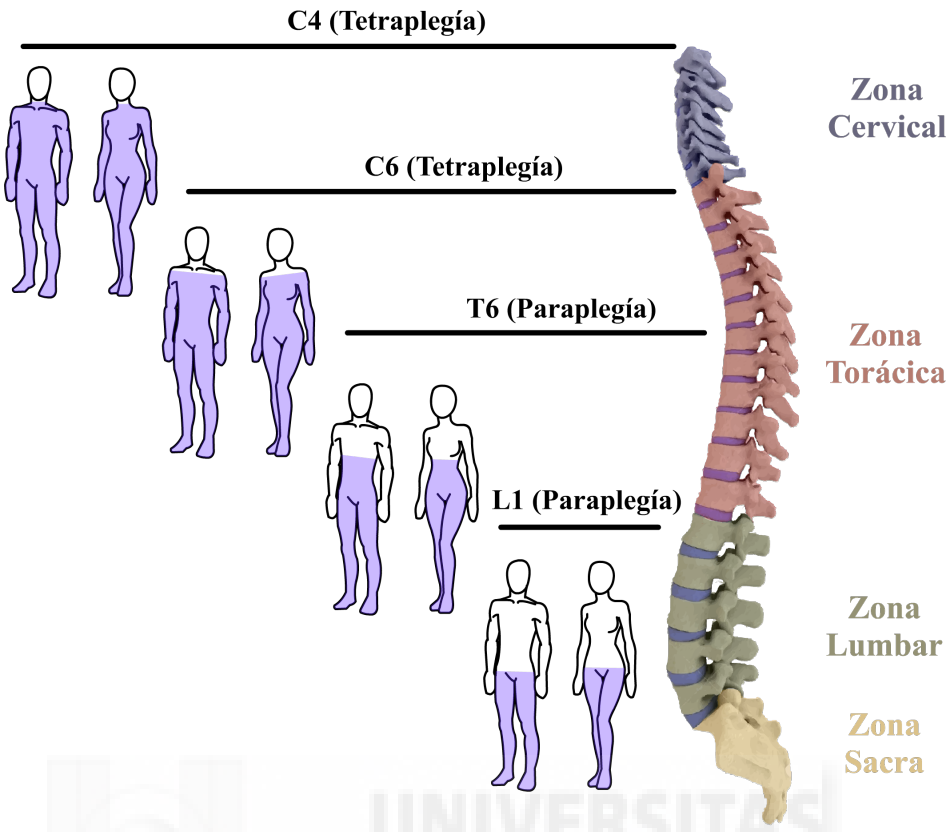

Figura 2.1: Niveles de lesión medular en función del área medular dañada.

de entre 3 y 12 meses. Las alteraciones que perduran tras los primeros 6 meses de rehabilitación suelen ser permanentes, por lo que es necesario optimizar la rehabilitación durante ese periodo de tiempo [35]. El nivel final de recuperación viene definido tanto por la eficacia de estas terapias como por la severidad de la lesión.

2.4. Accidente cerebrovascular

El accidente cerebrovascular (ACV), infarto cerebral o ictus es una lesión cerebral que se produce debido a una anomalía grave en el comportamiento del sistema cardíaco en el cerebro. Estas anomalías bloquean la llegada de sangre a las células cerebrales produciendo, de esta forma, una falta de los recursos básicos necesarios para el correcto funcionamiento de las mismas. Dado que el cerebro es el principal centro de control del organismo, un fallo en un conjunto de sus células puede tener grandes repercusiones en el cuerpo humano.

2.4.1. Causas del accidente cerebrovascular

En función de la anomalía circulatoria que cause la lesión cerebral, se puede distinguir entre ACV isquémico y ACV hemorrágico (Figura 2.2).

El accidente cerebrovascular isquémico se produce por una obstrucción en las vías que permiten la llegada de sangre a las células del cerebro. Estas células nerviosas necesitan un suministro constante de oxígeno y glucosa. Al cesar el flujo de sangre, se interrumpe dicho suministro, lo que provoca la muerte de las células. Cuanto mayor sea el tiempo durante el que se bloquea la respiración celular, mayor será la zona infartada del cerebro. Esta obstrucción o isquemia de las arterias del cerebro puede tener tres causas distintas en función de su origen:

- *Vasoconstricción*: consiste en el estrechamiento de una arteria, y la consecuente reducción del flujo de sangre, producido por la contracción del músculo liso presente en la superficie del vaso sanguíneo [36].
- *Trombo*: se trata de la detención del flujo sanguíneo por la coagulación de sangre en un punto concreto de una arteria cerebral [37].
- *Embolia*: producida por un coágulo de sangre generado en alguna de las venas del cuerpo que se desprende y viaja hasta el cerebro, provocando en él la obstrucción sanguínea [38].

El ACV isquémico el que más casos de lesión cerebral produce en la actualidad, suponiendo alrededor del 88 % de los accidentes cerebrovasculares.

Por otro lado, el accidente cerebrovascular hemorrágico o hemorragia cerebral se produce por la rotura de un vaso sanguíneo encefálico y el consecuente derrame sobre las células nerviosas. Este derrame conduce al accidente cerebrovascular por dos medios: la falta de riego sanguíneo del área dependiente del vaso roto y la compresión que la sangre extravasada ejerce sobre las estructuras cerebrales. Las principales causas del ACV hemorrágico son descritas a continuación:

- *Hipertensión arterial*: se trata de una enfermedad crónica que se manifiesta como un incremento de la presión del flujo sanguíneo en las arterias. Este

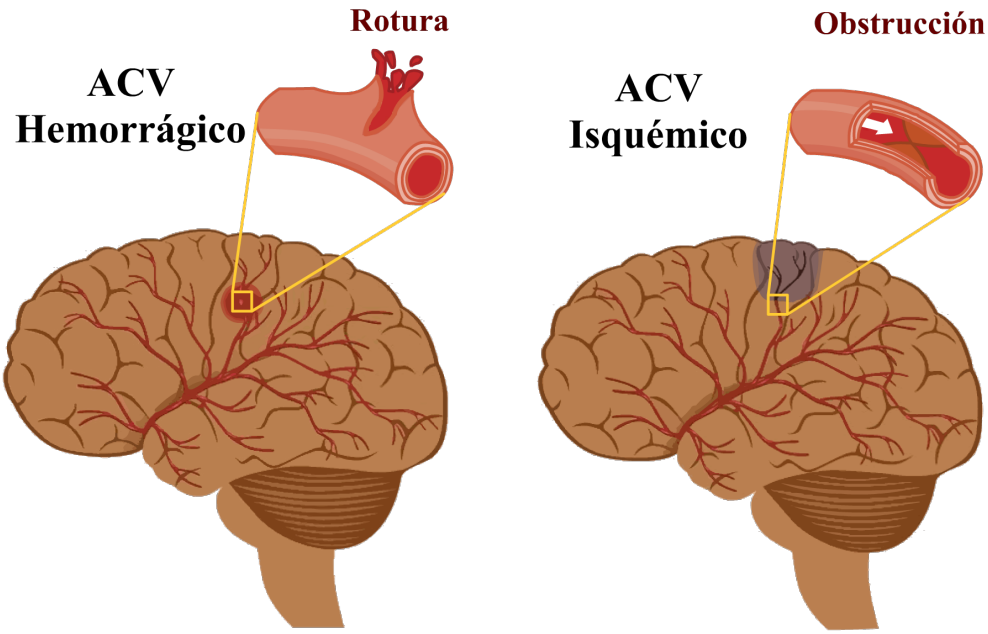

Figura 2.2: Los dos principales tipos de accidente cerebrovacular.

incremento aumenta el riesgo de que se produzca en las arterias cerebrales un derrame y la consecuente lesión encefálica [39].

- *Aneurisma*: se trata de una inflamación que se produce en una arteria debido a la existencia de una zona dañada. Estas protuberancias acumulan parte de la sangre que circula por la arteria a la que van anexionadas, pudiendo, en última instancia, desgarrarse y producir el derrame sanguíneo al cerebro [40].

El ACV hemorrágico no solo afecta a las zonas del cerebro dependientes de la arteria rota sino que, debido al derrame cerebral, se bloquean otros vasos encefálicos. Esto contribuye a un incremento del área afectada por la lesión.

2.4.2. Efectos del accidente cerebrovascular

Un accidente cerebrovascular puede causar la muerte o discapacidad permanente o temporal. Aproximadamente, el 20 % personas que sufren un ACV mueren dentro del primer mes, el 30 % en el primer año, y el 50 % mueren en los primeros 5 años [41].

Dependiendo de la zona encefálica afectada por el accidente cerebrovascular, los efectos que causa en el cuerpo humano pueden ser variados. Aunque estas

lesiones provocan efectos diferentes, existen algunos problemas comunes en las personas que sufren estos accidentes. Los más visibles son la parálisis muscular y los dimanantes problemas en el balance y la movilidad, problemas de visión, problemas para tragar, pérdida de control sobre los intestinos y la vejiga y exceso de cansancio. También existen otros efectos menos visibles, aunque igual de importantes, como los problemas de comunicación, tanto verbal como escrita, problemas de memoria y asociación de ideas, cambios emocionales como depresión y ansiedad y, como resultado de todos ellos, cambios en el comportamiento de las personas que sufren estos efectos.

2.4.3. Tratamiento del accidente cerebrovascular

El tratamiento de estas lesiones varía tanto en formas como en duración dependiendo de la intensidad y áreas de afectación, pero de forma general puede dividirse en cuatro fases [42]:

- *Tratamiento*: primera fase tras la lesión cerebral. Los médicos determinan el origen del accidente cerebrovascular y administran las cirugías o medicamentos oportunos para aliviar sus efectos (eliminación de coágulos, drenado de sangre o reparación de arterias rotas)

- *Recuperación*: se deja al paciente unas semanas de reposo bajo cuidados médicos. Durante este tiempo es común que algunas de las capacidades perdidas retornen gracias a mecanismos naturales de recuperación del organismo humano.

- *Rehabilitación*: durante este periodo, fisioterapeutas y especialistas trabajan en terapias de rehabilitación para recuperar las habilidades perdidas del paciente. Supone el paso más crítico de cara al bienestar futuro de la persona, ya que el paciente advierte grandes dificultades realizando tareas que antes podía realizar fácilmente. Es muy importante que los terapeutas sepan guiarlos a través de estas frustraciones, ya que en la mayoría de casos, con la terapia adecuada es posible recuperar casi todas las funciones perdidas.

- *Vuelta a casa*: el paciente vuelve a casa y mantiene algunas de las terapias de rehabilitación iniciadas en el hospital. El paciente debe realizar ciertos

ajustes sobre su forma de vida, ya que sus capacidades físicas no son las mismas. Algunos de estos ajustes son temporales y otros pueden durar toda la vida.

2.5. Técnicas y tecnologías de rehabilitación

La fisioterapia es un campo muy amplio de la medicina física. La asociación americana *American Board of Physical Therapy Specialties* (ABPTS) certifica ocho áreas de especialización en función de la orientación de las terapias de rehabilitación aplicadas por la fisioterapia: cardiovascular y pulmonar, electrofisiológica, geriátrica, neurológica, ortopédica, pediátrica, deportiva, y de salud en mujeres [43].

La rehabilitación neurológica es una parte muy importante en la recuperación de pacientes que han sufrido alguna lesión nerviosa. Las mejoras físicas más relevantes que se producen en pacientes con movilidad reducida se dan en la fase de rehabilitación [44]. Para lograr que estas mejoras sean máximas es necesario que las terapias rehabilitadoras se apliquen cuanto antes después de haber sufrido la lesión. Las terapias de rehabilitación han evolucionado a lo largo de la historia. En un principio los fisioterapeutas asistían físicamente a los pacientes y con el tiempo otras tecnologías y técnicas han ido añadiéndose a estas terapias.

2.5.1. Fisioterapia de rehabilitación neurológica

La fisioterapia de rehabilitación neurológica está enfocada a personas que han sufrido algún accidente o enfermedad neurológica, tales como el accidente cerebrovascular, el alzhéimer, la esclerosis múltiple, el Parkinson y la lesión de médula espinal. Los desórdenes asociados a disfunciones neurológicas incluyen problemas de visión, balance, marcha humana, realización de actividades cotidianas, fuerza muscular y pérdida de dependencia funcional. Esta especialidad se basa en la propiedad del cerebro humano conocida como plasticidad cerebral o neuroplasticidad.

2.5.2. Neuroplasticidad

Se ha demostrado, tanto en humanos [45] como en animales [46], que un gran número de experiencias pueden provocar cambios en la estructura cerebral en términos de interconexiones neuronales. Esta neuroplasticidad supone la base del aprendizaje y la memoria. La plasticidad cerebral juega un papel de gran relevancia durante la recuperación funcional en pacientes que han sufrido algún desorden neurológico. El cerebro es capaz de generar conexiones neuronales perdidas tras un accidente o incluso crear caminos neuronales nuevos que permitan a los pacientes recuperar las funciones perdidas. El método que usará el cerebro para lograr este objetivo varía en gran medida dependiendo de la lesión sufrida. En el caso de un paciente que haya perdido una extremidad, el cerebro generará nuevas conexiones corticales que le permitan realizar tareas cotidianas sirviéndose de otras partes del cuerpo. En el caso de un accidente cerebrovascular, el cerebro tratará de volver a generar los caminos neuronales que haya perdido y si no es capaz, creará nuevos.

La rehabilitación neurológica trata de sacar partido de esta propiedad cortical, utilizando diferentes técnicas que potencian la plasticidad cerebral. Se ha demostrado que es posible incrementar los efectos de la neuroplasticidad de tres formas distintas:

- *Realización de movimientos*: cualquier tipo de movimiento sobre la zona del cuerpo afectada por la lesión motriz incrementa la plasticidad cerebral. Esto favorece la recuperación del movimiento perdido. Los movimientos pueden ser realizados por un terapeuta, por un dispositivo de rehabilitación o por el propio paciente. Además, cuanto más involucrado se encuentre el paciente en su rehabilitación, mayor será la velocidad a la que se creen conexiones neuronales y menor será tiempo de recuperación [47].

- *Visualización de movimientos*: la observación de elementos móviles que puedan recordar a los movimientos que se desean recuperar activan las neuronas espejo de nuestro cerebro que tratan internamente de imitar lo que ven. Esto, de nuevo, favorece la regeneración de caminos neuronales [48]. Los movimientos observados pueden ser propios (con lo que se combinaría con

la realización de movimientos), de otra persona, o de elementos no humanos externos como puede ser un robot móvil o un avatar de un entorno de realidad virtual.

- *Imaginación de movimientos*: el mero hecho de imaginar un movimiento fomenta la reestructuración de las conexiones neuronales [49]. Este método está muy relacionado con el nivel de involucración del paciente. Si además de realizar y visualizar el movimiento, el paciente está lo suficientemente involucrado en su terapia como para concentrarse en la imaginación mental del movimiento, los efectos positivos de la rehabilitación serán mayores.

En este campo, la ciencia se centra en desarrollar técnicas y dispositivos que, añadidos a las terapias de rehabilitación, permitan estimular las propiedades plásticas del cerebro.

2.5.3. Dispositivos de rehabilitación

Existen multitud de dispositivos y técnicas orientadas a mejorar las terapias de rehabilitación. Puesto que se trata de una preocupación social en auge, cada día surgen nuevas investigaciones relevantes en este campo. Este apartado se centra en los sistemas de asistencia y rehabilitación y en las interfaces cerebro-máquina (BMI del inglés *Brain-Machine Interface*) por tratarse de los sistemas en los que se basa la presente Tesis Doctoral.

2.5.3.1. Sistemas de asistencia y rehabilitación

Los sistemas de asistencia son dispositivos y programas diseñados para realizar tareas cotidianas que una persona con movilidad reducida no es capaz de realizar por s sola, incluyendo desde pantallas táctiles que les permiten comunicarse [50] hasta dispositivos robóticos que realizen acciones físicas como acercarles objetos, desplazarlos de un sitio a otro, alimentarlos, etc [51].

Por otro lado, los sistemas orientados a la rehabilitación son dispositivos, generalmente robóticos, que facilitan los movimientos que un paciente debe realizar durante su terapia de rehabilitación. Dentro de estos sistemas cabe destacar, por

el gran impacto científico que están teniendo en los último años, los exoesqueletos. Se trata de robots vestibles (WR del inglés *Wearable Robots*) que se acoplan a las extremidades de una persona para asistir sus movimientos durante la rehabilitación [52]. Se dividen en exoesqueletos de miembro superior o inferior en función de si están orientados a la rehabilitación de brazos o de piernas.

2.5.3.2. Interfaces cerebro-máquina

Como se ha mencionado con anterioridad, para conseguir grandes mejoras en los resultados de la rehabilitación es necesario que el paciente se encuentre involucrado en su terapia. Las condiciones de movilidad reducida que experimentan los pacientes que deben someterse a estas terapias, pueden llevar a la frustración y al abandono de la misma si no se dispone de mecanismos que doten al paciente de autonomía. Como hemos descrito, las lesiones que sufren estos pacientes afectan principalmente al sistema nervioso bloqueando de esa forma los caminos biológicos de comunicación entre las órdenes del cerebro y los músculos del resto del cuerpo.

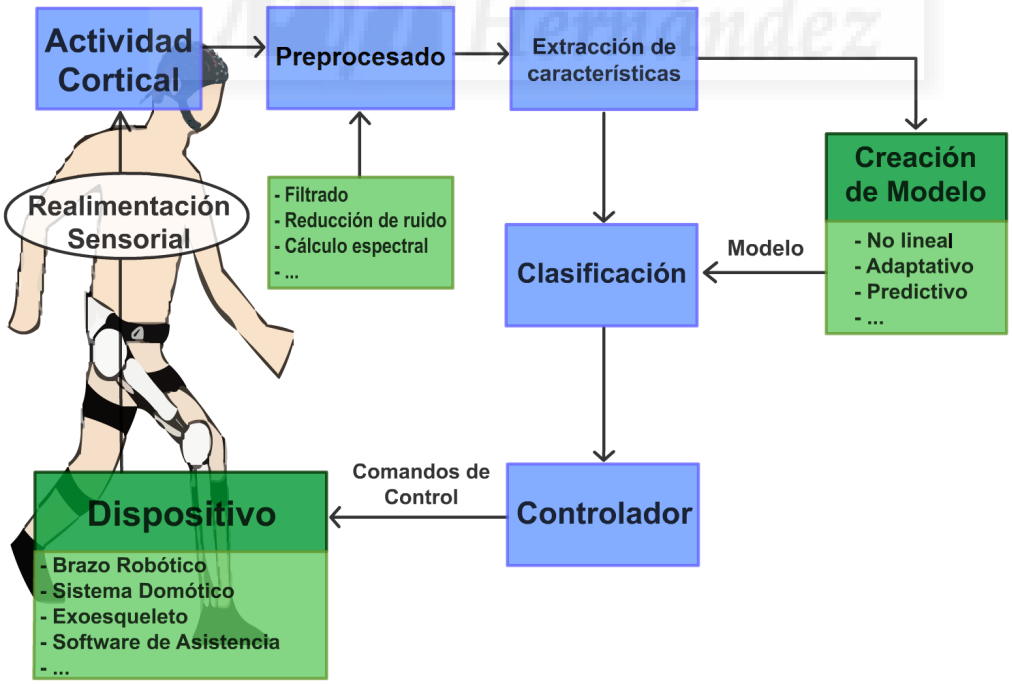

Figura 2.3: Esquema de funcionamiento de un sistema BCI.

Las interfaces cerebro-máquina o BMI son sistemas que proporcionan un ca-

mino de comunicación alternativo entre el cerebro humano y un dispositivo externo. La figura 2.3 muestra la arquitectura básica de un sistema BMI. Mediante el uso de diferentes tecnologías, es posible extraer señales procedentes de los impulsos eléctricos de cerebro humano. Estas señales responden a diferentes comportamientos corticales y, tras su estudio, es posible decodificar, en cierta medida, los estados cognitivos e intenciones de una persona. Para ello, es necesario someter las señales corticales a una etapa de procesamiento en la que se filtren y acentúen los fenómenos corticales bajo evaluación. Las señales filtradas pasan por un módulo de extracción de características donde se obtienen sus parámetros más representativos. Estos parámetros se comparan durante la etapa de clasificación con un modelo (establecido durante una fase previa de análisis), permitiendo la decodificación del estado mental e intenciones de una persona para su transformación en comandos de control. Finalmente, estos comandos son enviados a un dispositivo externo que está programado para realizar diferentes funciones de asistencia.

Estos sistemas permiten que una persona que sufre una discapacidad adquiera un cierto nivel de control sobre su entorno. En [53] y [54] se utilizan sistemas BMI para permitir a una persona controlar el movimiento de una silla de ruedas. Estos sistemas también se han empleado para el control de navegadores de internet y aplicaciones de comunicación [55, 56]. En [57] y [58] se ha evaluado las ventajas del uso de robots de asistencia controlados por sistemas BMI en pacientes que sufren tetraplejia. Aún con las limitaciones que estos sistemas presentan, su potencial en lo referente a las tecnologías asistivas ha sido ampliamente probado.

Además de los beneficios funcionales que proporciona esta tecnología, dotar de este nivel de autonomía a personas que habían visto reducidas sus capacidades físicas provoca sustanciales incrementos en su motivación. Por este motivo la comunidad científica ha propuesto el uso de sistemas BMI en las terapias de rehabilitación [49, 47, 59]. Mediante el uso de BMIs es posible informar a un sistema rehabilitador del estado mental e intenciones de un paciente para adaptar la terapia a sus necesidades específicas. Cuando el paciente se da cuenta de que el sistema responde favorablemente a sus intenciones y necesidades, incrementa

su nivel de involucración en la terapia y, por lo tanto, se favorece el fenómeno de plasticidad cerebral. En última instancia se mejoran los resultados finales de la rehabilitación en términos de velocidad de recuperación y de índice de mejora. En [48], se compara el uso o no de un BMI en combinación con un sistema de rehabilitación de miembro superior en personas que han sufrido un accidente cerebrovascular. Los resultados prueban que, para este tipo de pacientes, el uso del sistema BMI produce una mejora motora superior de la que se consigue sin él. Los mismos autores en [60] emplean este sistema para la rehabilitación de muñeca y mano obteniendo resultados similares. Actualmente, han comenzado a surgir estudios que combinan sistemas BMI con terapias de rehabilitación de miembro inferior [61] y marcha humana [62, 63]. Sin embargo, estos sistemas todavía se encuentran en unas fases muy preliminares debido a los problemas asociados a la adquisición de señales corticales durante el movimiento humano.

2.6. El cerebro humano

El cerebro es el órgano principal del sistema nervioso central. En él se procesan todos los datos biológicos de nuestro organismo y la información que recibimos del exterior. El cerebro utiliza toda esta información para generar los comandos de control convenientes en cada caso. Este puede dividirse en dos zonas con funciones concretas dentro del sistema nervioso como se muestra en la figura 2.4:

- *Zona subcortical*: esta zona está formada por una serie de elementos que yacen bajo el córtex cerebral y que se encargan principalmente de todas aquellas tareas relacionadas con el subconsciente. Entre ellas, la coordinación motora, el equilibrio, el control de la presión arterial y la respiración.

- *Zona cortical*: está formada principalmente por la corteza cerebral, se encarga de experimentar sensaciones y de relacionarlas con experiencias previas. Además también se encarga de la memoria y el pensamiento. Esta zona trabaja en asociación con el sistema nervioso periférico. Por ello es posible relacionar diferentes zonas de la corteza cerebral con funciones propias de partes del cuerpo concretas.

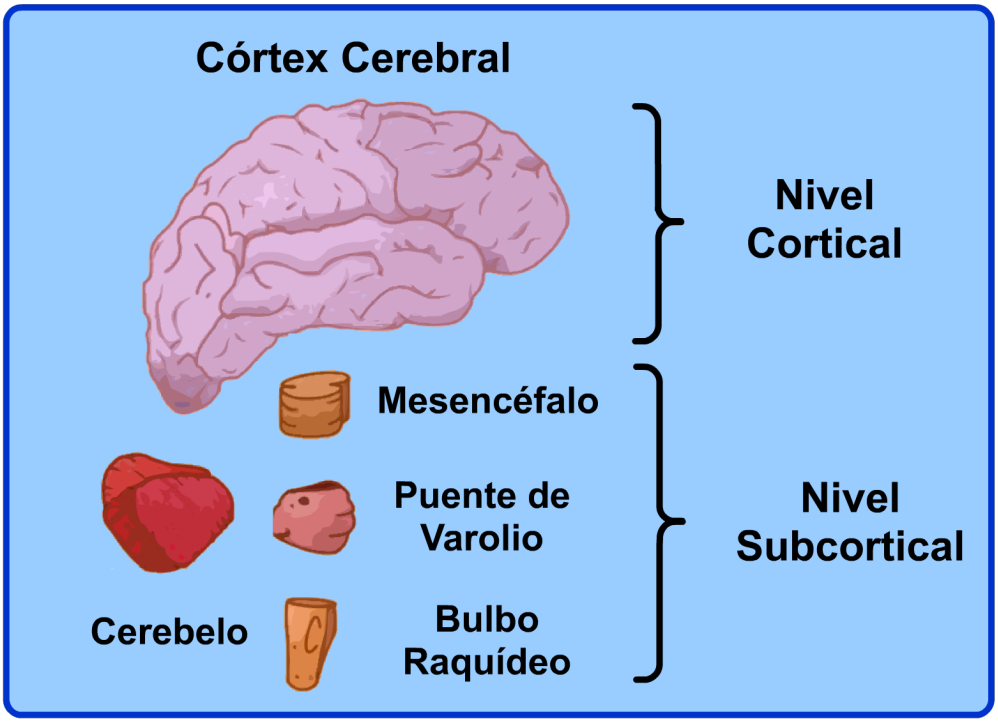

Figura 2.4: Niveles corticales del sistema nervioso.

En la figura 2.5a se muestran las partes en las que se puede dividir la corteza cerebral. Estas áreas se denominan lóbulos y tienen asociadas diferentes tareas de percepción y control.

- *Lóbulo frontal*: es el más grande de los lóbulos cerebrales, incluye las zonas corticales motoras y premotoras. Se encarga principalmente de procesar las funciones cognitivas de alto nivel como la planificación, coordinación y ejecución de movimientos. Además también se encarga de la articulación del lenguaje y la regulación de las emociones.

- *Lóbulo occipital*: es el más pequeño de los lóbulos principales del cerebro y se encuentra en la zona posterior. Aunque esta zona cortical no tiene la capacidad de crear imágenes coherentes, es la primera a la que llega la información visual haciéndola una parte muy importante en el reconocimiento de objetos.

- *Lóbulo parietal*: se encuentra entre los lóbulos frontal y occipital. Se encarga principalmente de procesar información sensorial, ya que contiene la zona somatosensorial. Por su cercanía con los lóbulos frontal y occipital, también

desarrolla funciones de control de movimientos y crea asociaciones entre información visual proveniente del lóbulo occipital y otras áreas corticales.

- *Lóbulos temporales*: son dos lóbulos, uno en cada hemisferio cerebral, situados en los laterales del córtex. Contienen el hipocampo y la corteza cerebral auditiva lo que hace que jueguen un papel importante en la memoria y el reconocimiento del lenguaje hablado.

La corteza motora juega un papel fundamental en la planificación y ejecución de movimiento y se encuentra principalmente en el lóbulo frontal (Figura 2.5b). Se puede dividir en tres zonas que se encargan de funciones diferentes:

- *Corteza motora primaria*: se encuentra en la parte posterior del lóbulo frontal. Trabaja conjuntamente con la zona premotora y con otras partes del cerebro. Las neuronas que la forman tienen largos axones que se conectan con las zonas de la médula espinal que controlan movimientos musculares periféricos. Además recibe información sensorial desde el cerebelo que usa para perfeccionar los movimientos.
- *Corteza premotora*: se encuentra en el lóbulo frontal inmediatamente antes de la zona motora primaria. Sus funciones son diversas y actualmente todavía no se conocen con certeza. Se cree que juega un importante papel en la planificación, preparación y guiado espacial de movimiento así como en la comprensión de acciones ajenas.
- *Área motora suplementaria*: se localiza frente de la corteza motora primaria y trabaja en conjunto con el área premotora. Sus funciones se asocian a control del movimiento en relación con la estabilización de postura y coordinación de ambos lados del cuerpo durante tareas que lo requieran.

El papel de la corteza motora en el movimiento hace de ella un área de gran relevancia para las investigaciones orientadas a la recuperación de función motora. Para investigar el comportamiento de esta zona, existen diferentes procedimientos que permiten extraer información de los impulsos eléctricos que se generan en las neuronas corticales.

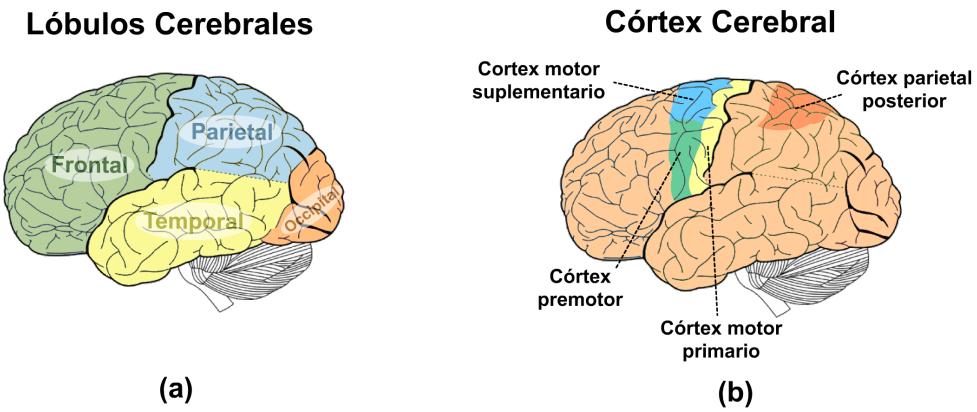

Figura 2.5: (A) Lóbulos en lo que está dividido el cerebro humano. (B) Principales áreas corticales según su función durantes los procesos motores.

2.7. Procedimientos de medida de la actividad cerebral

Todos los procesamientos que realiza el cerebro tienen su base en impulsos eléctricos que se transmiten entre neuronas. Estos impulsos son señales físicas susceptibles de ser registradas. Existen diferentes procedimientos para registrar estas señales que pueden dividirse en métodos invasivos y no invasivos. Dentro de estos dos grandes grupos, es posible encontrar diferentes procedimientos. La Tabla 2.1 muestra las ventajas e inconvenientes de los métodos de adquisición de señales corticales más conocidos.

Tabla 2.1: Métodos de medicin de la actividad cerebral: comparativa (ECoG: Electrocorticografía, EEG: Electroencefalografía, fMRI: Resonáncia Magnética Funcional, MEG: Magnetoencefalografía).

Sin Exoesqueleto			
U1	U2	U3	U4

2.7.1. Procedimientos invasivos

Estos métodos requieren de una intervención quirúrgica durante la cual se introducen sensores corticales en el interior del cráneo. Estas técnicas permiten obtener señales cerebrales con gran nitidez y resolución espacial debido a su cercanía a las fuentes de generación de potenciales cerebrales (tabla 2.1). En función de la localización de los electrodos implantados se diferencia entre electrocortico-

grafía (ECoG), en la que se colocan electrodos sobre el córtex cerebral que permiten el registro de señales de grupos de neuronas, y las técnicas intracorticales, en las que se introducen microelectrodos en el cerebro llegando a obtener impulsos eléctricos de neuronas individuales 2.6.

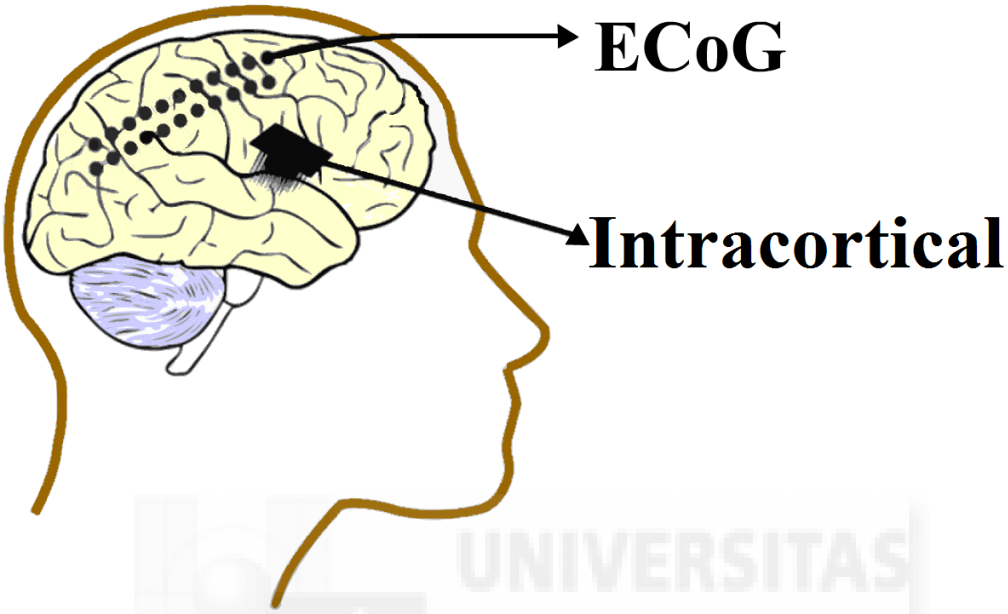

Figura 2.6: Sistemas invasivos de adquisición de señales corticales

En 1969, se publicó el primer trabajo en el que se registraban señales de neuronas individuales del córtex precentral de monos [64]. Tras varias sesiones en las que se premiaba con comida y estímulos visuales, los monos fueron capaces de controlar los niveles de actividad neuronal de la zona registrada. En 1980 se propuso el uso de estos sistemas como mecanismo de control de dispositivos externos, con todas las consecuencias positivas que podría tener para personas con movilidad reducida [65].

No fue hasta las década del 2000 cuando comenzó a haber un auge en este tipo de investigaciones que se centraban principalmente en la reconstrucción de movimientos a partir de señales extraídas de neuronas individuales [66, 67, 68]. En la actualidad se ha comenzado a realizar experimentaciones en humanos en los que se consigue que personas con tetraplejia sean capaces de controlar un cursor en la pantalla de un ordenador [69] o un brazo robótico en las tres dimensiones espaciales para realizar tareas de alcance y agarre [70, 71].

Aún con los avances mencionados, estos procedimientos son poco usados en

la actualidad por múltiples motivos. Los principales son las cuestiones éticas que plantea y el riesgo al que se expone a los usuarios intervenidos, no solo por la cirugía en sí, sino también por los problemas de rechazo que se pueden producir al introducir electrodos en el córtex. Las técnicas actuales requieren de una extracción de los electrodos pasadas unas semanas desde la intervención, ya que el cuerpo humano los identifica como una anomalía y genera tejido cicatrizante a su alrededor. Además, los procedimiento médicos que se realizan, dada su singularidad, suelen requerir grandes inversiones de dinero.

Electrocorticografía (ECoG)

Esta técnica de registro de señales corticales se basa en la localización de electrodos bajo el cráneo, justo sobre la superficie del córtex. Para ello es necesario separar temporalmente parte del cráneo del sujeto y dejar el cerebro al descubierto con los riesgos que ello conlleva.

El ECoG fue usado por primera vez en la década de 1950 por neurocirujanos del Instituto Neurológico de Montreal [72]. Se utilizó para identificar las zonas del cerebro que en las que se originasen ataques epilépticos y poder extirparlas durante una cirugía. Además también se aplicaban impulsos eléctricos a través de los electrodos implantados para identificar zonas sensorimotoras que no debían ser extraídas. Aunque actualmente se sigue considerando la técnica más efectiva para detectar zonas corticales epilépticas, también se ha usado con otros fines. En [73] se consiguió el control unidimensional de un cursor a partir de tareas de imaginación motora recogidas por un sistema ECoG. Este sistema fue mejorado en [74] añadiendo una segunda dimensión de control. Además, también se han desarrollado sistemas de inserción de texto [75] y predictores de movimientos de brazo [76].

Técnicas Intracorticales

Estas técnicas se basan en la medición de señales corticales a partir de electrodos insertados dentro del cerebro permitiendo obtener información de neuronas individuales. Por su nivel de invasión, estos métodos resultan más peligrosos que otras técnicas invasivas. El primer registro de actividad intracortical en monos se realizó en 1996 [77] y no fue hasta 2004 que se probó en humanos [78]. La infor-

mación cortical recogida con estas técnicas permite un control rápido con muy poco entrenamiento. Estos sistemas se han utilizado en para diseñar sistemas de control y escritura orientados a personas con tetraplejia [79, 80, 81].

2.7.2. Procedimientos no-invasivos

Existen multitud de sistemas no invasivos. Se trata de los más usados en la actualidad, ya que conllevan un menor coste económico y no plantean los dilemas éticos propios de los sistemas invasivos. En esta sección se definirán los tres métodos más utilizados en la actualidad: Imagen por resonancia magnética funcional (fMRI del inglés *functional Magnetic Resonance Imaging*), magnetoencefalografía (MEG) y electroencefalografía (EEG). Este último procedicimiento se describirá en mayor profundidad por tratarse del método utilizado en esta Tesis Doctoral para la adquisición de actividad cortical.

Imagen por resonancia magnética funcional (fMRI)

Esta técnica se basa en la relación que existe entre la actividad eléctrica cortical y el incremento de oxígeno en la sangre de las vías circulatorias encefálicas. Los vasos sanguíneos del área cerebral que experimenta un incremento de su actividad neuronal sufren una dilatación, lo que provoca una mayor llegada de oxígeno. Cuando las moléculas de sangre cargadas de oxígeno (oxihemoglobina) lo ceden al resto de células, provocan cambios en el campo magnético convirtiendo a estas moléculas en micro imanes [82]. Estas variaciones magnéticas son detectadas por el resonador magnético del sistema fMRI (ver figura 2.7).

Su principal ventaja es que permite obtener señales con alta resolución espacial en comparación con otras técnicas no invasivas. Sin embargo, su resolución temporal es más baja y existe un retardo importante entre las señales obtenidas y las señales eléctricas corticales reales, ya que la medición se realiza sobre el flujo sanguíneo (tabla 2.1). Este sistema se usa principalmente para localizar las zonas corticales asociadas a funciones cerebrales críticas en pacientes que requieren cirugía cerebral [83]. Aunque se usa principalmente para caracterización de respuestas cerebrales [84, 85, 86], existen estudios basados en esta tecnología orientados al control de dispositivos [87, 88], al entrenamiento en el control de actividad cortical por parte de un usuario [89, 90] y a la monitorización de movimientos

Figura 2.7: Dispositivo de resonancia magnética funcional.

[91, 92].

Magnetoencefalografía (MEG)

Este procedimiento se basa en la medición de los pequeños campos magnéticos producidos en las neuronas mediante el uso de un magnetómetro (figura 2.8). La comunicación entre neuronas se lleva a cabo a través de una transmisión sináptica de corriente entre ellas. De acuerdo con las ecuaciones de Maxwell, cualquier corriente eléctrica induce la aparición de un campo magnético. Sin embargo, los campos magnéticos inducidos por la actividad cortical son aproximadamente 10^7 veces más pequeños que el ruido magnético en ambientes urbanos. Para obtener mediciones válidas es necesario que el registro se haga bajo estrictas condiciones de aislamiento magnético y que se realice sobre las neuronas piramidales que conforman los centros de máxima activación cortical [93]. Esto último reduce la resolución espacial que el sistema puede ofrecer. Por otro lado, puesto que los campos magnéticos que se registran están directamente relacionados por las leyes de la inducción con la corriente eléctrica de las neuronas, este procedimiento presenta una buena resolución temporal [94] (tabla 2.1).

Figura 2.8: Magnetómetro para la adquisición de magnetoencefalografía.

El empleo de este método fue introducido por David Cohen en 1968 [95]. Este sistema se usa principalmente para medir con precisión la evolución temporal de la actividad cortical, ya que puede detectar eventos temporales con una precisión de 10 milisegundos. Mediante el uso de MEG es posible localizar áreas motoras, somatosensoriales y auditivas primarias [96, 97, 98]. Estudios más recientes han sido capaces de utilizar esta técnica para identificar respuestas corticales de pacientes con esquizofrenia [99] y respuestas psicológicas como dependencia emocional y comprensión del lenguaje [100]. Por estos motivos se plantea su uso como método de diagnosis de diferentes enfermedades como esclerosis múltiple, Alzheimer y síndrome de Sjögren [101].

Electroencefalografía (EEG)

La electroencefalografía es una técnica para adquirir señales eléctricas corticales a partir de electrodos situados en el cuero cabelludo. Estas señales tienen su origen en la corteza cerebral y se transmiten a través del cráneo y la piel gracias a las propiedades conductivas del cuerpo humano [102]. La principal ventaja de este sistema, además de su precio relativamente económico, es su gran resolución temporal ya que las señales registradas provienen de forma directa de los impulsos eléctricos de la capa superficial del cerebro. Por otra parte, los impulsos eléctricos que se generan en zonas concretas del córtex, al transmitirse, se mezclan con las contribuciones de áreas adyacentes provocando una disminución consi-

derable de la resolución espacial de la información registrada (tabla 2.1).

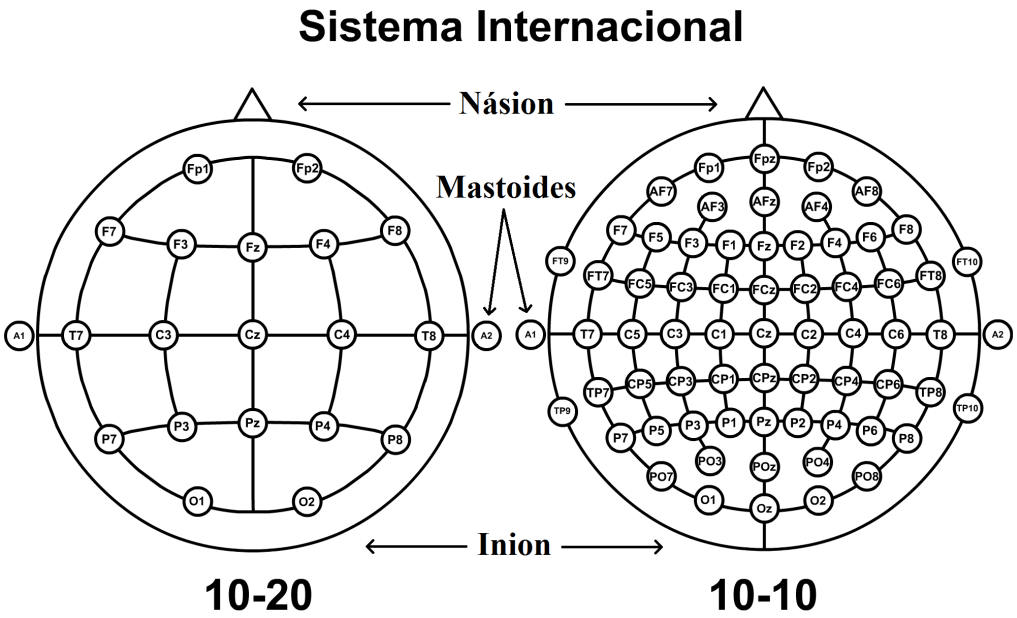

Figura 2.9: Sistemas 10-20 y 10-10 de posicionamiento de electrodos corticales en los sistemas de adquisición EEG.

Para registrar la actividad cerebral existen modelos estandarizados en los que se define la distribución y separación entre electrodos en función de la fisionomía craneal. El sistema internacional 10-20 y su modificación 10-10 (ver figura 2.9) son los modelos de distribución más conocidos internacionalmente. Este sistema se definió para asegurar la reproducibilidad experimental entre estudios realizados con diferentes sujetos. La localización de cada electrodo está directamente asociada con áreas concretas del córtex cerebral. Los valores 10-20 y 10-10 se refieren a los porcentajes de distancia entre electrodos adyacentes con respecto a las longitudes craneales inion-nasin y mastoide-mastoide, respectivamente. Habitualmente los sistemas de adquisición EEG emplean un gorro elástico en el que se encuentran distribuidos los electrodos para facilitar su correcta distribución en el cuero cabelludo. Las señales EEG registradas son del orden de las pocas decenas de microvoltios,7 por lo que se requiere de una fase de amplificación tras la adquisición. Además, para mejorar la relación señal a ruido durante el registro es necesario mejorar las propiedades conductivas entre los electrodos y la superficie de la cabeza. En este aspecto es posible diferenciar entre 2 tipos de electrodos:

- *Electrodos húmedos*: estos electrodos requieren de la aplicación de un gel conductivo, normalmente con base salina, situado entre el electrodo y el cuero

cabelludo. Este gel dieléctrico mejora las propiedades conductivas entre el cuero cabelludo y los electrodos haciendo al sistema más resistente a ruidos. Sin embargo, complica la instrumentación del sistema y, hace necesario lavar y secar los sensores tras cada sesión de registro.

- *Electrodos secos*: son electrodos acabados en varios salientes que permiten sortear el pelo y entrar en contacto directo con la piel del cráneo. Estos sistemas requieren de una fase de amplificación mayor que los basados en electrodos húmedos. Además, su robustez ante ruidos fisiológicos es menor. Su principal ventaja es que su instrumentación es mucho más rápida y no requiere la limpieza de los electrodos entre registros.

La información obtenida de las señales EEG se describe habitualmente en términos de ritmos corticales. Estos ritmos van asociados a diferentes rangos de frecuencias en los que vibran los diferentes potenciales cerebrales. El ancho de banda de las señales EEG está contenido aproximadamente en el rango de entre 1 y 100 Hz. En este aspecto es posible diferenciar entre cinco bandas frecuenciales: delta (<4 Hz), theta (4-7 Hz), alfa (8-15 Hz), beta (16-31 Hz) y gamma (>32 Hz) [103]. En función de los rangos de predominancia frecuencial de las señales que se registren, se diferencia entre multitud de fenómenos corticales asociados a distintas respuestas neurológicas.

2.8. Potenciales EEG

Los potenciales corticales adquiridos mediante señales EEG se pueden diferenciar en dos grandes grupos en función de sus orígenes y del control que tenga una persona sobre ellos: potenciales endógenos y exógenos.

2.8.1. Potenciales endógenos

Los potenciales corticales endógenos o espontáneos son aquellos cuya amplitud es susceptible de ser controlada a voluntad por una persona a través de la práctica. Por este motivo es común el desarrollo de sistemas BCI endógenos para

el control voluntario de dispositivos. Estos potenciales pueden dividirse a su vez en tres grandes grupos en función del tipo de acción o tarea que los provoque.

- *Ritmos sensoriomotores (SMR del inglés Sensorimotor Rhythms)*: se trata de potenciales que vibran en la banda alfa (8-15 Hz) y se registran principalmente en las zonas sensoriomotoras del córtex cerebral. Estos potenciales se manifiestan como una variación de potencia frequencial durante la ejecución de movimientos en las áreas corticales contrapuestas al mismo. Estos fenómenos se denominan sincronización (ERS del inglés *Event-Related Syncronization*) y desincronización (ERD del inglés *Event-Related Desyncronization*) (ver figura 2.10A) y se ha demostrado que la imaginación de tareas motoras también los provoca [104]. Mediante la práctica es posible adquirir un alto grado de control sobre estos ritmos y por ello se han empleado ampliamente para el diseño de sistemas de asistencia orientados a personas con discapacidades [105, 106, 107].

- *Potenciales corticales lentos (SCPs del inglés Slow Cortical Potentials)*: se trata de variaciones eléctricas negativas y positivas asociadas al incremento y decremento (respectivamente) de la actividad neuronal. Se producen en la banda delta (<4 Hz) y por lo tanto se caracterizan por su amplia extensión temporal, de entre 300 milisegundos y varios segundos (ver figura 2.10B). La aparición de este tipo de potenciales está asociada a la anticipación de una persona a un evento cercano en el tiempo, como por ejemplo, la preparación para iniciar un movimiento [108] o la intención de reaccionar ante un obstáculo [109]. Los sistemas BMI basados en estos potenciales suelen proporcionar eficiencias bajas de detección, dado que hay que esperar al menos la duración completa del potencial para poder detectarlo. Además, al estar relacionados con eventos que suceden puntualmente, el control de los falsos positivos en este tipo de sistemas es crucial para aplicaciones en tiempo real.

- *Tareas cognitivas*: existen multitud de tareas relacionadas con mecanismos cognitivos como la realización de operaciones matemáticas, la lectura o el nivel de atención que producen variaciones en los potenciales corticales a

diferentes frecuencias. Aunque se trata de un campo menos explorado, en la actualidad se están dando importancia a estos estudios por su utilidad como método para involucrar a pacientes en sus terapias de rehabilitación [110, 111, 112]. Se han encontrado evidencias de mecanismos cognitivos en multitud de rangos de frecuencia dependiendo en gran parte del proceso neurológico que se esté estudiando [113].

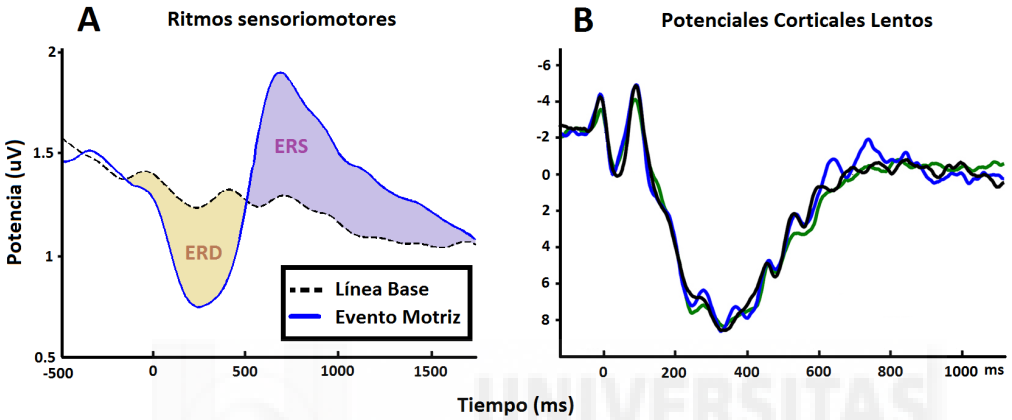

Figura 2.10: Formas de onda de los potenciales endógenos. Ritmos sensorimotores (A) y potenciales corticales lentos (B).

2.8.2. Potenciales exógenos

Los potenciales exógenos o evocados son cambios de la actividad cortical que aparecen como respuesta a un estímulo externo. Estos potenciales pueden aparecer en un amplio rango de frecuencias. La mayoría de sistemas BCI exógenos se utilizan para caracterizar la respuesta cerebral durante la diagnosis. Aun así, también existen BCI exógenos orientados a tareas de asistencia, como la implementación de teclados digitales. Existen multitud de estos potenciales en función del estímulo externos que los cause. A continuación se describirán los tipos de potenciales más comunes en investigaciones BMI:

- *Potenciales visuales (VEP del inglés Visual Evoked Potential)*: se trata de señales corticales que se registran principalmente en el córtex occipital (zona visual) en respuesta a estímulos luminosos (ver figura 2.11A) [114]. Un parpadeo luminoso a una frecuencia determinada genera un incremento de la potencia de las señales EEG del cortex visual en la misma banda de frecuencia.

Este fenómeno se conoce como potencial visual de estado estacionario (SSVEP del inglés *Steady-State Visual Evoked Potential*) y se ha empleado para el diseño de BMIs de toma de decisiones [115].

- *Potenciales auditivos (AEP del inglés Auditory Evoked Potentials)*: son cambios en la actividad cortical producidos en respuesta a un sonido externo (ver figura 2.11B). Dentro de estos potenciales cabe destacar el potencial auditivo de latencia media (AMLR del inglés *Auditory Middle Latency Response*) y el potencial auditivo de estado estacionario de 40 Hz (40Hz- ASSR del inglés *40 Hz-Auditory Steady-State Response*), principalmente usados para la evaluación de los efectos de la anestesia en humanos [116]. Los potenciales auditivos se emplean mayormente para la diagnosis de problemas auditivos y de otros trastornos como la demencia o el déficit de atención [117, 118].

- *Potenciales cognitivos*: existen multitud de potenciales relacionados con estados cognitivos que aparecen en respuesta al nivel de atención prestada a diferentes estímulos externos como pueden ser parpadeos de luz, sonidos u otros estímulos sensoriales. El potencial P300 es uno de los más estudiados de este campo. Se presenta como una deflexión positiva (P) unos 300 milisegundos (300) después de que se haya presentado el estímulo que lo dispara [119]. Existen otros muchos potenciales similares como el N70, el N150 o el P100. Un potencial que se usa para el estudio de los mecanismos de atención selectiva es el N2PC. Se manifiesta como una deflexión negativa 200 milisegundos después del estímulo [120]. Por último, otro potencial ampliamente estudiado es el denominado potencial de error (ErrP del inglés *Error-Related Potential*). Este potencial aparece como una deflexión positiva cuando se introduce un estímulo que rompe con la lógica de una sucesión de eventos sensoriales presentados a una persona en un orden considerado correcto [121].

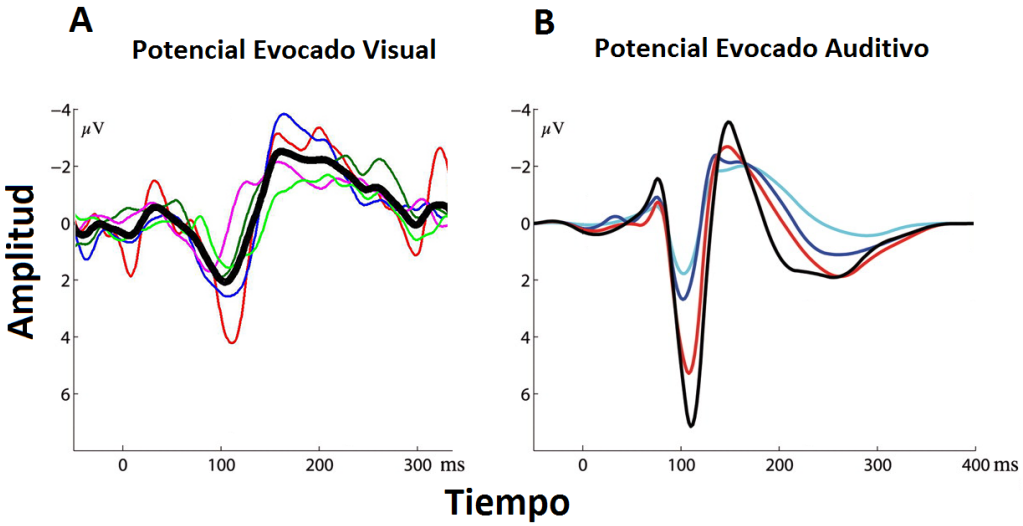

Figura 2.11: Formas de onda de los potenciales exógenos visuales (A) y auditivos (B).

2.9. Artefactos en sistemas BMI basados en EEG

En el ámbito del registro y análisis de señales, se denomina artefacto a cualquier señal que aparezca acoplada a la señal de interés que estamos evaluando y que no nos proporcione información útil en nuestro análisis. La identificación de artefactos es un punto clave en el análisis de señales EEG. Cualquier sistema BMI basado en señales EEG debe preveer las posibles condiciones adversas relacionadas con aparición de señales indeseadas para tratar de reducirlas o eliminarlas. De no hacerlo se corre el riesgo de obtener una caracterización no válida de los fenómenos EEG bajo evaluación.

2.9.1. Tipos de artefactos en los sistemas BMI basados en EEG

Para la identificación de artefactos es muy importante caracterizar todas las propiedades y condiciones de nuestro sistema. En el caso de los sistemas BMI basados en EEG hay que tener en cuenta tres factores de gran importancia. El primero es la conductividad del cuerpo, que además de reducir la resolución espacial de las señales EEG, hacen a estos sistemas susceptibles del acople de otras señales fisiológicas de origen no cortical. Por otro lado hay que tener en cuenta los dispositivos que se utilizan para el registro y para la realización de experimentos, que en ocasiones, resultan en fuentes de ruidos eléctricos y físicos. Y por último,

el entorno ajeno al experimento en el que se realicen las mediciones también juega un papel fundamental. Al ser las señales EEG del orden de microvoltios, los campos eléctricos y magnéticos o incluso las vibraciones cercanas pueden provocar deterioro en la calidad de las señales registradas. En función de estos tres factores se definen tres tipos de ruidos: de origen fisiológico, de entorno y de equipo experimental.

- *Artefactos fisiológicos*: son todas aquellas señales indeseadas que produce nuestro propio cuerpo. Algunas de ellas tienen un origen no eléctrico como la presión sanguínea o la tensión de la piel. Estas señales suelen tener una influencia baja y constante en las señales EEG, por lo que el uso de un sistema de tierra y referencia robusto es suficiente para eliminarlas. Por otro lado, existen muchas señales de origen eléctrico que se mezclan con las señales EEG de forma más errática y por lo tanto resultan más problemáticas. Los movimientos oculares y los parpadeos generan una diferencia de potencial entre la córnea y la membrana de Bruch. Cuando los movimientos oculares son bruscos, estas señales electrooculográficas (EOG) son muy susceptibles a acoplarse a las señales EEG dada la cercanía física entre el cuero cabelludo y los ojos [122, 123] (ver figura 2.12). Los impulsos eléctricos de activación muscular (EMG del inglés *Electromyiographic*) también suponen una fuente de ruidos en las señales EEG, sobre todo aquellos que se producen en la zona facial como gesticulaciones o presiones de mandíbula [124, 125] (ver figura 2.12). Por último, dada la propia definición de artefacto, puede suceder que una señal EEG inesperada, como potenciales evocados sensitivos, contamine los fenómenos EEG bajo evaluación. El campo de los artefactos fisiológicos es muy amplio y por ello existen muchas investigaciones orientadas a caracterizarlos y eliminarlos o reducir su influencia. Se han diseñado técnicas de regresión lineal [126] y de análisis de componentes independientes (ICA del inglés *Independent Component Analisys*) [127] para encontrar y eliminar artefactos EOG y EMG.

- *Artefactos de entorno*: son señales cuyo origen se encuentra en el entorno en el que se realiza la adquisición de datos EEG. Parpadeos luminosos o sonidos externos pueden provocar la aparición de potenciales corticales inde-

seados [128]. Sistemas ajenos al experimento pueden provocar la aparición de campos eléctricos y magnéticos que distorsionen las señales eléctricas registradas por el equipo EEG. Este tipo de artefactos son los más fácilmente evitables durante la fase de investigación, ya que basta con realizar los registros en un entorno controlado libre de señales externas.

- *Artefactos del equipo experimental*: se trata de señales cuyo origen es el equipo y los métodos usados para la adquisición de señales EEG. Estos artefactos suponen un reto mayor, ya que los elementos que los producen son necesarios para la obtención de las señales deseadas. El ejemplo más claro de este tipo de artefactos es la interferencia de la red eléctrica. La red eléctrica introduce una corriente con una alta potencia a 50/60 Hz (dependiendo de la región mundial). El método más común para lidiar con esta interferencia es el uso de un filtro Notch elimina banda, aunque también es posible usar un aislador eléctrico al que se conecten todos los dispositivos. Otros muchos factores pueden influir en la aparición de este tipo de artefactos y por lo general están asociados a las condiciones específicas del equipo que se esté usando, entre ellos, las pérdidas o contaminación de datos por el uso de equipos inalámbricos, cables en mal estado, fallos en el hardware de los equipos, etc.

2.9.2. Artefactos EEG durante el movimiento

En la historia de los sistemas BMI, la mayoría de estudios realizaba la adquisición de datos sobre usuarios inmóviles o bajo condiciones de movimiento muy reducidas. En los últimos años se ha comenzado a estudiar la evolución de las ondas corticales durante la marcha humana con el objetivo de comprender mejor los mecanismos cognitivos que se producen durante este proceso. Con estos conocimientos se pretende mejorar las terapias de rehabilitación de miembro inferior. Cuando se realizan registros EEG durante la marcha humana, existe un mayor riesgo de acople de señales EMG musculares, ya que el cuerpo se encuentra en un continuo movimiento [129]. Además aparecen otros artefactos a los cuales la literatura se refiere como artefactos de movimiento que, están directamente aso-

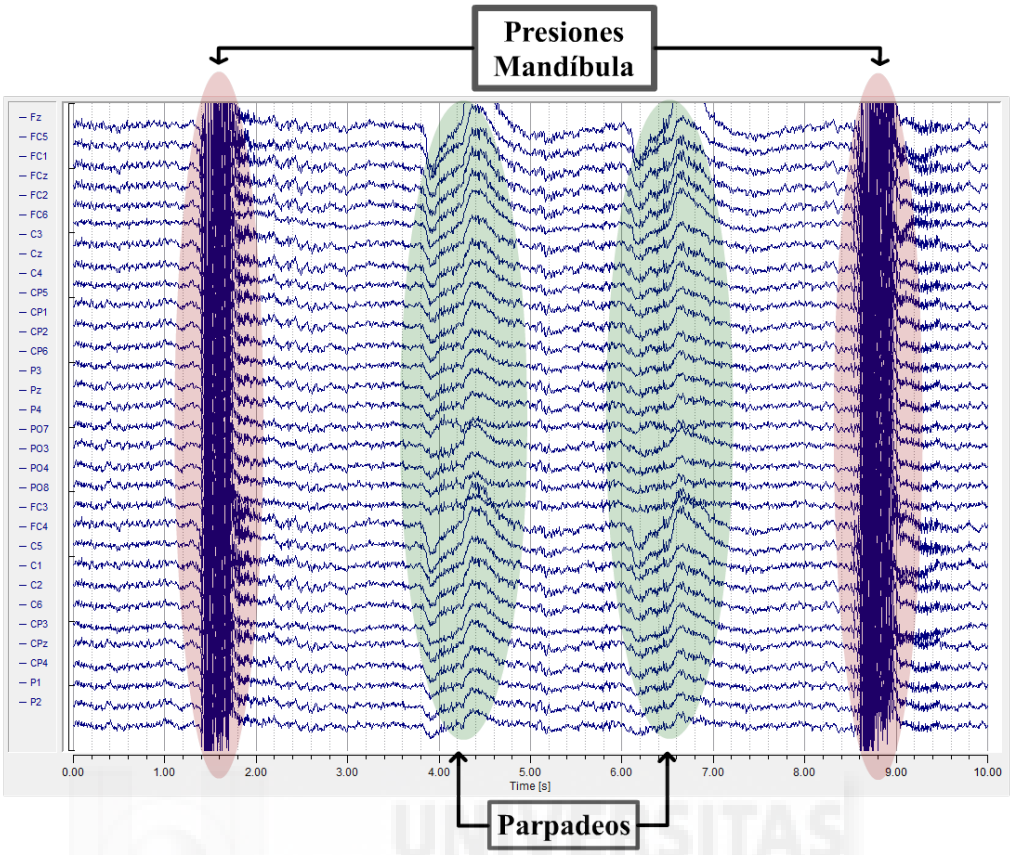

Figura 2.12: Artefactos electrooculares y musculares acoplados a las señales EEG registradas en 31 canales

ciados al movimiento al que se ve sometido el usuario y el equipo [130]. Estos artefactos tienen su origen en variaciones de conductividad, que se producen entre los electrodos y la cabeza por desplazamientos y asentamientos del gel dieléctrico usado en los sistemas BMI [131]. Se trata de un tipo de artefactos que afectan principalmente a los registros EEG durante movimientos complejos y que, hasta la fecha, han sido poco estudiados. En [132, 133], tras registrar señales EEG durante marcha humana, el 47.41 % de los datos tuvieron que ser eliminados por la afectación de artefactos de movimiento. En la presente Tesis Doctoral se evaluarán los artefactos producidos por cambios de conductividad durante la marcha humana con el objetivo de caracterizar sus efectos y evitar grandes pérdidas de datos durante los registros en movimiento [131].

UNIVERSITAS
Miguel
Hernández

Capítulo 3

RESUMEN DE LAS APORTACIONES

En este capítulo se describe de forma resumida cada una de las publicaciones en revista que conforman las investigaciones realizadas en el marco de la presente Tesis Doctoral. Además, también se describe una contribución a conferencia internacional en la que se publicó los primeros resultados de uno de los trabajos. Cada trabajo va acompañado de las figuras y tablas que se han considerado más relevantes para comprender los objetivos perseguidos y los resultados obtenidos. Todas las publicaciones pueden ser consultadas en los anexos B y C.

3.1. Sistema de control bidimensional basado en artefactos electromiográficos como sistema suplementario a un BMI

En este apartado se describen los primeros estudios que se realizaron sobre algunos de los artefactos que afectan a las señales EEG y cómo se emplearon para el diseño de un sistema de control bidimensinal. Esta parte de la Tesis Doctoral cuenta con la siguiente publicación en revista impactada [134]:

- *R1*: Á. Costa, E. Hortal, E. Iáñez, J. M. Azorín, *A Supplementary System for a Brain-Machine Interface Based on Jaw Artifacts for the Bidimensional Control of a Robotic Arm*, PLOS ONE, 9(11), Páginas: 1-13, 2014. Factor de Impacto (2014): 3.234. Posición 9/57 en el área de Multidisciplinary Sciences (Q1). DOI: 10.1371/journal.pone.0112352

3.1.1. Introducción

Este trabajo comienza como una primera toma de contacto con los artefactos más comunes en las señales EEG. Estos artefactos son los de origen EMG producidos en el área facial por gesticulaciones o movimientos mandibulares. Las presiones de mandíbula generan alteraciones en las ondas EEG registradas. Estas alteraciones son de gran amplitud en comparación a las señales EEG no contaminadas, lo que las hace fácilmente detectables. Se trata de señales muy fáciles de modular por un usuario, por lo que se decidió diseñar un sistema basado en ellas que permitiese a una persona controlar el movimiento bidimensional de un cursor en la pantalla y el movimiento bidimensional de un brazo robot para probar su utilidad en el campo de la asistencia.

3.1.2. Materiales y Métodos

Inicialmente se realizan registros de señales EEG ante diferentes tipos de presión mandibular. La figura 3.1 muestra el paradigma utilizado durante estos registros que consta de varias repeticiones en las que al usuario se le pide, de

forma pseudo-aleatoria, que realice diferentes tareas en periodos de 15 segundos. Las tareas consistén en leves presiones de la zona izquierda y derecha de la mandíbula. Este paradigma tiene como base uno similar utilizado en trabajos previos [135, 136].

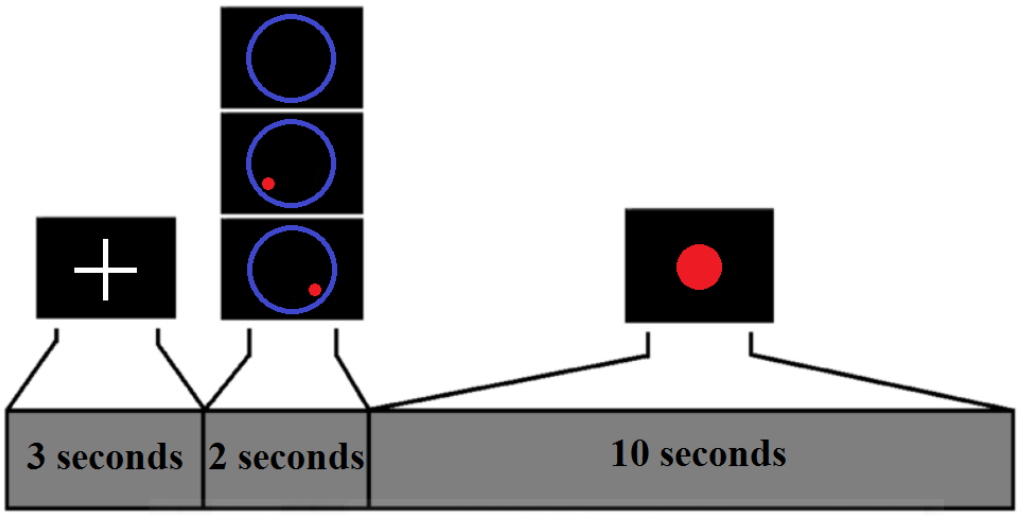

Figura 3.1: Esquema del paradigma utilizado durante la adquisición de señales EEG para gestionar la petición de tareas experimentales al sujeto.

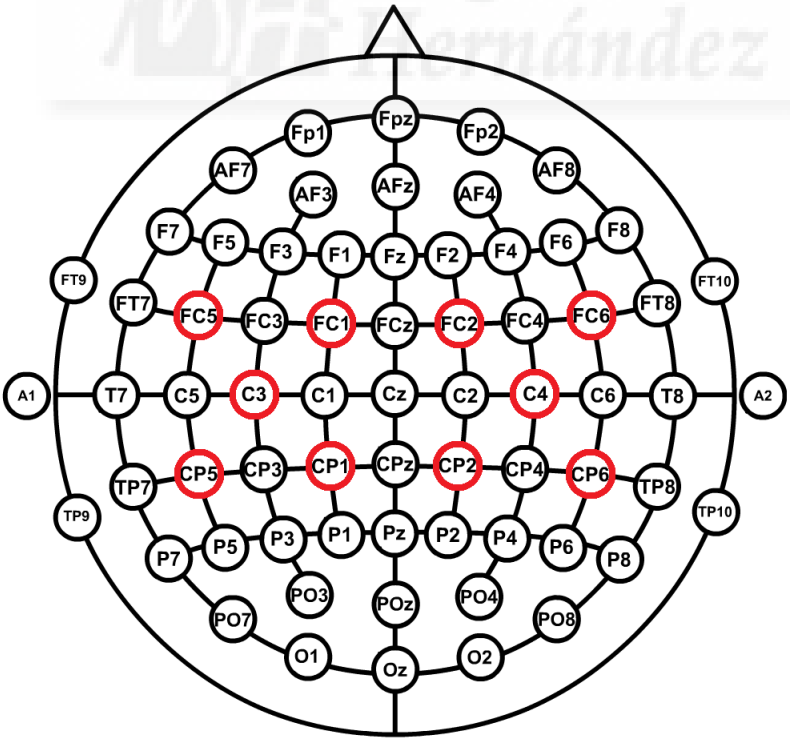

Figura 3.2: Configuración de electrodos utilizada. Se obtiene la información principal de los electrodos C3 y C4. Se utiliza la información cortical de los electrodos de alrededor para aplicar un filtrado espacial.

La adquisición se realizó con la distribución de 10 electrodos que se muestra en la figura 3.2 donde C3 y C4 se comparan para diferenciar presiones a derecha e izquierda. Los electrodos de alrededor se utilizan para aplicar un filtrado espacial y resaltar las componentes de interés de C3 y C4. Para la adquisición señales EEG en este experimento se utiliza el amplificador comercial de la compañía g.Tec (ver anexo A.1)

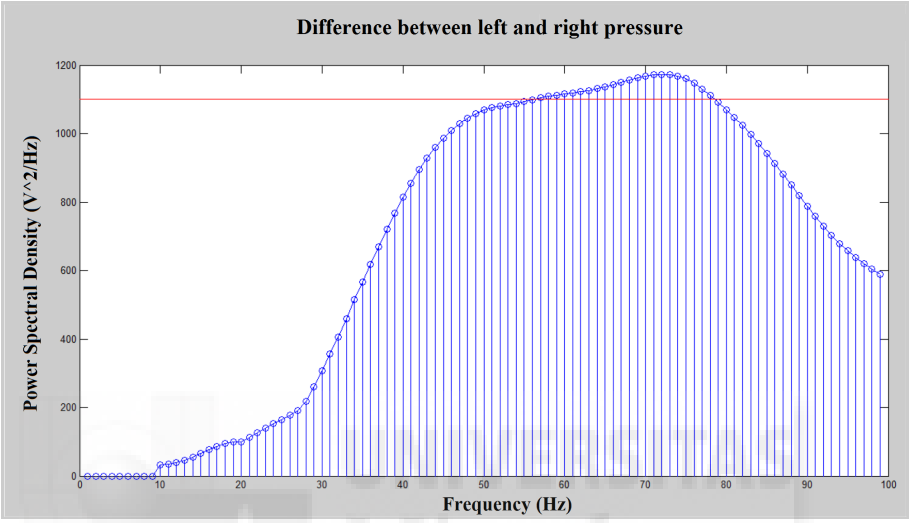

Figura 3.3: Estudios frecuencial de la diferencia de potencial entre los electrodos C3 y C4 ante presiones mandibulares a derecha e izquierda.

Se evaluá todo el ancho de banda de las señales mediante el método de máxima entropía de cálculo espectral (MEM del inglés *Máximum Enthropy Method*) [137]. La figura 3.3 muestra que el pico de máxima diferenciación entre presión a derecha e izquierda se produce alrededor de 75 Hz. El análisis de este rango de frecuencias permite la diferenciación de 5 tareas diferentes relacionadas con movimientos mandibulares (ver figura 3.4):

- Presión derecha fuerte ($Hard\_R$).
- Presión derecha suave ($Soft\_R$).
- Relax (Relax)
- Presión izquierda suave ($Soft\_L$).
- Presión izquierda fuerte ($Hard\_L$).

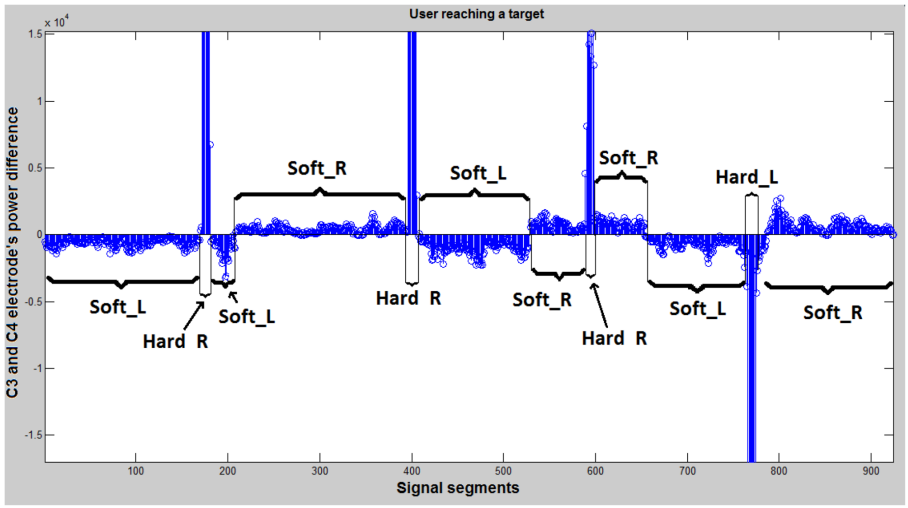

Figura 3.4: Diferencia de potencia entre C3 y C4 ante las diferentes tareas mandibulares pedidas al usuario durante los experimentos.

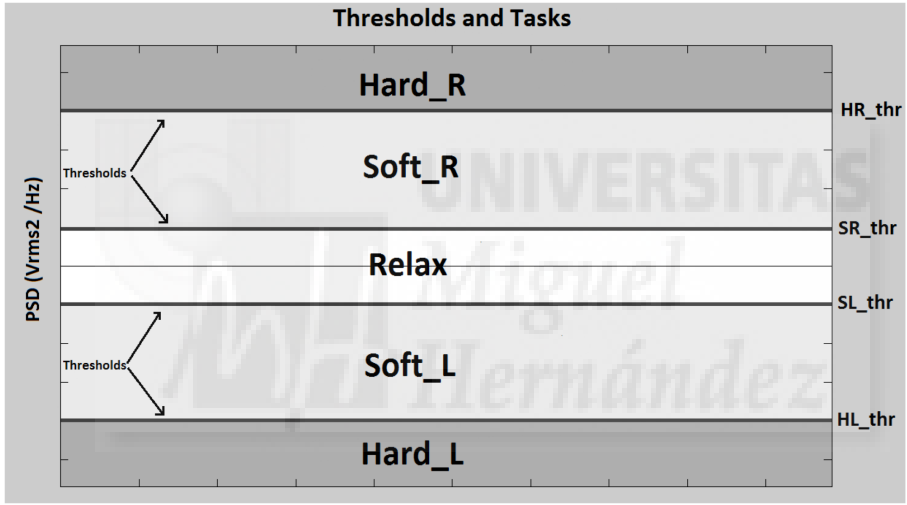

Figura 3.5: División de tareas clasificables en función de los cuatro umbrales definidos.

Además, es posible clasificarlas mediante el uso de los cuatro umbrales definidos en la figura 3.5 (HR_thr, SR_thr, SL_thr y HL_thr). Tras ser capaces de diferenciar entre 5 tareas se diseñan dos sistemas de control bidimensional basados en su clasificación.

3.1.3. Sistema de control de cursor

Este sistema permite controlar el movimiento de un cursor por la pantalla del ordenador. Las presiones suaves a derecha e izquierda controlan los movimientos en ambos sentidos de un eje y las presiones fuertes se utilizan para conmutar

entre los ejes X e Y. La figura 3.6 muestra la máquina de estados de control de este sistema y la figura 3.7 muestra la interfaz de movimiento del cursor. Este sistema fue validado por 4 usuarios que realizaron 8 repeticiones de un experimento en las que debían alcanzar 10 objetivos mediante el cursor. La tabla 3.1 muestra el porcentaje de objetivos alcanzados por cada usuario en cada repetición. En la tabla 3.2 se representa un coeficiente que indica el porcentaje de tiempo necesario para alcanzar cada objetivo en relación al tiempo mínimo necesario para alcanzarlo con el sistema diseñado.

Tabla 3.1: Número de objetivos alcanzados por cada usuario en cada una de las repeticiones del experimento.

	Run 1	Run 2	Run 3	Run 4	Run 5	Run 6	Run 7	Run 8
Usuario 1	30	70	90	90	100	90	100	90
Usuario 2	100	100	100	100	100	100	100	100
Usuario 3	40	80	90	90	100	100	80	100
Usuario 4	80	80	100	100	90	90	100	100

Tabla 3.2: Coeficientes que indican el porcentaje de tiempo necesario para alcanzar cada objetivo con el cursor en relación al tiempo mínimo necesario para alcanzarlo con el sistema diseñado.

		Run 1	Run 2	Run 3	Run 4	Run 5	Run 6	Run 7	Run 8	Avg
Usuarios	1	0.636	0.688	0.815	0.790	0.784	0.824	0.733	0.801	0.759
	2	0.868	0.915	0.891	0.927	0.856	0.802	0.900	0.914	0.884
	3	0.657	0.768	0.812	0.740	0.739	0.791	0.825	0.784	0.765
	4	0.834	0.742	0.838	0.814	0.727	0.801	0.767	0.820	0.793
	Media	0.749	0.778	0.839	0.818	0.777	0.804	0.806	0.830	**0.800**

3.1.4. Sistema de control de un brazo robótico

Este sistema está basado en el control bidimensional del brazo robótico Fanuc LR Mate 200iB (ver anexo A.2). Para ello es necesario implementar un sistema de comunicación entre los algoritmos EEG de toma de decisiones y el controlador del brazo robótico utilizado. La figura 3.8 muestra la máquina de estados de control del brazo robótico a partir de las tareas detectadas por el sistema.

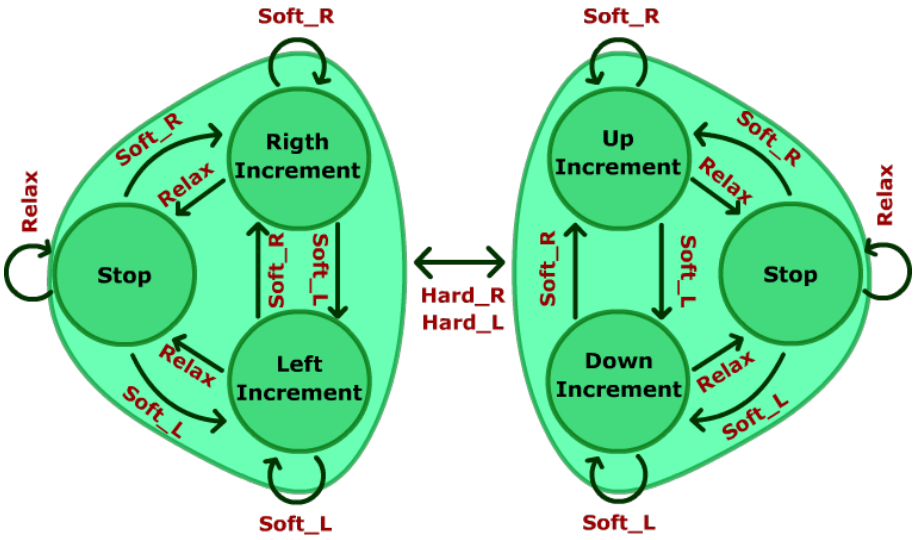

Figura 3.6: Máquina de estados de control del cursor a partir de las tareas de presión de mandíbula.

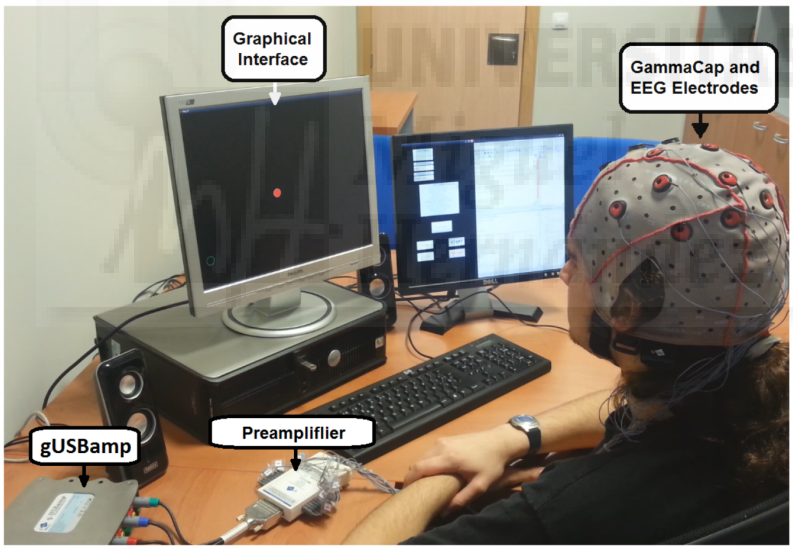

Figura 3.7: Usuario realizando un experimento con la interfaz gráfica para el control del cursor.

Este sistema es validado por los mismos 4 usuarios que el sistema de control del cursor. En este caso se pide que alcanzasen 8 objetivos localizados en el espacio de trabajo (ver figura 3.9) y se calcula el ratio de tiempo necesitado para alcanzar cada uno de ellos (ver tabla 3.2)

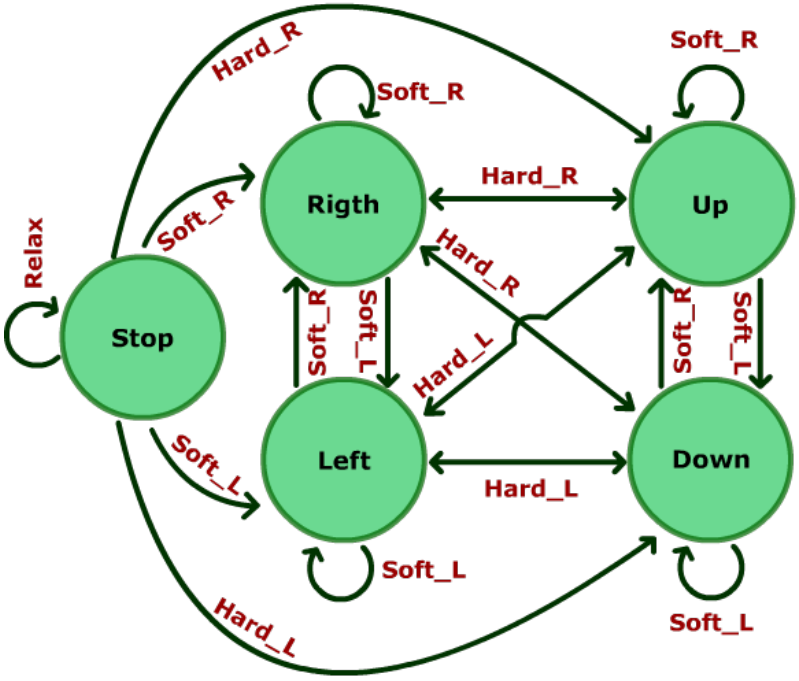

Figura 3.8: Máquina de estados de control del brazo robótico a partir de las tareas de presión de mandíbula.

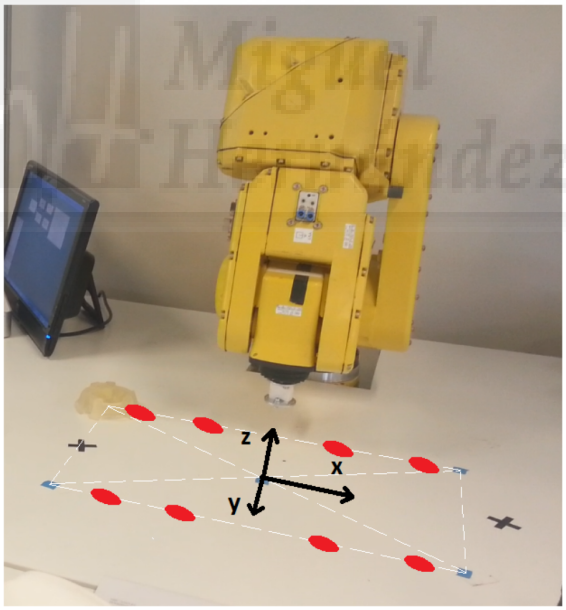

Figura 3.9: Espacio de trabajo del brazo robótico y localización de objetivos.

3.1.5. Resultados

En el primer sistema se puede observar un rápido incremento del control por parte de los usuarios durante las primeras 3 repeticiones (Tabla 3.1). Tras estas repeticiones, en la mayoría de casos, se alcanzan sin problemas todos los objeti-

vos en tiempos muy cercanos al óptimo (Tabla 3.2). En el segundo sistema, dado que los usuarios contaban con la experiencia adquirida en el primero, consiguen alcanzar todos los objetivos en porcentajes de tiempo similares al caso anterior (Tabla 3.3).

Tabla 3.3: Coeficientes que indican el porcentaje de tiempo necesario para alcanzar cada objetivo con el brazo robótico en relación al tiempo mínimo necesario para alcanzarlo con el sistema diseñado.

		Run 1	Run 2	Run 3	Run 4	Run 5	Run 6	Run 7	Run 8	Avg
Users	1	0.856	0.768	0.931	0.894	0.680	0.904	0.833	0.816	0.835
	2	0.904	0.955	0.707	0.669	0.904	0.899	0.855	0.859	0.844
	3	0.879	0.990	0.837	0.946	0.837	0.938	0.821	0.911	0.895
	4	0.994	0.837	0.890	0.755	0.788	0.764	0.988	0.622	0.830
	Avg	0.908	0.890	0.841	0.816	0.802	0.876	0.874	0.802	**0.851**

A parte de estos resultados, se realizá una comparativa en términos de velocidad entre el sistema diseñado y otros sistemas desarrollados por nuestro grupo de investigación: un sistema de control electrooculográfico (EOG) [138] y un sistema BCI jerárquico basado en la detección de tareas mentales [105], ambos orientados al control bidimensional. La comparación muestra que el sistema desarrollado en este trabajo es 1.4 veces más rápido que el sistema de control EOG y 24.78 veces más rápido que el BMI de tareas mentales.

3.1.6. Conclusiones

Los sistemas diseñados son aportaciones novedosas de la tesis, teniendo un gran potencial como tecnologías asistenciales orientadas a facilitar las condiciones de vida de personas que sufren problemas motores.

Las interfaces desarroladas se plantean como sistema suplementario a un BMI, ya que emplean el mismo set de electrodos. La figura 3.10 muestra como el sistema desarrollado durante este trabajo interactuaría con un sistema BMI. El sistema BMI se encargaría de funciones no relacionadas con el control como la monitorización de parámetros cognitivos del usuario y mediante una presión de mandíbula se cambiaría el control al sistema suplementario propuesto. Este sistema suple-

mentario estaría orientado a tareas de control como seleccionar mediante una interfaz otros modos de funcionamiento del BMI. Para devolver el control al sistema BMI bastaría con relajar la mandíbula durante unos segundos.

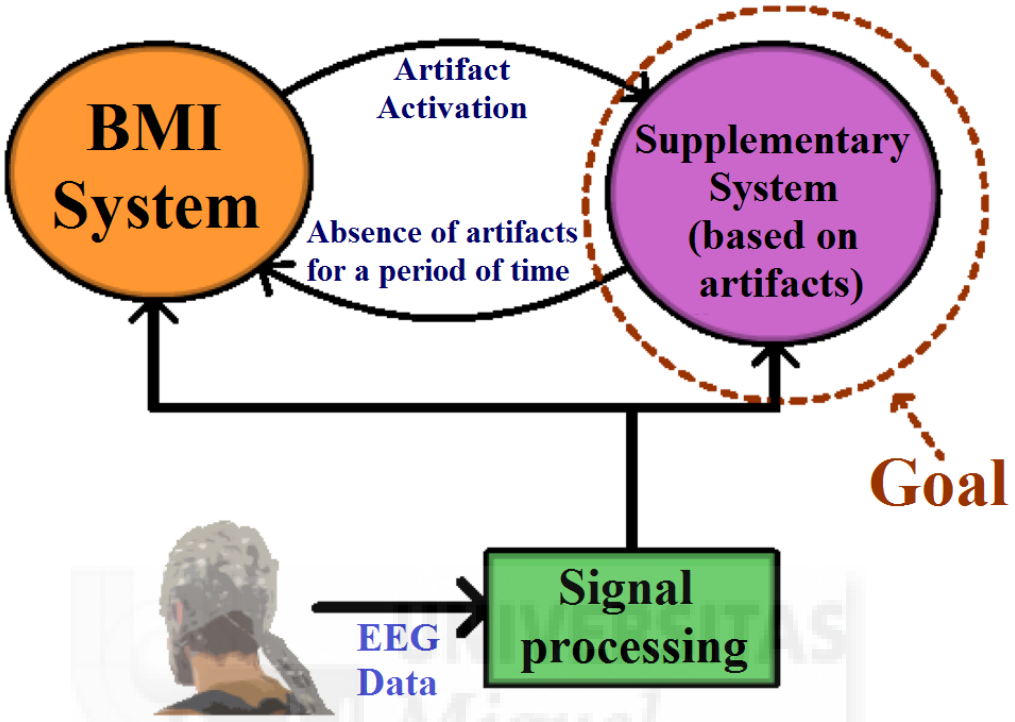

Figura 3.10: Esquema de la iteractuación entre el sistema suplementario desarrollado en este trabajo y un sistema BMI.

UNIVERSITAS
Miguel
Hernández

3.2. Análisis de artefactos de movimiento en las señales EEG durante la marcha humana

En este trabajo se comparan señales EEG de experimentos realizados durante la marcha humana con otros realizados sin movimiento. Esta parte de la Tesis Doctoral cuenta con una publicación en revista impactada [131]:

- *R2*: Á. Costa, E. Iáñez, R. Salazar-Varas, A. Úbeda, J. M. Azorín, *Characterization of Artifacts Produced by Gel Displacement on Non-invasive Brain-Machine Interfaces during Ambulation*, Frontiers in Neuroscience, 10, Páginas: 1-14, 2016. Factor de Impacto (2014): 3.656. Posición 82/252 en el área de Neuroscience (Q2). DOI: 10.3389/fnins.2016.00060

3.2.1. Introducción

Con los conocimientos adquiridos en el trabajo anterior sobre artefactos en señales EEG se comienzan una serie de investigaciones que requieren de mediciones EEG durante el movimiento. Esto genera la aparición de nuevos tipos de artefactos que, hasta la fecha, han sido poco estudiados y que se pretende abordar durante este trabajo.

3.2.2. Participantes y experimento

Se parte de registros de cuatro experimentos distintos. El primero se trata de un experimento de imaginación de tareas motoras realizado por usuarios que permanecen sentados en una silla sin realizar movimientos durante las pruebas. Este experimento forma parte de diferentes trabajos previos [135]. En los otros tres experimentos se registran señales corticales durante la marcha humana. En las figuras 3.11A y 3.11B se pueden observar los entornos experimentales de cada tipo de registro. Además, en la tabla 3.4 se muestran las especificaciones de cada uno de los experimentos realizados.

Tabla 3.4: Número de participantes, runs, duración y condiciones de cada set de datos.

Set de Datos	Participantes	Edad (media±STD)	N^o Runs Total	Duración Run (min)	Condición
1	3	26.6±4.0	24	5	Movimiento
2	10	26.6±3.9	160	4	Movimiento
3	3	25.6±2.8	48	3	Movimiento
4	12	27.3±4.6	144	4	No Movimiento

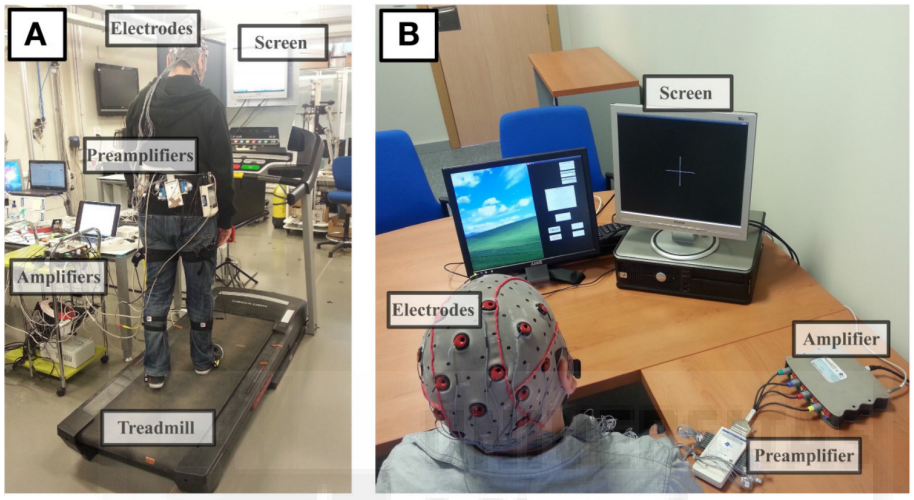

Figura 3.11: Entornos en los que se desarrollaron los registros utilizados en este trabajo. (A) Entorno de registros realizados durante la marcha.(B) Entorno de registros realizados sin movimiento.

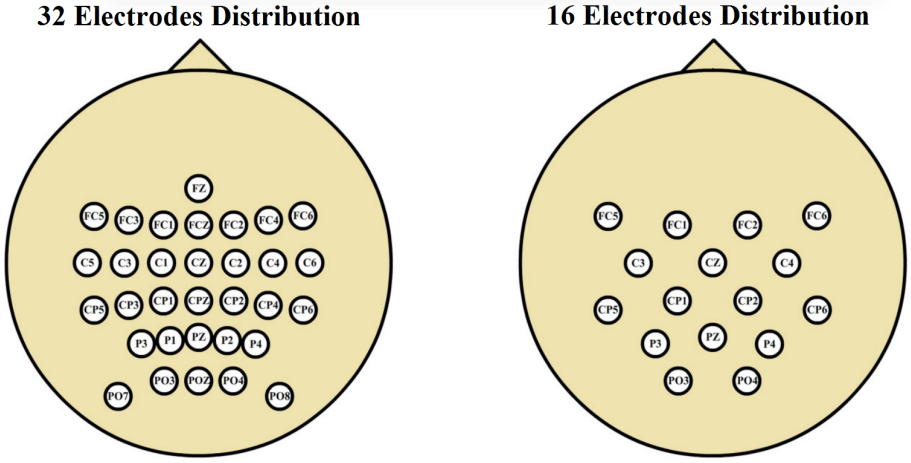

Figura 3.12: Configuraciones de electrodos para los experimentos durante la marcha (32 electrodos) y para los experimentos sin movimiento (16 electrodos).

Todos los experimentos se realizan con el el equipo de adquisición cortical de la compañia g.Tec (ver anexo A.1). La distribución de electrodos utilizada en ambos experimentos cubre las áreas motoras y premotoras. Como se puede ver en la

figura 3.12, para los experimentos realizados durante la marcha, se utilizaba una distribución espacial de electrodos mayor (32 electrodos) que para el experimento de tareas motoras (16 electrodos).

3.2.3. Identificación de ruidos

Tras un primer análisis de todos los registros se identifican dos tipos de artefactos de alta amplitud relacionados con fallos de conductividad entre los electrodos y el cuero cabelludo. Estos artefactos se manifiestan como amplitudes por encima del rango tipico de los potenciales EEG durante repeticiones completas de algún experimento (primer tipo de ruido denominado HA_noise) y como cambios repentinos de la amplitud en puntos intermedios de una repetición (segundo tipo de ruido denominado SA_noise) (ver figura 3.13).

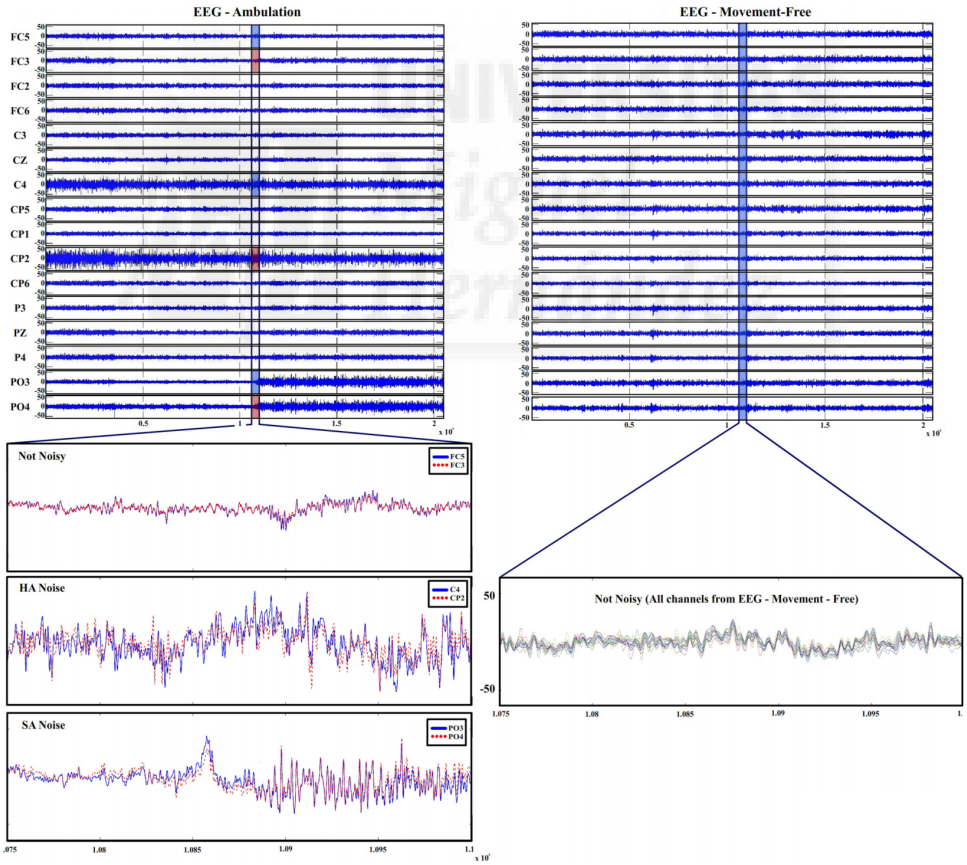

Figura 3.13: Tipos de ruidos identificados tras la inspección de las señales evaluadas.

Se diseña un algoritmo de identificación y clasificación de estos artefactos a partir de la desviación estándar de cada electrodo. En la figura 3.14 se muestra

las áreas afectadas en cada experimento por el ruido. Por otro lado, en la figura 3.15 se representan los niveles de afectación de cada tipo de ruido para los experimentos realizados durante la marcha humana, remarcando el nivel de afectación con respecto al total de datos analizados y las áreas en las que se producen más ruidos.

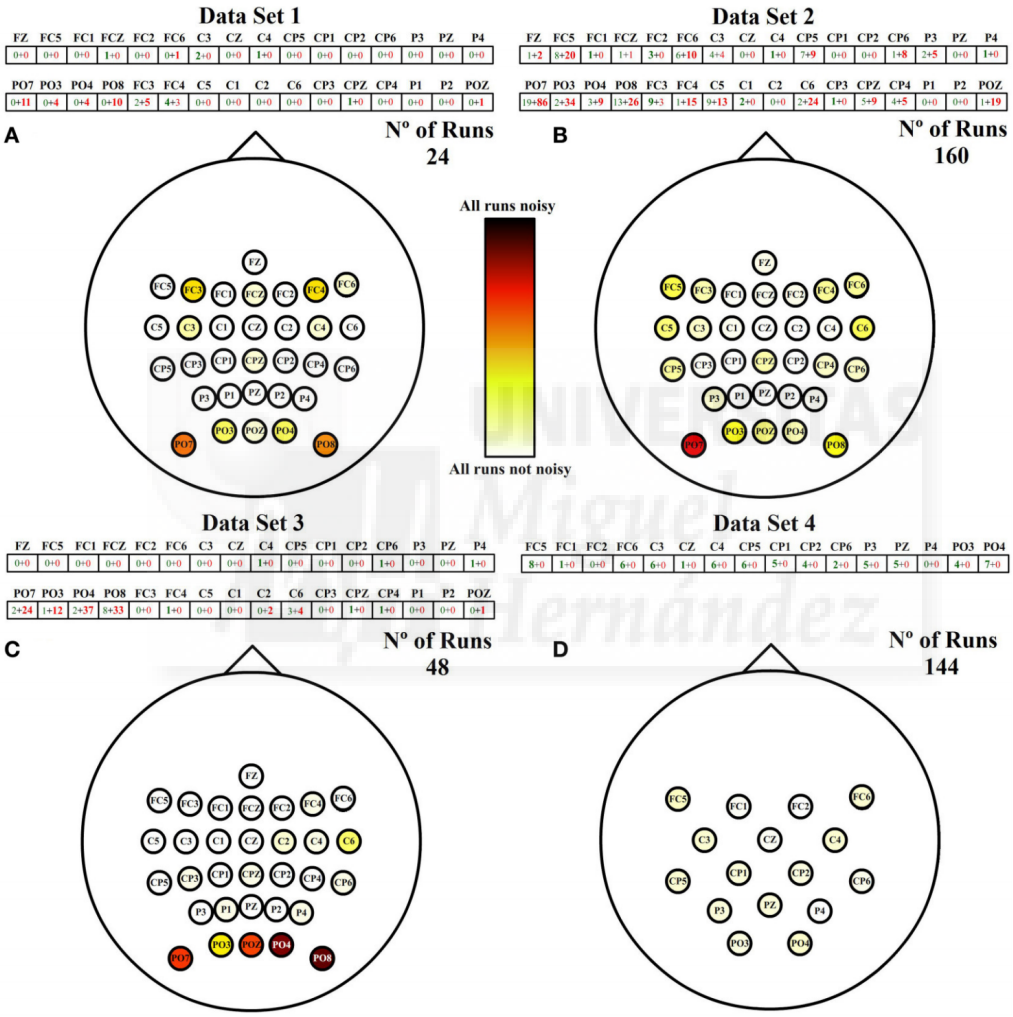

Figura 3.14: Áreas afectadas por los fallos de conductividad en cada uno de los experimentos realizados.

Estos resultados se resumen en la tabla 3.5, donde se muestra para cada experimento, la cantidad de ruidos de cada tipo y los porcentajes en los que afectan a las señales EEG.

Tabla 3.5: Número de cada tipo de ruido encontrado, porcentajes con respecto al número total de ruidos y con respecto al número total de datos para cada uno de los sets evaluados.

	Movimiento				No Movimiento
	DS 1	DS 2	DS 3	**Media**	DS 4
HA-N (n° canales)	11	107	22	-	66
SA-N (n° canales)	39	302	113	-	0
Total-N (n° canales)	50	409	135	-	66
Total-R (n° canales)	768	5120	1536	-	2304
HA-N vs Total-N (%)	22.00	26.16	16.30	**21.49**	100.00
SA-N vs Total-N (%)	78.00	73.84	83.70	**78.51**	0.00
HA-N vs Total-R (%)	1.43	2.09	1.43	**1.65**	2.86
SA-N vs Total-R (%)	5.08	5.90	7.36	**6.11**	0.00
Total-N vs Total-R (%)	6.51	7.99	8.79	**7.76**	2.86

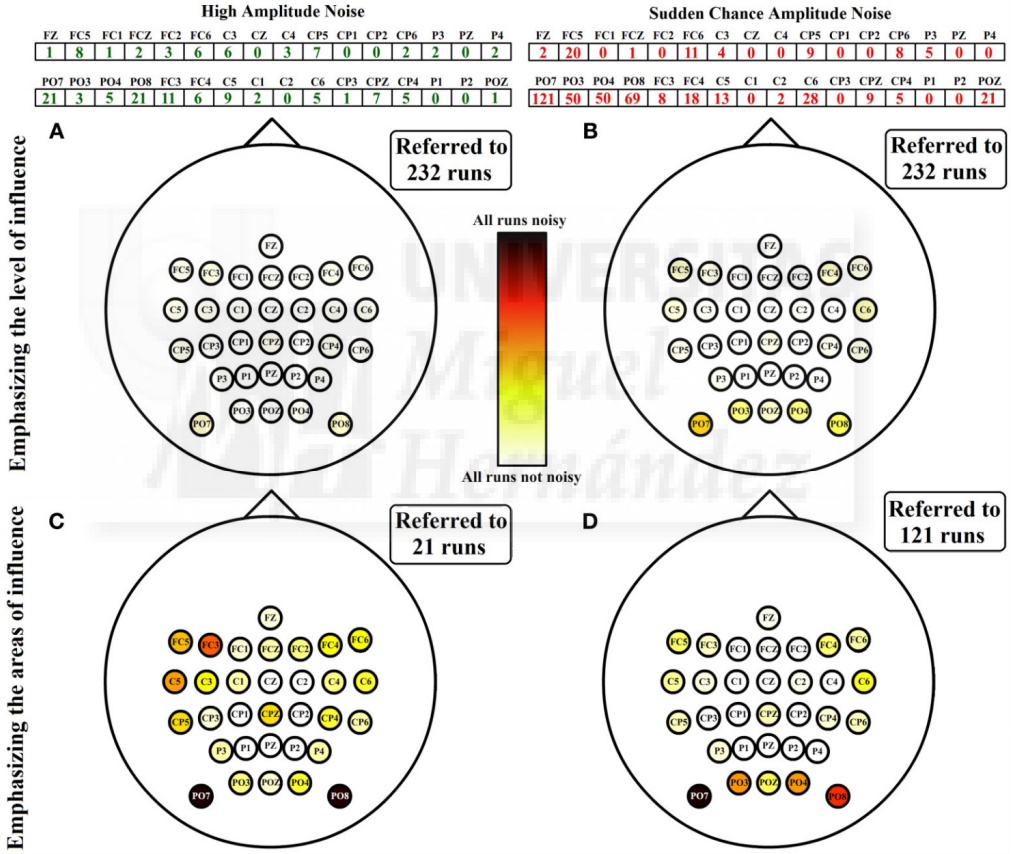

Figura 3.15: Nivel de afectación de cada tipo ruido en los experimentos realizados durante la marcha humana.

3.2.4. Caracterización temporal de ruidos

Además, se analizan los máximos de la señal segmentada (SMA del inglés *Segment Maximum Average*) para varias repeticiones consecutivas de los cuatro experimentos. Se trata de un parámetro desarrollado durante este trabajo que se

calcula de acuerdo al algoritmo de la figura 3.16 y que proporciona una aproximación de la amplitud máxima media de la señal durante un periodo de tiempo concreto. En la figura 3.17 se muestra la evolución de este parámetro para cada experimento.

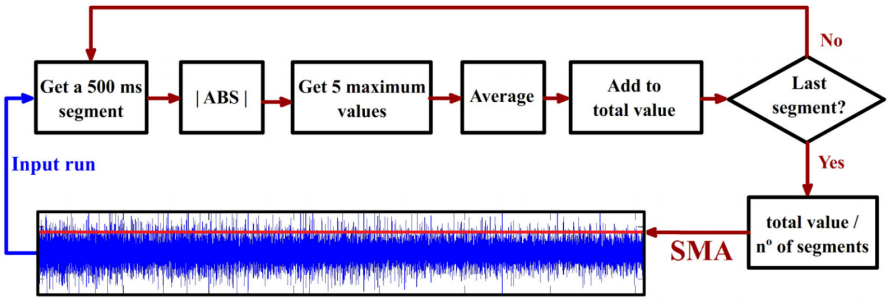

Figura 3.16: Procedimiento para el cálculo del Segment Maximun Average (SMA).

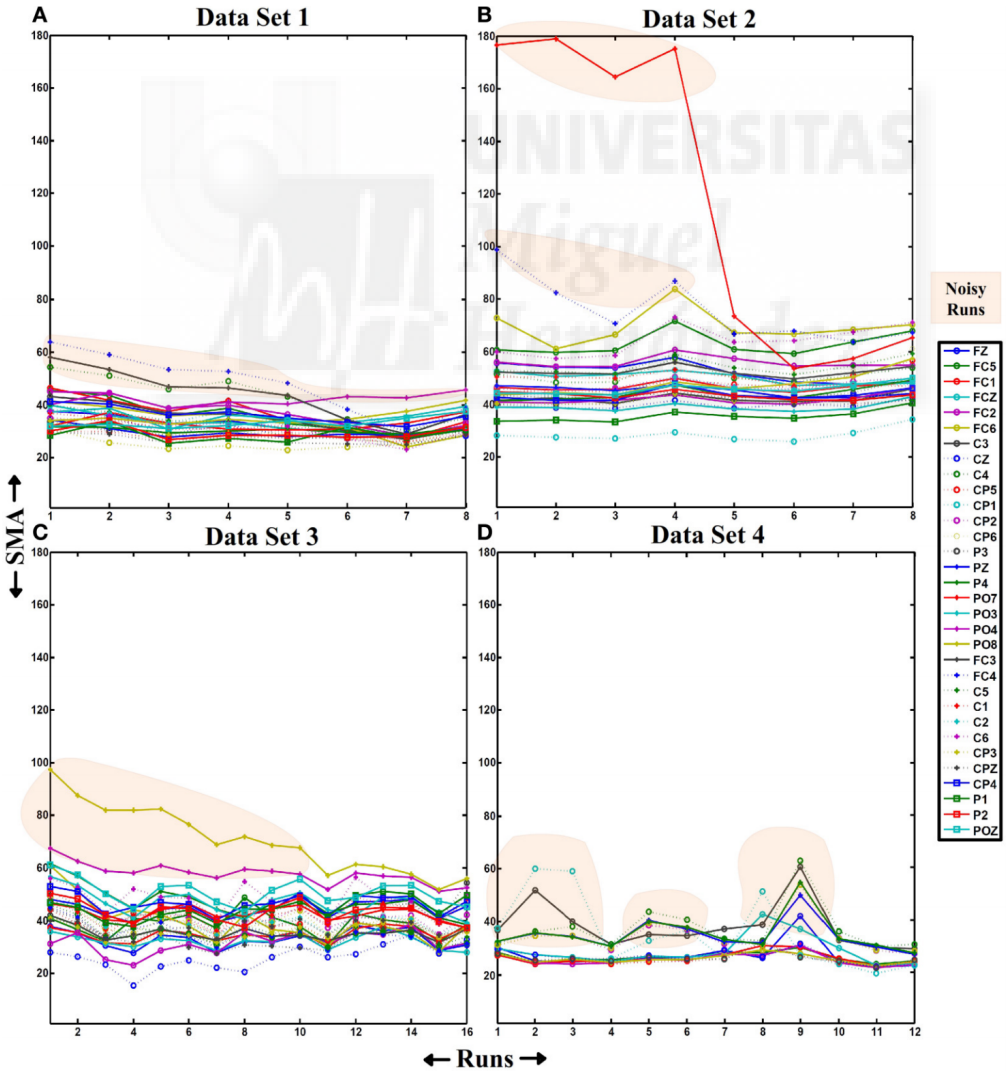

Figura 3.17: Evolucin del parámetro SMA a lo largo de repeticiones consecutivas de cada uno de los experimentos.

3.2.5. Caracterización frequencial de ruidos

Por último, se calculá el espectro de todas las repeticiones ruidosas y se comparan en media con el de las señales no ruidosas mostrando diferencias significativas a todas las frecuencias entre 5 y 90 Hz (ver figura 3.18).

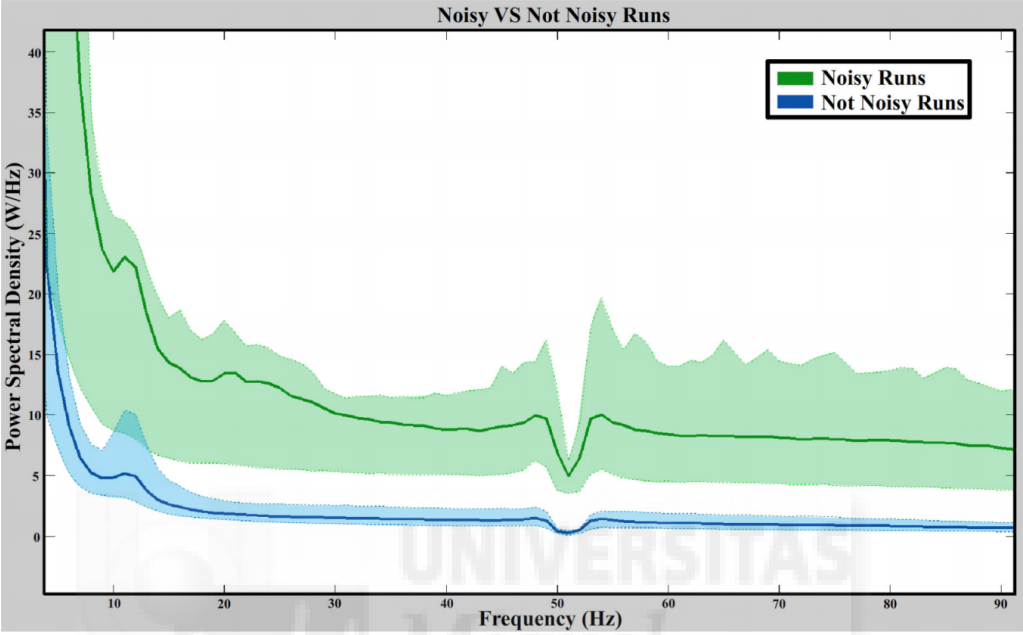

Figura 3.18: Comparativa de las medias de todos los electrodos ruidosos contra los no ruidosos. Las areas sombreadas muestran los percentiles 25 y 75 del total de señales promediadas.

3.2.6. Conclusiones

De estos resultados se comprueba que el HA_noise es la única fuente de ruido de los registros realizados sin movimiento (tabla 3.5) y que, bajo estas condiciones, los registros permanecen ruidosos durante repeticiones consecutivas del experimento (figura 3.17). Esto se debe a fallos en la conductividad entre el electrodo y la cabeza por una mala colocación del gel durante la instrumentación. Por otro lado, estos ruidos son los que menos afectan a los registros durante la marcha (tabla 3.5), ya que el movimiento inherente a estos experimentos provoca asentamientos del gel mal colocado mejorando la conductividad a lo largo de repeticiones consecutivas (figura 3.17). Por otro lado, se comprueba que el SA_noise es la mayor fuente de ruido de los registros durante la marcha habiendo contaminado el 6.11 % de todos los datos obtenidos bajo estas condiciones.

Con este trabajo se obtuvo una novedosa caracterización de artefactos que se deben tener en cuenta durante la realización de estudios que impliquen movimientos complejos como la marcha humana. Con ello se pretende evitar que los resultados que se obtengan al realizar estos experimentos estén condicionados por los artefactos y puedan ser malinterpretados.

3.3. Detección del nivel de atención en la marcha a partir de señales EEG

Este último trabajo se centra en la evaluación del nivel de atención que un usuario experimenta durante la marcha humana a partir de sus señales EEG con el objetivo de proporcionar realimentación cortical a un exoesqueleto robótico de rehabilitación de miembro inferior. Esta parte de la Tesis Doctoral cuenta con una publicación en congreso [139] y una en revista impactada [140]:

- *R3*: Á. Costa, E. Iáñez, A. Úbeda, E. Hortal, A. J. Del-Ama, Á. Gil-Agudo, J. M. Azorín. *Decoding the Attentional Demands of Gait through EEG Gamma Band Features*, PLOS ONE, 11(4), Páginas: 1-21, 2016. Factor de Impacto (2014): 3.234. Posición 9/57 en el área de Multidisciplinary Sciences (Q1). DOI: 10.1371/journal.pone.0154136
- *C1*: Á. Costa, E. Iáñez, A. Úbeda, D. Planelles, E. Hortal, J.M. Azorín. *Experimental Setup and First Results of a BCI System for Attention Levels Classification During Gait*. Workshop Proceedings on Neuro-Robotics for Patient-Specific Rehabilitation. International Conference on Autonomous Intelligent Systems (IAS-13), Padova, Italia, Páginas: 470-473, 2014.

3.3.1. Introducción

Este trabajo se basa en el diseño de un entorno experimental que permita el registro de señales EEG asociadas a diferentes niveles de atención. Sobre estos registros, se aplican los protocolos de eliminación de artefactos presentados en secciones anteriores y, las señales resultantes, se someten a diferentes algoritmos de procesamiento, separabilidad de clases y classificación para extraer aquellas caracteristicas que nos permitan identificar mejor el nivel de atención.

3.3.2. Materiales y Métodos

Para registrar señales EEG que correspondan con diferentes niveles de atención en la marcha humana se diseñó un experimento basado en el paradigma de

la tarea dual. Se basa en que un usuario debe realizar simultáneamente dos tareas. Una de estas tareas será siempre fija, en nuestro caso, la marcha humana. La otra tarea será distinta en diferentes repeticiones con el objetivo de modificar el nivel de atención que el usuario tiene sobre la primera tarea. En la figura 3.11A se puede apreciar el entorno experimental. El usuario camina en una cinta de andar (ver anexo A.3) equipado con el equipo de adquisición EEG de g.Tec (ver anexo A.1). De nuevo se utiliza la configuración de 32 electrodos mostrada en la figura 3.12.

La figura 3.19 muestra el paradigma experimental. Una repetición del experimento consta de cuatro tareas en las cuales el usuario siempre se encuentra andando en la cinta. La primera tarea se considera nivel medio de atención y consiste en andar sin distracciones mirando una pantalla en blanco situada frente al usuario. Durante la segunda y tercera tarea se pide al usuario que realice mentalmente unas operaciones matemáticas (tarea 2) y que vea un video sin audio y con subtítulos que aparecen por pantalla (tarea 3). Ambas tareas se consideran nivel bajo de atención en la marcha, ya que el usuario centra su atención en tareas externas no relacionadas con el proceso motriz. Por último, en la cuarta tarea el usuario debe seguir unas marcas situadas en la cinta de correr con un patrón no estable. Esta tarea lo fuerza a concentrarse en donde poner los pies en cada pisada, por lo que se considera como nivel alto de atención en la marcha.

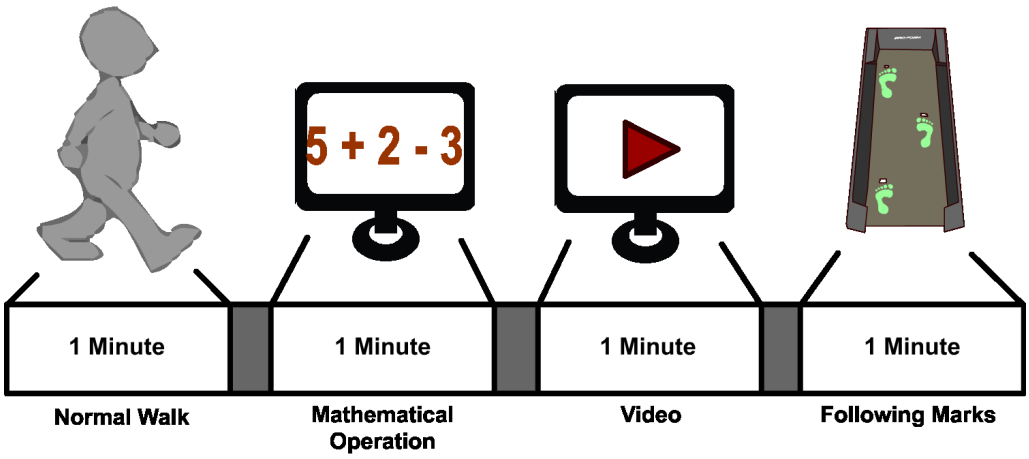

Figura 3.19: Paradigma utilizado durante la adquisicin de señales EEG ante diferentes niveles de atención durante la marcha.

Puesto que en la literatura existen multitud de fenómenos EEG asociados con

el nivel de atención en diferentes rangos frecuenciales se decidió realizar un estudio espectral de las 6 bandas de frecuencias que componen el ancho de banda de las señales EEG: delta (1-4Hz), theta (4-8 Hz), alpha (8-12 Hz), beta (12-30 Hz), gamma baja (30-50 Hz) y gamma alta (50-90 Hz). En la figura 3.20 se pueden apreciar las distribuciones espaciales de cada una de las 4 tareas a las diferentes bandas frequenciales.

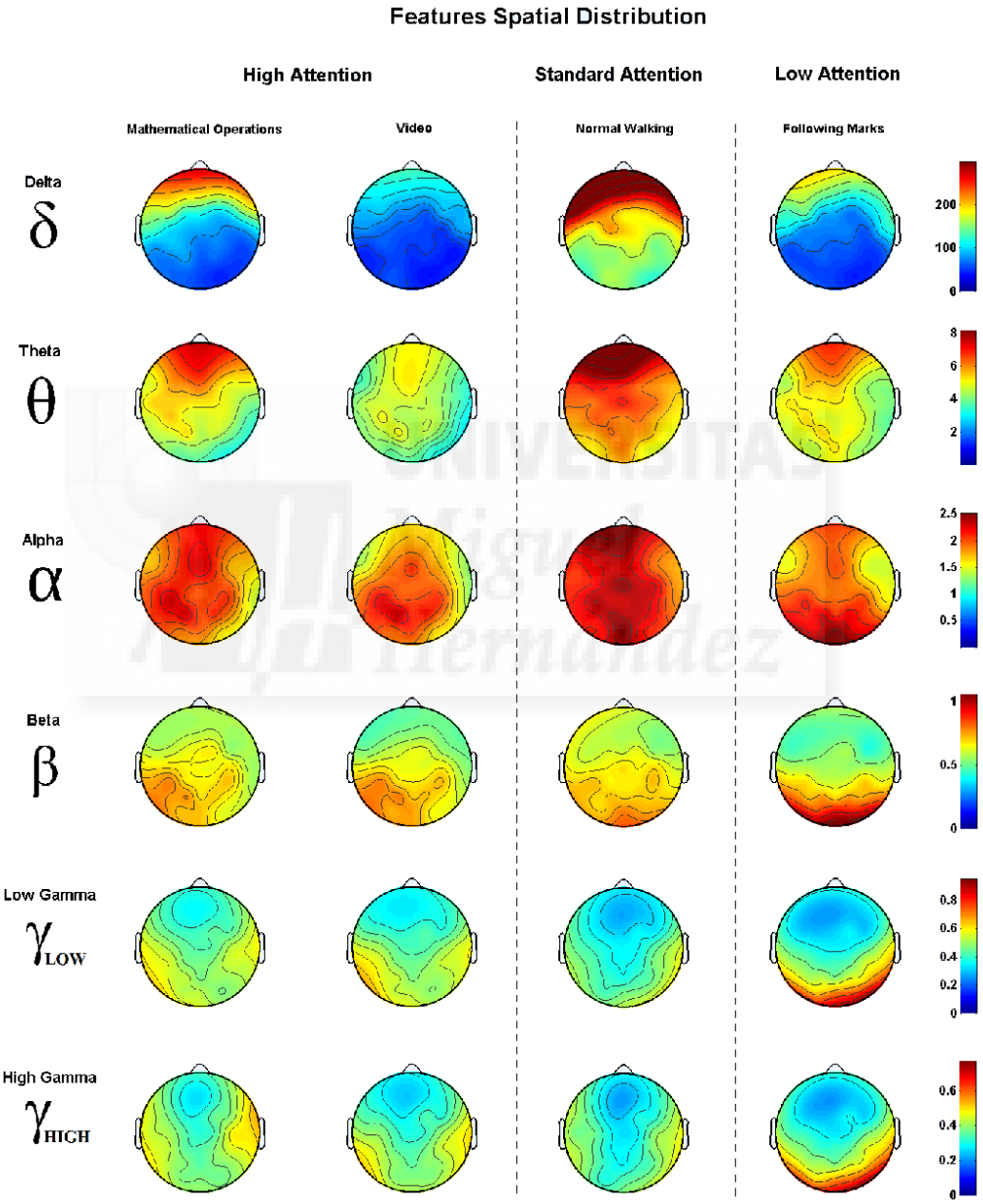

Figura 3.20: Distribución espacial de la media de las características frecuenciales para cada una de las bandas de frecuencia y las tareas de atención

Este experimento fue realizado por 10 usuarios sanos y 3 pacientes con lesión incompleta de médula espinal del Hospital Nacional de Parapléjicos de Toledo.

Las señales fueron evaluadas de acuerdo al protocolo definido en la sección 3.2 en busca de electrodos ruidosos. La información contaminada, que supuso un 2,71 % de los datos, fue sustituida utilizado información de electrodos vecinos no contaminados. Tras extraer las características de cada rango de frecuencia se calculó la distancia de Bhattacharyya entre las clases para saber dónde se producía la máxima separabilidad. La tabla 3.6 muestra que las bandas gamma baja y alta presentaban los mejores valores de separabilidad, por lo que se usaron para una etapa de clasificación.

Tabla 3.6: Distancias de Bhattacharyya para cada combinación de tareas:*A* es andar sin distracciones, *B* es andar realizando operaciones, *C* es andar viendo un video y *D* es andar siguiendo las marcas.

	AB	**AC**	**AD**	**BC**	**BD**	**CD**
1-4Hz	**16.62***	**17.86***	**16.32***	1.68	1.52	1.68
4-8Hz	**9.25**	**9.76**	**9.63**	0.85	1.36	1.20
8-12Hz	**8.68**	**9.32**	**9.35**	1.06	1.84	1.60
12-30Hz	**8.82**	**9.32**	**9.89**	1.35	2.95	2.61
30-50Hz	**8.22**	**8.88**	**9.64**	1.86**	**4.96****	**4.19****
50-90Hz	**9.41****	**10.81****	**11.40****	**3.98***	**7.23***	**5.91***

En la fase de clasificación se emplearon 5 classificadores diferentes: máquina de vector soporte (SVM, del inglés *Support Vector Machine*), bayesiano ingenuo (NB del inglés *Naive Bayes*), análisis discriminante lineal (LDA), K-vecinos más cercanos (KNN) y árbol de decisión (DTL del inglés *Decision Tree Learning*). Se aplicó un proceso de validación cruzada para obtener los resultados de clasificación de cada usuario sano y paciente.

3.3.3. Resultados

En la tabla 3.7 se muestran los resultados medios de clasificación y las desviaciones estándar para las características de las bandas gamma baja y gamma alta. En ella se puede observar que los valores máximo se obtienen para el clasificación SVM en la banda gamma alta con un 66.98 % de aciertos. Además en la figura 3.21 se muestra la clasificación media y desviación de cada clasificador dividido en bandas de frecuencia y usuarios sanos y pacientes. Además, se muestra el valor matemático del nivel aleatorio (chance level) para un sistema de las carac-

terísticas descritas. Aunque a simple vista se observa que los resultados obtenidos están por encima del aleatorio, se realizó un test Wilcoxon de significancia entre cada clasificador y el nivel aleatorio calculado que confirmó esta significancia.

Tabla 3.7: Valores de clasificación y desviación estandar de cada usuario para las bandas gamma alta y gamma baja.

		γ_{low}				
		SVM	**NB**	**LDA**	**KNN**	**DTL**
Sujetos	**H1**	77.38±12.38	52.02±12.37	78.10±5.66	73.38±14.03	73.29±6.49
	H2	68.86±12.05	44.17±9.60	67.74±9.54	65.99±13.27	59.43±13.36
	H3	76.89±6.45	53.52±7.43	72.99±7.38	73.71±9.96	69.76±7.13
	H4	68.38±3.99	36.44±3.82	62.74±4.16	66.18±3.59	61.25±4.71
	H5	76.37±7.62	60.62±8.01	72.31±8.05	72.73±8.54	66.32±5.81
	H6	70.31±15.06	45.79±8.94	69.62±14.81	67.40±14.44	61.31±9.92
	H7	59.36±6.47	33.81±6.73	54.52±6.43	58.05±9.09	52.07±6.63
	H8	68.74±7.79	37.09±6.28	59.40±5.13	66.60±8.71	60.29±6.77
	H9	67.00±6.85	39.22±9.82	63.37±6.16	65.31±8.36	58.94±4.69
	H10	57.42±6.57	31.38±7.49	54.87±5.67	52.31±9.84	50.81±5.08
	H11	60.51±8.24	47.41±8.93	75.38±9.71	67.24±6.69	62.39±6.86
	H12	71.66±9.22	61.37±5.09	72.31±6.65	72.63±7.90	68.00±5.92
	P1	53.66±7.00	40.95±4.33	62.72±3.92	54.09±3.94	51.83±6.47
	P2	67.56±4.33	37.28±5.65	62.39±10.71	71.12±5.40	63.36±4.42
	P3	48.28±2.96	28.99±4.16	50.54±4.18	52.05±6.54	49.14±5.15
	Media	**66.16±11.54**	**43.34±12.02**	**65 .27±10.53**	**65.27±11.84**	**60.55±9.95**
		γ_{high}				
	H1	77.15±13.33	36.31±11.68	78.47±7.49	74.03±14.94	73.35±7.55
	H2	69.89±14.41	41.48±8.54	71.53±12.24	67.79±14.63	62.97±11.89
	H3	77.15±7.15	47.11±6.30	74.51±7.22	72.99±10.63	69.79±7.79
	H4	68.99±3.20	26.83±2.98	63.80±4.34	67.79±4.25	62.83±4.19
	H5	77.65±7.88	62.36±8.19	78.32±7.60	73.31±9.61	68.75±7.78
	H6	71.49±16.78	50.18±10.00	71.17±14.90	67.78±14.64	60.83±12.74
	H7	59.87±8.66	33.39±6.06	57.39±6.44	56.37±10.95	52.17±8.54
	H8	73.88±10.11	33.46±6.57	66.18±10.10	72.32±12.57	67.92±9.48
	H9	65.80±7.84	38.87±7.00	63.51±6.74	62.89±8.56	57.00±6.90
	H10	58.48±5.70	32.69±5.83	55.66±5.94	56.96±8.24	53.74±9.91
	H11	63.63±9.86	60.08±10.63	67.30±8.67	66.43±10.38	61.48±7.91
	H12	71.07±10.81	60.67±5.62	75.86±7.47	78.45±10.88	74.46±6.04
	P1	50.75±5.27	36.75±5.65	59.81±4.39	58.19±6.96	53.77±6.59
	P2	69.94±6.85	39.55±8.42	67.46±9.34	73.81±6.38	68.00±7.02
	P3	48.92±2.47	28.34±3.98	53.45±5.89	55.50±6.96	54.20±4.94
	Media	**66.98±12.46**	**41.87±11.95**	**66.96±11.59**	**66.97±12.52**	**62.75±10.82**

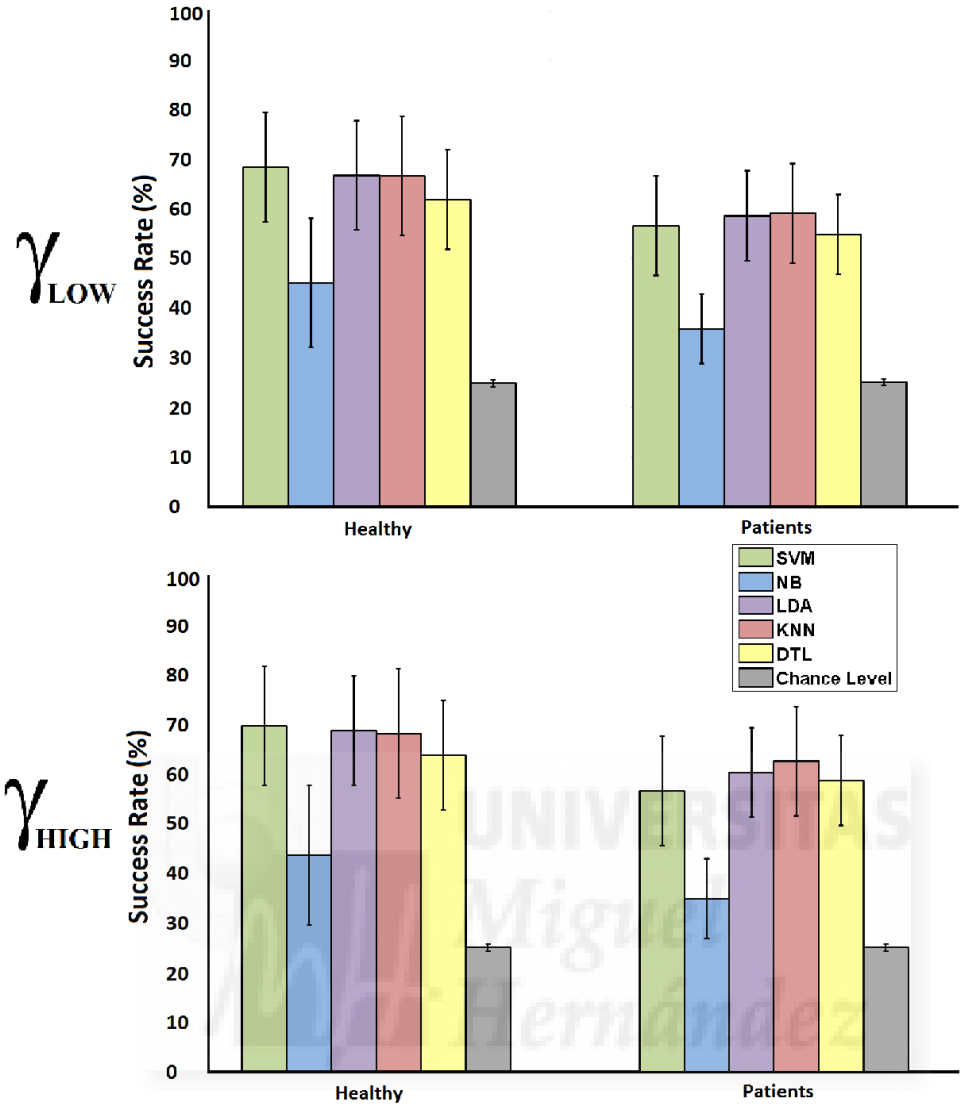

Figura 3.21: Resultados medios de la classificación de las 4 tareas de atención para usuarios sanos y pacientes. Se validan caracterísitcas de las bandas gamma alta y gamma baja con 5 clasificadores

3.3.4. Conclusiones

Los resultados obtenidos en este trabajo son una aportación relevante de esta Tesis Doctoral demuestran que existe información cortical relacionada con el nivel de atención durante la marcha en la banda gamma de frecuencia. También resultan prometedores de cara al diseño de sistemas en tiempo real que permitan calcular este nivel durante terapias de rehabilitación. Para ello, sin embargo, es necesario realizar ciertos ajustes para adaptar el sistema presentado en este trabajo. Por un lado, es necesario reducir la cantidad de tareas de cuatro a tres ya que

dos de las tareas corresponden al mismo nivel de atención. Con esto, se reducen los tiempo necesarios para entrenar el sistema y se incrementan los porcentajes de acierto. También es necesaria la implementación de algoritmos robustos de eliminación de artefactos en tiempo real para evitar que los resultados de clasificación pierdan su validez. Y por último se debe proveer un índice de atención en función de los valores de clasificación para reducir la influencia de las tareas mal clasificadas.

Capítulo 4

CONCLUSIONES Y TRABAJOS FUTUROS

4.1. Conclusiones

Todos los años, entre un cuarto y medio millón de personas en el mundo sufren lesiones medulares [2]. En su mayoría se trata de personas entre 16 y 30 años que han sufrido accidentes o caídas evitables. Estas lesiones se asocian a menores tasas de escolarización y participación económica, lo que supone un costo importante a la sociedad y a quienes las padeces. En los 6 primeros meses de rehabilitación, se obtienen los mayores beneficios motores y psicológicos, por lo que es necesario disponer de herramientas que nos permitan aplicar terapias muy focalizadas según la lesión especifica de cada paciente. Por todos estos motivos, existe un interés creciente orientado a mejorar las terapias de rehabilitación de estas personas y desarrollar investigaciones que les proporcionen una mayor autonomía.

Esta tesis se ha centrado en el desarrollo de interfaces cerebrales de asistencia y en la edición de mecanismos cognitivos durante la marcha humana. Estas herramientas proporcionan mecanismos de asistencia durante las terapias, así como información sobre el estado cognitivo del paciente, de forma que el sistema de rehabilitación podría ser reajustado para adaptarse a cada persona.

Las aportaciones más relevantes de esta tesis son las siguientes:

- Se han identificado los artefactos faciales que más afectan a las señales EEG.

Mediante esta identificación, se ha desarrollado un sistema basado en electrodos EEG capaz de detectar 5 niveles de presiones de mandíbula para el movimiento bidimensional de un dispositivo. Este sistema ha sido implementando para el control de un cursor y de un brazo robótico.

- Se ha demostrado la existencia de artefactos asociados a cambios de conductividad en los electrodos EEG, cuya contribución se incrementa durante la marcha humana. A partir de este estudio, se han caracterizado las zonas del cuero cabelludo donde se originan, en mayor medida, estos artefactos en función del tipo de experimento realizado.

- Se han aplicado estos conocimientos en experimentaciones realizadas durante la marcha con el objetivo de obtener información de los mecanismos cognitivos humanos a partir de señales EEG.

- Se han obtenido resultados de gran relevancia en la clasificación del nivel de atención durante la marcha humana a partir de la evaluación de las componentes de la banda gamma. Los resultados son prometedores de cara a la implementación de un sistema en tiempo real orientado a la rehabilitación.

4.2. TRABAJOS FUTUROS

Dado que el estudio de señales EEG durante la marcha humana es un campo que ha comenzado a ser investigado por la comunidad científica en la última década, todavía hay que hacer grandes avances en el mismo. En este trabajo se han establecido las bases para realizar estas investigaciones teniendo en cuenta la influencia de los artefactos y se han realizado diversos estudios prometedores en el campo de la evaluación de mecanismos cognitivos y la asistencia Sin embargo, es necesario seguir desarrollando las siguientes líneas para que, a partir de estos resultados, puedan desarrollarse aplicaciones reales en el campo de la asistencia y de la rehabilitacin::

- Mejora de la interfaz de control bidimensional: esta investigación permitiría gran precisión en la clasificación de presiones mandibulares. Un estudio más profundo podría permitir el desarrollo de interfaces de control en 2

dimensiones de forma simultánea e incluso en 3 dimensiones modulando el nivel de presión de mandibular a derecha e izquierda de forma individual referenciándolos a un tercer electrodo.

- Estudio de artefactos fisiológicos durante la marcha: en este trabajo se han evaluado los artefactos producidos por cambios de conductividad. Pero ante el movimiento, también se incrementa la actividad EMG. Esta es otra importante fuente de ruido que puede afectar a las ondas corticales registradas y que debe ser evaluada para dotar de mayor validez a los estudios basados en señales EEG adquiridas durante la marcha.

- Detección de niveles de atención en tiempo real: el objetivo consiste en proporcionar a un exoesqueleto de rehabilitación de miembro inferior, un índice representativo del nivel de atención, que pueda ser utilizado para adaptar el nivel de asistencia proporcionado al paciente durante su terapia.

- Evaluación de artefactos de BMI junto con los sistemas de rehabilitación: es común el uso de exoesqueletos orientado a la rehabilitación. Estos sistemas se acoplan a las extremidades de los pacientes para asistirles. Dadas sus propiedades mecánicas y eléctricas, es necesario evaluar su influencia sobre las señales EEG en el caso de que se desarrollen sistemas multidisciplinares en las que se apliquen ambas técnicas.

- Evaluación de las terapias: en este trabajo se han realizados pruebas preliminares con pacientes, sin embargo, de cara a los sistemas finales de rehabilitación basados en estas tecnologías, es necesario realizar pruebas con un mayor número de pacientes. Además los resultados se deben comparar con una población de control para asegurar los beneficios de estos sistemas respecto a las terapias más clásicas.

UNIVERSITAS
Miguel
Hernández

Bibliografía

[1] T. Shakespeare y A. Officer, "World report on disability," *Disabil Rehabil*, vol. 33, no. 17-18, p. 1491, 2011.

[2] W. H. Organization. (Última visita Noviembre de 2013) Spinal cord injury. fact sheet n. 384 `http://www.who.int/mediacentre/factsheets/fs384/en/`.

[3] N. Tsukahara y M. Kawato, "Dynamic and plastic properties of the brain stem neuronal networks as the possible neuronal basis of learning and memory," *Competition and cooperation in neural nets*, pp. 430–441, 1982.

[4] C. V. Granger, B. B. Hamilton, R. A. Keith, M. Zielezny, y F. S. Sherwin, "Advances in functional assessment for medical rehabilitation." *Topics in geriatric rehabilitation*, vol. 1, no. 3, pp. 59–74, 1986.

[5] A. L. Behrman y S. J. Harkema, "Locomotor training after human spinal cord injury: a series of case studies," *Physical therapy*, vol. 80, no. 7, pp. 688–700, 2000.

[6] S. J. Harkema, "Neural plasticity after human spinal cord injury: application of locomotor training to the rehabilitation of walking," *The Neuroscientist*, vol. 7, no. 5, pp. 455–468, 2001.

[7] J. Classen, J. Liepert, S. P. Wise, M. Hallett, y L. G. Cohen, "Rapid plasticity of human cortical movement representation induced by practice," *Journal of neurophysiology*, vol. 79, no. 2, pp. 1117–1123, 1998.

[8] P. S. Lum, C. G. Burgar, P. C. Shor, M. Majmundar, y M. Van der Loos, "Robot-assisted movement training compared with conventional therapy

techniques for the rehabilitation of upper-limb motor function after stroke," *Archives of physical medicine and rehabilitation*, vol. 83, no. 7, pp. 952–959, 2002.

[9] B. Volpe, H. Krebs, N. Hogan, L. Edelstein, C. Diels, y M. Aisen, "A novel approach to stroke rehabilitation robot-aided sensorimotor stimulation," *Neurology*, vol. 54, no. 10, pp. 1938–1944, 2000.

[10] S. K. Banala, S. K. Agrawal, y J. P. Scholz, "Active leg exoskeleton (alex) for gait rehabilitation of motor-impaired patients," *Rehabilitation Robotics. ICORR 2007. IEEE 10th International Conference on*, pp. 401–407, 2007.

[11] S. Hesse, H. Schmidt, C. Werner, y A. Bardeleben, "Upper and lower extremity robotic devices for rehabilitation and for studying motor control," *Current opinion in neurology*, vol. 16, no. 6, pp. 705–710, 2003.

[12] G. Prasad, P. Herman, D. Coyle, S. McDonough, y J. Crosbie, "Using motor imagery based brain-computer interface for post-stroke rehabilitation," *Neural Engineering, 2009. NER'09. 4th International IEEE/EMBS Conference on*, pp. 258–262, 2009.

[13] A. Jackson y J. B. Zimmermann, "Neural interfaces for the brain and spinal cordrestoring motor function," *Nature Reviews Neurology*, vol. 8, no. 12, pp. 690–699, 2012.

[14] J. L. Contreras-Vidal y R. G. Grossman, "Neurorex: A clinical neural interface roadmap for eeg-based brain machine interfaces to a lower body robotic exoskeleton," *Engineering in medicine and biology society (EMBC), 2013 35th annual international conference of the IEEE*, pp. 1579–1582, 2013.

[15] T. Noda, N. Sugimoto, J.-i. Furukawa, M. Sato, S.-H. Hyon, y J. Morimoto, "Brain-controlled exoskeleton robot for bmi rehabilitation," *Humanoid Robots (Humanoids), 2012 12th IEEE-RAS International Conference on*, pp. 21–27, 2012.

[16] J. E. Kline, H. J. Huang, K. L. Snyder, y D. P. Ferris, "Isolating gait-related movement artifacts in electroencephalography during human walking," *Journal of neural engineering*, vol. 12, no. 4, p. 046022, 2015.

[17] K. P. Tee, C. Guan, K. K. Ang, K. S. Phua, C. Wang, y H. Zhang, "Augmenting cognitive processes in robot-assisted motor rehabilitation," *Biomedical Robotics and Biomechatronics, 2008. BioRob 2008. 2nd IEEE RAS & EMBS International Conference on*, pp. 698–703, 2008.

[18] H. Seddon, "A classification of nerve injuries," *British medical journal*, vol. 2, no. 4260, p. 237, 1942.

[19] K. Goulding, P. E. Beaulé, P. R. Kim, y A. Fazekas, "Incidence of lateral femoral cutaneous nerve neuropraxia after anterior approach hip arthroplasty," *Clinical Orthopaedics and Related Research®*, vol. 468, no. 9, pp. 2397–2404, 2010.

[20] P. M. Bridge, D. J. Ball, S. E. Mackinnon, Y. Nakao, K. Brandt, D. A. Hunter, y C. Hertl, "Nerve crush injuriesa model for axonotmesis," *Experimental neurology*, vol. 127, no. 2, pp. 284–290, 1994.

[21] D. G. Van Den Broecke, A. H. Schuurman, E. D. Borg, y M. Kon, "Neurotmesis of the lateral femoral cutaneous nerve when coring for iliac crest bone grafts." *Plastic and reconstructive surgery*, vol. 102, no. 4, pp. 1163–1166, 1998.

[22] R. F. P. Shih, *Bradley's Neurology in Clinical Practice 6th Edition. Trauma of the nervous system: Spinal cord trauma*. Elsevier, 2012.

[23] J. De La Torre, "Spinal cord injury: Review of basic and applied research." *Spine*, vol. 6, no. 4, pp. 315–335, 1981.

[24] S. Sabharwal, *Essentials of Spinal Cord Medicine*. Demos Medical Publishing, 2013.

[25] W. R. Frontera, J. K. Silver, y T. D. Rizzo, *Essentials of physical medicine and rehabilitation: Musculoskeletal disorders, pain, and rehabilitation*. Saunders/Elsevier, 2008.

[26] G. Scivoletto, F. Tamburella, L. Laurenza, M. Torre, y M. Molinari, "Who is going to walk? a review of the factors influencing walking recovery after spinal cord injury," *Neuro-motor control and feed-forward models of locomotion in humans*, p. 75, 2007.

[27] P. New, R. Cripps, y B. B. Lee, "Global maps of non-traumatic spinal cord injury epidemiology: towards a living data repository," *Spinal cord*, vol. 52, no. 2, pp. 97–109, 2014.

[28] M. E. Van den Berg, J. M. Castellote, J. de Pedro-Cuesta, y I. Mahillo-Fernández, "Survival after spinal cord injury: a systematic review," *Journal of neurotrauma*, vol. 27, no. 8, pp. 1517–1528, 2010.

[29] C. Tai, J. R. Roppolo, y W. C. de Groat, "Spinal reflex control of micturition after spinal cord injury," *Restorative neurology and neuroscience*, vol. 24, no. 2, pp. 69–78, 2006.

[30] Y. Bahena-Salgado y J. Bernal-Márquez, "Calidad de vida de los pacientes con paraplejía secundaria a lesión vertebral traumática," *Acta Ortopédica Mexicana*, vol. 21, no. 1, pp. 3–7, 2007.

[31] H. Frankel, D. Hancock, G. Hyslop, J. Melzak, L. Michaelis, G. Ungar, J. Vernon, y J. Walsh, "The value of postural reduction in the initial management of closed injuries of the spine with paraplegia and tetraplegia," *Spinal Cord*, vol. 7, no. 3, pp. 179–192, 1969.

[32] D. D. Nowak, J. K. Lee, D. E. Gelb, K. A. Poelstra, y S. C. Ludwig, "Central cord syndrome," *Journal of the American Academy of Orthopaedic Surgeons*, vol. 17, no. 12, pp. 756–765, 2009.

[33] M. Itzoe y D. M. Sciubba, "Anterior cord syndrome," *Encyclopedia of Trauma Care*, pp. 144–145, 2015.

[34] E. Roth, T. Park, T. Pang, G. Yarkony, y M. Lee, "Traumatic cervical brown-sequard and brown-sequard-plus syndromes: the spectrum of presentations and outcomes," *Paraplegia*, vol. 29, no. 9, pp. 582–589, 1991.

[35] A. S. Burns y J. F. Ditunno, "Establishing prognosis and maximizing functional outcomes after spinal cord injury: a review of current and future directions in rehabilitation management," *Spine*, vol. 26, no. 24S, pp. S137–S145, 2001.

[36] A. B. Singhal, "Cerebral vasoconstriction syndromes," *Topics in stroke rehabilitation*, vol. 11, no. 2, pp. 1–6, 2004.

[37] M. Fisher, A. Paganini-Hill, A. Martin, M. Cosgrove, J. F. Toole, H. J. Barnett, y J. Norris, "Carotid plaque pathology thrombosis, ulceration, and stroke pathogenesis," *Stroke*, vol. 36, no. 2, pp. 253–257, 2005.

[38] W. J. Koroshetz y A. H. Ropper, "Artery-to-artery embolism causing stroke in the posterior circulation," *Neurology*, vol. 37, no. 2, pp. 292–292, 1987.

[39] A. Kaufmann y C. D. Domnariu, "Arterial hypertension and strokes." *Acta Medica Transilvanica*, vol. 17, no. 4, 2012.

[40] G. Di Pasquale, A. Andreoli, P. Grazi, P. Dominici, y G. Pinelli, "Cardioembolic stroke from atrial septal aneurysm." *Stroke*, vol. 19, no. 5, pp. 640–643, 1988.

[41] A. Culebras. (Última visita 10 de Marzo de 2016) Stroke recovery learn, recover, prevent `http://www.strokeeducation.org.nz/Stroke_Information.html`.

[42] I. Stroke Network. (Última visita 10 de Marzo de 2016) Stroke education: The stroke network: Stroke recovery `http://www.strokeeducation.info/recovery/index.htm`.

[43] K. Gardner, "American board of physical therapy specialties recognizes certified clinical specialists," 2015.

[44] M. C. Staff. (Última visita 10 de Marzo de 2016) Stroke rehabilitation: What to expect as you recover `http://www.mayoclinic.org/stroke-rehabilitation/art-20045172`.

[45] T. Elbert, C. Pantev, C. Wienbruch, B. Rockstroh, y E. Taub, "Increased cortical representation of the fingers of the left hand in string players," *Science*, vol. 270, no. 5234, pp. 305–307, 1995.

[46] M. A. Lebedev, G. Mirabella, I. Erchova, y M. E. Diamond, "Experience-dependent plasticity of rat barrel cortex: redistribution of activity across barrel-columns," *Cerebral Cortex*, vol. 10, no. 1, pp. 23–31, 2000.

[47] M. A. Dimyan y L. G. Cohen, "Neuroplasticity in the context of motor rehabilitation after stroke," *Nature Reviews Neurology*, vol. 7, no. 2, pp. 76–85, 2011.

[48] K. K. Ang, C. Guan, K. S. G. Chua, B. T. Ang, C. Kuah, C. Wang, K. S. Phua, Z. Y. Chin, y H. Zhang, "A clinical study of motor imagery-based brain-computer interface for upper limb robotic rehabilitation," *Engineering in Medicine and Biology Society, 2009. EMBC 2009. Annual International Conference of the IEEE*, pp. 5981–5984, 2009.

[49] F. Kaneko, T. Hayami, T. Aoyama, y T. Kizuka, "Motor imagery and electrical stimulation reproduce corticospinal excitability at levels similar to voluntary muscle contraction," *Journal of neuroengineering and rehabilitation*, vol. 11, no. 1, p. 1, 2014.

[50] A. M. Noll, "Tactile man-machine communication system," Nov. 11 1975, uS Patent 3.919.691.

[51] D. Erol y N. Sarkar, "Coordinated control of assistive robotic devices for activities of daily living tasks," *Neural Systems and Rehabilitation Engineering, IEEE Transactions on*, vol. 16, no. 3, pp. 278–285, 2008.

[52] J. L. Pons *et al.*, "Wearable robots: biomechatronic exoskeletons," 2008.

[53] T. Carlson y J. d. R. Millan, "Brain-controlled wheelchairs: a robotic architecture," *IEEE Robotics and Automation Magazine*, vol. 20, no. EPFL-ARTICLE-181698, pp. 65–73, 2013.

[54] D. Huang, K. Qian, D.-Y. Fei, W. Jia, X. Chen, y O. Bai, "Electroencephalography (eeg)-based brain–computer interface (bci): A 2-d virtual wheelchair control based on event-related desynchronization/synchronization and state control," *Neural Systems and Rehabilitation Engineering, IEEE Transactions on*, vol. 20, no. 3, pp. 379–388, 2012.

[55] C. C. Postelnicu y D. Talaba, "P300-based brain-neuronal computer interaction for spelling applications," *Biomedical Engineering, IEEE Transactions on*, vol. 60, no. 2, pp. 534–543, 2013.

[56] M. Bensch, A. A. Karim, J. Mellinger, T. Hinterberger, M. Tangermann, M. Bogdan, W. Rosenstiel, y N. Birbaumer, "Nessi: an eeg-controlled web browser for severely paralyzed patients," *Computational intelligence and neuroscience*, vol. 2007, 2007.

[57] G. Onose, C. Grozea, A. Anghelescu, C. Daia, C. Sinescu, A. Ciurea, T. Spircu, A. Mirea, I. Andone, A. Spânu *et al.*, "On the feasibility of using motor imagery eeg-based brain–computer interface in chronic tetraplegics for assistive robotic arm control: a clinical test and long-term post-trial follow-up," *Spinal Cord*, vol. 50, no. 8, pp. 599–608, 2012.

[58] J. P. Donoghue, A. Nurmikko, M. Black, y L. R. Hochberg, "Assistive technology and robotic control using motor cortex ensemble-based neural interface systems in humans with tetraplegia," *The Journal of physiology*, vol. 579, no. 3, pp. 603–611, 2007.

[59] T. Ros, M. A. Munneke, D. Ruge, J. H. Gruzelier, y J. C. Rothwell, "Endogenous control of waking brain rhythms induces neuroplasticity in humans," *European Journal of Neuroscience*, vol. 31, no. 4, pp. 770–778, 2010.

[60] K. K. Ang, C. Guan, K. S. Phua, C. Wang, L. Zhou, K. Y. Tang, G. J. E. Joseph, C. W. K. Kuah, y K. S. G. Chua, "Brain-computer interface-based robotic end effector system for wrist and hand rehabilitation: results of a three-armed randomized controlled trial for chronic stroke," *Frontiers in neuroengineering*, vol. 7, 2014.

[61] M. Duvinage, T. Castermans, M. Petieau, K. Seetharaman, T. Hoellinger, G. Cheron, y T. Dutoit, "A subjective assessment of a p300 bci system for lower-limb rehabilitation purposes," *Engineering in Medicine and Biology Society (EMBC), 2012 Annual International Conference of the IEEE*, pp. 3845–3849, 2012.

[62] G. Chéron, M. Duvinage, C. De Saedeleer, T. Castermans, A. Bengoetxea, M. Petieau, K. Seetharaman, T. Hoellinger, B. Dan, T. Dutoit *et al.*, "From spinal central pattern generators to cortical network: integrated bci for walking rehabilitation," *Neural plasticity*, vol. 2012, 2012.

[63] M. Rea, M. Rana, N. Lugato, P. Terekhin, L. Gizzi, D. Brötz, A. Fallgatter, N. Birbaumer, R. Sitaram, y A. Caria, "Lower limb movement preparation in chronic stroke a pilot study toward an fnirs-bci for gait rehabilitation," *Neurorehabilitation and neural repair*, vol. 28, no. 6, pp. 564–575, 2014.

[64] E. E. Fetz, "Operant conditioning of cortical unit activity," *Science*, vol. 163, no. 3870, pp. 955–958, 1969.

[65] E. M. Schmidt, "Single neuron recording from motor cortex as a possible source of signals for control of external devices," *Annals of biomedical engineering*, vol. 8, no. 4-6, pp. 339–349, 1980.

[66] M. A. Nicolelis, "Brain–machine interfaces to restore motor function and probe neural circuits," *Nature Reviews Neuroscience*, vol. 4, no. 5, pp. 417–422, 2003.

[67] A. B. Schwartz, D. M. Taylor, y S. I. H. Tillery, "Extraction algorithms for cortical control of arm prosthetics," *Current opinion in neurobiology*, vol. 11, no. 6, pp. 701–708, 2001.

[68] M. A. Nicolelis y N. Birbaumer, "Editorial," *Biomedical Engineering, IEEE Transactions on*, vol. 51, no. 6, pp. 877–880, 2004.

[69] S.-P. Kim, J. D. Simeral, L. R. Hochberg, J. P. Donoghue, y M. J. Black, "Neural control of computer cursor velocity by decoding motor cortical spiking

activity in humans with tetraplegiadisclosure." *Journal of neural engineering*, vol. 5, no. 4, p. 455, 2008.

[70] L. R. Hochberg, D. Bacher, B. Jarosiewicz, N. Y. Masse, J. D. Simeral, J. Vogel, S. Haddadin, J. Liu, S. S. Cash, P. van der Smagt *et al.*, "Reach and grasp by people with tetraplegia using a neurally controlled robotic arm," *Nature*, vol. 485, no. 7398, pp. 372–375, 2012.

[71] J. L. Collinger, B. Wodlinger, J. E. Downey, W. Wang, E. C. Tyler-Kabara, D. J. Weber, A. J. McMorland, M. Velliste, M. L. Boninger, y A. B. Schwartz, "High-performance neuroprosthetic control by an individual with tetraplegia," *The Lancet*, vol. 381, no. 9866, pp. 557–564, 2013.

[72] A. Palmini, "The concept of the epileptogenic zone: a modern look at penfield and jaspers views on the role of interictal spikes," *Epileptic disorders*, vol. 8, no. 2, pp. 10–15, 2006.

[73] E. C. Leuthardt, G. Schalk, J. R. Wolpaw, J. G. Ojemann, y D. W. Moran, "A brain–computer interface using electrocorticographic signals in humans," *Journal of neural engineering*, vol. 1, no. 2, p. 63, 2004.

[74] G. Schalk, K. Miller, N. Anderson, J. Wilson, M. Smyth, J. Ojemann, D. Moran, J. Wolpaw, y E. Leuthardt, "Two-dimensional movement control using electrocorticographic signals in humans," *Journal of neural engineering*, vol. 5, no. 1, p. 75, 2008.

[75] P. Brunner, A. L. Ritaccio, J. F. Emrich, H. Bischof, y G. Schalk, "Rapid communication with a p300 matrix speller using electrocorticographic signals (ecog)," *Frontiers in Neuroscience*, vol. 5, no. 5, pp. 1–9, 2011.

[76] T. Pistohl, T. Ball, A. Schulze-Bonhage, A. Aertsen, y C. Mehring, "Prediction of arm movement trajectories from ecog-recordings in humans," *Journal of neuroscience methods*, vol. 167, no. 1, pp. 105–114, 2008.

[77] P. R. Kennedy y R. A. Bakay, "Activity of single action potentials in monkey motor cortex during long-term task learning," *Brain research*, vol. 760, no. 1, pp. 251–254, 1997.

[78] P. R. Kennedy, M. T. Kirby, M. M. Moore, B. King, y A. Mallory, "Computer control using human intracortical local field potentials," *Neural Systems and Rehabilitation Engineering, IEEE Transactions on*, vol. 12, no. 3, pp. 339–344, 2004.

[79] T. Fitzpatrick, "Teenager moves video icons just by imagination, washington university in st. louis," 2012.

[80] J. Bartels, D. Andreasen, P. Ehirim, H. Mao, S. Seibert, E. J. Wright, y P. Kennedy, "Neurotrophic electrode: method of assembly and implantation into human motor speech cortex," *Journal of neuroscience methods*, vol. 174, no. 2, pp. 168–176, 2008.

[81] B. Jarosiewicz, A. A. Sarma, D. Bacher, N. Y. Masse, J. D. Simeral, B. Sorice, E. M. Oakley, C. Blabe, C. Pandarinath, V. Gilja *et al.*, "Virtual typing by people with tetraplegia using a self-calibrating intracortical brain-computer interface," *Science translational medicine*, vol. 7, no. 313, p. 313ra179, 2015.

[82] S. Ogawa y T.-M. Lee, "Magnetic resonance imaging of blood vessels at high fields: in vivo and in vitro measurements and image simulation," *Magnetic resonance in medicine*, vol. 16, no. 1, pp. 9–18, 1990.

[83] T. N. Nadkarni, M. J. Andreoli, V. A. Nair, P. Yin, B. M. Young, B. Kundu, J. Pankratz, A. Radtke, R. Holdsworth, J. S. Kuo *et al.*, "Usage of fmri for pre-surgical planning in brain tumor and vascular lesion patients: Task and statistical threshold effects on language lateralization," *NeuroImage: Clinical*, vol. 7, pp. 415–423, 2015.

[84] R. L. Buckner, W. Koutstaal, D. L. Schacter, A. D. Wagner, y B. R. Rosen, "Functional–anatomic study of episodic retrieval using fmri: I. retrieval effort versus retrieval success," *Neuroimage*, vol. 7, no. 3, pp. 151–162, 1998.

[85] M. Ullsperger y D. Y. von Cramon, "Subprocesses of performance monitoring: a dissociation of error processing and response competition revealed by event-related fmri and erps," *Neuroimage*, vol. 14, no. 6, pp. 1387–1401, 2001.

[86] K. J. Mitchell y M. K. Johnson, "Source monitoring 15 years later: what have we learned from fmri about the neural mechanisms of source memory?" *Psychological bulletin*, vol. 135, no. 4, p. 638, 2009.

[87] A. Eklund, H. Ohlsson, M. Andersson, J. Rydell, A. Ynnerman, y H. Knutsson, "Using real-time fmri to control a dynamical system by brain activity classification," *Medical Image Computing and Computer-Assisted Intervention–MICCAI 2009*, pp. 1000–1008, 2009.

[88] J. H. Lee, J. Ryu, F. A. Jolesz, Z.-H. Cho, y S.-S. Yoo, "Brain–machine interface via real-time fmri: preliminary study on thought-controlled robotic arm," *Neuroscience letters*, vol. 450, no. 1, pp. 1–6, 2009.

[89] G. Rota, R. Sitaram, R. Veit, M. Erb, N. Weiskopf, G. Dogil, y N. Birbaumer, "Self-regulation of regional cortical activity using real-time fmri: The right inferior frontal gyrus and linguistic processing," *Human brain mapping*, vol. 30, no. 5, pp. 1605–1614, 2009.

[90] N. Weiskopf, R. Veit, M. Erb, K. Mathiak, W. Grodd, R. Goebel, y N. Birbaumer, "Physiological self-regulation of regional brain activity using real-time functional magnetic resonance imaging (fmri): methodology and exemplary data," *Neuroimage*, vol. 19, no. 3, pp. 577–586, 2003.

[91] J. Hidler, T. Hodics, B. Xu, B. Dobkin, y L. G. Cohen, "Mr compatible force sensing system for real-time monitoring of wrist moments during fmri testing," *Journal of neuroscience methods*, vol. 155, no. 2, pp. 300–307, 2006.

[92] D. R. Gitelman, T. B. Parrish, K. S. LaBar, y M.-M. Mesulam, "Real-time monitoring of eye movements using infrared video-oculography during functional magnetic resonance imaging of the frontal eye fields," *Neuroimage*, vol. 11, no. 1, pp. 58–65, 2000.

[93] Y. Okada, "Neurogenesis of evoked magnetic fields," *Biomagnetism, an interdisciplinary approach*, pp. 399–408, 1983.

[94] J. Malmivuo, V. Suihko, y H. Eskola, "Sensitivity distributions of eeg and meg measurements," *Biomedical Engineering, IEEE Transactions on*, vol. 44, no. 3, pp. 196–208, 1997.

[95] D. Cohen, "Magnetoencephalography: evidence of magnetic fields produced by alpha-rhythm currents," *Science*, vol. 161, no. 3843, pp. 784–786, 1968.

[96] P. Tass, T. Fieseler, J. Dammers, K. Dolan, P. Morosan, M. Majtanik, F. Boers, A. Muren, K. Zilles, y G. Fink, "Synchronization tomography: a method for three-dimensional localization of phase synchronized neuronal populations in the human brain using magnetoencephalography," *Physical review letters*, vol. 90, no. 8, p. 088101, 2003.

[97] A. M. Dale y M. I. Sereno, "Improved localizadon of cortical activity by combining eeg and meg with mri cortical surface reconstruction: a linear approach," *Journal of cognitive neuroscience*, vol. 5, no. 2, pp. 162–176, 1993.

[98] M. F. Rushworth, M. Krams, y R. E. Passingham, "The attentional role of the left parietal cortex: the distinct lateralization and localization of motor attention in the human brain," *Journal of cognitive neuroscience*, vol. 13, no. 5, pp. 698–710, 2001.

[99] Y. Hirano, S. Hirano, T. Maekawa, C. Obayashi, N. Oribe, A. Monji, K. Kasai, S. Kanba, y T. Onitsuka, "Auditory gating deficit to human voices in schizophrenia: a meg study," *Schizophrenia research*, vol. 117, no. 1, pp. 61–67, 2010.

[100] A. Ihara, Q. Wei, A. Matani, N. Fujimaki, H. Yagura, T. Nogai, H. Umehara, y T. Murata, "Language comprehension dependent on emotional context: A magnetoencephalography study," *Neuroscience research*, vol. 72, no. 1, pp. 50–58, 2012.

[101] A. P. Georgopoulos, E. Karageorgiou, A. C. Leuthold, S. M. Lewis, J. K. Lynch, A. A. Alonso, Z. Aslam, A. F. Carpenter, A. Georgopoulos, L. S.

Hemmy *et al.*, "Synchronous neural interactions assessed by magnetoencephalography: a functional biomarker for brain disorders." *Journal of neural engineering*, vol. 4, no. 4, p. 349, 2007.

[102] P. Olejniczak, "Neurophysiologic basis of eeg," *Journal of clinical neurophysiology*, vol. 23, no. 3, pp. 186–189, 2006.

[103] M. Teplan, "Fundamentals of eeg measurement," *Measurement science review*, vol. 2, no. 2, pp. 1–11, 2002.

[104] A. Schnitzler, S. Salenius, R. Salmelin, V. Jousmäki, y R. Hari, "Involvement of primary motor cortex in motor imagery: a neuromagnetic study," *Neuroimage*, vol. 6, no. 3, pp. 201–208, 1997.

[105] E. Hortal, A. Úbeda, E. Iáñez, y J. M. Azorín, "Control of a 2 dof robot using a brain–machine interface," *Computer methods and programs in biomedicine*, vol. 116, no. 2, pp. 169–176, 2014.

[106] E. Hortal, D. Planelles, Á. Costa, E. Iáñez, A. Ubeda, J. M. Azorín, y E. Fernández, "Svm-based brain–machine interface for controlling a robot arm through four mental tasks," *Neurocomputing*, vol. 151, pp. 116–121, 2015.

[107] C. Neuper, G. R. Müller-Putz, R. Scherer, y G. Pfurtscheller, "Motor imagery and eeg-based control of spelling devices and neuroprostheses," *Progress in brain research*, vol. 159, pp. 393–409, 2006.

[108] R. Salazar-Varas, Á. Costa, E. Iáñez, A. Úbeda, E. Hortal, y J. Azorín, "Analyzing eeg signals to detect unexpected obstacles during walking," *Journal of neuroengineering and rehabilitation*, vol. 12, no. 1, p. 1, 2015.

[109] D. Planelles, E. Hortal, Á. Costa, A. Úbeda, E. Iáñez, y J. M. Azorín, "Evaluating classifiers to detect arm movement intention from eeg signals," *Sensors*, vol. 14, no. 10, pp. 18 172–18 186, 2014.

[110] M. M. Sohlberg y C. A. Mateer, "Cognitive rehabilitation: An integrative neuropsychological approach," 2001.

[111] T. P. Tinius y K. A. Tinius, "Changes after eeg biofeedback and cognitive retraining in adults with mild traumatic brain injury and attention deficit hyperactivity disorder," *Journal of Neurotherapy*, vol. 4, no. 2, pp. 27–44, 2000.

[112] N. H. Engelberts, M. Klein, H. J. Adèr, J. J. Heimans, D. G. Trenité, y H. M. Van der Ploeg, "The effectiveness of cognitive rehabilitation for attention deficits in focal seizures: a randomized controlled study," *Epilepsia*, vol. 43, no. 6, pp. 587–595, 2002.

[113] E. Başar, C. Başar-Eroglu, S. Karakaş, y M. Schürmann, "Gamma, alpha, delta, and theta oscillations govern cognitive processes," *International journal of psychophysiology*, vol. 39, no. 2, pp. 241–248, 2001.

[114] F. Di Russo, A. Martínez, M. I. Sereno, S. Pitzalis, y S. A. Hillyard, "Cortical sources of the early components of the visual evoked potential," *Human brain mapping*, vol. 15, no. 2, pp. 95–111, 2002.

[115] G. R. Müller-Putz, R. Scherer, C. Brauneis, y G. Pfurtscheller, "Steady-state visual evoked potential (ssvep)-based communication: impact of harmonic frequency components." *Journal of neural engineering*, vol. 2, no. 4, pp. 123–130, 2005.

[116] G. Plourde, "Auditory evoked potentials," *Best Practice & Research Clinical Anaesthesiology*, vol. 20, no. 1, pp. 129–139, 2006.

[117] A. Starr, "Long latency event-related components of the auditory evoked potential in dementia," *Brain*, vol. 101, p. 648, 1978.

[118] T. Picton y S. Hillyard, "Human auditory evoked potentials. ii: Effects of attention," *Electroencephalography and clinical neurophysiology*, vol. 36, pp. 191–200, 1974.

[119] J. Polich y A. Kok, "Cognitive and biological determinants of p300: an integrative review," *Biological psychology*, vol. 41, no. 2, pp. 103–146, 1995.

[120] M. Eimer, "The n2pc component as an indicator of attentional selectivity," *Electroencephalography and clinical neurophysiology*, vol. 99, no. 3, pp. 225–234, 1996.

[121] P. W. Ferrez *et al.*, "Error-related eeg potentials generated during simulated brain–computer interaction," *Biomedical Engineering, IEEE Transactions on*, vol. 55, no. 3, pp. 923–929, 2008.

[122] J. C. Corby y B. S. Kopell, "Differential contributions of blinks and vertical eye movements as artifacts in eeg recording," *Psychophysiology*, vol. 9, no. 6, pp. 640–644, 1972.

[123] T. Elbert, W. Lutzenberger, B. Rockstroh, y N. Birbaumer, "Removal of ocular artifacts from the eega biophysical approach to the eog," *Electroencephalography and clinical neurophysiology*, vol. 60, no. 5, pp. 455–463, 1985.

[124] I. I. Goncharova, D. J. McFarland, T. M. Vaughan, y J. R. Wolpaw, "Emg contamination of eeg: spectral and topographical characteristics," *Clinical Neurophysiology*, vol. 114, no. 9, pp. 1580–1593, 2003.

[125] A. Achaibou, G. Pourtois, S. Schwartz, y P. Vuilleumier, "Simultaneous recording of eeg and facial muscle reactions during spontaneous emotional mimicry," *Neuropsychologia*, vol. 46, no. 4, pp. 1104–1113, 2008.

[126] J. Woestenburg, M. Verbaten, y J. Slangen, "The removal of the eye-movement artifact from the eeg by regression analysis in the frequency domain," *Biological psychology*, vol. 16, no. 1, pp. 127–147, 1983.

[127] T. P. Jung, C. Humphries, T.-W. Lee, S. Makeig, M. J. McKeown, V. Iragui, T. J. Sejnowski *et al.*, "Extended ica removes artifacts from electroencephalographic recordings," *Advances in neural information processing systems*, pp. 894–900, 1998.

[128] U. Mitzdorf, "Current source-density method and application in cat cerebral cortex: investigation of evoked potentials and eeg phenomena," *Physiological reviews*, vol. 65, no. 1, pp. 37–100, 1985.

[129] M. Severens, B. Nienhuis, P. Desain, y J. Duysens, "Feasibility of measuring event related desynchronization with electroencephalography during walking," *Engineering in Medicine and Biology Society (EMBC), 2012 Annual International Conference of the IEEE*, pp. 2764–2767, 2012.

[130] T. Castermans, M. Duvinage, G. Cheron, y T. Dutoit, "About the cortical origin of the low-delta and high-gamma rhythms observed in eeg signals during treadmill walking," *Neuroscience letters*, vol. 561, pp. 166–170, 2014.

[131] Á. Costa, R. Salazar-Varas, A. Úbeda, y J. M. Azorín, "Characterization of artifacts produced by gel displacement on non-invasive brain-machine interfaces during ambulation," *Frontiers in neuroscience*, vol. 10, pp. 1–14, 2016.

[132] J. T. Gwin, K. Gramann, S. Makeig, y D. P. Ferris, "Removal of movement artifact from high-density eeg recorded during walking and running," *Journal of neurophysiology*, vol. 103, no. 6, pp. 3526–3534, 2010.

[133] J. T. Gwin, K. Gramann, S. Makeig, y D. Ferris, "Electrocortical activity is coupled to gait cycle phase during treadmill walking," *Neuroimage*, vol. 54, no. 2, pp. 1289–1296, 2011.

[134] Á. Costa, E. Hortal, E. Iáñez, y J. M. Azorín, "A supplementary system for a brain-machine interface based on jaw artifacts for the bidimensional control of a robotic arm," *PloS one*, vol. 9, no. 11, p. e112352, 2014.

[135] E. Hortal, E. Iáñez, A. Úbeda, D. Planelles, A. Costa, y J. M. Azorín, "Selection of the best mental tasks for a svm-based bci system," *Systems, Man and Cybernetics (SMC), 2014 IEEE International Conference on*, pp. 1483–1488, 2014.

[136] E. Iáñez, J. M. Azorín, A. Úbeda, J. M. Ferrández, y E. Fernández, "Mental tasks-based brain–robot interface," *Robotics and Autonomous Systems*, vol. 58, no. 12, pp. 1238–1245, 2010.

[137] I. Barrodale y R. Erickson, "Algorithms for least-squares linear prediction and maximum entropy spectral analysis-part i: Theory," *Geophysics*, vol. 45, no. 3, pp. 420–432, 1980.

[138] E. Iánez, J. Azorín, E. Fernández, y R. Morales, "Electrooculography-based human interface for robot controlling," *Proceedings of the 13th Annual Conference of the International Functional Electrical Stimulation Society (IFESS), York, Walter de Gruyter-Berlin-New, Freiburg, Germany*, vol. 53, pp. 305–307, 2008.

[139] Á. Costa, E. Iáñez, A. Úbeda, D. Planelles, E. Hortal, y J. Azorín, "Experimental setup and first results of a bci system for attention levels classification during gait," *International Conference on Autonomous Intelligent Systems, Workshop Proceedings of (IAS-13)*, pp. 470–473, 2014.

[140] Á. Costa, E. Iáñez, A. Úbeda, E. Hortal, A. J. Del-Ama, Á. Gil-Agudo, y J. M. Azorín, "Decoding the attentional demands of gait through eeg gamma band features," *PLoS one*, vol. 11, no. 4, p. e0154136, 2016.

UNIVERSITAS
Miguel
Hernández

Apéndice A

MATERIAL Y EQUIPOS

UNIVERSITAS
Miguel
Hernández

A.1. Equipo de adquisición EEG: gTec

El g.USBAmp (Figura A.1e) es un sistema de adquisicion/procesamiento y amplificación de bioseñales de alto rendimiento y precisión comercializado por *g.tec medical engineering*. Este equipo permite la adquisición de multiples tipos de señales como encefalográficas, cardiacas, musculares, electrooculares y respiratorias entre otros muchos parámetros fisiológicos y físicos. Este amplificador permite la adquisición simultánea de 16 canales. Cada uno de estos canales puede tener una frecuencia de muestreo de hasta 38.400 Hz con una resolución de 24 bits. Las señales adquiridas tienen un rango de voltaje de $\pm$ 250 mV, con una resolución inferior a 30 nV. Internamente, el equipo dispone de filtros hardware paso banda y notch configurables.

El resto de los componentes utilizados para la adquisición de las señales EEG son los siguientes:

- g.GAMMAbox (Figura A.1f): caja de preamplificacón para los 16 canales. Hace de interfaz entre el amplificador g.USBAmp y los electrodos.
- g.GAMMAconnector (Figure A.1g): cable de conexión entre el amplificador g.USBAmp y la caja de interfaz g.GAMMAbox. Tiene una longitud de unos 40 cm.
- g.GAMMAcap (Figura A.1a): gorro con corte optimizado para un ajuste perfecto, costuras flexibles para la colocación de electrodos de alta densidad, etiquetado con 74 posiciones estándar (siguiendo el sistema internacional 10-10 o 10-20 extendido) además de 86 posiciones intermedias adicionales. Se puede utilizar tanto con un conjunto de correas en el pecho como con una correa de la barbilla.
- g.LADYbird (Figura A.1b): electrodo de anillo activo que se puede utilizar con g.GAMMAcap (para señales EEG) o con una arandela adhesiva (para ECG, EMG, EOG). Está formado por una corona sintetizada de Ag/AgCl, con una longitud de 125 cm y conector de seguridad de 2 pines.
- g.LADYbirdGND (Figura A.1c): electrodo de anillo pasivo para conexión de tierra. Al igual que el electrodo g.LADYbird se puede utilizar con g.GAMMAcap

(EEG) o con la arandela adhesiva (ECG, EMG, EOG). El resto de características también son idénticas a estos electrodos pero de color amarillo.

- g.GAMMAearclip Ag/AgCl (Figure A.1d): pinza para sujeción en la oreja con conector de seguridad de dos polos. Al igual que los electrodos anteriores, está formado por una corona sintetizada de Ag/AgCl, con una longitud de 125 cm.

- Tierra ESD (Figura A.1e): pulsera antiestática que permite conectar la muñeca de un usuario a la tierra del g.USBamp.

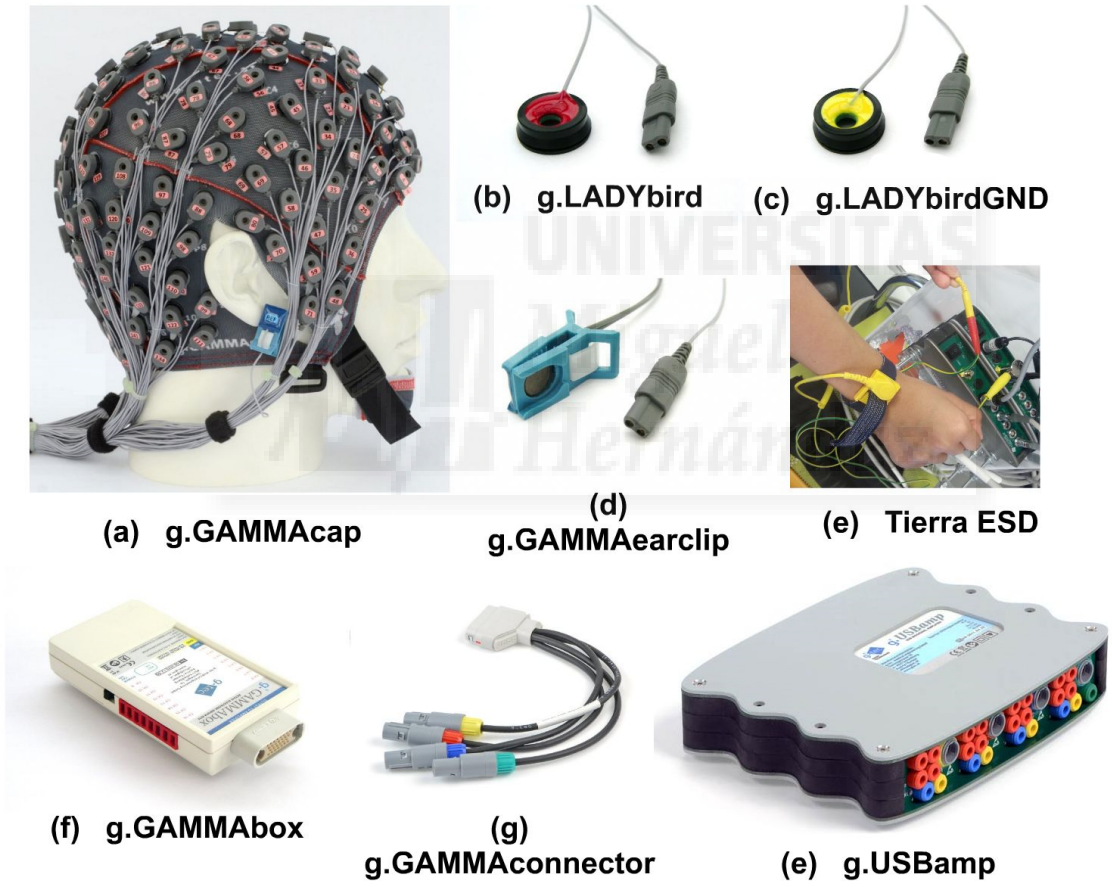

Figura A.1: Equipo de registro EEG de g.Tec.

A.2. Robot industrial: Fanuc

El Fanuc LR Mate 200iB (ver Figura A.2a) es un robot industrial de seis ejes fabricado por Fanuc Robotics. Se trata de un robot de construccin modular impulsado por servos eléctricos. Es un robot para montaje en mesa diseñado para una amplia variedad de procesos de fabricación y está diseñado para proporcionar la máxima flexibilidad y precisión con un diseño compacto. Este sistema dispone de la consola de control manual Teach Pendant A05B-2301-C301 (ver Figura A.2b) así como de unas librerías de C para la programación de rutinas por software.

Entre sus aplicaciones se pueden destacar el manejo de materiales, procesos de carga y descarga, electrónica y sala blanca, tareas de limpieza de piezas, montaje/ensamblado o extracción de material. Sus características principales son la velocidad de 480° por segundo de sus ejes, su conector de efector final integrado en la muñeca, frenos a prueba de fallos, servomotores sin escobillas AC para minimizar el mantenimiento del motor, rodamientos y unidades selladas y motores y cableado ubicados internamente para la protección del medio ambiente. Además, el sistema cumple con el estándar IP65 para evitar el daño por polvo y líquidos.

(a) Fanuc LR Mate 200iB

(b) Teach Pendant A05B-2301-C301

Figura A.2: Robot industrial Fanuc LR Mate 200iB.

A.3. Cinta de correr: Proform Performance 750

Esta cinta (ver figura A.3) dispone de un potente motor que permite un movimiento constante y suave. Puede alcanzar una velocidad punta de 18 Km/h en incrementos de 0.1 Km/h. Permite un cambio rápido de velocidad desde la consola mediante la pulsación de un botón y sin interrumpir el movimiento. Además hace posible el cambio de inclinación durante el movimiento, entre 0 y 10 % con intervalos de 1 %. Dispone de una superficie antideslizante de carrera de 51 cm x 140 cm.

Figura A.3: Cinta de correr Pro-form Performance 750.

UNIVERSITAS
Miguel
Hernández

Apéndice B

PUBLICACIONES EN REVISTA

B.1. Publicación 1

OPEN ACCESS Freely available online

PLOS ONE

A Supplementary System for a Brain-Machine Interface Based on Jaw Artifacts for the Bidimensional Control of a Robotic Arm

Álvaro Costa*, Enrique Hortal, Eduardo Iáñez, José M. Azorín

Brain-Machine Interface Systems Lab, Miguel Hernández University, Elche, Spain

Abstract

Non-invasive Brain-Machine Interfaces (BMIs) are being used more and more these days to design systems focused on helping people with motor disabilities. Spontaneous BMIs translate user's brain signals into commands to control devices. On these systems, by and large, 2 different mental tasks can be detected with enough accuracy. However, a large training time is required and the system needs to be adjusted on each session. This paper presents a supplementary system that employs BMI sensors, allowing the use of 2 systems (the BMI system and the supplementary system) with the same data acquisition device. This supplementary system is designed to control a robotic arm in two dimensions using electromyographical (EMG) signals extracted from the electroencephalographical (EEG) recordings. These signals are voluntarily produced by users clenching their jaws. EEG signals (with EMG contributions) were registered and analyzed to obtain the electrodes and the range of frequencies which provide the best classification results for 5 different clenching tasks. A training stage, based on the 2-dimensional control of a cursor, was designed and used by the volunteers to get used to this control. Afterwards, the control was extrapolated to a robotic arm in a 2-dimensional workspace. Although the training performed by volunteers requires 70 minutes, the final results suggest that in a shorter period of time (45 min), users should be able to control the robotic arm in 2 dimensions with their jaws. The designed system is compared with a similar 2-dimensional system based on spontaneous BMIs, and our system shows faster and more accurate performance. This is due to the nature of the control signals. Brain potentials are much more difficult to control than the electromyographical signals produced by jaw clenches. Additionally, the presented system also shows an improvement in the results compared with an electrooculographic system in a similar environment.

Citation: Costa Á, Hortal E, Iáñez E, Azorín JM (2014) A Supplementary System for a Brain-Machine Interface Based on Jaw Artifacts for the Bidimensional Control of a Robotic Arm. PLoS ONE 9(11): e112352. doi:10.1371/journal.pone.0112352

Editor: Mikhail A. Lebedev, Duke University, United States of America

Received June 19, 2014; **Accepted** October 5, 2014; **Published** November 12, 2014

Data Availability: The authors confirm that all data underlying the findings are fully available without restriction. All relevant data are within the paper and its Supporting Information files.

Funding: This research has been funded by the Commission of the European Union under the BioMot project - Smart Wearable Robots with Bioinspired Sensory-Motor Skills (Grant Agreement number IFP7-ICT- 2013-10-611695). The funders had no role in study design, data collection and analysis, decision to publish, or preparation of the manuscript.

Competing Interests: The authors have declared that no competing interests exist.

* Email: acosta@umh.es

Introduction

In our society there is an increasing concern about helping and assisting people who suffer from motor disabilities. Emerging from this concern, each day, different areas of research are focusing their efforts on developing Human-Machine systems to help people suffering from these conditions [1,2]. Brain-Machine Interfaces (BMIs) are a clear example of these systems. Depending on the nature of the neural phenomenons analyzed, these systems can be classified as evoked or spontaneous. On the one hand, spontaneous BMIs study those brainwaves that can be voluntarily controlled by a subject. To achieve this control it is usually necessary to have a training period during which the users learn how to control their brain potentials. On the other hand, evoked BMIs rely on the analysis of brain potentials that cannot be controlled by the users. These potentials appear in response to a external stimulus like flashlights or sounds among others [3,4]. Spontaneous systems are usually focused on generating commands to control a device taking advantage of the users capability to control their EEG signals [5–7]. Regarding evoked systems, there are studies focused on generating control commands [8,9] and also on the evaluation of the brain response to different external stimulus with diagnosis purposes [10–12]. Besides, BMIs (both spontaneous and evoked) are used on other topics in the field of human health, such as the measurement of the mental state of a patient (workload, attention level, emotional state,...) [13] or as support systems on rehabilitation processes [14].

BMI systems can also be divided into two big groups depending on the invasion level needed to register signals. Invasive BMI systems register signals directly from the brain using electrodes implanted inside the cortex [15,16]. This method provides an excellent signal to noise ratio because the electrodes used are placed much closer to the source of the electrical signals. However, their use is limited due to the risk and ethical questions associated to the surgery needed to implant the electrodes under the scalp. On the other hand, for non-invasive BMIs, surgery is not needed. Instead, a set of electrodes is placed over the scalp in order to register the EEG signals. Nowadays, there are many studies

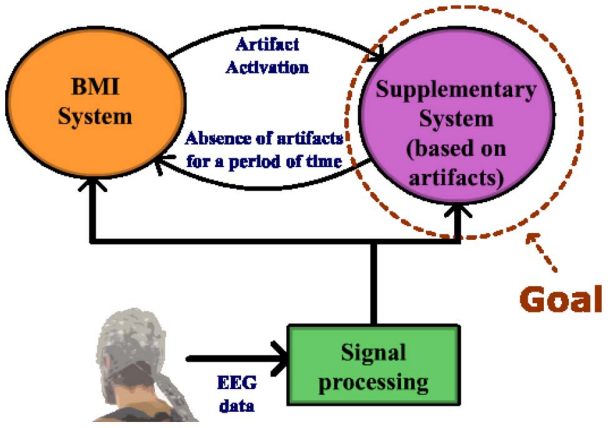

Figure 1. Block interconnection diagram. EEG data from the scalp is acquired, processed and classified in real time. The classification results are used as control commands for 2 different systems. The Supplementary System block is the main goal of the present work. It should be activated and controlled with EMG signals registered from a BMI set of electrodes. If no EMG signals are detected in the EEG data, the BMI system is used. When the user wants to use the Supplementary System, he/she has to generate an EMG signal.
doi:10.1371/journal.pone.0112352.g001

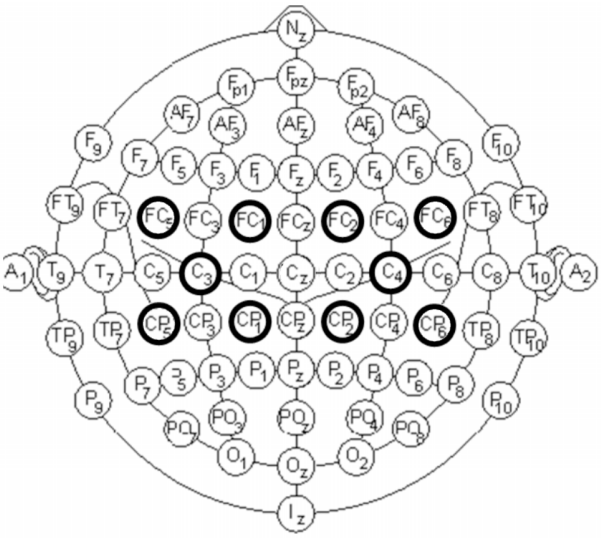

Figure 2. Electrode distribution. FC5, FC1, FC2, FC6, C3, C4, CP5, CP1, CP2 and CP6 (darker circles) according to the International 10/10 System.
doi:10.1371/journal.pone.0112352.g002

focused on helping people with motor diseases based on non-invasive BMI systems, like [17–19]. The main disadvantage of non-invasive BMI systems is the quality of the registered signals. Due to volume conduction which is defined as the property, associated to biological tissues, of transmiting electric and magnetic fields from an electric primary source current, the scalp filters electric signals from the brain and there is mixing of signals from different sources. This makes difficult to isolate the signals produced in a single brain area. Due to the localization of those electrodes, EEG signals are also contaminated by several noise sources produced by other physiological factors like blood pressure, skin tension, muscular and ocular movements, etc. All of these unwanted signals are considered artifacts when the goal of the study is to evaluate how EEG signals behave. For that reason, on non-invasive systems, the signal to noise ratio is a critical factor and detecting and filtering artifacts is a fundamental part of the data analysis [20–22].

Some signals (usually considered artifacts on BMI systems) can be controlled by users, like those produced by voluntary movements of the eyes (electrooculographic (EOG)) and muscles (electromyographic (EMG)). In this work, the use of EMG signals generated voluntarily by subjects is proposed in order to implement a supplementary system for a BMI. The architecture that appears in Figure 1 shows how this system and the BMI system will coexist. The main advantage of this architecture is that they share the same set of EEG electrodes, instead of including EMG electrodes or other sensors.

The supplementary system proposed uses EMG signals (extracted from the EEG signals of the BMI), which are generated by the users clenching their jaws, in order to control the 2-dimensional movement of a robotic arm. These clench signals affect a wide range of frequencies (1–128 Hz) according to [23]. For that reason is not possible to use this system simultaneously with a BMI system. However, it is possible to freely alternate between both systems (non-simultaneous control). The proposed system, controlled voluntarily by the user as in a spontaneous BMI, has a decreased training time, improved classifier stability and accuracy, and an increased number of the detected tasks. Since this system allows users a better control of a device, it could be used as a complement for a BMI focused on solving other problems also related with the improvement of the quality of life of people with disabilities. For example, internet browsers based on evoked potentials [24] can be complemented with the supplementary system described on this article. Thus the evoked BMI could be used to write text in the browser, while our system could be used to control the cursor.

Materials and Methods

Data Acquisition

EEG signals are acquired using an amplifier (g.USBamp, g.Tec, GmbH, Austria) with active electrodes to increase their signal/noise ratio by introducing a pre-amplification stage (g.GAMMAbox, g.Tec, GmbH, Austria). The acquisition of EEG signals is done using 10 electrodes placed over the scalp with the following distribution: FC5, FC1, FC2, FC6, C3, C4, CP5, CP1, CP2 and CP6 (see Figure 2) according to the International 10/10 System, with a monoauricular reference in the right earlobe and ground in AFz. Information is digitalized at 1200 Hz. A bandpass filter from 0.1 to 100 Hz has been applied. Also, a 50 Hz Notch filter to remove the power line interference is used. Finally, all the data are sent to a computer system where the processing and classification algorithms are applied. Figure 3 shows an image of the equipment used for the EEG recordings. Electrodes C3 and C4 are the main goal of our analysis. Their readings show the best classification results compared to the other electrodes analyzed. These electrodes are also associated with the sensorimotor areas where right and left motor imagery tasks are detected. The other electrodes shown in Figure 2 (FC5, FC1, FC2, FC6, CP5, CP1, CP2, CP6) are used in the processing stage to remove their power contribution from electrodes C3 and C4.

Data analysis

The signals are processed in real time as in [25]. To do that, the time between data windows must be small enough for the algorithm to provide feedback to the user in real time. Also, the

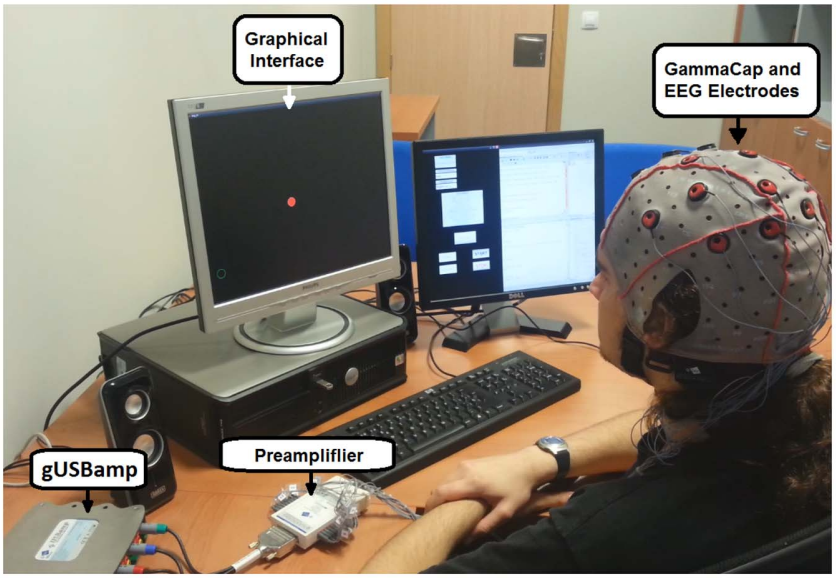

Figure 3. Equipment. Amplifier and GammaCap from g.Tec are used to register EEG Signals. Data are processed and classified in the computer, which is also used to provide visual feedback to the user.
doi:10.1371/journal.pone.0112352.g003

window length should not be too long to avoid delays in the feedback. Every 50 ms a data window of 400 ms is stored, resulting in a 350 ms overlap between the windows. This overlap increases the stability of the classification results by using the information of previous data windows. Then, a four nearest neighbor Laplacian algorithm [26] is applied to the temporal data from electrodes C3 and C4. This algorithm uses the information received from the four nearest electrodes of C3 and C4 and their distances from them in order to reduce the unwanted signal contribution that these electrodes have on C3 and C4. The result is a smoother time signal where the main contribution comes from the electrode of interest. The Laplacian is computed according to the formula,

$$V_i^{LAP} = V_i^{CR} - \sum_{j \epsilon S_i} g_{ij} V_j^{CR} \quad (1)$$

where V_i^{LAP} is the result of applying this algorithm to the electrode i, V_i^{CR} is the electrode i signal before the transformation and,

$$g_{ij} = \frac{\frac{1}{d_{ij}}}{\sum_{j \epsilon S_i} \frac{1}{d_{ij}}} \quad (2)$$

where S_i is the set of electrodes that surround electrode i and d_{ij} is the distance between i and j electrodes.

Then, the power spectral density of the Laplacian waveforms is computed through the maximum entropy method (MEM) [27]. To differentiate between left and right clenches a frequency analysis is made. For each frequency from 1 to 100 hz, the power spectral density (PSD) of electrodes C3 and C4 is calculated. The difference between these 2 values (C4-C3) is computed when the user clenches the left side of the jaw (C4-C3)L and when the clench is produced on the right side (C4-C3)R. After that, the difference (C4-C3)L - (C4-C3)R is calculated and represented on Figure 4. This initial analysis shows that most differences in the signal power for left and right clenches were present between 57 and 77 Hz and for algorithm only the integral of power spectrum between 57 and 77 Hz was calculated.

Classification

We have developed a classifier based on the application of different thresholds. First of all, each incoming feature is stored in the first position of a 10 position vector (at first filled with zeros) and the rest of the vector is shifted so the oldest value is lost. Every 50 ms, when a new data window (400 ms length with 350 ms overlap with the previous window) arrives, the average of this vector is compared with four thresholds in order to classify the signals. Five tasks have been established according to the power levels received from this average. Each task is associated with a jaw area and the level of clench pressure, and they are defined as follows:

- HardR: Hard right clench
- SoftR: Soft right clench
- Relax: Not clenching
- SoftL: Soft left clench
- HardL: Hard left clench

These tasks are classified through the comparison of 4 thresholds defined as HRthr, SRthr, SLthr and HLthr. Horizontal lines on Figure 5 show a representation of these thresholds, and the areas represent the 5 possible tasks. In Figure 6, PSD levels of tasks SoftR, Relax and SoftL are shown. The central graph shows two vectors of the classifier input from a subject who is not clenching the jaw (Relax). The right and left graphs display the waveforms caused by clenching right and left jaw areas respectively (SoftR and SoftL). This analysis shows that PSD levels from electrode C3 are higher than PSD levels from C4 when the clenching occurs on the left side of the jaw. In a similar way, C4 levels become dominant when clenching is produced on the right side. On the relax task, the PSD from C3 and C4 are similar so the absolute value of the factor C4-C3 is considerably lower. The absolute value of C4-C3 becomes higher when the clench pressure is higher. If the subjects clench the jaw in such a way that the thresholds HRthr or HLthr are exceeded, tasks HardR and

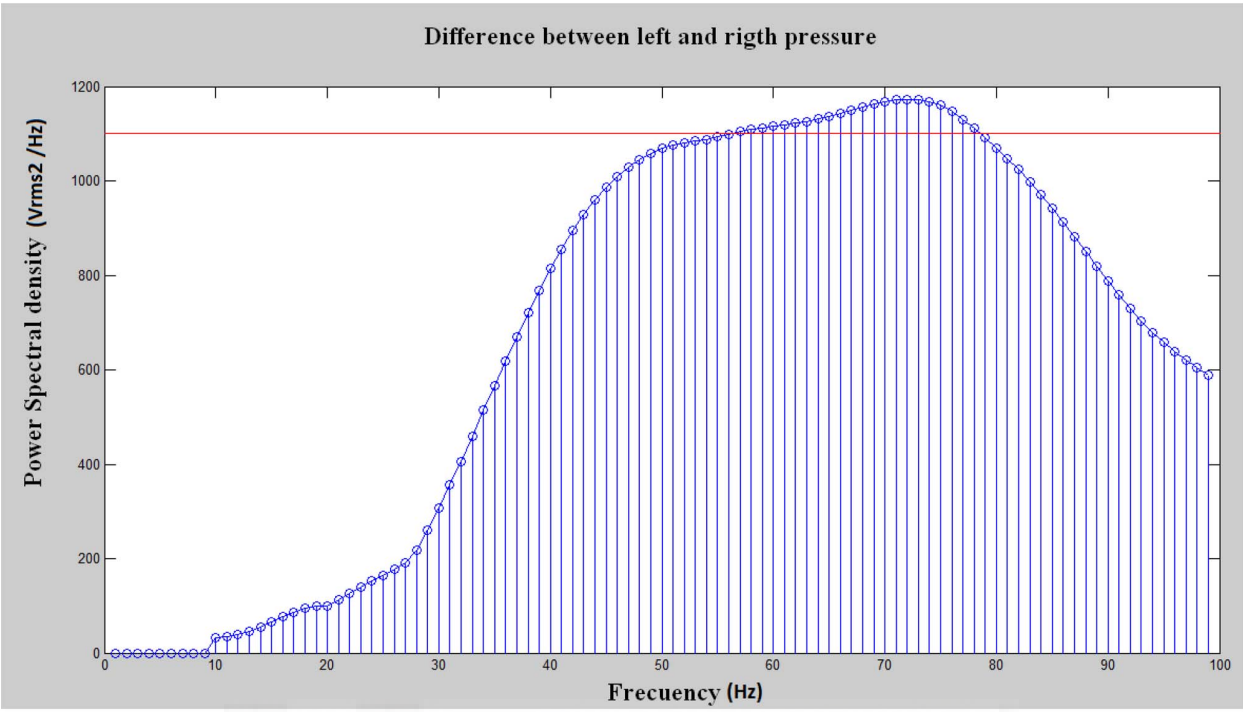

Figure 4. Frequency analysis results. The blue line represent the average Power Spectral Density(PSD) difference between electrodes C3 and C4 for each frequency. The red line represents the minimum spectral level required for a frequency to be target of analysis. These results were obtained from the user 2 (system developer) and compared with the other 3 volunteers to confirm that the optimum range of frequencies does not experience huge changes between users.
doi:10.1371/journal.pone.0112352.g004

HardL (depending on the jaw side) are detected. If the subjects clench the jaw in such a way that the thresholds SRthr or SLthr are exceeded without reaching HRthr or HLthr, tasks SoftR or SoftL are detected depending, again, on the jaw area where the clench is produced. Finally, if the subject is not clenching his/her jaw, no threshold is exceeded and the relax task is detected.

User Training

In order to learn how to control the 2-dimensional movement of a cursor on a screen, two graphical interfaces and a three steps training program have been defined. Training steps 1 and 2 use the first graphical interface, while training step 3 uses the second one. Real time data are processed during all three steps and the interfaces provide visual feedback to the users. This way, the users know how the training is progressing in order to improve their results by adapting the way they clench the jaw. In next section, both graphical interfaces are described. The model used through the training is further described on the section Training Steps.

Graphical Interfaces. Two graphical interfaces are designed. Both of them show a red cursor with a diameter of 25 pixels (about 1.2 cm with a screen size of 38.5×33 cm). The 2-dimensional movement of this cursor is controlled by the user. Depending on the interface, training step and task, the feedback will be different. This is properly explained on each training step on the section Training Steps.

First Interface. This interface is shown on Figure 7. A white cross is shown for 3 seconds on the screen. During this time, the user rests. Afterwards, an image is shown for 2 seconds to indicate the required task to the user. During these seconds, the user is asked to start performing the task. Finally, a red cursor appears on the screen for 10 seconds. This cursor provides feedback of the task detected by making different movements (in this case only left and right movement are used as feedback, which are further explained in the Training Step section). The control of the cursor depends on the training step. Over one run, this sequence is repeated 15 times making each run 4 minutes long. This interface is used to register data of concrete tasks and create a model adapted to each user.

Second Interface. Figure 8 shows how the second interface works. First, a white cursor appears on the screen for 3 seconds. After that, a target appears randomly on the screen and both the target and the white cursor remain on the screen for 2 more seconds. Finally, the cursor starts moving depending on the users commands generated by jaw clenches. The main goal of this interface is to simulate the bidimensional movement of the cursor controlled by the user. To do that, the model defined during the training is used. If the user reaches the target, the cursor becomes white and blinks several times as a reward.

Training Steps. During these three steps, the user is going to gradually learn how to control the two dimensional cursor movement by clenching the jaw. Each step uses one of the graphical interfaces previously described. All data are processed in real time. From the beginning of the training, the interfaces provide visual feedback to the user by generating cursor movements. In order to produce these movements, a model must exist along the three steps. At first, a default model is defined. During the training, this model is modified to be adapted to the signals of each user.

Step 1: Getting used to the clench. The first step starts with the default model (set of thresholds) [10000 100 -100 -10000] (HRthr, SRthr, SLthr and HLthr, respectively from Figure 6). The first graphical interface is used in order to provide visual feedback. The user is asked randomly by the interface to clench softly the

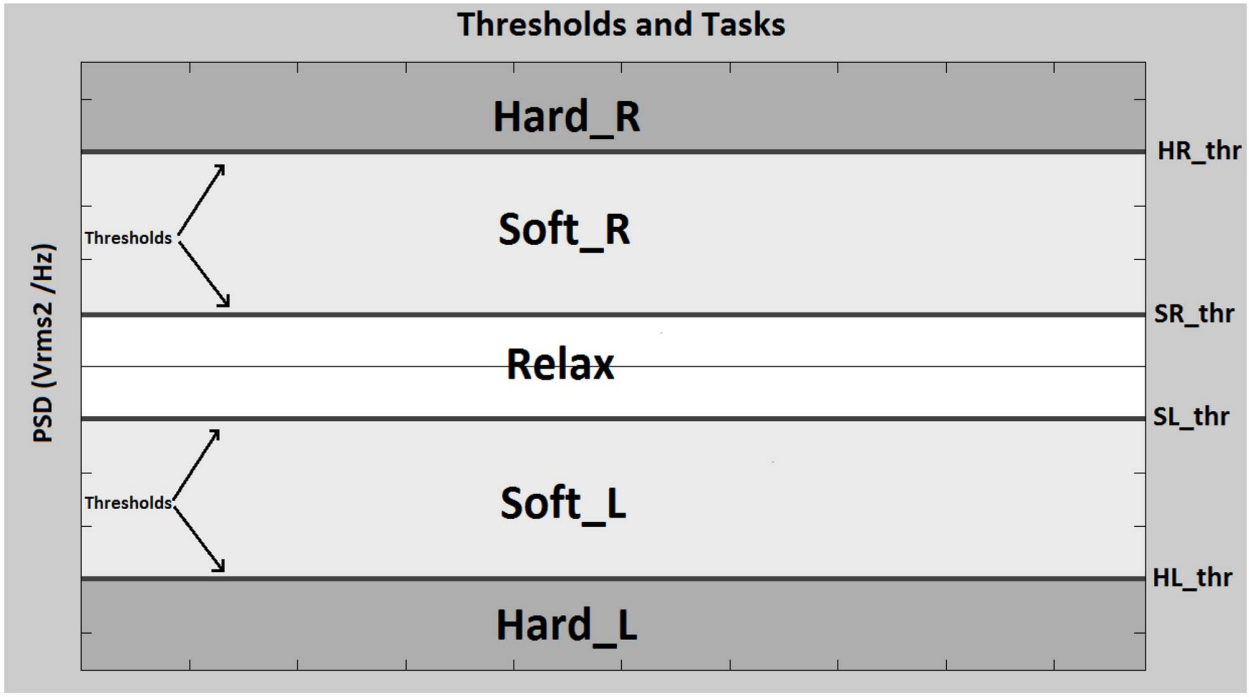

Figure 5. Thresholds and Tasks. Horizontal lines represent the set of thresholds used as model to classify the processed signals. Each threshold represents a level of Power Spectral Density (PSD). Each value on X-axis represents one processed data window. Each data window is classified depending their position on the Y-axis (PSD). Each area delimited by the thresholds represents one of the 5 possible tasks.
doi:10.1371/journal.pone.0112352.g005

right and left jaw areas (tasks SoftR and SoftL). The model is not modified along this step. If the tasks are correctly classified, the red cursor moves right if the clench is produced on the right side, and left if it is produced on the left side. If the clench exceeds thresholds HRthr or HLthr, tasks HardR and HardL are detected and the cursor becomes blue and stops moving. If no threshold is reached, task Relax is detected and the cursor remains red and stopped. During this step, the user gets used to the kind of clench which feels more comfortable with. It has been found that by using this default threshold set, after one 4-minutes run, a user who has never used the system before, is able to control right and left cursor movements. The fact that this default model provides similar results in different users means that the signals do not experience big changes between users.

Step 2: Creating the model. The second step also starts with the default threshold set [10000 100 -100 -10000]. The same interface from step 1 is used but, this time, tasks SoftR, SoftL and Relax are randomly asked. As in step 1, the user has to clench right and left jaw areas softly when tasks SoftR and SoftL are asked (respectively) and keeps the jaw released when the system asks for Relax task. The visual feedback provided by the interface is the same provided in step 1. Tasks SoftR and SoftL move the cursor right and left, respectively, task Relax makes the cursor stop, and tasks HardR and HardL stop the cursor and makes it blue. In this step, after each 10 seconds performed task by the user, a matrix

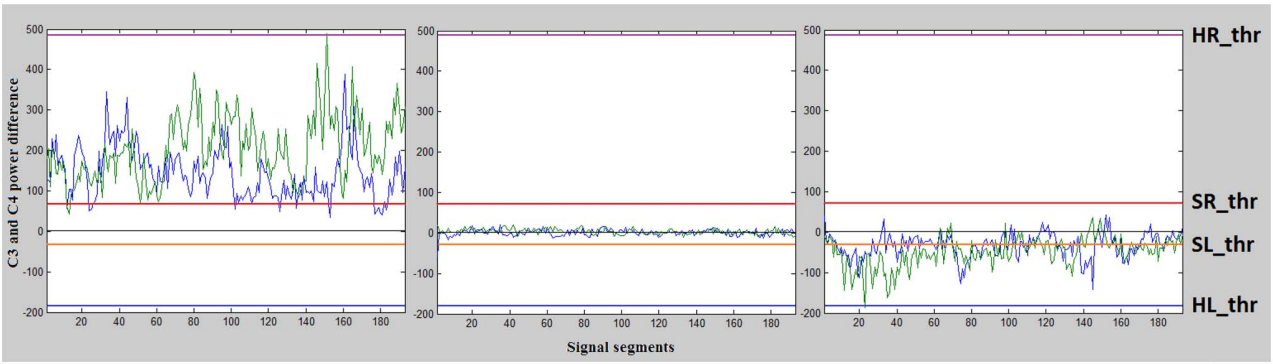

Figure 6. Results obtained for three different tasks during two trials. Signals from the right graph represent two trials (blue and green) where the user clenches the right area of the jaw (SoftR). Signals from the left graph represent two trials where the user clenches the left area of the jaw (SoftL). Signals from the center graph represent two trials where the user releases the jaw (Relax). These signals were recorded from user 2.
doi:10.1371/journal.pone.0112352.g006

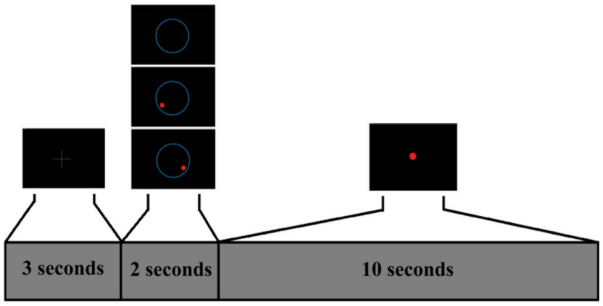

Figure 7. First Interface Protocol. The user is asked to relax during the first 3 seconds, after that, an image appears for 2 seconds to show the task (one of three possible ones) that the user has to perform. For the next 10 seconds, the cursor moves left, right or remains stopped depending on the classified task. After these 10 seconds, the sequence is repeated.
doi:10.1371/journal.pone.0112352.g007

like the one shown in Figure 9 is modified. It is a 3×5 matrix whose rows represent each requested task, while the columns represent the number of classified data windows according to the established set of thresholds (there are three rows because only tasks SoftR, SoftL and Relax are requested while there are five columns because tasks HardR and HardL can be also classified). Each 50 ms a new data window is classified, and the matrix is updated by increasing in one the value of the position indicated by the row requested and the column classified. This way, every 10 seconds it is possible to know which tasks were requested and which tasks were classified by looking at the matrix. According to the amount of wrong classified data windows, thresholds are modified to adjust each task area to the users' skills. If the success rate is 100%, those thresholds that delimit the requested task are reduced by 30%. This way, it is possible to reduce the strength of the clench if the user is able to achieve the same results with softer clenches. Also, reducing the area of the tasks performed could allow the inclusion of new tasks above HardR and below HardL in future works. Otherwise, the thresholds will be increased according to the percentage of misclassified tasks. This process makes threshold values converge to their optimal point. However, this process is endless. Therefore, when thresholds are close to their optimal values, they oscillate around them. After five 4-minutes runs, thresholds reach their oscillation point around their optimal values. The final values are decided by seeing the thresholds evolution and manually selecting them. On Figure 10 this evolution and the final set of thresholds selected are shown for all the users. These final thresholds become the model that best fits the signals produced by each user.

Step 3: 2-dimensional movement. In the last step, the starting model is the one obtained from step 2 and it does not evolve during this training step. This time, the second interface is used. Eight targets (with the same cursor size) are defined in eight fixed positions and they appear randomly during this step. The user is requested to reach them by controlling the movement of a two dimensional cursor before a time limit is reached. A target is successfully reached when there is less that 15 pixels (0.72 cm) on each axis (X and Y) between the cursor and the target position. Figure 11 shows a state machine that describes the behavior of the cursor depending on the tasks performed by the user. The 2-dimensional axes are not simultaneously controlled by the user but he/she is able to alternate between movement axis using HardR and HardL tasks. This axis alternation is represented by the change of the color of the cursor from red to blue and viceversa.

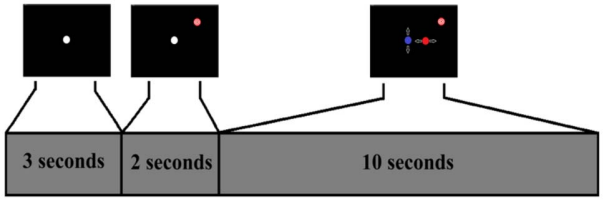

Figure 8. Second Interface Protocol. The user is asked to relax during the first 3 seconds, after that, the user is asked to reach a target. The cursor moves left, right, up, down or remains stopped depending on the classified task until it reaches the target.
doi:10.1371/journal.pone.0112352.g008

When the cursor turns red, the horizontal dimension is controlled and when it becomes blue, the vertical dimension is controlled. Tasks HardR and HardL are achieved by making a strong clench for a short period of time (less than 0.5 seconds, like a quick bite) on right or left areas of the jaw, respectively. The cursor movement is controlled by tasks SoftR and SoftL (right and left, or up and down according to the current selected axis, respectively). Tasks SoftR and SoftL are achieved by clenching softly the respective area of the jaw. Task Relax stops the cursor movement.

During this step, the user gets used to the 2-dimensional movement of the cursor and learns how to control it. Figure 12 shows the signals produced by a user when the two dimensional movement is being controlled. It clearly shows the difference between tasks SoftR, SoftL, HardR and HardL. Eight sessions are performed during this step and in each run, 10 targets appear. The user has 25 seconds to reach each target. Otherwise, the target counts as not reached and a new target appears.

Protocol Summary

Each run is approximately four minutes long, taking one minute break between them. The total training time needed to control the two dimensions with the cursor can be computed as:

- Step 1: One start up run to get used to the kind of jaw movements the system requires.
- Step 2: Five runs where a model is defined for the user (selection of thresholds).
- Step 3: Eight final runs where the user learns how to control the two dimensional movement.

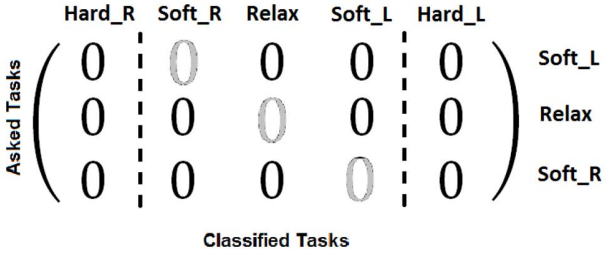

Figure 9. Task classification matrix. Rows represent the tasks requested by the interface and columns represent the tasks classified by the system. Only tasks SoftR, SoftL and Relax are requested while all five tasks (HardR, SoftR, Relax, SoftL and HardL) can be detected. The matrix is initialized with zeros at the beginning of each run and these values are updated with every classification. The thresholds are modified trying to get a diagonal matrix.
doi:10.1371/journal.pone.0112352.g009

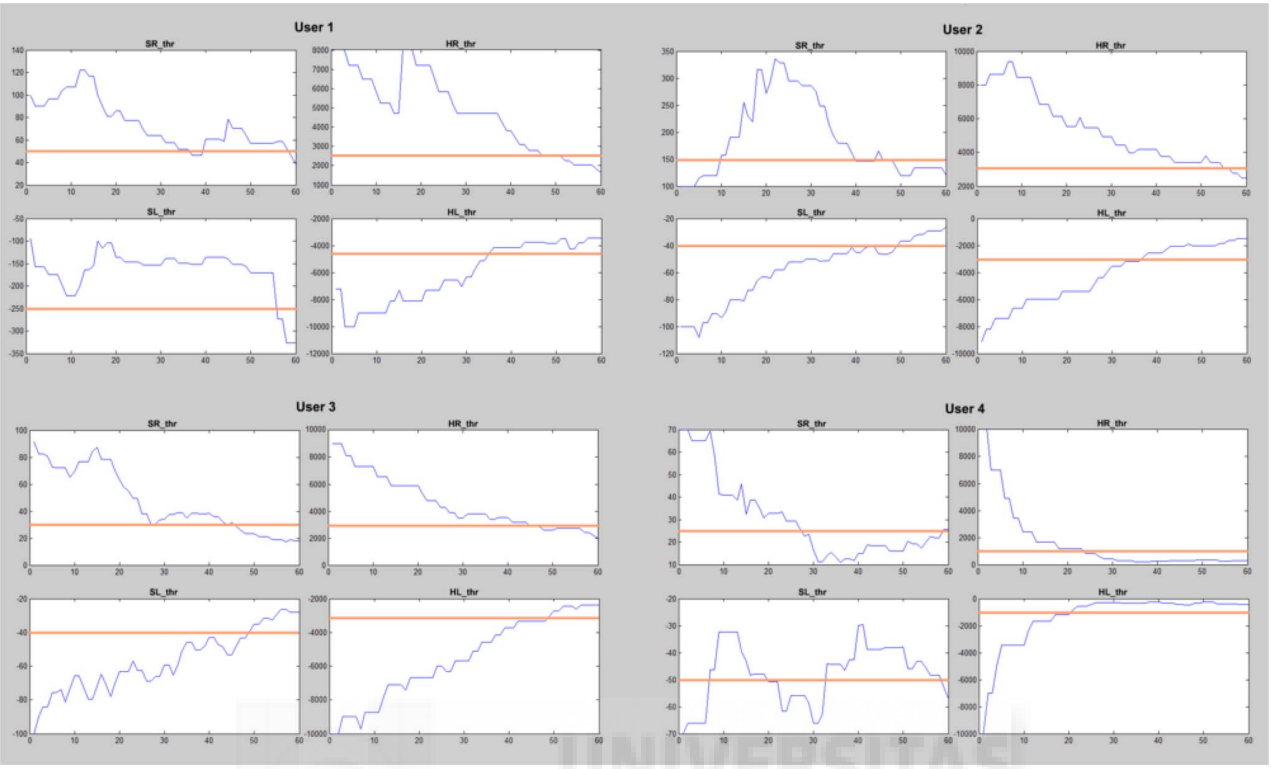

Figure 10. Threshold convergence. The evolution of HRthr, SRthr, SLthr and HLthr are shown for all users. Also the final value selected for each threshold and user is represented with a horizontal line. Y-axis represents the Power Spectral Density and the X-axis represents the number of tasks requested to the user along the 5 runs.
doi:10.1371/journal.pone.0112352.g010

The training process takes approximately 70 minutes. After that, the user has an accurate control of the system and he/she is ready to start controlling the robotic arm as it is shown on the next section.

Robot Control System

After the user is trained in the 2-dimensional control of the cursor, the system is going to be adapted to control the end-effector of a robotic arm on a 2-dimensional plane. Two different

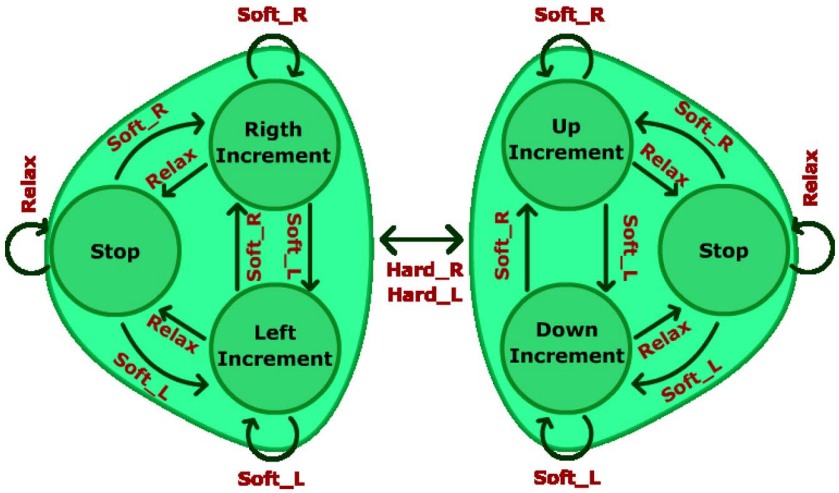

Figure 11. Cursor State Machine. Each group of 3 states represents one of the dimensions. The left group represents the horizontal dimension and the right group represents the vertical dimension. Tasks HardL and HardR are used to alternate between horizontal and vertical dimensions. Once the dimension is selected, tasks SoftR and SoftL control the direction of the movement (on the horizontal dimension, SolfR moves the cursor to the right and SoftL moves the cursor to the left, on the vertical dimension, SoftR moves the cursor up and SoftL moves the cursor down). Relax task stops the cursor no matter the dimension selected.
doi:10.1371/journal.pone.0112352.g011

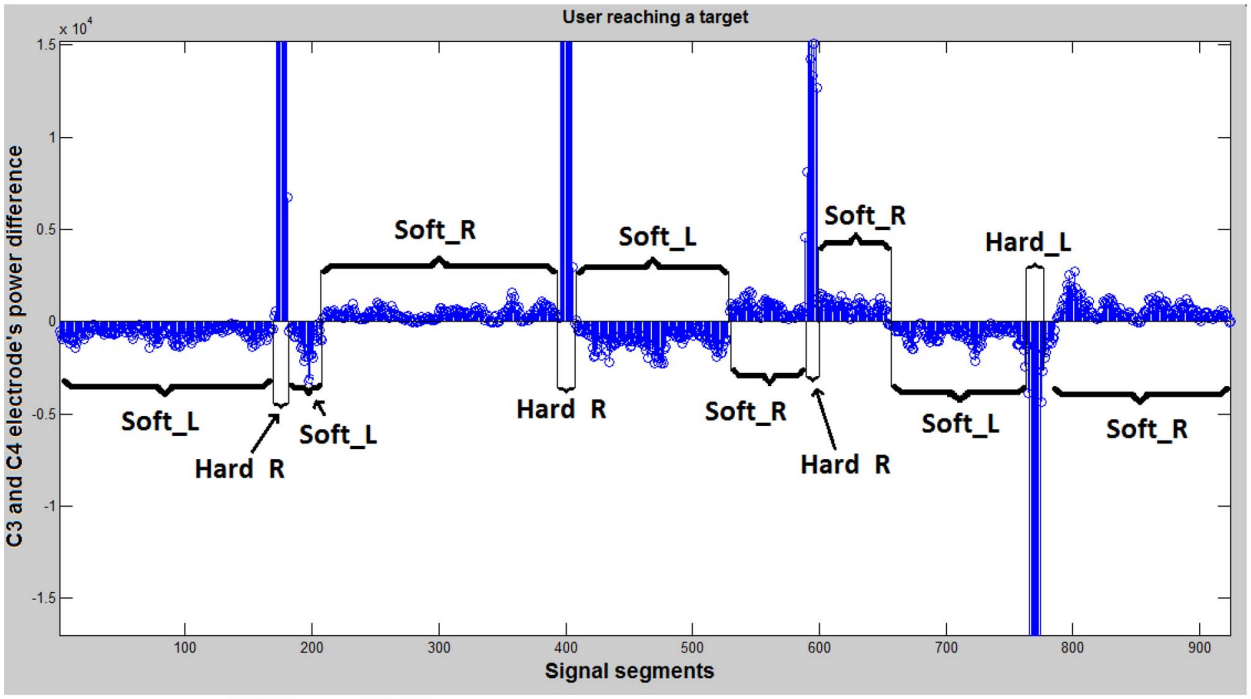

Figure 12. Online results from a user reaching a target (3rd step). SoftR corresponds to the low positive values, SoftL to the low negative values, HardR to the high positive values, and HardL to the high negative values. Relax task is not used (its power level is lower than SoftR and SoftL). Y-axis represents the PSD difference between C3 and C4. X-axis represents the number of analyzed data windows (each 50 ms a new data window is analyzed).
doi:10.1371/journal.pone.0112352.g012

processes are running simultaneously to achieve this goal. A Matlab function is in charge of the processing and classification of signals and it also provides a simple graphical interface to help the users on their first contact with the robotic arm. A C++ program translates the classification results into control commands and sends them to the robotic arm.

Robotic Arm. For the kind of movements wanted on this research, a 2.5D plotter robot may be a more suitable option but due to equipment already available in the research facility, the robotic arm used is the Fanuc LR Mate 200iB. It is a six degrees of freedom robot that can be moved in a three dimensional workspace. Figure 13 shows the robot appearance. The robotic arm is controlled using a C++ program through a local computer network. This program is used to send movement instructions to the LR Mate 200iB. It also receives information about the current position of the robot. Moreover, the C++ program runs a control panel whose main goal is to provide a set of simple instructions to control the interaction with the robot [1]. Through this panel, it is possible to connect and disconnect the robot. It also implements a function to send the robot to a home position and another function is in charge of sending movement instructions to the robot in real time according to the classification results provided by Matlab.

Graphical Interface. A Matlab-based application algorithm registers, processes and classifies the information recorded from the sensorimotor scalp areas. The C++ program uses the final data provided by Matlab in order to send movement instructions to the robotic arm. A communication system has been implemented to make possible the interaction between both processes. This communication introduces a small delay (less than 0.5 seconds) between the moment when the user executes the task and the moment when the robotic arm starts moving. For that reason, a graphical interface has been designed to provide visual feedback of each classified direction. This visual feedback uses the image shown in Figure 14. Each circle represents a direction in a two dimensional plane. This way, it is possible for a user to move the robotic arm to one of these directions. The full circle corresponding to the direction where the robot is moving gets coloured blue while the others remain empty. This interface is only used on the

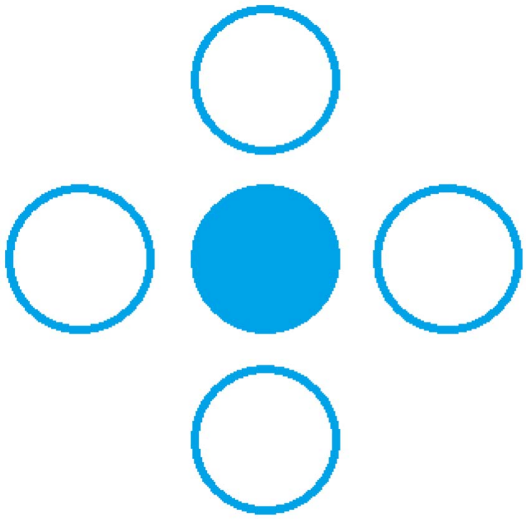

Figure 13. Robotic Arm Environment. It allows movements in a three dimensional workspace. Z-axis remains fixed during tests. The spots show the position of the 8 targets defined.
doi:10.1371/journal.pone.0112352.g013

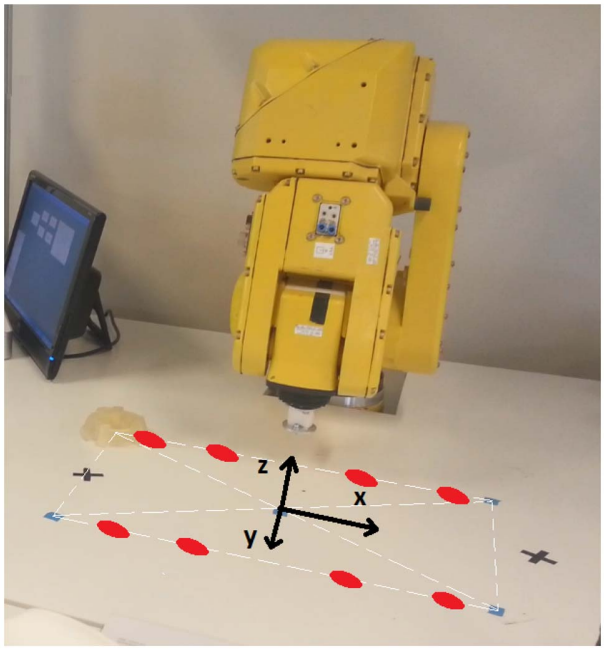

Figure 14. Visual feedback. The full circle represents the direction identified by the algorithm. The robotic arm moves according to the direction shown on this interface.
doi:10.1371/journal.pone.0112352.g014

first run performed with the robotic arm. After that, the user gets used to the small delay and the interface can be removed.

Real Time Test. Tests have been made over a two dimensional workspace. Z-axis is fixed and X-axis and Y-axis are restricted to a rectangle area DIN-A3 size. This way, the users who trained on a computer screen are familiar with the movement area. Figure 13 shows the mentioned workspace. As it can be seen, 8 targets have been placed on the workspace. The users were requested to reach these targets by controlling the robotic arm. Each user has performed nine runs. In the first run no target is requested. The user uses this run to get used to the system delay. The eight remaining runs are used to reach the eight possible targets shown on Figure 13. On each run, a different target is requested and the robotic arm movement stops when the target is reached. Robotic arm movement is controlled by the user through the five tasks previously described. In order to keep HardR and HardL as short duration tasks, a state machine (Figure 15) is designed. As it can be seen, the control of the two dimensional movement is similar to the one used on training step 3. The differences are due to the delay limitations introduced by the robot. Although the movement increment is detected by the system each 50 ms, the robotic arm cannot respond with such speed. For this reason, movement commands are sent only when a change of direction is detected in order to reduce the delay times. For instance, if a right movement state is detected, the robotic arm starts a right continuous movement until a new state is detected. At that moment, the current robot movement is stopped and a new movement begins.

Results and Discussion

The system was tested with four healthy volunteers (capable of moving their jaws) with ages between 22 and 28 (24.25 ± 2.62) (three men with previous experience with this kind of tests and one woman without any, all of them right-handed). All the volunteers

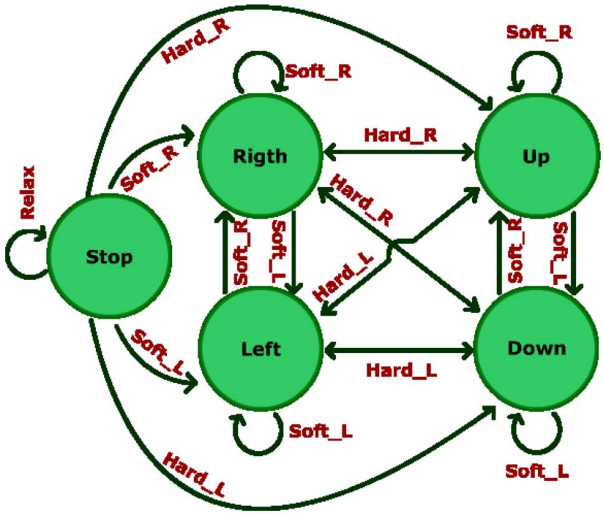

Figure 15. Robotic Arm State Machine. When a state changes, a continuous movement starts in the direction indicated by the current state.
doi:10.1371/journal.pone.0112352.g015

were sat while performing the experiment. They were told not to blink nor perform neck movements, except in rest periods indicated during the tests. The results presented on this work were obtained over a period of 3 months. The data of the cursor movement were registered in the first month and the robot arm control data in the third month. Human data presented in this article have been acquired under an experimental protocol approved by the ethics committee for experimental research of the Miguel Hernández University of Elche, Spain. Written consent according to the Helsinki declaration was obtained from each subject. Also the participants shown in Figure 3 and on referred videos have given written informed consent (as outlined in PLOS consent form) to publish these case details.

Cursor Movement Results

During step 1, all users got used to the kind of clenching that the system is able to identify. They also achieved a successful threshold convergence during the 5 runs from step 2. On the third step, users 1, 2 and 4 noticed that tasks SoftR and SoftL are correctly detected by making a small jaw movement to the side the user wants to move the cursor without the need of clenching their teeth. User 3 kept clenching the jaw. All the users achieved tasks HardR and HardL by making a quick bite with the right or left side of the jaw. Table 1 shows the success and fail rate depending on the number of targets reached by a user in each run. User 2 is the system developer so it has more experience than the rest. As a consequence, he reached all the targets under the time limit. As it has been mentioned, the learning process takes place from runs 1 to 3. During these 3 runs, success rate experiences a huge improvement and after that it remains constant. The control that the user achieves after the third run is very similar to the control anyone can achieve using a joystick or other manual control as shown on video S1. In section Protocol Summary, the training time was estimated as 70 minutes, but by seeing these results, in 3 runs the control of the system is really close to its optimum. Thus it is reasonable to say that the training process could be reduced to 45 min. Table 2 shows the time efficiency in the reaching of targets where the time efficiency coefficient has been defined as follows:

Table 1. Targets Reached.

	Run 1	Run 2	Run 3	Run 4	Run 5	Run 6	Run 7	Run 8
User 1	30	70	90	90	100	90	100	90
User 2	100	100	100	100	100	100	100	100
User 3	40	80	90	90	100	100	80	100
User 4	80	80	100	100	90	90	100	100

Percentage (%) of targets reached by the user on each run.
doi:10.1371/journal.pone.0112352.t001

Table 2. Coefficient of Spent Time to Reach the Target with the Cursor.

		1	2	3	4	5	6	7	8	Avg
	1	0.636	0.688	0.815	0.790	0.784	0.824	0.733	0.801	0.759
	2	0.868	0.915	0.891	0.927	0.856	0.802	0.900	0.914	0.884
Users										
	3	0.657	0.768	0.812	0.740	0.739	0.791	0.825	0.784	0.765
	4	0.834	0.742	0.838	0.814	0.727	0.801	0.767	0.820	0.793
	Avg	0.749	0.778	0.839	0.818	0.777	0.804	0.806	0.830	**0.800**

The values show the C_{opT} for each user to reach every target.
doi:10.1371/journal.pone.0112352.t002

$$C_{opT} = \frac{Optimum\ Time}{Time\ used} \quad (3)$$

The *time used* is the time spent for the user to reach the target, and *optimum time* is the time needed to reach the target if the cursor is controlled manually. To obtain the optimum time, an algorithm that allows a subject to control the cursor by using the key arrows is implemented. All users were asked to reach each target using this manual control. The *optimum time* for each target is calculated as the average of the time employed by all users using this manual control (this average presents a very small deviation meaning that the optimum times are very similar between users). The non-reached targets were not computed to obtain these results. C_{opT} is in average 0.8 throughout the 8 runs for all subjects. In order to prove the efficiency of this system, the average value of the obtained C_{opT} is compared with the average C_{opT} of a BMI system based on motor imagery tasks and a system based in electrooculography (which usually provides better results than motor imagery systems). The optimum time is calculated on these systems according to the methodology previously explained. Analyzing the results from [27,28] (which are previous works done by our group in a similar environment with a hieralchical motor imagery BMI system and a electrooculographic system) the average C_{opT} obtained in the BMI system is 0.033, which is 30.30 times worse than the optimum time, and the average C_{opT} obtained in the electrooculographic system is 0.588, which is 1.7 times worse than the optimum time. Using our system to move a cursor on a screen, the average C_{opT} for all runs and users is 0.8, which is 24.24 times quicker than the motor imagery BMI system (0.033) and 1.36 times quicker than the electrooculographic system (0.588).

Robotic Arm Movement Trials Results

After the training section, users are ready to control the robotic arm in two dimensions. They are requested to reach eight different targets. Time required to reach each target is measured. Table 3 shows the values of C_{opT} obtained by the users to reach each target referred to the minimum time needed by the robot to reach them (manually controlled) under the same conditions. The strategy used in the previous section was applied here to obtain the values of the *optimum time*. All users were also requested to reach the targets using the arrow keys. In this case, there is no improvement along runs due to the similarities between the cursor movement system (Training section) and the robot movement system. Results are also compared with the needed time percentages to reach targets using a system based on motor imagery tasks seen on the last section (0.033). This time, the improvement is, in average, 0.818, which is 24.78 times better than a motor imagery BMI system and 1.4 times better than the electrooculographic system. On videos S2 and S3 are shown 2 subjects who have completed the training in a free movement test reaching a target with and without obstacles in the workspace.

System Limitations

The number of states able to be detected on this system is limited by the behavior of the measured signals. For soft clenching, the PSD increment can be easily controlled by the user, but when the clench is higher, the PSD behaves similar to an exponential function, increasing considerably the control difficulty. Also, thresholds have been defined in order to benefit tasks SoftR, SoftL, HardR and HardL, but making hard for some users the

Table 3. Robotic Arm Time Percentage.

Users	1	2	3	4	5	6	7	8	Avg
1	0.856	0.768	0.931	0.894	0.680	0.904	0.833	0.816	0.835
2	0.904	0.955	0.707	0.669	0.904	0.899	0.855	0.859	0.844
3	0.879	0.990	0.837	0.946	0.837	0.938	0.821	0.911	0.895
4	0.994	0.837	0.890	0.755	0.788	0.764	0.988	0.622	0.830
Avg	0.908	0.890	0.841	0.816	0.802	0.876	0.874	0.802	**0.851**

The values shown indicate the C_{opT} for each user to reach every target.

doi:10.1371/journal.pone.0112352.t003

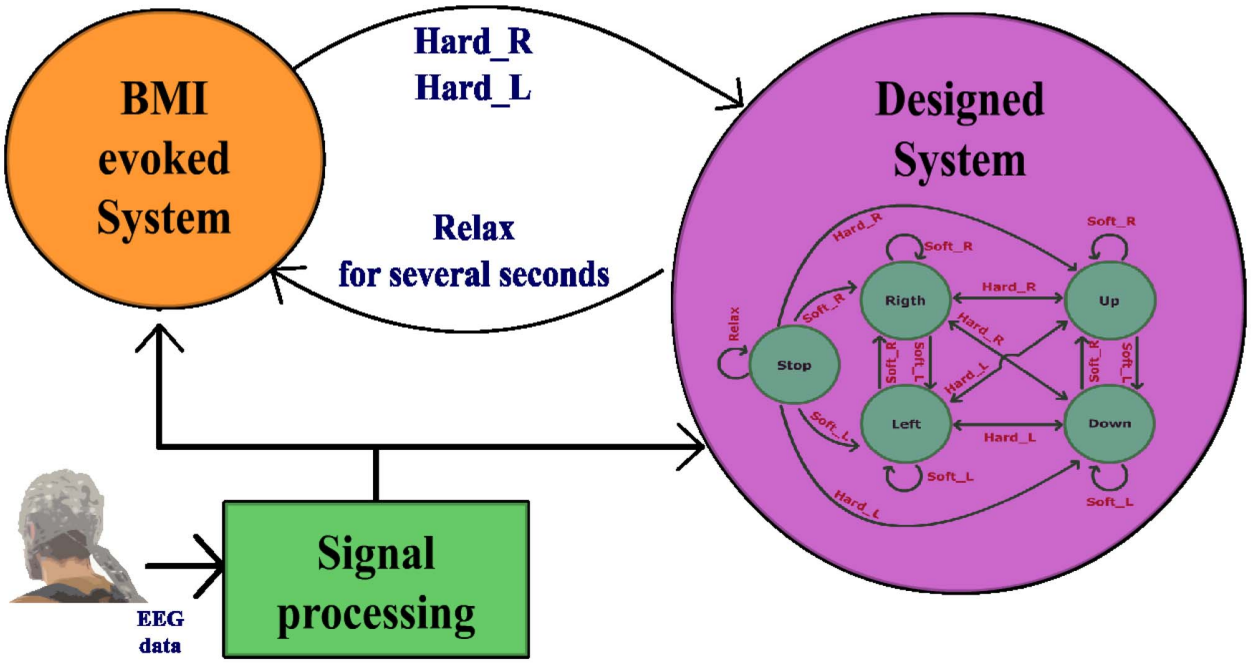

Figure 16. Block interconnection diagram. The supplementary system is activated with tasks HardR or HardL, while the control is returned to the BMI system when the user stays on the Relax state for several seconds.
doi:10.1371/journal.pone.0112352.g016

control of the Relax state. This point should be further studied in future works.

Conclusion

A supplementary application for a BMI system has been designed. A very similar system could also be implemented placing a couple of electromyographic electrodes on both cheeks or placing pressure sensors on the teeth. However, the goal of this research is to use the electrodes of a BMI system in order to implement a supplementary system based on the skill of a user to control EMG signals produced by clenching different areas of the jaw. Results prove that the control acquired by users who can move their jaws is close to the control that a healthy user can acquire using a joystick or the movement arrows of a keyboard.

On the basis of this study, the architecture shown on Figure 16 is proposed as a future work. A BMI system would work while the jaw is relaxed. At the moment the user wants to alternate to jaw control, a quick bite (tasks HardR or HardL) would activate the jaw control algorithm. The change to the BMI system should be produced when the user remains several consecutive seconds on the Relax state. Our supplementary system should be complemented with an appropriate BMI system, i.e. a menu application that allows a patient to select the rehabilitation strategy desired while a BMI system measures the mental state of the patient in order to evaluate how the selected strategy affects the mental workload of the patient. It is also proposed its use in combination with a BMI system previously developed by our group [24], where visual evoked potentials were used to control an internet browser, allowing a user to write and move the cursor on the screen. The BMI system provides a quick and fluid writing but the cursor control can be improved by using the supplementary system designed. On the same work, the BMI system is used to control a robot arm in 3 dimensions. For that purpose, the user first selects the movement plane and then, a 2-dimensional control also based on evoked potentials is used. Using the 2-dimensional control implemented in the current work, it would be possible to improve the performance of the 3-dimensional control described in [24], by combining the plane selection algorithm of the evoked BMI system and the 2-dimensional control implemented in our supplementary system. As a conclusion, this supplementary system allows us to implement a control system in combination with a BMI system using the same set of sensors. This system is oriented to help people who suffer from motor disabilities which deprive them from moving their arms or legs but still have mobility on the jaw. In the future, this system should be tested on this kind of patients. The system might be also adapted for 3-dimensional movement by alternating between three space axes instead of two. Another research line would be to compare a third electrode from a central position (like Cz or CPz) with C3 and C4 in order to measure separately the level of clench from left and right areas of the jaw so both dimensions, X and Y, would be simultaneously controlled.

Supporting Information

Video S1 User 2 controlling a cursor on a screen.
(MP4)

Video S2 User 2 controlling the robotic arm.
(MP4)

Video S3 User 1 controlling the robotic arm.
(MP4)

Author Contributions

Conceived and designed the experiments: AC EI JMA. Performed the experiments: AC EH. Analyzed the data: AC. Contributed reagents/materials/analysis tools: EI JMA. Wrote the paper: AC EI EH JMA.

References

1. Iáñez E, Úbeda A, Hortal E, Azorín JM, Fernández E (2013) Empirical analysis of the integration of a bci and an eog interface to control a robot arm. In: IWINAC (1)′13. pp. 151–160.
2. Takahashi K, Kashiyama T (2005) Remarks on multimodal nonverbal interface and its application to controlling mobile robot. In: Mechatronics and Automation, 2005 IEEE International Conference. volume 2, pp. 999–1004 Vol. 2. doi:10.1109/ICMA.2005.1626688.
3. Sokol S (1976) Visually evoked potentials: Theory, techniques and clinical applications. Survey of Ophthalmology 21: 18–44.
4. Ruth R, Lambert P (1991) Auditory evoked potentials. Otolaryngologic clinics of North America 24: 349370.
5. Volosyak I, Guger C, Graser A (2010) Toward bci wizard - best bci approach for each user. In: Engineering in Medicine and Biology Society (EMBC), 2010 Annual International Conference of the IEEE. pp. 4201–4204. doi:10.1109/IEMBS.2010.5627390.
6. Marshall D, Coyle D, Wilson S, Callaghan M (2013) Games, gameplay, and bci: The state of the art. Computational Intelligence and AI in Games, IEEE Transactions on 5: 82–99.
7. Hamadicharef B (2010) Brain-computer interface (bci) literature - a bibliometric study. In: Information Sciences Signal Processing and their Applications (ISSPA), 2010 10th International Conference on. pp. 626–629. doi:10.1109/ISSPA.2010.5605421.
8. Bi L, Fan X, Jie K, Teng T, Ding H, et al. (2014) Using a head-up display-based steady-state visually evoked potential brain; computer interface to control a simulated vehicle. Intelligent Transportation Systems, IEEE Transactions on 15: 959–966.
9. Trejo L, Rosipal R, Matthews B (2006) Brain-computer interfaces for 1-d and 2-d cursor control: designs using volitional control of the eeg spectrum or steady-state visual evoked potentials. Neural Systems and Rehabilitation Engineering, IEEE Transactions on 14: 225–229.
10. Dasey T, Micheli-Tzanakou E (2000) Detection of multiple sclerosis with visual evoked potentials - an unsupervised computational intelligence system. Information Technology in Biomedicine, IEEE Transactions on 4: 216–224.
11. Fujita T, Yamasaki T, Kamio Y, Hirose S, Tobimatsu S (2011) Parvocellular pathway impairment in autism spectrum disorder: Evidence from visual evoked potentials. Research in Autism Spectrum Disorders 5: 277–285.
12. Nakamae T, Tanaka N, Nakanishi K, Fujimoto Y, Sasaki H, et al. (2010) Quantitative assessment of myelopathy patients using motor evoked potentials produced by transcranial magnetic stimulation. European Spine Journal 19: 685–690.
13. Roy R, Bonnet S, Charbonnier S, Campagne A (2013) Mental fatigue and working memory load estimation: Interaction and implications for eeg-based passive bci. In: Engineering in Medicine and Biology Society (EMBC), 2013 35th Annual International Conference of the IEEE. pp. 6607–6610. doi:10.1109/EMBC.2013.6611070.
14. Duvinage M, Castermans T, Petieau M, Seetharaman K, Hoellinger T, et al. (2012) A subjective assessment of a p300 bci system for lower-limb rehabilitation purposes. In: Engineering in Medicine and Biology Society (EMBC), 2012 Annual International Conference of the IEEE. pp. 3845–3849. doi:10.1109/EMBC.2012.6346806.
15. Carmena JM, Lebedev MA, Crist RE, O′Doherty JE, Santucci DM, et al. (2003) Learning to control a brainmachine interface for reaching and grasping by primates. PLoS Biol 1: e42.
16. Velliste M, Perel S, Spalding MC, Whitford AS, Schwartz AB (2008) Cortical control of a prosthetic arm for self-feeding. Nature 453: 1098–1101.
17. Huang D, Qian K, Fei DY, Jia W, Chen X, et al. (2012) Electroencephalography (eeg)-based brain-computer interface (bci): A 2-d virtual wheelchair control based on event-related desynchronization/synchronization and state control. Neural Systems and Rehabilitation Engineering, IEEE Transactions on 20: 379–388.
18. Frisoli A, Loconsole C, Leonardis D, Banno F, Barsotti M, et al. (2012) Systems, man, and cybernetics. part c: Applications and reviews. IEEE Transactions 42: 1169–1179.
19. Postelnicu CC, Talaba D (2013) P300-based brain-neuronal computer interaction for spelling applications. Biomedical Engineering, IEEE Transactions on 60: 534–543.
20. Fatourechi M, Bashashati A, Ward RK, Birch GE (2007) Emg and eog artifacts in brain computer interface systems: A survey. Clinical Neurophysiology118: 480–494.
21. Daly I, Billinger M, Scherer R, Muller-Putz G (2013) On the automated removal of artifacts related to head movement from the Neural Systems and Rehabilitation Engineering, IEEE Transactions on 21: 427–434.
22. Savelainen A (2010) An introduction to eeg artifacts. Independent research projects in applied mathematics.
23. Yong X, Ward R, Birch G (2008) Facial emg contamination of eeg signals: Characteristics and effects of spatial filtering. In: Communications, Control and Signal Processing, 2008. ISCCSP 2008. 3rd International Symposium on. pp. 729–734. doi:10.1109/ISCCSP.2008.4537319.
24. Blasco JS, Iez E, beda A, Azorn J (2012) Visual evoked potential-based brainmachine interface applications to assist disabled people. Expert Systems with Applications 39: 7908–7918.
25. Guger C, Ramoser H, Pfurtscheller G (2000) Real-time eeg analysis with subject-speci c spatial patterns for a brain-computer interface (bci). Rehabilitation Engineering, IEEE Transactions on 8: 447–456.
26. Hjorth B (1975) An on-line transformation of fEEGg scalp potentials into orthogonal source derivations. Electroencephalography and Clinical Neurophysiology 39: 526–530.
27. Hortal E, Úbeda A, Iáñez E, Azorín JM (2014) Control of a 2 dof robot using a brainmachine interface. Computer Methods and Programs in Biomedicine
28. Úbeda A, Iáñez E, Azorín J (2011) Wireless and portable eog-based interface for assisting disabled people. Mechatronics, IEEE/ASME Transactions on 16: 870–873.

UNIVERSITAS
Miguel
Hernández

B.2. Publicación 2

UNIVERSITAS
Miguel
Hernández

frontiers in Neuroscience

ORIGINAL RESEARCH
published: 25 February 2016
doi: 10.3389/fnins.2016.00060

Characterization of Artifacts Produced by Gel Displacement on Non-invasive Brain-Machine Interfaces during Ambulation

Álvaro Costa[1]*, *Rocio Salazar-Varas*[2], *Andrés Úbeda*[1] and *José M. Azorín*[1]

[1] Brain-Machine Interface Systems Lab, Systems Engineering and Automation Department, Miguel Hernández University, Elche, Spain, [2] Center of Research and Advanced Studies (Cinvestav), Monterrey, Mexico

So far, Brain-Machine Interfaces (BMIs) have been mainly used to study brain potentials during movement-free conditions. Recently, due to the emerging concern of improving rehabilitation therapies, these systems are also being used during gait experiments. Under this new condition, the evaluation of motion artifacts has become a critical point to assure the validity of the results obtained. Due to the high signal to noise ratio provided, the use of wet electrodes is a widely accepted technic to acquire electroencephalographic (EEG signals). To perform these recordings it is necessary to apply a conductive gel between the scalp and the electrodes. This work is focused on the study of gel displacements produced during ambulation and how they affect the amplitude of EEG signals. Data recorded during three ambulation conditions (gait training) and one movement-free condition (BMI motor imagery task) are compared to perform this study. Two phenomenons, manifested as unusual increases of the signals' amplitude, have been identified and characterized during this work. Results suggest that they are caused by abrupt changes on the conductivity between the electrode and the scalp due to gel displacement produced during ambulation and head movements. These artifacts significantly increase the Power Spectral Density (PSD) of EEG recordings at all frequencies from 5 to 90 Hz, corresponding to the main bandwidth of electrocortical potentials. They should be taken into consideration before performing EEG recordings in order to asses the correct gel allocation and to avoid the use of electrodes on certain scalp areas depending on the experimental conditions.

Keywords: artifact, human gait, brain-machine interface, conductive gel, electroencephalography, rehabilitation

OPEN ACCESS

Edited by:
Mikhail Lebedev, Duke University, USA

Reviewed by:
Balaji Narayanan, Hartford Hospital/Institute of Living/Yale University, USA
Giovanni Mirabella, Sapienza University, Italy
Vahab Youssofzadeh, University of Ulster, UK

***Correspondence:**
Álvaro Costa
acosta@umh.es

Specialty section:
This article was submitted to Neural Technology, a section of the journal Frontiers in Neuroscience

Received: *02 September 2015*
Accepted: *09 February 2016*
Published: *25 February 2016*

Citation:
Costa Á, Salazar-Varas R, Úbeda A and Azorín JM (2016) Characterization of Artifacts Produced by Gel Displacement on Non-invasive Brain-Machine Interfaces during Ambulation. Front. Neurosci. 10:60. doi: 10.3389/fnins.2016.00060

1. INTRODUCTION

Non-invasive Brain-Machine Interface (BMI) technologies have become very popular during the last decade. These technologies are based on the measurement of brainwaves using electrodes located over the scalp. Since it is based on passive sensors, this placement does not require surgery and has no other medical implications. By analysing brain potentials it is possible to decode several parameters related to the mental state of the subject. Biologically, this process is mainly performed (in a complex way) in the cerebral cortex, in the cerebellum and in the basal ganglia (Cisek and Kalaska, 2010; Mirabella, 2014). Normally motor commands are sent to the peripheral

nerves and muscles through the spinal cord. However, in Spinal Cord Injured (SCI) patients, these communication pathways are interrupted at different levels depending on the severity of the injury. BMIs provide an alternative way to communicate the brain with external devices or even, indirectly, with the rest of the body using exoskeletons. In Carlson and Millán (2013) a BMI is used to control a wheelchair. In Escolano et al. (2012) a telepresence mobile robot is BMI-controlled allowing handicapped people to perform daily tasks. Currently, many works based on this technology have been oriented to rehabilitation. Classic rehabilitation techniques are based on therapist-patient interaction (O'Sullivan et al., 2013). Recent techniques are trying to obtain more natural movement patterns introducing exoskeletons in the rehabilitation process (Chen et al., 2013; Metzger et al., 2014). As these emerging systems are controllable devices , BMIs have been proposed by several researchers (Daly and Wolpaw, 2008; Pfurtscheller et al., 2008; King et al., 2013) as a method for increasing the level of the patients' involvement in the rehabilitation process. In the last 30 years it has been demonstrated that, both in humans (e.g., Elbert et al., 1995) and animal models (e.g., Lebedev et al., 2000), a wide range of experiences promotes physical changes of the brain structure. This brain plasticity represents the neural basis of learning and memory (for a review see Kolb and Gibb, 2014). It has been hypothesized that neuroplasticity could help functional recovery following brain injury by maximizing the use of the spared circuitry. In fact, some works have shown an increase in plastic changes in patients when they experience higher levels of involvement on their rehabilitations (Dimyan and Cohen, 2011; Kaneko et al., 2014). In Ang et al. (2014), a BMI based on motor imagery tasks is used to control a Haptic Knob robot providing patients a way to be involved with their rehabilitation.

Notwithstanding the remarkable results achieved with BMIs (Nicolelis and Lebedev, 2009), this approach still have limitations which explain why we are still far from approximating voluntary behavior using external devices. For instance, the speed of information transfer rates is currently not high enough (Baranauskas, 2014). Another problem is that the current understanding of brain processes underlying motor decision-making is not accurate enough. For example, volitional inhibition or the ability to cancel pending actions (Logan, 1994) has been disregarded several times by the BCI scientific community (Mirabella, 2012). Although there have been attempts to face this issue (Ifft et al., 2012), the current understanding of volitional control is not enough to properly adapt behavior to unattended changes either in the external environment or in our thoughts. In addition in the last few years, BMIs have been applied on lower limb rehabilitation. These studies involve the acquisition of data during gait processes and other body movements produced during ambulation (Chéron et al., 2012; Duvinage et al., 2012). The use of BMIs on these conditions involve several issues that should be addressed. The volume conduction of the scalp and the consequent smearing of signals produce a poor signal spatial resolution (da Silva, 2004) during electroencephalografic (EEG) acquisition. This scalp property produces the appearance of redundant information on nearby scalp areas. Due to volume conduction, several signals from other sources (artifacts) can be coupled to the EEG signals of interest. Usually, BMI research is performed on movement-free conditions where only electro-ocular and facial artifacts (Fatourechi et al., 2007) need to be taken into account. However, when a subject is walking, artifacts must be properly studied to know if there are new sources of noise affecting the recorded signals. To understand the importance of this study it is necessary to have a global view of the possible noises affecting EEG signals and knowledge of the state of the art techniques or methods developed to detect, reduce and removal of such artifacts. Depending on their source, EEG artifacts can be divided into three large groups: biological artifacts, environment artifacts, and equipment artifacts.

Biological artifacts are signals from biological sources that distort the EEG activity. Some of these signals come from physiological sources like blood pressure or skin tension. They have low and constant influence on EEG signals so the usual way of correcting them is by using a reference electrode. Others have an electrical source like electrooculographic (EOG) signals, electromyographic (EMG) signals or even other EEG potentials that mask the signals of interest. The appearance of these artifacts can lead to misleading results and to the development of systems that are really not studying the targeted phenomena. For that reason, there are lots of studies focused on understanding the nature of these signals in order to learn how to detect and reduce them. There are studies characterizing the influence of EMG signals and the scalp areas affected by them (Goncharova et al., 2003). There are several methods oriented to reduce EOG artifacts, from their removal by visual inspection to the use of linear regression techniques (Schlögl et al., 2007). More complex studies use independent component analysis (ICA) to decompose the signals into independent components and remove those related to artifacts (Gwin et al., 2010; Akhtar et al., 2012).

Environment artifacts are produced by the surrounding conditions of the experimental environment. Loud noises, flashlights and other visual stimuli can produce the appearance of evoked EEG potentials (Mitzdorf, 1985) that contaminate the EEG phenomena under research. Other factors like floor vibrations or electromagnetic fields produced by external devices can affect the subject and the equipment devices adding undesired signals coupled to the recorded data. These artifacts can be avoided by performing the experiment in a controlled isolated environment.

Finally, equipment artifacts are produced by those devices and methods included in the experiment. The most common is the power line interference which is a 50/60 Hz (depending on the world region) signal affecting the electrical network that gets coupled with the recorded data. Current systems include a 50/60 Hz notch filter to remove this interference. It can also be removed by connecting all the equipment to an isolation transformer. Most of these artifacts depend on the specific conditions of each experiment and they should be characterized to develop a systematic protocol that contribute to their removal or reduction. Also, current studies (Castermans et al., 2014; Kline et al., 2015) have found motion artifacts focalized on low-delta and high-gamma bands on the EEG signals during ambulation and head movements. In non-invasive BMI systems based on wet electrodes there is a common source of noise

shared by many experiments. This technology is based on the placement of electrodes over the scalp applying a conductive gel between both surfaces. To easily place the electrodes over the scalp, an elastic cap that fits the subject's head is used. When an experiment does not require head movements, the conductive gel and the electrodes do not experience changes by settlement. However, when the experiment is performed during ambulation, due to the elasticity of the cap, the electrodes and the gel present displacements that induce undesired changes of the signals' amplitude. Both electrode and gel are not fully fixed elements of the acquisition system, electrode movements induce gel displacement and viceversa. As a consequence, the conductivity between the scalp and the electrode change during these movements producing changes in the signals' amplitude. For simplification reasons, hereafter, conductivity changes are going to be referred as gel movements as they could be seen like relative changes of position between the three elements that conform the acquisition system: scalp, gel and electrode. These artifacts have been considered on other works as artifacts from unknown sources. To remove them, data rejection techniques are usually used producing, in some cases, a significant decrease in the amount of data available for each study. This problem has become the main motivation to evaluate and understand these artifacts. Having these artifacts characterized, makes possible the development of experimental protocols focused on their avoidance.

The main goal of this work is to characterize, during EEG recordings, two types of noise produced by the displacement of conductive gel comparing ambulation vs. non-ambulation (thereafter referred to as movement free) conditions. These artifacts can be easily identified by measuring the electrodes' impedance, unfortunately, not all acquisition devices allow the computation of this parameter. To obtain the optimal signal, both noises should be evaluated. The first noise identified is produced by an initial misplacement of gel, producing a significant increase in the signals' amplitude and standard deviation over a whole run. The second noise is manifested as a sudden amplitude increase in a long segment of one run. To perform this study, EEG data from four experiments (three performed during ambulation and one performed movement-free) are used. To understand the nature of these artifacts, noisy channels are identified after evaluating parameters related to the signal's amplitude. Noisy channels are isolated and divided into groups depending on the type of noise, the experimental conditions and the scalp areas evaluated. The characterization of these noises is necessary to properly understand how they affect the EEG recordings and to develop experimental protocols oriented to avoid them in experiments involving human gait. To our knowledge this is the first study to carry out the characterization of this artifacts. Current works usually discard noisy electrodes and signal trials affected by these artifacts to perform their analysis. This could be a valid approach for offline analysis but not valid to perform online studies. In addition, the amount of information loss after applying data rejection techniques from gait experiments is a factor to take into account. If the scalp areas affected by these artifacts are known, it is possible to avoid them during experiments. It will be also possible to develop gel allocation protocols that reduce their influence. This approach is also helpful for avoiding unnecessary trial rejections and the consequent loss of information.

2. MATERIALS AND METHODS

2.1. Experiments and Data Sets

To perform this study, EEG data from four experiments are analyzed. Data sets 1, 2, and 3 are registers from experiments performed under the framework of BioMot (Smart Wearable Robots with Bioinspired Sensory-Motor Skills), an European project oriented to the development of an exoskeleton controlled by physiological signals for lower limb rehabilitation. These experiments were oriented to evaluate several parameters associated to the human gait. In them, EEG signals were recorded during treadmill walk. On the other hand, data set 4 is composed of EEG data related to motor imagery tasks where participants were not moving. Below, each set of recordings is presented with the relevant information related to the experiments performance, the environmental conditions and the procedure.

The evaluated recordings have been acquired from two different experimental conditions. **Figure 1A** shows the experimental condition of data sets 1, 2, and 3. In this case, participants carried the equipment and walked on a treadmill. On the other hand, **Figure 1B** shows the second condition, where participants sat in front of a computer screen performing motor imagery tasks. Human data presented in this article have been acquired under an experimental protocol approved by the ethics committee for experimental research of the Miguel Hernández University of Elche, Spain. Written consent according to the Helsinki declaration was obtained from each participant. **Table 1** shows specific participant and run features regarding each experiment. The specific conditions of the experiments were defined to fit the main goals of different studies. In the current study, these data sets are used to evaluate the observed artifacts produced by gel displacement.

2.1.1. Data Set 1 (Speed and Tilt Changes during Gait)

The participants were asked to change several times their speed and tilt level. The sequence of tasks was: walk at 2 km/h and 10° of tilt, walk at 2 km/h and 5° of tilt, walk at 2 km/h and 0° of tilt, walk at 3 km/h and 0° of tilt, and walk 4 km/h and 0° of tilt. Each condition was performed for 60 s. Tilts positive values refer to positive inclinations. During a whole run participants were always looking forward.

2.1.2. Data Set 2 (Gait Attention Changes)

Participants were asked to walk over the treadmill at a constant velocity of 2 km/h and 0° of tilt. During a run, the participant performed four activities: normal walk looking to a white screen, walking while performing mathematical operations shown on a screen, walking while watching a video, and walking following some adhesive marks on the treadmill. The duration of each activity was fixed by the experimenter to 60 s periods each. In the last activity the adhesive marks were placed to provide an irregular gait cycle, so the participant had to look down to follow them.

2.1.3. Data Set 3 (Obstacle Appearance during Gait)

During this experiment the participants walked while several visual stimuli were presented simulating the appearance of unexpected obstacles. The walking was performed at 2 km/h with 0° of tilt. Each run was composed of two different tasks. In the first task, the participants were asked to stop their gait for a second when a laser projection appeared over the treadmill. In the second one, they were asked to stop their gait for a second when they saw a change of the screen color. Each condition lasts for 90 s. During the laser projection task, participants were looking down to see the laser appearance.

2.1.4. Data Set 4 (Motor Imagery Task)

The participants were asked to sit in front of a screen and imagine the performance of different motor tasks. In each run the participant were instructed to imagine four specific motor movements related to right and left limbs. During the whole experiment participants remained seated in a movement-free condition.

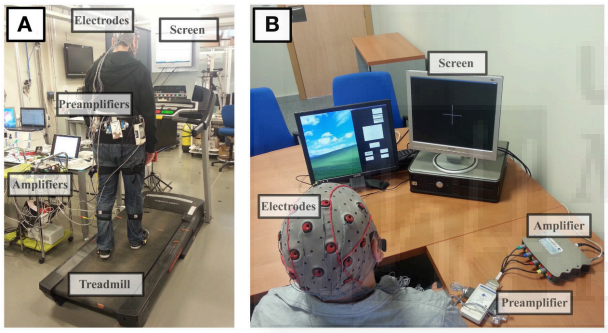

FIGURE 1 | Experimental conditions. Panel **(A)** shows the experimental conditions of the experiment performed during ambulation: amplifiers are on the desk connected by cable to the preamplifiers. Electrodes are placed over the subject who is walking on a treadmill. A computer screen is placed in front of the subject to provide, if needed, visual feedback. All unnecessary electronic devices were disconnected during experiments and signals were visually analyzed prior to the experiment performance to confirm the absence of environmental noises affecting the recordings. Panel **(B)** shows the experimental conditions of motor imagery experiments: the subject sits in front of a screen that provides feedback about the experimental procedure. Signals are acquired using the electrodes placed over the scalp before the preamplification and digitalization stage.

2.2. Data Acquisition

Data acquisition conditions were similar over all the data sets. The only appreciable changes were in the number of electrodes used. Thirty-two electrodes were used on ambulation recordings (data sets 1, 2, and 3) and 16 electrodes were used during movement-free recodings (data set 4). The spatial distribution of the electrodes was the same for all data sets, being smaller the spatial resolution on data set 4, as shown in **Figure 2**.

The EEG data were acquired using 32/16 pseudo-active electrodes to improve the signal to noise ratio with the distributions shown in **Figure 2** according to the International System 10/10 (Klem et al., 1999) with a monoauricular reference in the right earlobe using AFZ electrode as ground. The scalp is measured to place the electrodes on the same anatomic areas for all participants (Towle et al., 1993). The conductive gel used to reduce the impedance between the electrodes and the scalp is a salt-base electrolyte gel (SignaGel, Parker Laboratories, USA). The electrical signals were preamplified (g.GAMMAbox, g.Tec, GmbH, Austria) and digitalized at 1200 Hz using two commercial amplifiers (g.USBamp, g.Tec, GmbH, Austria). These devices were also configured to apply a hardware low pass filter from 0.5 to 100 Hz, and a 50 Hz notch filter to remove the power line interference.

2.3. Analysis Procedure

The presented data sets were studied and compared throughout this section in order to characterize the equipment and set up artifacts produced on EEG signals during both conditions. In

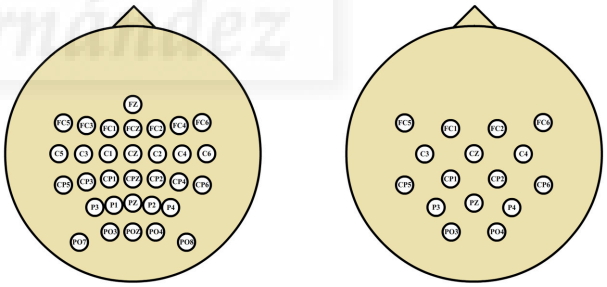

FIGURE 2 | Electrode distributions. Thirty-two electrode scalp distribution corresponding to gait experiments and 16 electrode scalp distribution corresponding to motor imagery experiments. Both distributions cover the same spatial area with different spatial resolutions.

TABLE 1 | Experiment specifications.

	Number of participants					Run duration		
Data set	Male	Female	Ages(mean ± STD)	Sessions	Runs per session	(min)	Total number of runs	Condition
1	3	0	26.66 ± 4.04	1	8	5	24	Ambulation
2	8	2	26.60 ± 3.94	2	8	4	160	Ambulation
3	3	0	25.66 ± 2.88	1	16	3	48	Ambulation
4	12	0	27.33 ± 4.67	1	12	4	144	Movement-Free

Specific values of each data set regarding the number of participants, age, number of sessions, runs, and duration. All subjects were right-handed.

Figure 3, the 16 channels recorded from data set 4 (movement-free experiment) and the same 16 channels from data set 2 (ambulation experiment) are shown. By comparing both signals, two phenomenons mostly associated to ambulation data are described as follows:

1. **A sudden amplitude change** (hereafter, we call it as SA noise) as it is seen in electrodes FC5 and CP6.
2. **A higher amplitude** (hereafter, we call it as HA noise) during the whole run like those shown in C3 and CP5.

The run shown in **Figure 3** has been selected for noise definition purposes. Not all the runs of ambulation data present both kind of noises and when they appear, they are not always associated to the same electrodes. Furthermore, the HA noise appears in some runs of data set 4 (movement-free). Regardless of their origin, all visible noise sources are associated to an unusual increase in the signal's amplitude. aAccording to literature, typical EEG amplitudes ranges differ throughout studies a(between 0.5 and 100 μV; Teplan, 2002 or between 50 and 200 μV; Srinivasan, 2007). It is important to characterize the typical amplitude of the recorded EEG signals in specific experimental and equipment conditions. In our case, it is clear that the increase of amplitude presented in electrodes FC5 and CP6, and the amplitude in C3 and CP5 are not produced just by EEG variations. In order to remove or reduce the appearance of these phenomena, it is necessary to know their origin. For that purpose, in this paper, both phenomenons are going to be studied using the four data sets previously introduced. To study and compare the signals, three parameters related to the amplitude of the signals are described:

1. Standard Deviation that measures the amount of variation or dispersion of a signal.

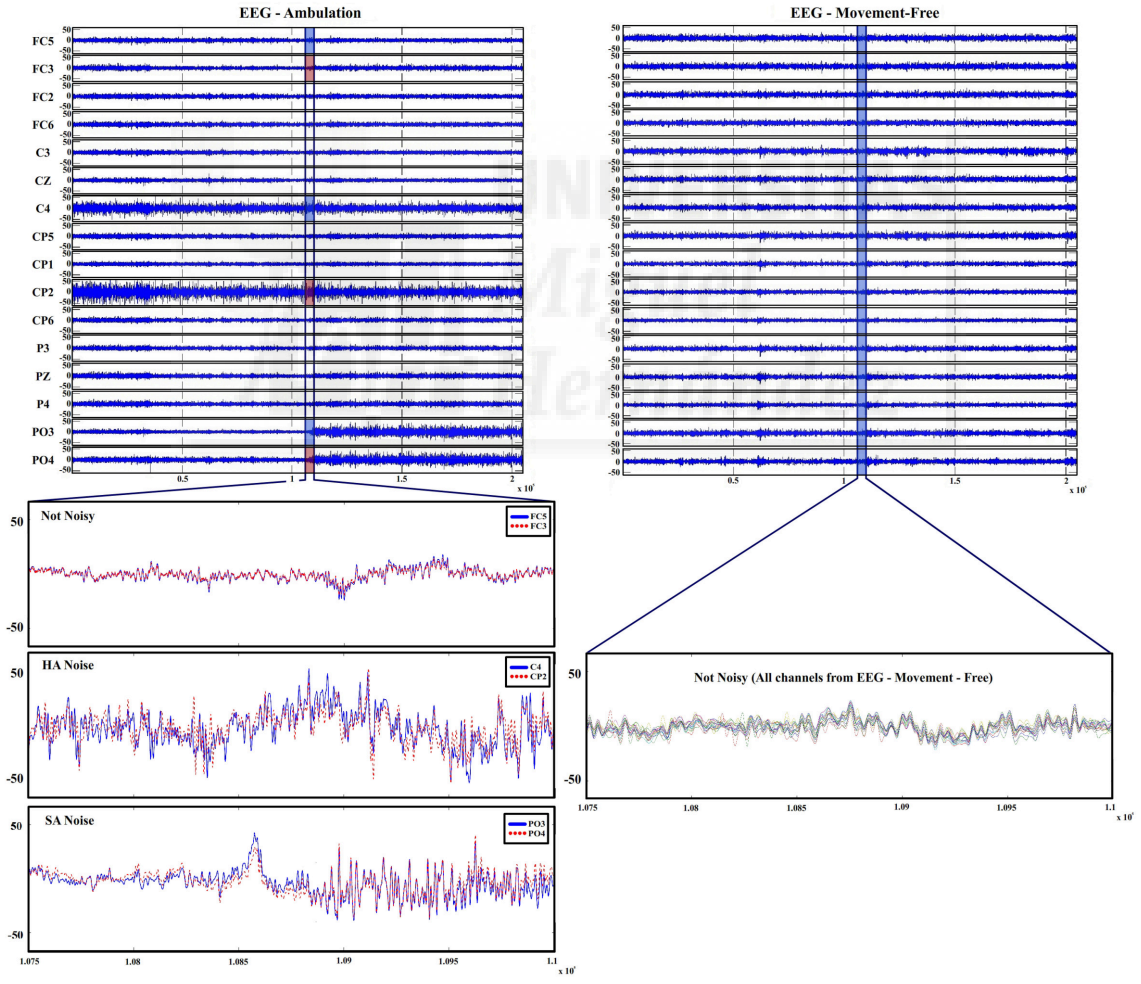

FIGURE 3 | EEG recordings during ambulation and movement-free conditions. Top left shows EEG ambulation graphs with the data registered on channels from experiments performed during ambulation. **Bottom left** shows 2-s trials with detailed amplitudes and vibration of two not noisy channels (FC5 and FC3), two HA noise affected channels (C4 and CP2) and two SA noise affected channels (PO3 and PO4). **Top right** shows EEG movement-free graphs with the data registered on channels from the movement-free experiment. **Bottom right** shows 2-s trials with detailed amplitudes and vibration of all channels of EEG movement-free. Only the 16 electrodes shared on both distribution are shown to keep the figure dimensionality

2. Segments Maximum Average (SMA) which is a parameter developed for this work that obtains the average of the maximum values of the signal once it has been divided into smaller segments. This parameter is related to the averaged maximum amplitudes of the signal during a run. The value obtained is similar to the average of the signal's envelope. The method followed to obtain this value is explained in the following sections.
3. Power Spectral Density (PSD) which provide a measurement of the power distribution across each frequency component.

2.3.1. Analysis of the Standard Deviation

The standard deviation of EEG signals is a widely used parameter due to the statistical properties of this waves. High pass filtered EEG signals follow a normal distribution with mean zero (Blanco et al., 1995). Also all channels are referred to a free of noise electrode consistently gripped to the right earlobe. Under this circumstances, the standard deviation can be considered constant for long trials. For that reason this parameter is commonly used for normalization purposes (Cincotti et al., 2008). Cortical signals recorded from different scalp areas have similar amplitudes and constant standard deviations. If a high amplitude noise appears in a channel during EEG recording, it can be easily detected by evaluating outliers standard deviation values from an electrode distribution. This method has been widely used in literature as data rejection technique (Gwin et al., 2010, 2011; Salazar-Varas et al., 2015). By studying the standard deviation of EEG recordings, it is possible to select the noisy electrodes in each run. **Figure 4** shows the standard deviation values for each electrode of ambulation and movement-free runs from **Figure 3**. From this representation it is easy to distinguish the noisy electrodes. To perform an automatic labeling of the noisy electrodes of a run, two fixed thresholds and one variable threshold are applied to the values of standard deviation computed for each run (**Figure 4**):

- Variable Threshold: It is computed for each run as:

$$Variable\ Threshold = SDAverage + (SDAverage - SDmin) \quad (1)$$

  where *SDAverage* is the average value of the standard deviation of all the electrodes of one run, and *SDMin* is the minimum standard deviation value of all the electrodes of one run. Standard deviation values above this threshold are labeled as noisy electrodes and those under it are labeled as not noisy. This method performs correct classification during runs where just a few channels present noise contribution.
- High Threshold: It is fixed at 15 μV. Standard deviation values above this threshold are classified as noisy. Its purpose is to avoid bad classification in the case that all electrodes present noise contribution. This is an uncommon scenario usually associated to abrupt conductivity changes on the ground electrode due to a bad allocation of the conductive gel.
- Low Threshold: It is fixed at 5 μV. Standard deviation values under this threshold are classified as not noisy. Its purpose is to avoid bad classification in the case that all electrodes present not noise contribution. This is a common scenario where all channels show stable conductivity values between the scalp and the electrodes.

The range between both fixed thresholds (5 and 15 μV) correspond to the typical values of standard deviations observed throughout runs of the 4 data sets. The variable threshold is defined to select noisy electrodes with standard deviation within this range.

In **Figure 3**, only electrodes FC5, C3, CP5, and CP6 from the ambulation data are labeled as noisy. This labeling is applied to

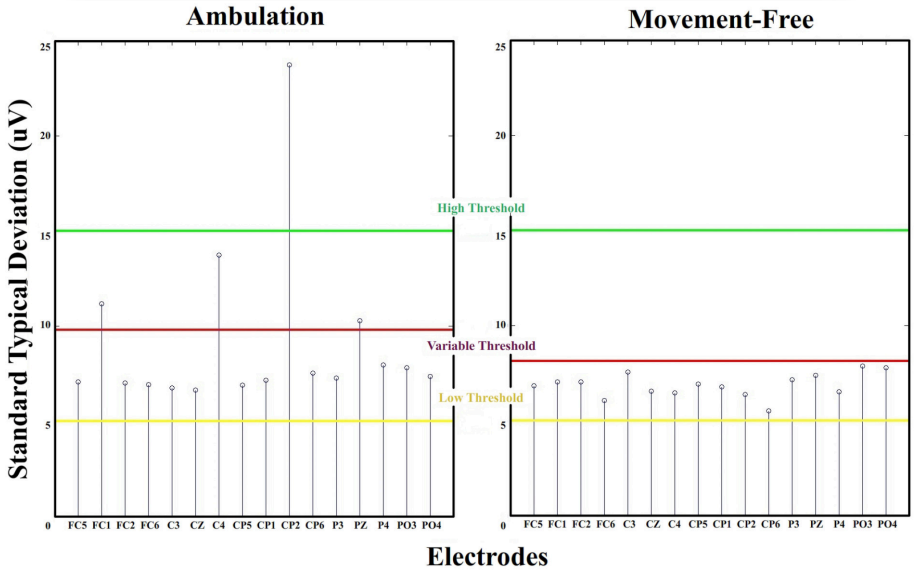

FIGURE 4 | Standard deviation thresholds. Standard deviations for electrodes FC5 to PO4 from a run of ambulation and movement-free data. High threshold and low threshold are fixed. Electrodes above high threshold are classified as noisy, and electrodes under low threshold are classified as not noisy. For middle standard deviation values, the variable threshold is defined dynamically. Electrodes are classified noisy and not noisy depending on if they exceed or not this threshold.

each run for all data sets. The length of labeled vectors differs between data sets as they are recorded using different number of electrodes. Both kind of noises are recognized following this method. They share similar statistical parameters and the only difference between them is the moment where the amplitude changes. For that reason, once a channel is identified as noisy, it is classified as HA or SA by visual inspection. After performing this labeling over a set of runs and updating the value of the vector, it is possible to see which electrodes are more sensitive to the phenomena under research.

2.3.2. Analysis of the Segments Maximum Average (SMA) Related with HA Noise

This parameter provides a measure about the average of the maximum values of the signal amplitudes once a run is divided into segments (the segmentation is trying to emulate real time conditions). On each run, the SMA is calculated for each channel. **Figure 5** illustrates how this parameter is computed and the results provided in a random run and electrode. The length of the consecutive and non-overlapped segments used (500 ms) has been selected to fit the usual requirement of real time systems used in other works performed by our group (Hortal et al., 2015). This parameter is used to evaluate the evolution of the channel's amplitude across consecutive runs.

2.3.3. Analysis of the Noise Power Spectral Distribution

The PSD of each run and electrode of all data sets is computed from 5 to 90 Hz with a spectral resolution of 1 Hz using the pwelch method (Welch, 1967). The output of this process provides 86 values vector per run and electrode (a total of 9728 frequency vectors counting all channels of all runs for the four data sets). Using the standard deviation previously described, these vectors are divided into two groups corresponding to noisy and not noisy signals. A Wilcoxon Sum-Rank test is performed with a confidence interval of 95% and applying a Bonferroni correction for multiple comparisons (Cabin and Mitchell, 2000) to validate the significance between noisy and not noisy signals at each frequency (86 statistical comparisons).

2.3.4. Noise Significance between Ambulation and Movement-Free Data

After dividing between HA and SA (see Section 2.2.1), noisy data are associated to the data set and channel where they were found. From this classification several parameters related to the distribution of noise are obtained: The number of HA noises (*HA-N*), the number of SA noises (*SA-N*), the total number of noises ($Total\text{-}N = HA\text{-}N + SA\text{-}N$) and the total number of channels evaluated ($Total\text{-}R = Total\text{-}N + Not\ noisy\ channels$). These parameters are used to compute the ratio of each noise against the total amount of noise (*HA-N* vs. *Total-N* and *SA-N* vs. *Total-N*) and against the total amount of channels analyzed (*HA-N* vs. *Total-R* and *SA-N* vs. *Total-R*). This ratios are computed for complete data sets (three values per ratio for ambulation data from data set 1–3 and one value per ratio for movement-free data from data set 4) and also for single channels of each data set (32×3 values per ratio for ambulation data and 16×1 values per ratio for movement-free data). These last vectors are used to test the significance in the apparition of the noises described between ambulation and movement-free data running a Wilcoxon Sum-Rank test (Wilcoxon et al., 1970) with a confidence interval of 95% and applying a Bonferroni correction for multiple comparisons.

3. RESULTS

Figure 6 shows the labeled vector of each data set after applying the thresholds defined on the standard deviation of each run. Each vector is followed by a spatial representation of the electrodes in the scalp with different shades of red. The shades are assigned to each electrode depending on the following coefficient:

$$\frac{\text{Number of noisy classified runs}}{\text{Total number of runs analyzed}} \tag{2}$$

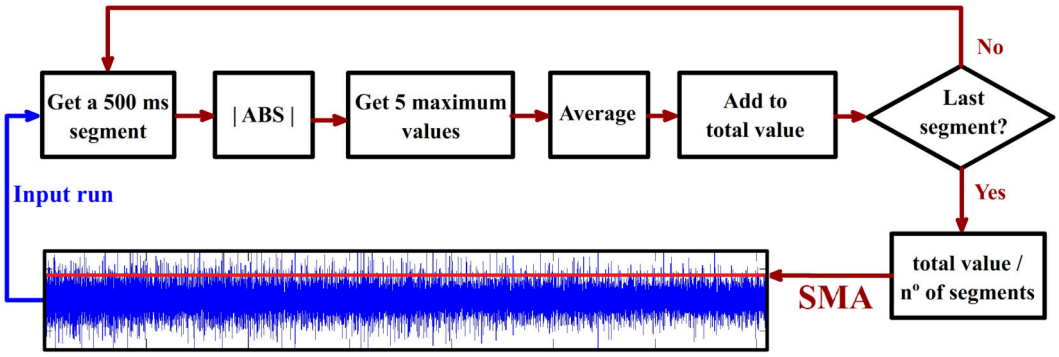

FIGURE 5 | Segments maximum average (SMA) calculus. The time signal is divided into 500 ms consecutive non-overlapped epochs. The absolute value of the epoch is computed. The five maximum values for each epoch are averaged and the result is added to a variable called "total value." This process is repeated on every epoch. The final value of "total value" is divided into the total number of epochs providing as a result the SMA parameter represented with a red line over the blue time signal. This value is calculated for all the electrodes and runs.

where the 0 is represented as white and 1 as black. This coefficient works as a standardization parameter to compensate the variable number of runs of each data set.

The addition of both numbers represented inside each electrode is the total number of noisy runs detected per electrode. The first factor (green) is the number of noisy runs produced by a high amplitude (HA) during the whole run, and the second factor (red) is the number of noisy electrodes produced by a sudden amplitude (SA) change. A deeper analysis of **Figure 6** shows that data sets related to ambulation present higher numbers of noisy runs, being the noisiest electrodes those located on posterior peripheral scalp areas. In addition, ambulation data are principally contaminated by SA noises while movement-free data are only contaminated by HA noises.

To appreciate the influence of each noise, **Figure 7** shows the spatial distribution of both noises separately. For each noise there are two representations. The first one (**Figures 7A,B**) is referenced to the total number of runs of ambulation data (24 from data set 1 + 160 from data set 2 + 48 from data set 3 = 232 runs). This representation highlight the level of contamination that each noise produces in the data. The second one (**Figures 7C,D**) is referenced to the highest number of noisy runs (21 in the case of HA noise vector and 121 for SA noise vector) to emphasize the most affected areas of each noise. **Figure 7** also shows how SA noise is very focused on peripheral areas, while HA noise affects most of the scalp with a lower ratio of occurrence. In the case of data set 4, all the noises detected are HA noises, suggesting that SA noises are caused by performing EEG recordings during ambulation. **Table 2** shows the percentage of SA and HA noises against the total number of noisy electrodes and against the total number of channels in each data set. On ambulation experiments, HA noise represents the 21.49% of the noises and the 1.65% of the total amount of data. On the other hand, SA noises represents the 78.51% of the noises and the 6.11% of all the data evaluated. Moreover, on movement-free experiment, the only noise identified (100%)

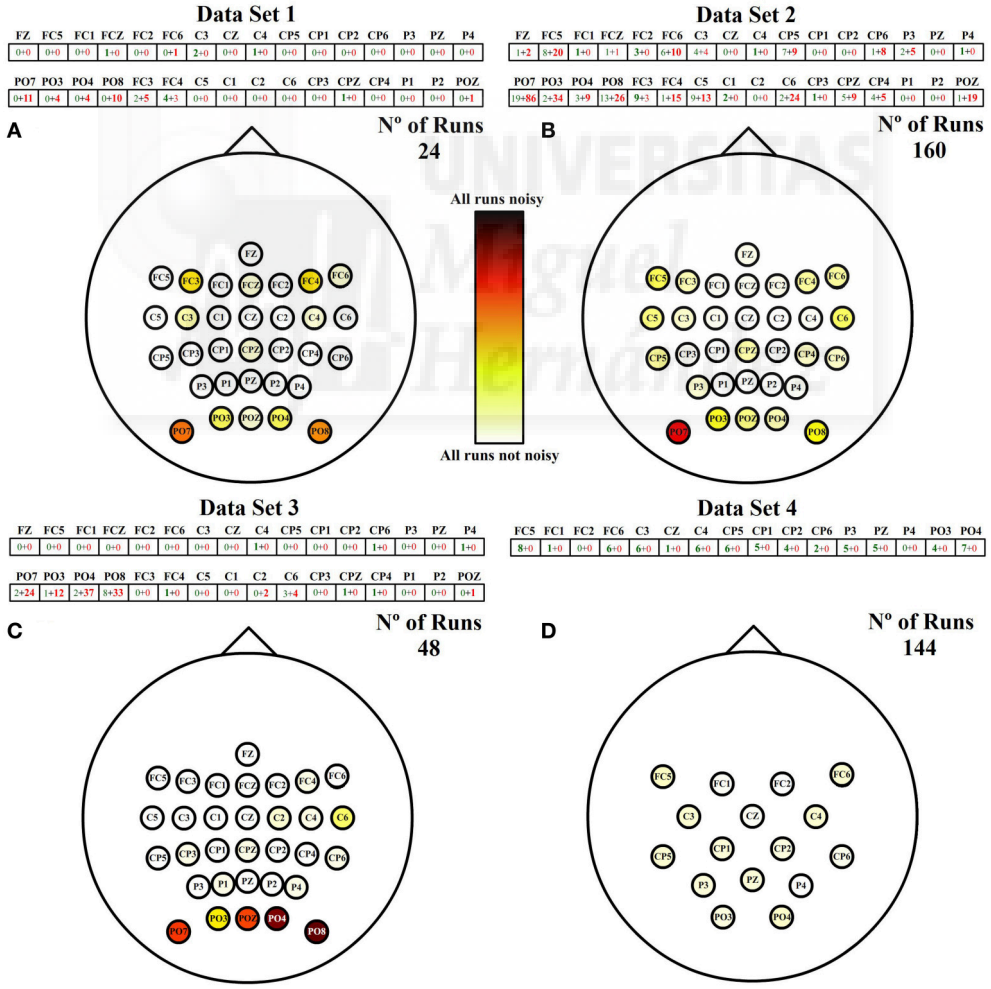

FIGURE 6 | Noises spatial distribution. Each cell of the vector on the top of each scalp represents the number of times an electrode has been classified as noisy after the analysis of all runs. Each number is divided into two values. Green and red values correspond to the number of HA and SA noises identified, respectively. The total number of noisy runs per electrode are spatially represented over each scalp in red shade colors between white and black. **(A)** Spatial distribution of noisy channels for runs of data set 1. **(B)** Spatial distribution of noisy channels for runs of data set 2. **(C)** Spatial distribution of noisy channels for runs of data set 3. **(D)** Spatial distribution of noisy channels for runs of data set 4.

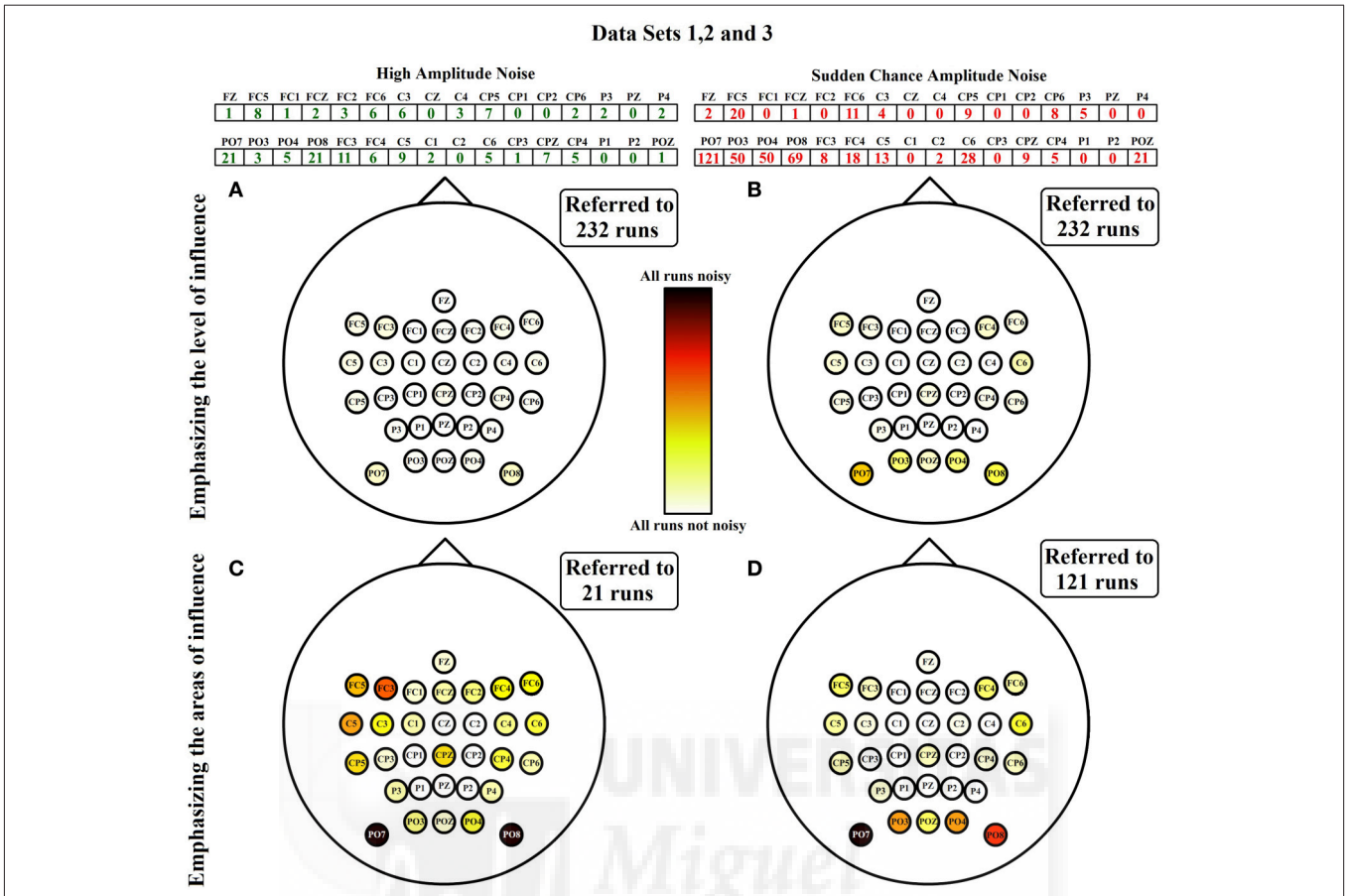

FIGURE 7 | HA and SA noises emphasizing level and areas of influence. HA and SA noises from data sets 1, 2, and 3 are separately analyzed. On the first column, the sum of HA noises from data sets 1, 2, and 3 are represented. The same representation is shown on column two with SA noises. In the first row, noises are represented over the total number of runs analyzed, showing that way the level of influence of the noise along all the runs. In the second row, noises are represented over the maximum number in the classification vector, emphasizing that way the areas affected by each noise. **(A)** Spatial distribution of channels with HA noise referred to the total amount of runs evaluated. **(B)** Spatial distribution of channels with SA noise referred to the total amount of runs evaluated. **(C)** Spatial distribution of channels with HA noise referred to the maximum number of HA noisy channels identified. **(D)** Spatial distribution of channels with SA noise referred to the maximum number of SA noisy channels identified.

TABLE 2 | SA and HA noises vs. total number of noisy channels and total number of channels analyzed.

	Ambulation				Movement-Free	Significance (p)
	Data set 1	Data set 2	Data set 3	Average	data set 4	Ambulation vs. Movement-Free
HA-N (number of channels)	11	107	22	–	66	–
SA-N (number of channels)	39	302	113	–	0	–
Total-N (number of channels)	50	409	135	–	66	–
Total-R (number of channels)	768	5120	1536	–	2304	–
HA-N vs. Total-N (%)	22.00	26.16	16.30	21.49	100.00	$\mathbf{4.74 \cdot 10^{-59}}$
SA-N vs. Total-N (%)	78.00	73.84	83.70	78.51	0.00	$\mathbf{4.74 \cdot 10^{-59}}$
HA-N vs. Total-R (%)	1.43	2.09	1.43	1.65	2.86	$\mathbf{5.58 \cdot 10^{-8}}$
SA-N vs. Total-R (%)	5.08	5.90	7.36	6.11	0.00	$\mathbf{3.28 \cdot 10^{-63}}$
Total-N vs. Total-R (%)	6.51	7.99	8.79	7.76	2.86	$\mathbf{1.09 \cdot 10^{-35}}$

SA-N and HA-N are the number of noisy channels affected by each kind of noise, Total-N is the sum of SA-N and HA-N and Total-R is the total number of channels analyzed. Each cell shows the relation between the parameters specified in the first column for each data set. Average values for all data sets related to the performed experiments during ambulation are also shown. In the last column, the confidence p-values provided by the Wilcoxon Sum-Rank Test, validate the significant differences between ambulation and movement-free experiments in terms of the comparisons performed.

is the HA, representing the 2.86% of the total amount of data acquired under this condition. This table is useful to compare the HA noise results from movement-free data (**Figure 6D**) and the noise results from ambulation data (**Figure 7A**). In the last column, the confidence *p*-values provided by the Wilcoxon Sum-Rank Test, validate the significant differences between ambulation and movement-free experiments in terms of the comparisons performed.

As shown in **Figure 6**, HA noise does not appear in a specific scalp area neither from ambulation nor from movement-free data. However, it has higher influence in movement-free data. To understand this phenomenon, the evolution of the amplitude of noisy electrodes is measured during a whole session. For each data set, a session where the HA noise phenomenon appears is selected and the SMAs of all electrodes are computed and represented for all the runs as shown in **Figure 8**. Each line corresponds to a EEG channel as shown in the legend. Runs of electrodes affected by HA noise (related to an unexpected high value of the SMA) are in the highlighted areas. **Figures 8A–C** corresponding to ambulation data (data sets 1–3) presents a similar behavior on their respective noisy electrodes. The noise decreases after the performance of several consecutive runs. On the other hand, **Figure 8D**, corresponding to movement-free data (data set 4), shows noisy electrodes presenting an erratic behavior during the whole session.

Figure 9 shows the average value of the spectral distribution of noisy signals (670 values per frequency corresponding to runs labeled as noisy) and not noisy signals (9058 values per frequency corresponding to runs labeled as not noisy). For each group, the 25 and 75% of each frequency is represented showing a clear PSD dominance of noisy signals over not noisy signals. The Wilcoxon Sum-Rank test is used to compare both

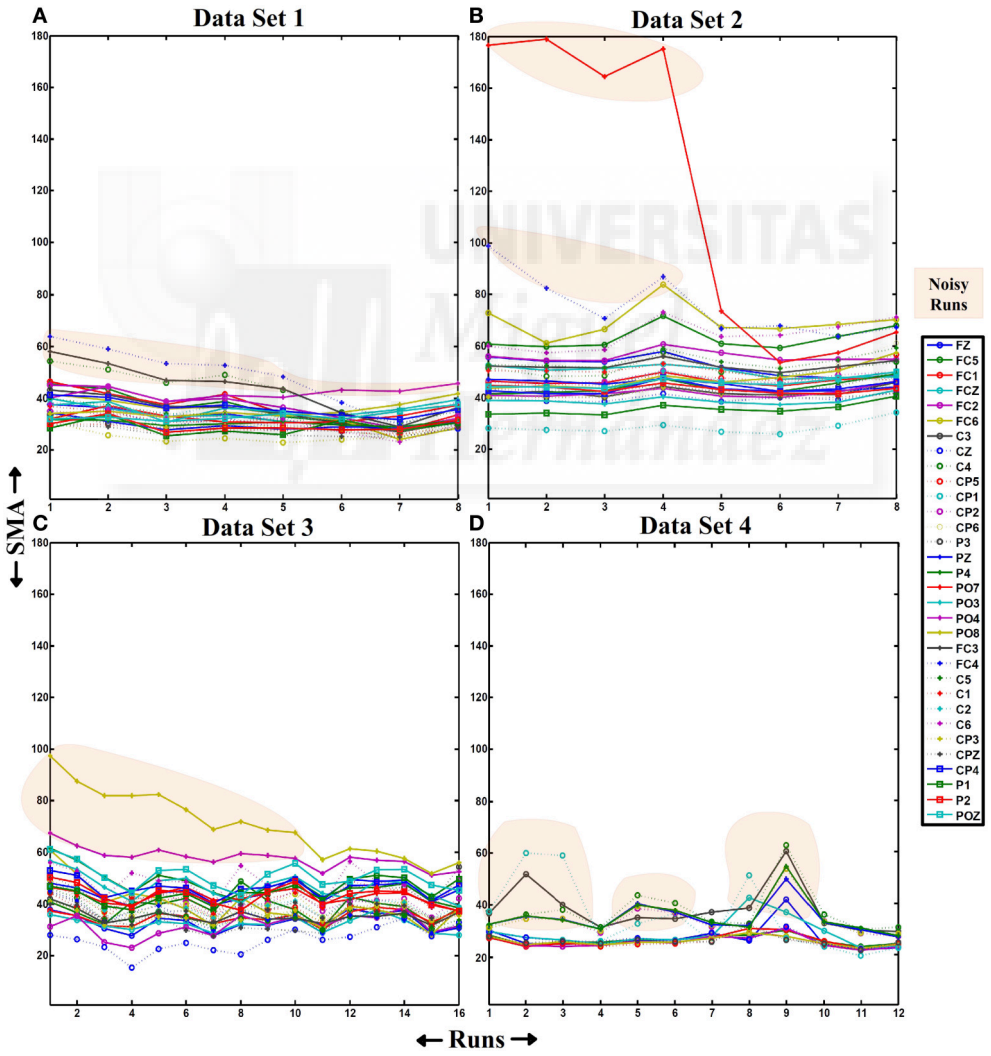

FIGURE 8 | SMA evolution. On each graph, the X-axis represents the number of runs of a single session and the Y-axis represents the value of the SMA. This parameter is represented from all the runs of a session from data sets 1, 2, 3, and 4 (graphs **(A–D)**, respectively). The SMA values for all the electrodes and runs are represented. The number of runs on a session depends on the experiment/data set represented (8 runs for data sets 1 and 2, 16 runs for data set 3, and 12 runs for data set 4). Also, the number of channels is different (32 for data sets 1, 2, and 3 and 16 for data set 4). The orange shadow marks SMAs for electrodes and runs identified as noisy.

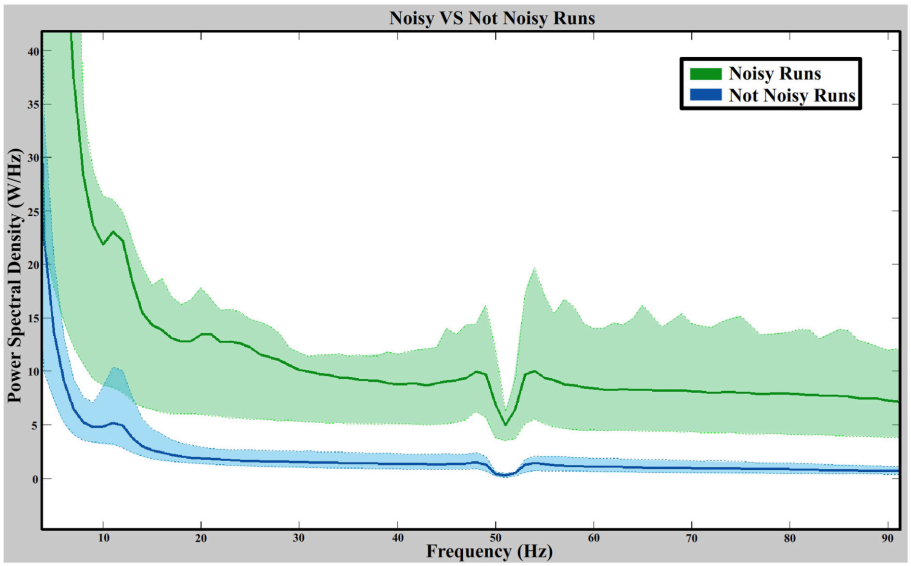

FIGURE 9 | Noisy vs. not noisy signals spectral distribution. The green and blue straight lines are the average value of the noisy and not noisy signals (from all data sets), respectively. Green and blue dashed lines represent the 25 and 75% of each distribution. The power spectral distribution is computed from 5 to 90 Hz with a resolution of 1 Hz.

groups (670 values for noisy signals and 9058 values for not noisy signals) at each frequency (86 frequencies). All confidence levels fulfill the confidence interval after applying a Bonferroni correction showing significance results between noisy and not noisy electrodes at all frequencies. The power decrease on 50 Hz is dued to the notch filter applied during the amplification stage.

4. DISCUSSION

We identify two kind of noises (HA and SA) which are related to equipment artifacts. Interestingly, the main source of noises in EEG recordings performed during ambulation are SA noises appearing only during ambulation and representing the predominant type of noise presented in the EEG signal recorded. Moreover, this noise is focused on peripheral areas corresponding to those scalp locations more sensitive to conductivity changes during head reorientations. These findings are further supported after comparing the spatial distributions of the noises from data sets 1, 2, and 3 with the typical head movements from the three experiments performed during ambulation. The clearest example can be seen on experiment three. During this experiment participants were asked several times to keep a normal walk while they reoriented their heads to the ground in order to see the appearance of visual stimulus. This reorientation produced gel displacements on occipital areas of the scalp inducing the appearance of this noise. The experiment two has a close relationship with experiment three. In this case, participants are also asked to look down but this time in order to follow some marks (with a non-periodic step length) placed over the treadmill which produce an unsteady gait pattern with the consequent left and right head movements. These movements also provoked electrodes displacement over the lateral areas. Experiment one does not imply any specific head reorientation but it includes changes on the ambulation speed producing in this case a different pattern of head movement. Occipital areas are not so affected as participants do not look down. The appearance of noise on occipital and frontal areas was probably caused by the increase of the backward and forward movement of the head during fast ambulation.

On the other hand, HA noises appear in both ambulation and movement-free data. They represent, approximately, one fifth of the noises evaluated. In the case of movement-free data, they are the only kind of noise appearing in the signal. In this case, the HA noise has significant and greater effect in movement-free data than in ambulation data. In addition, this noise present low intensity affecting all scalp areas. These two facts support the hypothesized idea that this noise is produced by a bad gel allocation during the set up of the equipment. This error is committed in random electrodes when the control population is big and its effects are gradually reduced on each run of ambulation experiments. A possible explanation of these effects is that ambulation provokes gel settlement improving the conductivity between the scalp and the electrodes. During movement-free experiment, noisy electrodes present an erratic behavior during the full session suggesting that the gel was bad allocated during the first run and it did not settle along runs. This behavior is supported by the fact that participants kept their heads still during movement-free experiment.

Finally, the spectral power of the noisy trials shows significant values (at all frequencies) against not noisy trials. This suggest that the artifact measured are not directly related to the motion artifacts described on (Kline et al., 2015; affecting mainly low frequencies) nor to the delta and high-gamma band rhythms observed on (Castermans et al., 2014)

5. CONCLUSION

An analysis of set up artifacts produced by conductivity variations between the scalp and the electrodes has been performed. During this work, data from four different experiments have been used: three of them performed during ambulation, and the fourth one performed movement-free. Two different phenomena have been characterized.

An unusual increase in the signal amplitude of some electrodes (referred as HA noise in the paper) appears in both ambulation and movement-free data with a low apparition rate (1.68% in ambulation and 2.86% in movement-free) and a random scalp distribution. Results suggest that they are provoked by gel bad allocation during the electrode's set up. This unusual amplitude is presented in complete sessions from movement-free experiments. On the other hand, in ambulation experiments, the amplitude experiences a reduction throughout runs of the same session converging to typical amplitudes.

A sudden change in the signals' amplitude of some electrodes (referred as SA noise) appears only in ambulation data with a higher rate of apparition (21.49%) and focused on peripheral areas. Results suggest that they are provoked by gel displacements produced by head movements on areas of the scalp where the cap presents critical movements due to its elasticity. These areas change depending on the head movements performed. Looking down triggers this change on occipital areas, moving the head forward and backward on occipital and frontal areas, and right and left head movements affect lateral areas.

These noises can be easily distinguished from other physiological noises like EOG, EMG or cardiac rhythms. Contribution of EOG artifacts is only noticeable in a single trial basis (Elbert et al., 1985) and EMG due to arms and legs movements and cardiac rhythms do not change the amplitude of the signal as much as the artifacts described in this work (Freeman et al., 2003; Moretti et al., 2003). Only EMG signals produced by continuous jaw clenching or heavy head movements have similar effects in the EEG signals but, in this case, these effects hugely affect all the electrodes and not just a random set of them as it was found during this work.

So far, most of works related to BMI do not require the performance of movements. Most studies present artifacts produced by physiological factors, sometimes unavoidable during recordings, like blinks. To deal with them, there are methods like linear regression that allow their removal during real time analysis. Still, many studies apply data rejection techniques in offline analysis suggesting that there are equipment and set up artifacts affecting the electrodes during recordings. Data rejected is usually discarded. In these studies the amount of data rejected represents a small percentage of the total data recorded and it is mostly produced by the noises described in this work. With the appearance of a relatively new branch of research where EEG signals are measured during gait, the amount of equipment and set up artifacts significantly increases. In Gwin et al. (2011) the electrocortical activity during the gait cycle is studied, using 248 electrodes array to measure EEG signals during treadmill ambulation. After an electrode rejection technique, an average of 117.6 electrodes were discarded, meaning that the 47.41% of the recorded data was unused. The same data (again with this 47.41% of rejection) was used in Gwin et al. (2010) to implement a real time artifact removal during walking and running. This research is focused on the study of physiological artifacts (like electrical muscles activation) providing really useful findings and removal methods based on independent component analysis (ICA). Even so, a previous analysis like the one presented in this paper could help to reduce the number of rejected electrodes and to avoid the register of noisy areas of the scalp depending on the kind of movements performed. Future works that intend to acquire EEG signals during ambulation should take into consideration the problems addressed on this work to avoid the processing and storage complications coming from contaminated data.

As mentioned in the introduction, there are many potential noise sources during EEG recordings. This paper is focused on the study of a kind of noise produced by conductivity changes due to gel displacements which are, at the same time, specific equipment noises. This study is helpful to design efficient experiments but it is not enough to ensure the absence of artifacts from other sources. Many studies have proved the appearance of EMG contributions in EEG signals during muscle activation (Brown et al., 1999; Hansen and Nielsen, 2004). These physiological noises are usually not avoidable during recordings, however there are studies focussed on removing them with specific mathematical techniques (Schlögl et al., 2007; Gwin et al., 2010). Research oriented to evaluate EEG phenomena should take into account all kind of potential noise sources and deal with each one of them on the correct stage of the experimental procedure.

AUTHOR CONTRIBUTIONS

AC and JA designed the study and contributed to writing the manuscript. AC analyzed dada and interpreted the results. All the authors participate conceiving the experiments. AC, RS, and AU collected the data and also participate in the drafting of the manuscript. All authors read and approved the final manuscript.

FUNDING

This research has been carried out in the framework of the project BioMot - Smart Wearable Robots with Bioinspired Sensory-Motor Skills (Grant Agreement number IFP7-ICT-2013-10-611695), funded by the Commission of the European Union, and the project Associate - Decoding and stimulation of motor and sensory brain activity to support long term potentiation through Hebbian and paired associative stimulation during rehabilitation of gait (DPI2014-58431-C4-2-R), funded by the Spanish Ministry of Economy and Competitiveness and by the European Union through the European Regional Development Fund (ERDF) "A way to build Europe".

REFERENCES

Akhtar, M. T., Mitsuhashi, W., and James, C. J. (2012). Employing spatially constrained ica and wavelet denoising, for automatic removal of artifacts from multichannel eeg data. *Signal Process.* 92, 401–416. doi: 10.1016/j.sigpro.2011.08.005

Ang, K. K., Guan, C., Phua, K. S., Wang, C., Zhou, L., Tang, K. Y., et al. (2014). Brain-computer interface-based robotic end effector system for wrist and hand rehabilitation: results of a three-armed randomized controlled trial for chronic stroke. *Front. Neuroeng.* 7:30. doi: 10.3389/fneng.2014.00030

Baranauskas, G. (2014). What limits the performance of current invasive brain machine interfaces? *Front. Syst. Neurosci.* 8:68. doi: 10.3389/fnsys.2014.00068

Blanco, S., Garcia, H., Quiroga, R. Q., Romanelli, L., and Rosso, O. (1995). Stationarity of the eeg series. *Eng. Med. Biol. Magaz. IEEE* 14, 395–399. doi: 10.1109/51.395321

Brown, P., Farmer, S., Halliday, D., Marsden, J., and Rosenberg, J. (1999). Coherent cortical and muscle discharge in cortical myoclonus. *Brain* 122, 461–472. doi: 10.1093/brain/122.3.461

Cabin, R. J., and Mitchell, R. J. (2000). To bonferroni or not to bonferroni: when and how are the questions. *Bull. Ecol. Soc. Am.* 81, 246–248. Available online at: http://www.jstor.org/stable/20168454

Carlson, T., and Millán, J. D. R. (2013). Brain-controlled wheelchairs: a robotic architecture. *IEEE Robot. Autom. Magaz.* 20, 65–73. doi: 10.1109/MRA.2012.2229936

Castermans, T., Duvinage, M., Cheron, G., and Dutoit, T. (2014). About the cortical origin of the low-delta and high-gamma rhythms observed in eeg signals during treadmill walking. *Neurosci. Lett.* 561, 166–170. doi: 10.1016/j.neulet.2013.12.059

Chen, G., Chan, C. K., Guo, Z., and Yu, H. (2013). A review of lower extremity assistive robotic exoskeletons in rehabilitation therapy. *Crit. Rev. Biomed. Eng.* 41, 343–363. doi: 10.1615/critrevbiomedeng.2014010453

Chéron, G., Duvinage, M., De Saedeleer, C., Castermans, T., Bengoetxea, A., Petieau, M., et al. (2012). From spinal central pattern generators to cortical network: integrated bci for walking rehabilitation. *Neural Plast.* 2012:375148. doi: 10.1155/2012/375148

Cincotti, F., Mattia, D., Aloise, F., Bufalari, S., Astolfi, L., Fallani, F. D. V., et al. (2008). High-resolution eeg techniques for brain–computer interface applications. *J. Neurosci. Methods* 167, 31–42. doi: 10.1016/j.jneumeth.2007.06.031

Cisek, P., and Kalaska, J. F. (2010). Neural mechanisms for interacting with a world full of action choices. *Annu. Rev. Neurosci.* 33, 269–298. doi: 10.1146/annurev.neuro.051508.135409

da Silva, F. L. (2004). Functional localization of brain sources using eeg and/or meg data: volume conductor and source models. *Magnet. Reson. Imag.* 22, 1533–1538. doi: 10.1016/j.mri.2004.10.010

Daly, J. J., and Wolpaw, J. R. (2008). Brain–computer interfaces in neurological rehabilitation. *Lancet Neurol.* 7, 1032–1043. doi: 10.1016/S1474-4422(08)70223-0

Dimyan, M. A., and Cohen, L. G. (2011). Neuroplasticity in the context of motor rehabilitation after stroke. *Nat. Rev. Neurol.* 7, 76–85. doi: 10.1038/nrneurol.2010.200

Duvinage, M., Castermans, T., Petieau, M., Seetharaman, K., Hoellinger, T., Cheron, G., et al. (2012). "A subjective assessment of a p300 bci system for lower-limb rehabilitation purposes," in *Engineering in Medicine and Biology Society (EMBC), 2012 Annual International Conference of the IEEE* (San Diego, CA: IEEE), 3845–3849. doi: 10.1109/EMBC.2012.6346806

Elbert, T., Lutzenberger, W., Rockstroh, B., and Birbaumer, N. (1985). Removal of ocular artifacts from the eega biophysical approach to the eog. *Electroencephalogr. Clin. Neurophysiol.* 60, 455–463. doi: 10.1016/0013-4694(85)91020-X

Elbert, T., Pantev, C., Wienbruch, C., Rockstroh, B., and Taub, E. (1995). Increased cortical representation of the fingers of the left hand in string players. *Science* 270, 305–307. doi: 10.1126/science.270.5234.305

Escolano, C., Antelis, J. M., and Minguez, J. (2012). A telepresence mobile robot controlled with a noninvasive brain–computer interface. *Syst. Man Cybernet. B Cybernet. IEEE Trans.* 42, 793–804. doi: 10.1109/TSMCB.2011.2177968

Fatourechi, M., Bashashati, A., Ward, R. K., and Birch, G. E. (2007). Emg and eog artifacts in brain computer interface systems: a survey. *Clin. Neurophysiol.* 118, 480–494. doi: 10.1016/j.clinph.2006.10.019

Freeman, W. J., Holmes, M. D., Burke, B. C., and Vanhatalo, S. (2003). Spatial spectra of scalp eeg and emg from awake humans. *Clin. Neurophysiol.* 114, 1053–1068. doi: 10.1016/S1388-2457(03)00045-2

Goncharova, I., McFarland, D. J., Vaughan, T. M., and Wolpaw, J. R. (2003). Emg contamination of eeg: spectral and topographical characteristics. *Clin. Neurophysiol.* 114, 1580–1593. doi: 10.1016/S1388-2457(03)00093-2

Gwin, J. T., Gramann, K., Makeig, S., and Ferris, D. P. (2010). Removal of movement artifact from high-density eeg recorded during walking and running. *J. Neurophysiol.* 103, 3526–3534. doi: 10.1152/jn.00105.2010

Gwin, J. T., Gramann, K., Makeig, S., and Ferris, D. P. (2011). Electrocortical activity is coupled to gait cycle phase during treadmill walking. *Neuroimage* 54, 1289–1296. doi: 10.1016/j.neuroimage.2010.08.066

Hansen, N. L., and Nielsen, J. B. (2004). The effect of transcranial magnetic stimulation and peripheral nerve stimulation on corticomuscular coherence in humans. *J. Physiol.* 561, 295–306. doi: 10.1113/jphysiol.2004.071910

Hortal, E., Planelles, D., Costa, A., Iáñez, E., Úbeda, A., Azorín, J., et al. (2015). Svm-based brain–machine interface for controlling a robot arm through four mental tasks. *Neurocomputing* 151, 116–121. doi: 10.1016/j.neucom.2014.09.078

Ifft, P. J., Lebedev, M. A., and Nicolelis, M. A. (2012). Reprogramming movements: extraction of motor intentions from cortical ensemble activity when movement goals change. *Front. Neuroeng.* 5:16. doi: 10.3389/fneng.2012.00016

Kaneko, F., Hayami, T., Aoyama, T., and Kizuka, T. (2014). Motor imagery and electrical stimulation reproduce corticospinal excitability at levels similar to voluntary muscle contraction. *J. Neuroeng. Rehabil.* 11:94. doi: 10.1186/1743-0003-11-94

King, C. E., Wang, P. T., Chui, L. A., Do, A. H., and Nenadic, Z. (2013). Operation of a brain-computer interface walking simulator for individuals with spinal cord injury. *J. Neuroeng. Rehabil.* 10:77. doi: 10.1186/1743-0003-10-77

Klem, G. H., Lüders, H. O., Jasper, H., and Elger, C. (1999). The ten-twenty electrode system of the international federation. *Electroencephalogr. Clin. Neurophysiol.* 52(Suppl.), 3.

Kline, J. E., Huang, H. J., Snyder, K. L., and Ferris, D. P. (2015). Isolating gait-related movement artifacts in electroencephalography during human walking. *J. Neural Eng.* 12:046022. doi: 10.1088/1741-2560/12/4/046022

Kolb, B., and Gibb, R. (2014). Searching for the principles of brain plasticity and behavior. *Cortex* 58, 251–260. doi: 10.1016/j.cortex.2013.11.012

Lebedev, M. A., Mirabella, G., Erchova, I., and Diamond, M. E. (2000). Experience-dependent plasticity of rat barrel cortex: redistribution of activity across barrel-columns. *Cereb. Cortex* 10, 23–31. doi: 10.1093/cercor/10.1.23

Logan, G. D. (1994). "On the ability to inhibit thought and action: a users' guide to the stop signal paradigm," in *Inhibitory Processes in Attention, Memory, and Language*, eds D. Dagenbach and T. H. Carr (San Diego, CA: Academic Press), 189–239.

Metzger, J.-C., Lambercy, O., Califfi, A., Dinacci, D., Petrillo, C., Rossi, P., et al. (2014). Assessment-driven selection and adaptation of exercise difficulty in robot-assisted therapy: a pilot study with a hand rehabilitation robot. *J. Neuroeng. Rehabil.* 11:154. doi: 10.1186/1743-0003-11-154

Mirabella, G. (2012). Volitional inhibition and brain–machine interfaces: a mandatory wedding. *Front. Neuroeng.* 5:20. doi: 10.3389/fneng.2012.00020

Mirabella, G. (2014). Should i stay or should i go? conceptual underpinnings of goal-directed actions. *Front. Syst. Neurosci.* 8:206. doi: 10.3389/fnsys.2014.00206

Mitzdorf, U. (1985). Current source-density method and application in cat cerebral cortex: investigation of evoked potentials and EEG phenomena. *Am. Physiol. Soc.* 65, 37–100.

Moretti, D., Babiloni, F., Carducci, F., Cincotti, F., Remondini, E., Rossini, P., et al. (2003). Computerized processing of eeg–eog–emg artifacts for multi-centric studies in eeg oscillations and event-related potentials. *Int. J. Psychophysiol.* 47, 199–216. doi: 10.1016/S0167-8760(02)00153-8

Nicolelis, M. A., and Lebedev, M. A. (2009). Principles of neural ensemble physiology underlying the operation of brain–machine interfaces. *Nat. Rev. Neurosci.* 10, 530–540. doi: 10.1038/nrn2653

O'Sullivan, S. B., Schmitz, T. J., and Fulk, G. (2013). *Physical Rehabilitation*. Philadelphia, PA: FA Davis.

Pfurtscheller, G., Muller-Putz, G. R., Scherer, R., and Neuper, C. (2008). Rehabilitation with brain-computer interface systems. *Computer* 41, 58–65. doi: 10.1109/MC.2008.432

Salazar-Varas, R., Costa, Á., Iáñez, E., Úbeda, A., Hortal, E., and Azorín, J. (2015). Analyzing eeg signals to detect unexpected obstacles during walking. *J. Neuroeng. Rehabil.* 12, 1. doi: 10.1186/s12984-015-0095-4

Schlögl, A., Keinrath, C., Zimmermann, D., Scherer, R., Leeb, R., and Pfurtscheller, G. (2007). A fully automated correction method of eog artifacts in eeg recordings. *Clin. Neurophysiol.* 118, 98–104. doi: 10.1016/j.clinph.2006.09.003

Srinivasan, N. (2007). Cognitive neuroscience of creativity: {EEG} based approaches. *Methods* 42, 109–116. doi: 10.1016/j.ymeth.2006.12.008

Teplan, M. (2002). Fundamentals of eeg measurement. *Measur. Sci. Rev.* 2, 1–11. Available online at: http://www.edumed.org.br/cursos/neurociencia/MethodsEEGMeasurement.pdf

Towle, V. L., Bolaños, J., Suarez, D., Tan, K., Grzeszczuk, R., Levin, D. N., et al. (1993). The spatial location of eeg electrodes: locating the best-fitting sphere relative to cortical anatomy. *Electroencephalogr. Clin. Neurophysiol.* 86, 1–6. doi: 10.1016/0013-4694(93)90061-Y

Welch, P. D. (1967). The use of fast fourier transform for the estimation of power spectra: a method based on time averaging over short, modified periodograms. *IEEE Trans. Audio Electroacoust.* 15, 70–73. doi: 10.1109/TAU.1967.1161901

Wilcoxon, F., Katti, S., and Wilcox, R. A. (1970). Critical values and probability levels for the wilcoxon rank sum test and the wilcoxon signed rank test. *Selected Tab. Math. Stat.* 1, 171–259.

Conflict of Interest Statement: The authors declare that the research was conducted in the absence of any commercial or financial relationships that could be construed as a potential conflict of interest.

B.3. Publicación 3

PLOS ONE

RESEARCH ARTICLE

Decoding the Attentional Demands of Gait through EEG Gamma Band Features

Álvaro Costa[1]*, Eduardo Iáñez[1], Andrés Úbeda[1], Enrique Hortal[1], Antonio J. Del-Ama[2], Ángel Gil-Agudo[2], José M. Azorín[1]

1 Brain-Machine Interface Systems Lab, Miguel Hernández University, Av. de la Universidad S/N, 03202 Elche, Spain, **2** Biomechanics and Technical Aids Units, Physical Medicine and Rehabilitation Department, National Hospital for Spinal Cord Injury, SESCAM, Finca de la Peraleda S/N, 45071, Toledo, Spain

* acosta@umh.es

Citation: Costa Á, Iáñez E, Úbeda A, Hortal E, Del-Ama AJ, Gil-Agudo Á, et al. (2016) Decoding the Attentional Demands of Gait through EEG Gamma Band Features. PLoS ONE 11(4): e0154136. doi:10.1371/journal.pone.0154136

Editor: Dezhong Yao, University of Electronic Science and Technology of China, CHINA

Received: November 17, 2015

Accepted: April 8, 2016

Published: April 26, 2016

Data Availability Statement: Due to consent procedure, data is available for all interested parties upon request to the Data Access Commitee of the Biomot Project at bgallegog@externas.sescam.jccm.es or maria.rodriguezu@umh.es.

Funding: This research has been funded by the Commission of the European Union under the BioMot project - Smart Wearable Robots with Bioinspired Sensory-Motor Skills (Grant Agreement number IFP7-ICT- 2013-10-611695). The funders had no role in study design, data collection and analysis, decision to publish, or preparation of the manuscript.

Abstract

Rehabilitation techniques are evolving focused on improving their performance in terms of duration and level of recovery. Current studies encourage the patient's involvement in their rehabilitation. Brain-Computer Interfaces are capable of decoding the cognitive state of users to provide feedback to an external device. On this paper, cortical information obtained from the scalp is acquired with the goal of studying the cognitive mechanisms related to the users' attention to the gait. Data from 10 healthy users and 3 incomplete Spinal Cord Injury patients are acquired during treadmill walking. During gait, users are asked to perform 4 attentional tasks. Data obtained are treated to reduce movement artifacts. Features from $\delta(1-4Hz)$, $\theta(4-8Hz)$, $\alpha(8-12Hz)$, $\beta(12-30Hz)$, $\gamma_{low}(30-50Hz)$, $\gamma_{high}(50-90Hz)$ frequency bands are extracted and analyzed to find which ones provide more information related to attention. The selected bands are tested with 5 classifiers to distinguish between tasks. Classification results are also compared with chance levels to evaluate performance. Results show success rates of $\sim$67% for healthy users and $\sim$59% for patients. These values are obtained using features from γ band suggesting that the attention mechanisms are related to selective attention mechanisms, meaning that, while the attention on gait decreases the level of attention on the environment and external visual information increases. Linear Discriminant Analysis, K-Nearest Neighbors and Support Vector Machine classifiers provide the best results for all users. Results from patients are slightly lower, but significantly different, than those obtained from healthy users supporting the idea that the patients pay more attention to gait during non-attentional tasks due to the inherent difficulties they have during normal gait. This study provides evidence of the existence of classifiable cortical information related to the attention level on the gait. This fact could allow the development of a real-time system that obtains the attention level during lower limb rehabilitation. This information could be used as feedback to adapt the rehabilitation strategy.

Competing Interests: The authors have declared that no competing interests exist.

Introduction

According to the World Report on Disability provided by the World Health Organization (WHO), more than 1000 million people from the entire world suffer some sort of disability, which represents the 15% of the world population. Between 110 and 190 millions of adults have significant difficulties to perform daily activities. The number of disabled people is rising due to the population ageing and the increase of chronic diseases [1]. Spinal Cord Injury (SCI) is one of the most concerning diseases that lead to motor disability. According to the National Institutes of Health (NIH), among neurological disorders, the cost to society of SCI is exceeded only by the cost of mental retardation [2]. These considerable costs come from the rehabilitation devices, clinical staff and the long time periods required to perform the rehabilitation therapies needed by SCI patients. Emerging from these problems, governments are investing on technologies oriented to improve rehabilitation therapies and many research groups are focusing their studies on this topic [3–5].

In classical physical rehabilitation, patients are rehabilitated by therapists or devices that induce on them the movements they cannot do on their own. Over the last years, the field of neurorehabilitation has proved in multiple occasions that this process could be widely improved by involving the patients in a neurological way [6]. The brain is a learning organ, capable of restoring lost neural paths during the rehabilitation process. Using this capability, known as neuroplasticity [7], it is possible to reduce rehabilitation periods and improve the recovery results. To that end, it is necessary to provide some sort of neurological feedback to the patient during the rehabilitation. In [8–10], a virtual reality has been used to provide the patients with visual feedback of an avatar performing, simultaneously, the rehabilitation movements. Results show high improvements in the rehabilitation process and also in the patient's motivation and involvement. Another way of providing neurological feedback is through the use of Brain-Computer Interfaces (BCI) [11, 12]. BCIs obtain neural information from the brain by acquiring the electrical signals on the scalp. This information can be used to obtain patient's intentions and mental state. Using patient intentions to trigger the rehabilitation strategy enhances the effectiveness of the therapy in terms of time and performance [13]. In [14], an upper limb rehabilitation system is tested on stroke patients showing evidence that, among this type of patients, a robotic rehabilitation based on a motor imagery BCI result in greater motor improvement than standard robotic rehabilitation. On the other hand, there are BCIs designed to obtain parameters related to cognitive mechanisms like concentration, workload and attention. These parameters play an important role during rehabilitation as the mental state of the patient has a huge influence over the therapy performance [15].

In the case of lower limb rehabilitation, attention has been proved to be an important parameter that affects the final performance of the therapy [16, 17]. Slow gait and poor stability have been also associated to a low attention and cognition capabilities [18, 19]. In [20, 21], dual-task strategies are also used to test the gait stability and variability in elder people according to the attention paid on the gait process showing similar results. In BCI studies, attention has been a well studied parameter, but it is susceptible to be subjectively understood depending on the focus of each specific work. Attention and cognitive mechanisms have been related to different electroencephalographic (EEG) phenomena produced mainly on the alpha, beta and gamma bands. Power spectral variations on alpha and beta bands have been related to changes on brain's attentional demands [22–24] and the increase of theta/beta bands power ratio and alpha band peaks have been used in [25] to diagnose attention-deficit and hyperactivity disorders. Phase synchronization on gamma band has been related to visual-spatial selective attention [26–29], which is the act of focusing on a particular object, action or stimulus for a period of time, while simultaneously ignoring irrelevant information that is also occurring. Also,

amplitude changes of evoked potentials like P300 have been related to the level of attention paid to an external stimulus [30, 31].

In the current work, a evaluation study is performed to find a relationship between the attention level that a user pays to the gait and the EEG brain signals. The main goal of this study is to set up the basis for a future system capable of classifying in real time the attention level of SCI patients during lower limb rehabilitation. The development of such system could have important implications on the rehabilitation strategies, being a first step to a rehabilitation system capable of changing the therapy parameters in order to fit the mental state of the patient. To perform this study, cortical information from experiments where healthy users and incomplete SCI patients walk on a treadmill are extracted during several tasks related to the attentional demands on gait. This study faces two critical points. The first one is to evaluate the validity of the EEG signals measured during walking, which is a subject of controversy in this field. In [32] it is stated that it is possible to measure good quality EEG signals during movements like walking, cycling and sitting to measure attention by evaluating P300 amplitudes (1–4 Hz), on the other hand, a recent study [33] claims that, during treadmill walking, the EEG signals are polluted with movement artifacts that change depending on the subject, conditions, electrodes and strides, affecting mainly low frequencies ($\sim 1-8$ Hz) and which cannot be removed just using the current artifact removal techniques. The second point is to correlate the results obtained with the state-of-the-art studies to find a relationship between the attention paid on the gait an the current investigations on attention and cognitive mechanisms.

To deal with these problems, all frequency bands associated to cortical signals are evaluated to find those optimal to classify the attention parameters of interest and, after that, several classifiers are tested to get the one that provides better results. The experimental conditions have been defined to avoid the maximum amount of noises and the signals are processed with artifact removal algorithms in order to reduce, as much as possible, their contributions and evaluate only the cortical contribution.

Materials and Methods

Acquisition system

EEG data are acquired through 32 channels using pseudo-active electrodes located on the scalp through an elastic cap (g.GAMMAcap, g.Tec, GmbH, Austria) with the following spatial distribution: FZ, FC5, FC3, FC1, FCZ, FC2, FC4, FC6, C5, C3, C1, CZ, C2, C4, C6, CP5, CP3, CP1, CPZ, CP2, CP4, CP6, P5, P3, PZ, P4, P6, PO7, PO3, POZ, PO4 and PO8 according to the international system 10/10 using AFz position as ground and a monoauricular reference in the right earlobe. Electrical signals are preamplified (g.GAMMAbox, g.Tec, GmbH, Austria) before their 1200 Hz digitalization using two commercial amplifiers (g.USBamp, g.Tec, GmbH, Austria). A 50 Hz Notch filter is also applied to remove the power line interference.

Experimental environment

Fig 1 shows an image of the environment of the experiments. The user is wearing the EEG cap which is connected to the amplifiers using a couple of extensor wires. A treadmill is used to create a steady gait pattern. An antistatic wrist strap connects the user's wrist to the amplifier ground to avoid noises related to the treadmill vibration. In front of the user, a screen placed on the treadmill is connected to the recording computer to provide visual guidance to the user during the experiments.

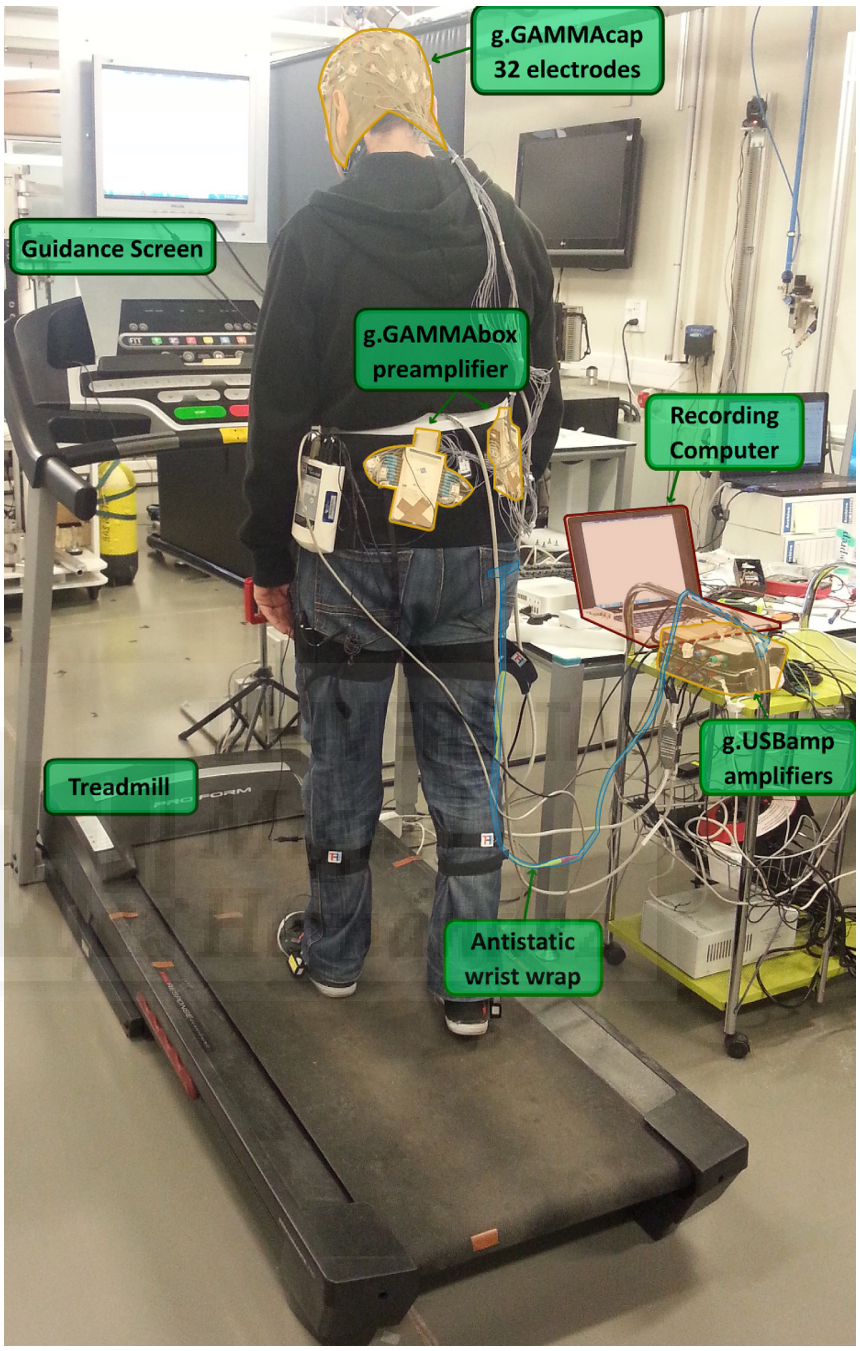

Fig 1. Experimental Environment. The user walks on a treadmill while a screen located at the eye-level provides guidance to perform different attention-related tasks. During the experiment, EEG signals are recorded from 32 channels located over the cortex through the g.GAMMAcap. Electrical signals are preamplified through 2 g.GAMMAboxes located in the user hip and digitalized in the g.USBamplifiers. An antistatic wrist strap connects the user's wrist with the amplifiers ground to remove treadmill's electrical noise. The digitalized data are recorded in a computer system.

doi:10.1371/journal.pone.0154136.g001

Experimental paradigm

The experiment performed is based on the dual task paradigm, commonly used in the literature to evaluate attention measurements [34, 35]. In this work, users walk on a treadmill at 2 km/h and 0 degrees of tilt while they are asked to perform 4 different 1-minute tasks that induce changes in the attention paid to gait. In Fig 2 a graphical representation of a run is shown. During the first task the subject walks normally, looking straight ahead, without any distraction. This task represents a standard attention level on the gait as the user is not fully focused on the gait but not distracted by any other task. In the second and the third task, the subject is asked to perform several mathematical operations and to watch a video on the screen, respectively. Mathematical operations are composed by simple additions and subtractions with numbers between 1 and 9 presented to the user in a friendly interface. The video is presented soundless with subtitles to avoid the appearance of auditory potentials and to keep the interest of the user. Both tasks represent a low attention level since the user is focusing on a non-related gait task. Finally, during the fourth task, the user is asked to walk following some marks located on the treadmill trail. These marks have been consciously located following an unsteady distribution to force the user to keep a high attention level on the variable gait pattern. The order of task performance was the same shown on Fig 2 for all sessions and subjects.

A complete session of the experiment is composed of 8 runs with 1 minute breaks between runs. The final duration of a session is approximately 40 min and it is composed of 32 min of useful data (8 minutes of each task).

Participants

Twelve healthy users have performed 2 sessions of the experiment, 4 women and 8 men, all of them right handed, with ages between 22 and 32 (26.3 ± 3.8). Also 3 incomplete SCI patients have performed 1 session of the experiment, all of them right handed men, with ages between 26 and 58 (44 ± 16.3). Healthy users are degree and Ph.D. students from the Miguel Hernández University of Elche with no known diseases, and patients are from the National Hospital for Spinal Cord Injury (Spain) and they have incomplete SCI with motor lesions between C5 and C6 level. All patients selected were able to walk by themselves or using simple assistive devices like crutches or walkers. They do not suffer from cerebral injury so their brain processes should not present huge differences from those manifested on healthy users [36]. All users have been previously informed about the experimental procedure and they have signed an informed consent according to the Helsinki declaration. The experimental procedure were approve by the ethics committee of the Miguel Hernández University of Elche (Spain).

Processing and features extraction

This section describes how to obtain the frequency features of the signal for all the bands where cortical information can be found. According to literature [37] these bands are: delta (δ = 1–4 Hz), theta θ (θ = 4–8 Hz), alpha (α = 8–12 Hz), beta (β = 12–30 Hz), low gamma (γ_{low} = 30–50 Hz) and high gamma (γ_{high} = 50–90 Hz) bands.

Time processing. Although cortical processes can be described and generalized, electrocortical signal's amplitudes experience huge changes in the time domain depending on the user and the recording day [38]. Also, recording EEG signals during human walking induces several sources of noise that contaminate the cortical signals of interest [33]. For these reasons it is important to apply processing methods to remove the artifacts affecting the brain signals and also a standardization of the signals to make possible the comparison between users and sessions.

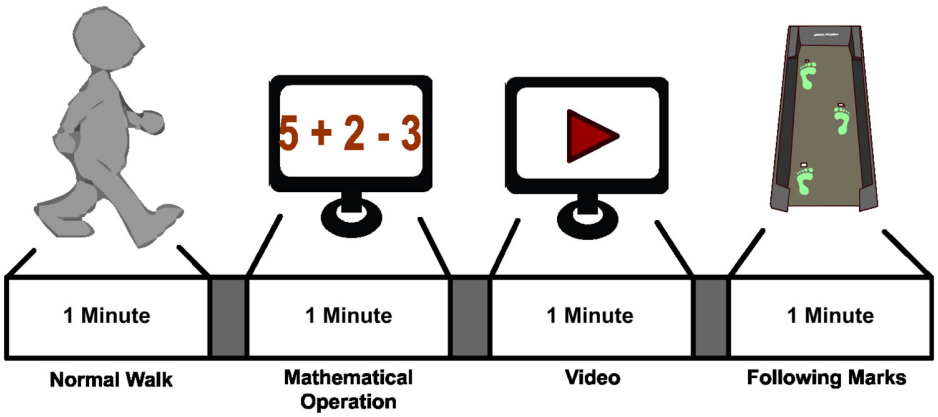

Fig 2. Experimental Cue. A single run is divided into 4 different tasks related to the attention level during gait: Normal walking as Standard Attention Level, performing mathematical operation and watching a video during walking as Low Attention Level, and following marks on the threadmill as High Attention Level.

doi:10.1371/journal.pone.0154136.g002

First, all data are bandpass filtered between 0.5 and 100 Hz to remove blink artifacts associated to low frequencies [39] and electromyographic (EMG) artifacts associated to high frequencies [40]. After that, each channel from every session is visually inspected to find outliers. On Fig 3A, the first session of user 1 is shown to graphically see the artifacts found on some channels during a recording. The simplest way to deal with these channels is their rejection with the consequent loss of information. In this work, to keep some information from these channels and preserve the data dimensionality and the final number of features extracted, the noisy channels are going to be removed and reconstructed using data from a spatially distributed set of recordings sites by means of spatial position as in [41]. Using this method no extra information is added to the signal (only redundant information from surrounding electrodes), allowing the recovery of some lost information from a specific scalp area using the information left on the neighbor areas due to volume conduction [42, 43]. Fig 3B shows the signals after replacing

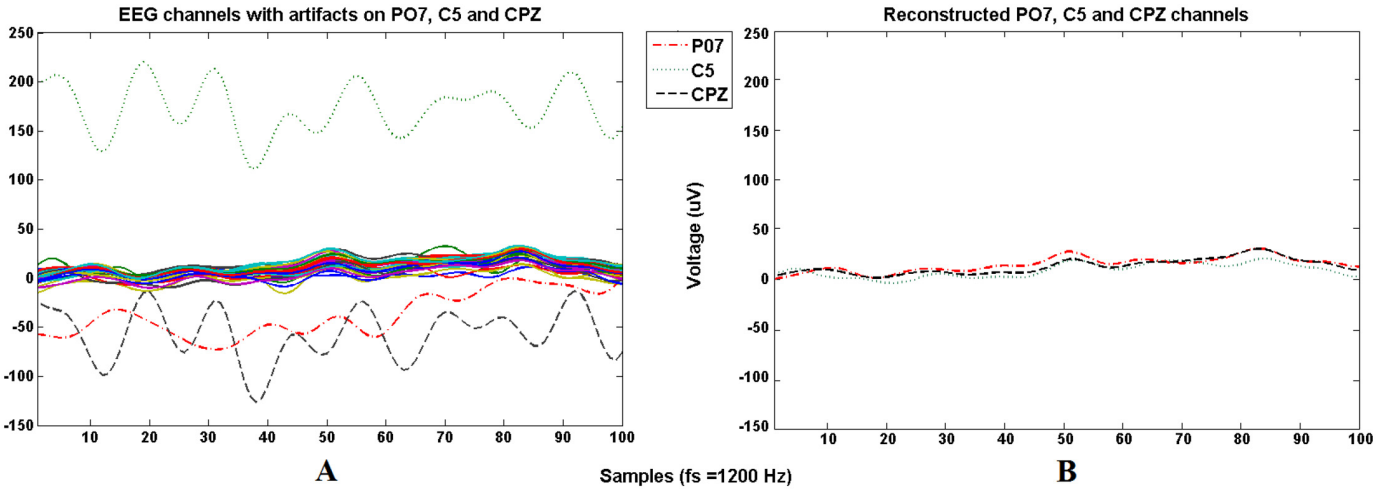

Fig 3. Noisy channels reconstruction. Graph A shows 100 samples of the 32 electrodes time signals from the first session of User 1. Solid lines represent the artifact-free electrodes (±50 uV, common range of EEG signals), dotted and dashed lines represent the noisy channels (PO7, C5 and CPZ, out of ±50 uV range). Each noisy channel is replaced by the average value of the surrounding channels. Graph B shows the reconstructed signal.

doi:10.1371/journal.pone.0154136.g003

the contaminated areas. The amount of reconstructed information from noisy electrodes is the 2.70% of the total available data from both healthy users and patients.

The next step is the standardization of the signals in the time domain. To do that it is necessary to find a parameter that represents the brain signals and that does not experience huge variations during a session. Also, an important aspect of this process is to reduce to its minimum the loss of information after applying the standardization processes. The selected parameter to perform this standardization has been developed during this research and for simplifications it is going to be referenced as Maximum Visual Threshold (MV Threshold). This parameter is computed by windowing an EEG channel in L-samples epochs and averaging the maximum value of each epoch. Eq (1) shows the formula to obtain the MV Threshold for the electrode e where $X^{e}_{(i-1)\cdot L+1:i*L)}$ is the L-samples epoch number i for $i = 1, 2, 3 \ldots N$ being N the total number of epochs.

$$MVThreshold^{e} = \frac{1}{N}\sum_{i=1}^{N} max(X^{e}_{(i-1)\cdot L+1:i*L)}) \quad (1)$$

In Fig 4A a highpass filtered EEG signal is shown in blue. The red line represents the MV Threshold calculated for L = 1200 samples (1 second). The green dotted line represents the step-by-step computation of the MV Threshold. During the initial epochs, the average variation (green line) presents an unsteady behavior but after averaging several tens of epochs, the variation is very small and it is robust against isolated high amplitude peaks. Since the value of the MV Threshold depends on the epoch width L, it is important to select this L value taking into account the width of the epochs that are going to be used to obtain the features of our signals. Fig 4B shows the MV Threshold for different values of L. The black point shows the one selected for the current work. For L values close to 1 (0.83 milliseconds), the value of MV Threshold is really close to the signal average which is almost 0. Prior to $L = 110$ (92 milliseconds) the value of MV Threshold presents an accelerated increase and it becomes more stable after this point. This phenomenon is closely related to the amount of spectral information of the signal. The minimum epoch length needed to get all the spectral information desired from a signal is computed as $t_{min} = 1/f_{min}$, being f_{min} the minimum frequency of interest in the signals analyzed. In this case, the $L = 110$ is associated to low frequencies ($\sim$ 10 Hz) corresponding to the α band, the activation of which is expected from EEG data obtained during motor tasks, implying that most of signal information appears in this band. However, current EEG data are bandpass filtered between 1–100 Hz which means that the minimum epoch length to have access to all the bandwidth is 1 seconds ($L = 1200$) which also in the range where MV Threshold presents a stable behaviour.

The MV Threshold is calculated for each electrode and it can be considered constant during a whole session. For each session, 32 MV Thresholds are computed, one per channel with L = 1200 samples. The signal standardization is computed according to Eq (2) where $V(t)_e$ is the time domain EEG signal of the electrode e and $MVThreshold_j$ is the MV Threshold of the channel j, with $j = 1, 2, 3, \ldots Ch$ being Ch the total number of channels.

$$SV(t)_e = \frac{V(t)_e}{\frac{1}{Ch}\cdot\sum_{j=1}^{Ch}\cdot MVThreshold_j} \quad (2)$$

The values of the MV Thresholds are different on each session and user, but they remain constant during a single session. The use of this standardization makes possible the comparison of data between users without the loss of information. The bandwidth of interest can be

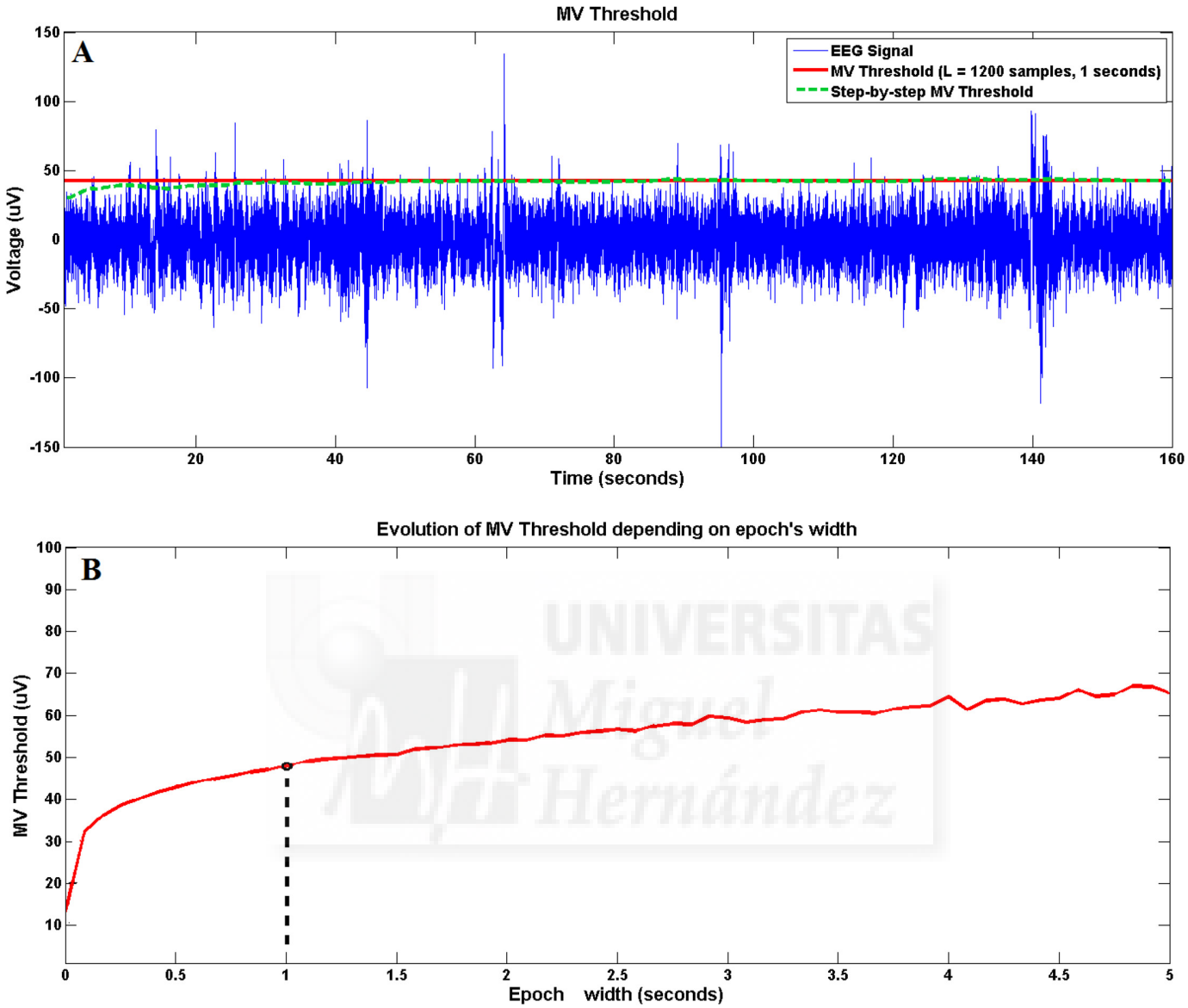

Fig 4. Maximum Visual Threshold. Graph A shows 160 seconds of a single channel EEG signal (in blue) and the MV Threshold computed for that signal with a epoch width (L) of 1200 samples (1 second) (in red). Graph B shows the evolution of the MV Threshold depending on the width L of the epochs for the same EEG channel. The black point shows the value selected and shown in graph A.

doi:10.1371/journal.pone.0154136.g004

recovered from the signals and the variation of spectral power between electrodes is not lost by averaging the MV Thresholds obtained for each of the channels.

Features extraction. Once the signals are filtered and standardized, breaks from each session are removed and the remaining data is divided into one minute tasks (4 per run). This division is performed prior to epoch segmentation to avoid the existence of epoch containing cortical information of two consecutive tasks. Each task is divided into 1 second epochs (1200 samples) with an overlap of 0.5 seconds (600 samples) between epochs obtaining 3840 epoch per session ($\frac{8\ Runs\ \cdot\ 4\ Tasks\ \cdot\ 60\ Seconds}{0.5\ Seconds\ (Overlap)}$) and 960 epochs per task (4 attention tasks). Epoch and overlap values are selected to fit future real time specifications and they are also useful for the analysis

proposed in this work related to frequency bands comparison and task classification. After that, the spectrum of every epoch is computed using the Maximum Entropy Method presented by Burg in [44]. This method is an autoregressive calculation technique introduced to compute the spectrum finite-length epochs of real time sampled data. The AR-parameters are computed by minimizing the sum of the square forward and backward prediction errors [45]. This method reduces the minimum entropy components of the signal which are associated to those components than provide less amount of information reducing this way the random components (usually associated with electronic noise) and improving the components with more information. For each epoch the spectrum is computed between 1 and 100 Hz with a spectral resolution of 1 Hz.

The computed spectrum of the epochs is used to obtain 6 different features sets according to the frequency bands analyzed. As it was mentioned at the beginning of the processing section, the frequency bands evaluated are delta δ (1–4 Hz), theta θ (4–8 Hz), alpha α (8–12 Hz), beta β (12–30 Hz), low gamma γ_{low} (30–50 Hz) and high gamma γ_{high} (50–90 Hz). For each frequency band and epoch, 32 features are obtained as the sum of all frequencies between the lowest and the highest frequency of each band (for each channel).

This feature extraction process is performed for each individual session, i.e twice per each healthy subject and once per each patient.

Frequency band selection. To take an objective decision regarding the optimal frequency band to classify the attention on the gait, there are several possibilities based on the use of mathematical parameters and indices that provide information related to class differentiation. In [46], Millán et al. introduce a coefficient that expresses the separability between 2 classes according to their mean and standard deviation across all the epochs. To use this coefficient it is necessary to obtain a single value of mean and standard deviation per class which is difficult when each task is represented by more than one feature per epoch. A more suitable parameter for the present study is the Battacharyya distance (*Bdist*) which was firstly introduced by Battacharyya in [47]. This parameter provides a measurement of the similarity of 2 sets of features and it is closely related to the Battacharyya coefficient which is a measure of the amount of overlap between 2 statistical samples or populations. According to literature, this measurement has widely proved its reliability for signal selection purposes [48–50]. As mentioned, *Bdist* is used to compare 2 classes, however in the current work, to obtain information related with the separability of 4 classes, the *Bdist* has been calculated for all the possible combinations of the 4 classes.

Since the *Bdist* can provide any value in the range $0 < Bdist < \infty$, it is necessary to use a selection criteria to decide which frequency bands present the higher class separability. In [51], Choi and Lee have performed a study where they represent the Bayes error [52] of 2 task classification against the Battacharyya distance between 2 classes. As a result, they obtain a logarithmic behavior being the Bayes error between $\sim$10% and 30% for *Bdist* = 0.5, $\sim$1% and 7% for *Bdist* = 2 and $\sim$0% and 2% for *Bdist* = 3.5. For this work, 2 classes are going to be selected as highly separable if their *Bdist* = $>$ 3.5. Only features from healthy subjects are used in the computation of *Bdist* values. They represent most of the cortical data recorded during this work and the attention level paid from patients is expected to be higher during non-attentional tasks. Best features selected by this method are applied to patients data during the classification stage.

Classification

Five different classifiers have been considered to test the capability of distinguishing between the 4 gait attention tasks. The classifiers used are properly enumerated below:

1. Support Vector Machine (SVM) [53] with Radial Base Function kernel with $C = 512$ and $y = 0.002$ (parameters obtained in a previous work [54]).
2. Naïve Bayes (NB)[55].
3. Linear Discriminant Analysis (LDA) which is a generalization of Fisher's linear discriminant [56].
4. K-Nearest Neighbors (KNN) [57] with the number of neighbors $k = 30$.
5. Decision Tree Learning (DTL) [58].

To validate the success rate results obtained by each classifier for each session (2 session x 12 healthy users + 1 session x 3 patients = 27 sessions) an 8-fold cross validation has been used where each run has been used as fold.

Chance level computation

To validate the results and to select the best classifier, it is necessary to confirm the significance level between the classification results and the chance level. Applying the simplest mathematical statement, the chance level for a 4-task classification system assuming class equality (which is the case of the current study) is 25%. But for real finite data analysis the chance level presents several variations according to the specific conditions of the data studied. In [59], Müller-Putz et al. introduce a mathematical method to calculate the range of values corresponding to the chance level according to the number of tasks classified and the number of epochs used in the classification stage for a 2-tasks classification system. According to Müller-Putz's work, the confidence interval around the expected chance level can be calculated using Eq (3) where n is the number of epochs, $z_{1-\frac{\alpha}{2}}$ is the $1-\frac{\alpha}{2}$ quantile of the standard normal distribution $N(0, 1)$, α is the level of confidence required (typically 0.1 and 0.05) and $\tilde{p}$ is the unbiased estimator computed according to Eq (4). In this case, n is still the number of epochs and $\bar{X}$ is the averaged probability of all the individual probabilities of a correct classified epoch X_i with a classifier that performs a random classification. The Eq (5) shows the mathematical formula to compute $\bar{X}$, which according to the definition provided corresponds to the mathematical value of the chance level for an ideal random classifier (50% for 2 tasks). For more than 2 classes the model can be extended as shown in [60].

$$Chance\ Level\ Range = \tilde{p} \pm \sqrt{\frac{\tilde{p} \cdot (1-\tilde{p}))}{n+4}} \cdot z_{1-\frac{\alpha}{2}} \tag{3}$$

$$\tilde{p} = \frac{n \cdot \bar{X} + 2}{n+4} \tag{4}$$

$$\bar{X} = \frac{1}{n} \cdot \sum_{i=1}^{n} \cdot X_i \tag{5}$$

Results

Features spatial representation

After the signal epoch segmentation and features extraction, a single 32 features vector is computed for each frequency band and task as the average of the epochs of all sessions (from both

healthy and patients data). This makes 6 frequency bands per 4 tasks, a total of 24 feature vectors. The spatial distribution of these features has been represented in Fig 5 in order to visually appreciate the difference between each task depending on the frequency range evaluated. On this representation it is possible to appreciate some differentiation between tasks and frequencies. Focusing on the minimum and maximum spectral power values used to represent each frequency, it is shown that the spectral power of EEG signals gets lower when the frequency evaluated increases. These results, based on visual inspection and spectral power level, are quite subjective in order to decide which frequency bands provides more information to differentiate between the attention tasks presented.

Frequency band separability

To obtain an objective measurement related to class differentiation, the *Bdist* is used. In Table 1 this parameter is shown for each 2-tasks combination and frequency band. The letter labelling for the class combination is the following one: *A* for "Normal Walking" class, *B* for "Mathematical Operations" class, *C* for "Video" class and *D* for "Following Marks" class. All the tasks combinations that achieve the criteria selected ($Bdist = > 3.5$) have been highlighted in bold in Table 1. Also the first and second maximum values for each combination are marked with one or two asterisks respectively.

Table 1 shows high *Bdist* values for all task combinations that include task A (Normal Walking) which means that it presents a huge separability from the rest of tasks on every frequency band. On the other hand, the remaining combinations present a low *Bdist* for low frequencies achieving the selection criteria only on γ_{low} band (except for BC combination) and γ_{high} band. Another interesting fact obtained from this table is that, for all frequencies, the combination BC ("Mathematical Operation" class and "Watching Video" class) has the lowest separability features. Taking into account that these tasks or classes have been defined as the same level of attention (low gait attention level), these results suggest that, indeed, both tasks present lots of similarities. For that reason, both γ_{low} and γ_{high} bands are going to be selected for the classification stage where several classifiers are going to be evaluated in the classification of the 4 tasks mentioned.

Classification results

The 5 classifiers previously described are applied to on the data. The average and the standard deviation for each user and classifier after an 8-fold cross validation are computed for γ_{low} and γ_{high} bands and represented on Table 2. For patients, 1 session is used to compute the success rate while results from 2 sessions are averaged in the case of healthy users. The total averaged values for each classifier and frequency band are also computed. These values are computed using all the single fold values obtained from every subject. From these results it is possible to approximate averaged classification results, e.g from high gamma band frequency features and KNN classifier, a 66.79% and a 59.08% of success rate are obtained from healthy subjects and patients respectively.

Significance against chance level. In the current work, for each session there are 3840 epochs but only 960 are used to test the classification results on each fold iteration. The chance level range of a single fold (from the 8-cross fold validation) is computed for $n = 960$, $\bar{X} = 0.25$ (4 tasks) and $\alpha = 0.05$ (according to Eq 3), obtaining the range $23.9 < successrate < 26.3$ (Fig 6). Any iteration of the 8-cross fold validation providing a classification result within this range should be considered random. Fig 7 shows the average success rate of each classifier for healthy users and patients on both frequency bands (24 *sessions* · 8 *folds* = 192 *success rate values* of healthy users and 3 *sessions* · 8 *folds* = 24 *success rate values for patients*) and the computed

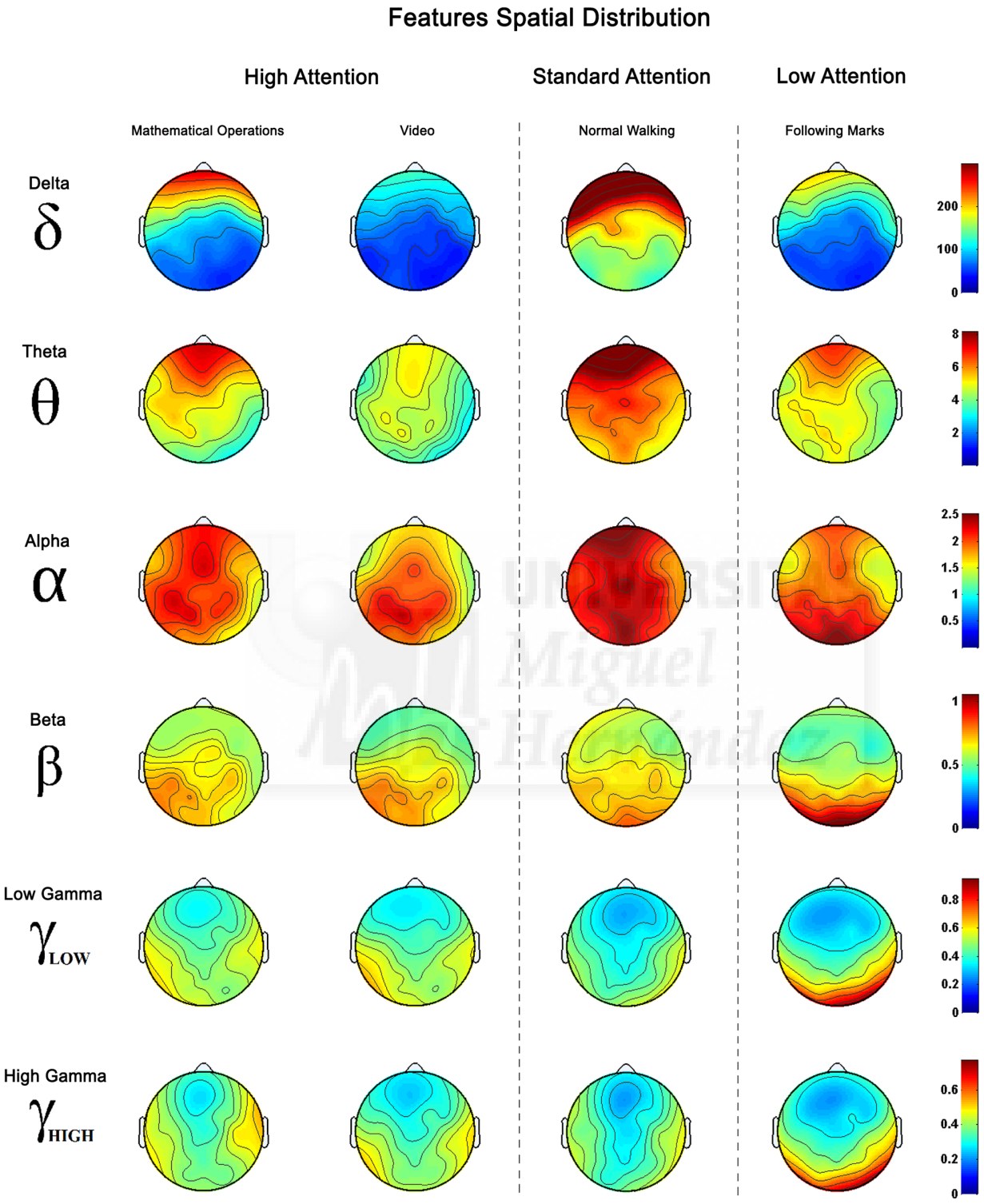

Fig 5. Features Spatial Distribution. Spatial distribution is represented for each task and frequency. Features used are computed by averaging the features of every subject (healthy users and patients) and sessions for each task and frequency band. Tasks are arranged according to the increasing attentional demand.

doi:10.1371/journal.pone.0154136.g005

Table 1. Bhattacharyya distance. Values of *bdist* for the paired combination of tasks on each frequency band. All *bdist* values > 3 are marked in bold. Highest *bdist* values for each task combinations are marked with * and second highest *bdist* values are marked with **.

	AB	AC	AD	BC	BD	CD
1–4Hz	**16.62***	**17.86***	**16.32***	1.68	1.52	1.68
4–8Hz	**9.25**	**9.76**	**9.63**	0.85	1.36	1.20
8–12Hz	**8.68**	**9.32**	**9.35**	1.06	1.84	1.60
12–30Hz	**8.82**	**9.32**	**9.89**	1.35	2.95	2.61
30–50Hz	**8.22**	**8.88**	**9.64**	1.86**	**4.96****	**4.19****
50–90Hz	**9.41****	**10.81****	**11.40****	**3.98***	**7.23***	**5.91***

doi:10.1371/journal.pone.0154136.t001

Table 2. Success Rates and Standard Deviation. Success rates for all subjects (10 healthy and 3 patients) and classifiers for both frequency band features.

				γ_{low}		
		SVM	**NB**	**LDA**	**KNN**	**DTL**
Users	**H1**	77.38±12.38	52.02±12.37	78.10±5.66	73.38±14.03	73.29±6.49
	H2	68.86±12.05	44.17±9.60	67.74±9.54	65.99±13.27	59.43±13.36
	H3	76.89±6.45	53.52±7.43	72.99±7.38	73.71±9.96	69.76±7.13
	H4	68.38±3.99	36.44±3.82	62.74±4.16	66.18±3.59	61.25±4.71
	H5	76.37±7.62	60.62±8.01	72.31±8.05	72.73±8.54	66.32±5.81
	H6	70.31±15.06	45.79±8.94	69.62±14.81	67.40±14.44	61.31±9.92
	H7	59.36±6.47	33.81±6.73	54.52±6.43	58.05±9.09	52.07±6.63
	H8	68.74±7.79	37.09±6.28	59.40±5.13	66.60±8.71	60.29±6.77
	H9	67.00±6.85	39.22±9.82	63.37±6.16	65.31±8.36	58.94±4.69
	H10	57.42±6.57	31.38±7.49	54.87±5.67	52.31±9.84	50.81±5.08
	H11	60.51±8.24	47.41±8.93	75.38±9.71	67.24±6.69	62.39±6.86
	H12	71.66±9.22	61.37±5.09	72.31±6.65	72.63±7.90	68.00±5.92
	P1	53.66±7.00	40.95±4.33	62.72±3.92	54.09±3.94	51.83±6.47
	P2	67.56±4.33	37.28±5.65	62.39±10.71	71.12±5.40	63.36±4.42
	P3	48.28±2.96	28.99±4.16	50.54±4.18	52.05±6.54	49.14±5.15
	Avg	**66.16±11.54**	**43.34±12.02**	**65.27±10.53**	**65.27±11.84**	**60.55±9.95**
				γ_{high}		
	H1	77.15±13.33	36.31±11.68	78.47±7.49	74.03±14.94	73.35±7.55
	H2	69.89±14.41	41.48±8.54	71.53±12.24	67.79±14.63	62.97±11.89
	H3	77.15±7.15	47.11±6.30	74.51±7.22	72.99±10.63	69.79±7.79
	H4	68.99±3.20	26.83±2.98	63.80±4.34	67.79±4.25	62.83±4.19
	H5	77.65±7.88	62.36±8.19	78.32±7.60	73.31±9.61	68.75±7.78
	H6	71.49±16.78	50.18±10.00	71.17±14.90	67.78±14.64	60.83±12.74
	H7	59.87±8.66	33.39±6.06	57.39±6.44	56.37±10.95	52.17±8.54
	H8	73.88±10.11	33.46±6.57	66.18±10.10	72.32±12.57	67.92±9.48
	H9	65.80±7.84	38.87±7.00	63.51±6.74	62.89±8.56	57.00±6.90
	H10	58.48±5.70	32.69±5.83	55.66±5.94	56.96±8.24	53.74±9.91
	H11	63.63±9.86	60.08±10.63	67.30±8.67	66.43±10.38	61.48±7.91
	H12	71.07±10.81	60.67±5.62	75.86±7.47	78.45±10.88	74.46±6.04
	P1	50.75±5.27	36.75±5.65	59.81±4.39	58.19±6.96	53.77±6.59
	P2	69.94±6.85	39.55±8.42	67.46±9.34	73.81±6.38	68.00±7.02
	P3	48.92±2.47	28.34±3.98	53.45±5.89	55.50±6.96	54.20±4.94
	Avg	**66.98±12.46**	**41.87±11.95**	**66.96±11.59**	**66.97±12.52**	**62.75±10.82**

doi:10.1371/journal.pone.0154136.t002

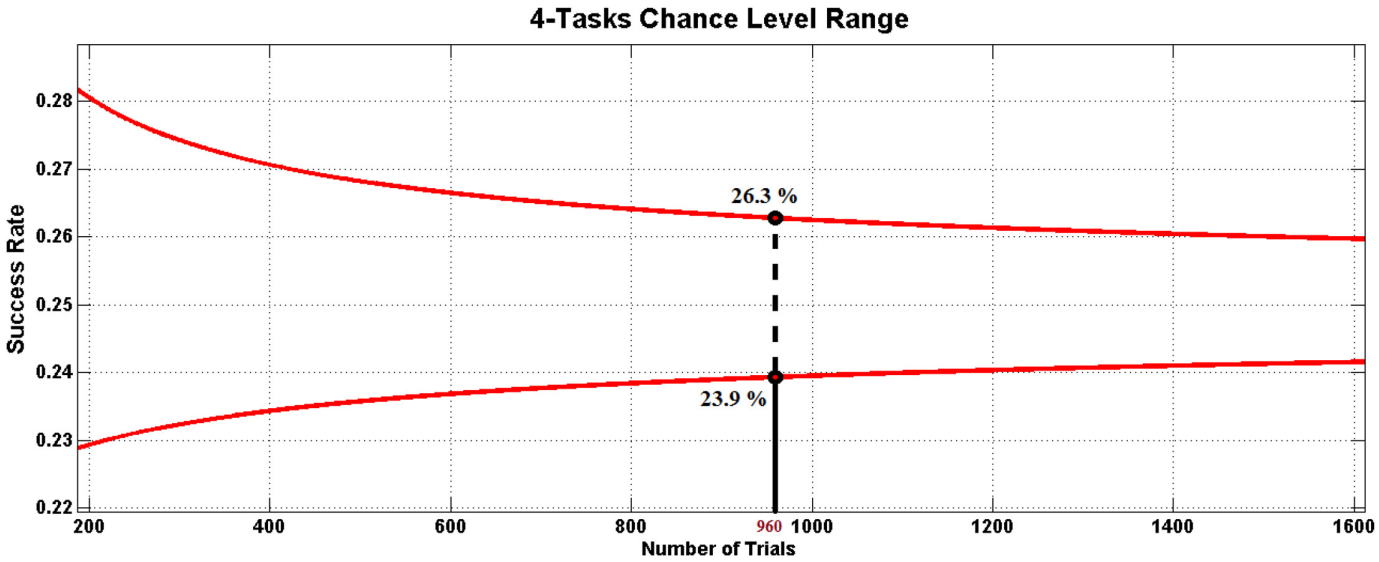

Fig 6. Chance Level Range. The range of variation of the chance level for a 4-task classification system is shown depending on the number of epochs classified. The top and bottom lines represent the highest and the minimum values admissible to consider the current classification random. These values are selected for the number of epochs of the current work ($n = 960$).

doi:10.1371/journal.pone.0154136.g006

value of the chance level for each group (a 192/24 vector, respectively, with random values from the chance level range computed). The significance of these success rates is analyzed from these results. To that end, the chance level is compared to the success rate obtained for each classifier running a Wilcoxon Sum-Rank Test with a confidence interval of 95% and then applying a Bonferroni correction for multiple comparisons. This analysis shows that the success rates are predominantly above chance levels ($p < 0.05$) for all 5 classifiers.

Significance between classifiers, features sets and subjects. To test the significance between classifier outputs, feature sets and subjects, the same statistical approach is applied. Table 3 shows the significance p values of comparing the same classifier for 4 different conditions: 1) γ_{low} features: healthy against patients; 2) γ_{high} features: healthy against patients; 3) Healthy: γ_{low} against γ_{high} features; 4) Patients: γ_{low} against γ_{high} features. Table 4, on the other hand, shows the significance p values for all the classifier combinations for the 4 graphs of Fig 7. On both tables, the significant p values are marked in bold after applying a Bonferroni correction.

Discussion

On the spatial distribution of the averaged features shown in Fig 5 it is possible to appreciate some differentiation between tasks and frequencies. Focusing on the minimum and maximum spectral power values used to represent each frequency, it is shown that the spectral power of EEG signals gets lower when the frequency evaluated increases. In δ and θ bands, the distributions present huge deviations between tasks and the main activation is located on the frontal lobe usually associated to blinks, head movements and other physiological artifacts [61]. These results fit the statements of Kline et al. in [33] claiming that motion artifacts have higher contributions on lower frequency bands and present huge variations depending on the subject and the walking speed. α band shows a main activation on the motor area which is an expected behavior during walking. According to literature, the motor cortex side activated depends on the real or imagined motor movement performed [62, 63]. For that reason, during walking, left

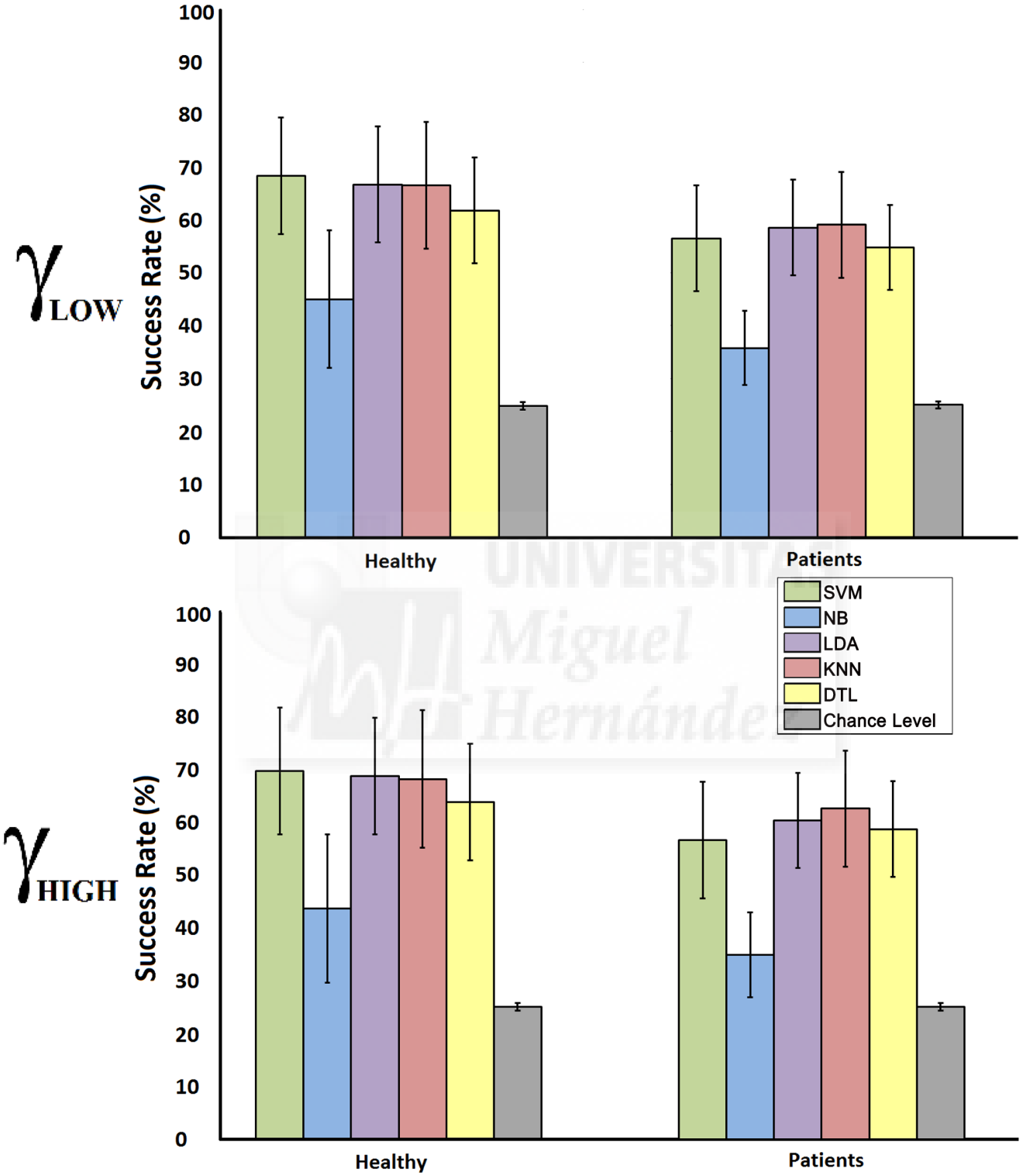

Fig 7. Chance Level Range. The graphs show the average success rate of each classifier and the computed chance level for 4 equally distributed tasks and the amount of epochs used during the cross validation. Graph A shows the results for γ_{high} features, while graph B shows the results for γ_{low} features.

doi:10.1371/journal.pone.0154136.g007

Table 3. Significance between classifiers. Significance values for the paired combination of classifiers for healthy and patient both using γ_{low} and γ_{high} features.

		Healthy$_{\gamma_{low}}$		
	SVM	NB	LDA	KNN
NB	**$2.2 \cdot 10^{-40}$**	-	-	-
LDA	**$2.0 \cdot 10^{-3}$**	**$5.4 \cdot 10^{-36}$**	-	-
KNN	$2.6 \cdot 10^{-2}$	**$4.1 \cdot 10^{-35}$**	$3.5 \cdot 10^{-1}$	-
DLT	**$6.2 \cdot 10^{-11}$**	**$1.5 \cdot 10^{-29}$**	**$4.9 \cdot 10^{-4}$**	**$8.0 \cdot 10^{-6}$**
		Healthy$_{\gamma_{high}}$		
NB	**$2.7 \cdot 10^{-8}$**	-	-	-
LDA	$5.8 \cdot 10^{-2}$	**$2.0 \cdot 10^{-41}$**	-	-
KNN	$4.3 \cdot 10^{-2}$	**$4.1 \cdot 10^{-38}$**	$8.5 \cdot 10^{-1}$	-
DLT	**$8.8 \cdot 10^{-5}$**	**$6.4 \cdot 10^{-35}$**	**$1.0 \cdot 10^{-4}$**	**$1.7 \cdot 10^{-4}$**
		Patient$_{\gamma_{low}}$		
NB	**$2.7 \cdot 10^{-8}$**	-	-	-
LDA	$5.1 \cdot 10^{-1}$	**$7.6 \cdot 10^{-9}$**	-	-
KNN	$2.7 \cdot 10^{-1}$	**$5.6 \cdot 10^{-9}$**	$9.8 \cdot 10^{-1}$	-
DLT	$5.0 \cdot 10^{-1}$	$2.5 \cdot 10^{-8}$	$2.0 \cdot 10^{-1}$	$1.8 \cdot 10^{-1}$
		Patient$_{\gamma_{high}}$		
NB	**$4.3 \cdot 10^{-14}$**	-	-	-
LDA	**$3.1 \cdot 10^{-5}$**	**$3.1 \cdot 10^{-10}$**	-	-
KNN	**$2.1 \cdot 10^{-3}$**	**$8.8 \cdot 10^{-11}$**	**$2.0 \cdot 10^{-2}$**	-
DLT	**$4.8 \cdot 10^{-6}$**	**$2.3 \cdot 10^{-9}$**	**$1.4 \cdot 10^{-4}$**	**$2.5 \cdot 10^{-4}$**

doi:10.1371/journal.pone.0154136.t003

and right areas of motor cortex are alternatively activated disguising any changes related with the attention. In the β band, the spectral power is softer in the motor area and experiences a smooth increase in the occipital area. Finally, for γ_{low} and γ_{high} bands there is a significant reduction on the motor cortex where the power and distribution seems to be related to the attention level classified. Compared with the motor cortex, the occipital area is much more active suggesting that visual information is being processed. These results and those provided in Table 1 about class separability suggest that the measurement of the attention level on the gait is closely related to the selective attention. As it was stated at the beginning of the paper, selective attention is described as the attention paid to an external object, action or stimulus while another object, action or stimulus, simultaneously happening, is ignored. In this case, the gait process and the environmental visual information are the event and action, respectively, confronted, and the gait attention changes depending on which event is more or less ignored or attended.

Classification values on Fig 7 and the test performed show that all classifiers tested provide significant values in the classification of this attention level, confirming the existence of discernible information related to the attention level on the gait obtained from γ band features. On rows 1 and 2 of Table 4, each classifier from healthy users is compared with its analog on patients showing, in most cases, significant differences between them. These results imply that the classification results from patients are significantly different than those obtained from healthy. This significance could be a consequence of the inherent increased attention on gait presented on incomplete SCI patients who are always more focused on the gait than healthy subjects regardless the distraction event presented to them [18, 19]. Both healthy subjects and patients performed the same tasks and the classification model was trained according to them, but patients' attention on gait was always higher than healthy's during standard and low

Table 4. Significance between bands and users. Rows 1 and 2: Significance values for both frequency features between healthy and patients. Rows 3 and 4: Significance values for both healthy and patients between frequency bands.

	SVM-SVM	NB-NB	LDA-LDA	KNN-KNN	DLT-DLT
γ_{low}: *Healthy–Patient*	$\mathbf{1.44 \cdot 10^{-6}}$	$\mathbf{2.90 \cdot 10^{-3}}$	$\mathbf{2.60 \cdot 10^{-3}}$	$\mathbf{3.00 \cdot 10^{-3}}$	$\mathbf{1.50 \cdot 10^{-3}}$
γ_{high}: *Healthy–Patient*	$\mathbf{1.64 \cdot 10^{-6}}$	$7.17 \cdot 10^{-2}$	$\mathbf{6.01 \cdot 10^{-4}}$	$\mathbf{3.30 \cdot 10^{-2}}$	$\mathbf{2.49 \cdot 10^{-2}}$
Healthy: $\gamma_{low} - \gamma_{high}$	$2.84 \cdot 10^{-1}$	$\mathbf{1.87 \cdot 10^{-2}}$	$\mathbf{3.46 \cdot 10^{-2}}$	$3.19 \cdot 10^{-1}$	$7.98 \cdot 10^{-2}$
Patient: $\gamma_{low} - \gamma_{high}$	$9.51 \cdot 10^{-1}$	$5.29 \cdot 10^{-1}$	$6.13 \cdot 10^{-1}$	$2.56 \cdot 10^{-1}$	$1.73 \cdot 10^{-1}$

doi:10.1371/journal.pone.0154136.t004

attention tasks. On the other hand, rows 3 and 4 for Table 4 show the same classifier comparison but this time between frequency bands, showing no significant values except for classifiers C2 (NB) and C3 (LDA) on healthy users. These values suggest that the information is similar in both bands and their combination in the feature extraction stage could improve the final classification results.

Finally, on Table 3, for each subject group (healthy and patients) and frecuency band (γ_{low} and γ_{high}), the classifiers are compared between them showing in most cases no significant results between them. In that case, the optimal classifiers selection could be performed by the maximum average success rate. Focusing on Fig 7, classifiers SVM, LDA and KNN provide, in general the best results, being SVM performance slightly higher on healthy users and LDA and KNN on patients.

Conclusion

In this paper, different frequency bands extracted from data of 10 healthy users and 3 incomplete SCI patients have been evaluated to find a relationship between cortical signals and the cognitive mechanisms related to the attenton during gait. The study emphasizes the difficulties to decode cortical information on low frequency (δ and θ) bands due to the artifacts generated by movement and also to classify the cortical information on α band related to attention which is covered up by the motor rhythms produced during gait on cortical signals. On the other hand, information related to selective attention mechanisms that relate the attention to the gait and the attention to the external environment have been found in the γ band. The band selection has been performed by computing a separability index between tasks using the Bhattacharyya distance and the features extracted have been tested using 5 classifiers with an 8-fold cross validation. Final results provide an average value of 67% of success rate classification for 4 attention tasks. Success rate values have been compared to chance level, showing clear significance. Healthy users have obtained significantly higher classification results suggesting that there was less class separability on patient's which is related to the higher level of attention they pay on non-attentional tasks due to their motor disabilities.

This work settles a basis for gait attention classification. For future works this offline analysis should be performed with a higher patient population. In addition, the features extraction should be improved combining both low and high γ bands and using mathematical algorithms for feature selection and reduction. The number of tasks used to train the model should be reduced to 3, removing one of the high gait attention tasks and improving this way the final success rate. Current processing algorithms should be changed to fit real time condition in order to perform online tests with healthy users and patients. Also the the reference electrode standardization technique (REST) [64] should be tested on the data to improve the quality of EEG signals in terms of spatial resolution and artifacts' identification. And, as a final goal, an online system that provides the attention level of an incomplete SCI patient under exoskeleton

rehabilitation could be used to change, in real time, the parameters of the rehabilitation to fit better to the cognitive state of the patients and improve the rehabilitation performance by involving them in a deeper level.

Author Contributions

Conceived and designed the experiments: AC JMA EI. Performed the experiments: AC EI EH AU AJDA. Analyzed the data: AC AU EH. Contributed reagents/materials/analysis tools: AC AJDA AGA JMA. Wrote the paper: AC EI AU EH AJDA AGA JMA.

References

1. Organization WH, et al. World report on disability. 2011;.
2. Westgren N, Levi R. Quality of life and traumatic spinal cord injury. Archives of physical medicine and rehabilitation. 1998; 79(11): 1433–1439. doi: 10.1016/S0003-9993(98)90240-4 PMID: 9821906
3. Kay E, Kilonzo C, Harris MJ. Improving rehabilitation services in developing nations: the proposed role of physiotherapists. Physiotherapy. 1994; 80(2):77–82. doi: 10.1016/S0031-9406(10)61012-7
4. Van Twillert S, Postema K, Geertzen JH, Hemminga T, Lettinga AT. Improving rehabilitation treatment in a local setting: a case study of prosthetic rehabilitation. Clinical rehabilitation. 2009; 23(10):938–947. doi: 10.1177/0269215509338125 PMID: 19717507
5. Kalra L, Dale P, Crome P. Improving stroke rehabilitation. A controlled study. Stroke. 1993; 24 (10):1462–1467. doi: 10.1161/01.STR.24.10.1462 PMID: 8378947
6. Dimyan MA, Cohen LG. Neuroplasticity in the context of motor rehabilitation after stroke. Nature Reviews Neurology. 2011; 7(2):76–85. doi: 10.1038/nrneurol.2010.200 PMID: 21243015
7. Stephenson R. A review of neuroplasticity: some implications for physiotherapy in the treatment of lesions of the brain. Physiotherapy. 1993; 79(10):699–704. doi: 10.1016/S0031-9406(10)60008-9
8. Zimmerli L, Duschau-Wicke A, Riener R, Mayr A, Lünenburger L. Virtual reality and gait rehabilitation Augmented feedback for the Lokomat. In: Virtual Rehabilitation International Conference, 2009. IEEE; 2009. p. 150–153.
9. Koenig A, Brütsch K, Zimmerli L, Guidali M, Duschau-Wicke A, Wellner M, et al. Virtual environments increase participation of children with cerebral palsy in robot-aided treadmill training. IEEE; 2008.
10. Lin TY, Hsieh CH, et al. A kinect-based system for physical rehabilitation: Utilizing tai chi exercises to improve movement disorders in patients with balance ability. In: Modelling Symposium (AMS), 2013 7th Asia. IEEE; 2013. p. 149–153.
11. Daly JJ, Wolpaw JR. Brain-computer interfaces in neurological rehabilitation. The Lancet Neurology. 2008; 7(11):1032–1043. doi: 10.1016/S1474-4422(08)70223-0 PMID: 18835541
12. Dobkin BH. Brain-computer interface technology as a tool to augment plasticity and outcomes for neurological rehabilitation. The Journal of physiology. 2007; 579(3):637–642. doi: 10.1113/jphysiol.2006.123067 PMID: 17095557
13. Stevens JA, Stoykov MEP. Using motor imagery in the rehabilitation of hemiparesis. Archives of physical medicine and rehabilitation. 2003; 84(7):1090–1092. doi: 10.1016/S0003-9993(03)00042-X PMID: 12881842
14. Ang KK, Guan C, Chua KSG, Ang BT, Kuah C, Wang C, et al. A clinical study of motor imagerybased brain-computer interface for upper limb robotic rehabilitation. In: Engineering in Medicine and Biology Society, 2009. EMBC 2009. Annual International Conference of the IEEE. IEEE; 2009. p. 5981–5984.
15. Heruti RJ, Lusky A, Dankner R, Ring H, Dolgopiat M, Barell V, et al. Rehabilitation outcome of elderly patients after a first stroke: effect of cognitive status at admission on the functional outcome. Archives of physical medicine and rehabilitation. 2002; 83(6):742–749. doi: 10.1053/apmr.2002.32739 PMID: 12048650
16. Woollacott M, Shumway-Cook A. Attention and the control of posture and gait: a review of an emerging area of research. Gait & posture. 2002; 16(1):1–14. doi: 10.1016/S0966-6362(01)00156-4
17. Yogev-Seligmann G, Hausdorff JM, Giladi N. The role of executive function and attention in gait. Movement disorders. 2008; 23(3):329–342. doi: 10.1002/mds.21720 PMID: 18058946
18. Martin KL, Blizzard L, Wood AG, Srikanth V, Thomson R, Sanders LM, et al. Cognitive function, gait, and gait variability in older people: a population-based study. The Journals of Gerontology

Series A: Biological Sciences and Medical Sciences. 2013; 68(6):726–732. doi: 10.1093/gerona/gls224

19. Mielke MM, Roberts RO, Savica R, Cha R, Drubach DI, Christianson T, et al. Assessing the temporal relationship between cognition and gait: slow gait predicts cognitive decline in the Mayo Clinic Study of Aging. The Journals of Gerontology Series A: Biological Sciences and Medical Sciences. 2013; 68 (8):929–937. doi: 10.1093/gerona/gls256
20. Parker TM, Osternig LR, Lee HJ, van Donkelaar P, Chou LS. The effect of divided attention on gait stability following concussion. Clinical biomechanics. 2005; 20(4):389–395. doi: 10.1016/j.clinbiomech.2004.12.004 PMID: 15737446
21. Springer S, Giladi N, Peretz C, Yogev G, Simon ES, Hausdorff JM. Dual-tasking effects on gait variability: The role of aging, falls, and executive function. Movement Disorders. 2006; 21(7):950–957. doi: 10.1002/mds.20848 PMID: 16541455
22. Ray WJ, Cole HW. EEG alpha activity reflects attentional demands, and beta activity reflects emotional and cognitive processes. Science. 1985; 228(4700):750–752. doi: 10.1126/science.3992243 PMID: 3992243
23. Ray WJ, Cole HW. EEG activity during cognitive processing: influence of attentional factors. International Journal of Psychophysiology. 1985; 3(1):43–48. doi: 10.1016/0167-8760(85)90018-2 PMID: 4044364
24. Klimesch W, Doppelmayr M, Russegger H, Pachinger T, Schwaiger J. Induced alpha band power changes in the human EEG and attention. Neuroscience letters. 1998; 244(2):73–76. doi: 10.1016/S0304-3940(98)00122-0 PMID: 9572588
25. Lansbergen MM, Arns M, van Dongen-Boomsma M, Spronk D, Buitelaar JK. The increase in theta/beta ratio on resting-state EEG in boys with attention-deficit/hyperactivity disorder is mediated by slow alpha peak frequency. Progress in Neuro-Psychopharmacology and Biological Psychiatry. 2011; 35(1):47–52. doi: 10.1016/j.pnpbp.2010.08.004 PMID: 20713113
26. Doesburg SM, Roggeveen AB, Kitajo K,Ward LM. Large-scale gamma-band phase synchronization and selective attention. Cerebral Cortex. 2008; 18(2):386–396. doi: 10.1093/cercor/bhm073 PMID: 17556771
27. Fell J, Fernandez G, Klaver P, Elger CE, Fries P. Is synchronized neuronal gamma activity relevant for selective attention? Brain Research Reviews. 2003; 42(3):265–272. doi: 10.1016/S0165-0173(03)00178-4 PMID: 12791444
28. Gruber T, Müller MM, Keil A, Elbert T. Selective visual-spatial attention alters induced gamma band responses in the human EEG. Clinical neurophysiology. 1999; 110(12):2074–2085. doi: 10.1016/S1388-2457(99)00176-5 PMID: 10616112
29. Müuller MM, Gruber T, Keil A. Modulation of induced gamma band activity in the human EEG by attention and visual information processing. International Journal of Psychophysiology. 2000; 38(3):283–299. doi: 10.1016/S0167-8760(00)00171-9
30. Polich J. Attention, probability, and task demands as determinants of P300 latency from auditory stimuli. Electroencephalography and clinical neurophysiology. 1986; 63(3):251–259. doi: 10.1016/0013-4694(86)90093-3 PMID: 2419083
31. Gray HM, Ambady N, Lowenthal WT, Deldin P. P300 as an index of attention to self-relevant stimuli. Journal of experimental social psychology. 2004; 40(2):216–224. doi: 10.1016/S0022-1031(03)00092-1
32. Killane I, Browett G, Reilly RB. Measurement of attention during movement: Acquisition of ambulatory EEG and cognitive performance from healthy young adults. In: Engineering in Medicine and Biology Society (EMBC), 2013 35th Annual International Conference of the IEEE. IEEE; 2013. p. 6397–6400.
33. Kline JE, Huang HJ, Snyder KL, Ferris DP. Isolating gait-related movement artifacts in electroencephalography during human walking. Journal of neural engineering. 2015; 12(4):046022. doi: 10.1088/1741-2560/12/4/046022 PMID: 26083595
34. Cicerone KD. Attention deficits and dual task demands after mild traumatic brain injury. Brain Injury. 1996; 10(2):79–90. doi: 10.1080/026990596124566 PMID: 8696318
35. Ryu K, Myung R. Evaluation of mental workload with a combined measure based on physiological indices during a dual task of tracking and mental arithmetic. International Journal of Industrial Ergonomics. 2005; 35(11):991–1009. doi: 10.1016/j.ergon.2005.04.005
36. Bruehlmeier M, Dietz V, Leenders K, Roelcke U, Missimer J, Curt A. How does the human brain deal with a spinal cord injury? European Journal of Neuroscience. 1998; 10(12):3918–3922. doi: 10.1046/j.1460-9568.1998.00454.x PMID: 9875370
37. Sanei S, Chambers JA. EEG signal processing. John Wiley & Sons; 2013.

38. Samek W, Meinecke FC, Muller KR. Transferring Subspaces Between Subjects in Brain-Computer Interfacing. Biomedical Engineering, IEEE Transactions on. 2013; 60(8):2289–2298. doi: 10.1109/TBME.2013.2253608

39. Gasser T, Sroka L, Möcks J. The transfer of EOG activity into the EEG for eyes open and closed. Electroencephalography and Clinical Neurophysiology. 1985; 61(2):181–193. doi: 10.1016/0013-4694(85)91058-2 PMID: 2410229

40. Grosse P, Cassidy M, Brown P. EEG-EMG, MEG-EMG and EMG-EMG frequency analysis: physiological principles and clinical applications. Clinical Neurophysiology. 2002; 113(10):1523–1531. doi: 10.1016/S1388-2457(02)00223-7 PMID: 12350427

41. Lachaux JP, Pezard L, Garnero L, Pelte C, Renault B, Varela FJ, et al. Spatial extension of brain activity fools the single-channel reconstruction of EEG dynamics. Human brain mapping. 1997; 5(1):26–47. doi: 10.1002/(SICI)1097-0193(1997)5:1%3C26::AID-HBM4%3E3.3.CO;2-S PMID: 20408208

42. Holsheimer J, Feenstra B. Volume conduction and EEG measurements within the brain: a quantitative approach to the influence of electrical spread on the linear relationship of activity measured at different locations. Electroencephalography and clinical neurophysiology. 1977; 43(1):52–58. doi: 10.1016/0013-4694(77)90194-8 PMID: 68872

43. Lotte F, Guan C. Spatially regularized common spatial patterns for EEG classification. In: Pattern Recognition (ICPR), 2010 20th International Conference on. IEEE; 2010. p. 3712–3715.

44. Rainford B, Daniell G. μSR frequency spectra using the maximum entropy method. Hyperfine Interactions. 1994; 87(1):1129–1134. doi: 10.1007/BF02068515

45. Schels HF, Haberl R, Jilge G, Steinbigler P, Steinbeck G. Frequency analysis of the electrocardiogram with maximum entropy method for identification of patients with sustained ventricular tachycardia. Biomedical Engineering, IEEE Transactions on. 1991; 38(9):821–826. doi: 10.1109/10.83601

46. Garipelli G, Chavarriaga R, del R Millan J. Single trial recognition of anticipatory slow cortical potentials: the role of spatio-spectral filtering. In: Neural Engineering (NER), 2011 5th International IEEE/EMBS Conference on. IEEE; 2011. p. 408–411.

47. Bhattacharyya A. On a measure of divergence between two multinomial populations. Sankhyā: The Indian Journal of Statistics. 1946; p. 401–406.

48. Guorong X, Peiqi C, Minhui W. Bhattacharyya distance feature selection. In: Pattern Recognition, 1996, Proceedings of the 13th International Conference on. vol. 2. IEEE; 1996. p. 195–199.

49. Chaudhuri G, Borwankar J, Rao P. Bhattacharyya Distance based linear discriminant function for stationary time series. Communications in Statistics-Theory and Methods. 1991; 20(7):2195–2205. doi: 10.1080/03610929108830627

50. Kailath T. The divergence and Bhattacharyya distance measures in signal selection. Communication Technology, IEEE Transactions on. 1967; 15(1):52–60. doi: 10.1109/TCOM.1967.1089532

51. Choi E, Lee C. Feature extraction based on the Bhattacharyya distance. Pattern Recognition. 2003; 36(8):1703–1709. doi: 10.1016/S0031-3203(03)00035-9

52. Antos A, Devroye L, Györfi L. Lower bounds for Bayes error estimation. Pattern Analysis and Machine Intelligence, IEEE Transactions on. 1999; 21(7):643–645. doi: 10.1109/34.777375

53. Thome ACG. SVM Classifiers-Concepts and Applications to Character Recognition. INTECH Open Access Publisher; 2012.

54. Flórez F, Azorín JM, Iáñez E, Ubeda A, Fernández E. Development of a Low-cost SVM-based Spontaneous Brain-computer Interface. In: IJCCI (NCTA); 2011. p. 415–421.

55. Murphy KP. Naive bayes classifiers. University of British Columbia. 2006;.

56. Scholkopft B, Mullert KR. Fisher discriminant analysis with kernels. Neural networks for signal processing IX. 1999; 1:1.

57. Cunningham P, Delany SJ. k-Nearest neighbour classifiers. Multiple Classifier Systems. 2007; p. 1–17.

58. Safavian SR, Landgrebe D. A survey of decision tree classifier methodology. IEEE transactions on systems, man, and cybernetics. 1991; 21(3):660–674. doi: 10.1109/21.97458

59. Mueller-Putz G, Scherer R, Brunner C, Leeb R, Pfurtscheller G. Better than random: A closer look on BCI results. International Journal of Bioelectromagnetism. 2008; 10(EPFL-ARTICLE-164768):52–55.

60. Genz A, Kwong KS. Numerical evaluation of singular multivariate normal distributions. Journal of Statistical Computation and Simulation. 2000; 68(1):1–21. doi: 10.1080/00949650008812053

61. Reyes CE, Rugayan JLC, Jason C, Rullan G, Oppus CM, Tangonan GL. A study on ocular and facial muscle artifacts in EEG signals for BCI applications. In: TENCON 2012–2012 IEEE Region 10 Conference. IEEE; 2012. p. 1–6.

62. Porro CA, Francescato MP, Cettolo V, Diamond ME, Baraldi P, Zuiani C, et al. Primary motor and sensory cortex activation during motor performance and motor imagery: a functional magnetic resonance imaging study. The Journal of neuroscience. 1996; 16(23):7688–7698. PMID: 8922425

63. Pfurtscheller G, Neuper C. Motor imagery activates primary sensorimotor area in humans. Neuroscience letters. 1997; 239(2):65–68. doi: 10.1016/S0304-3940(97)00889-6 PMID: 9469657

64. Yao D. A method to standardize a reference of scalp EEG recordings to a point at infinity. Physiological measurement. 2001; 22(4):693. doi: 10.1088/0967-3334/22/4/305 PMID: 11761077

Apéndice C

CONTRIBUCIONES EN CONGRESOS

C.1. Contribución 1

Experimental Setup and First Results of a BCI System for Attention Levels Classification During Gait

Álvaro Costa, Eduardo Iáñez, Andrés Úbeda, Daniel Panelles, Enrique Hortal and José M. Azorín[1]

Miguel Hernández University, Av. de la Universidad S/N 03202 Elche, Spain
acosta@umh.es,
WWW home page: http://bmi.umh.es/

Abstract. This paper presents preliminary results obtained in the classification of attention levels during gait. For that purpose an experimental environment and equipment is going to be presented. EEG signals are measured while a user walks on a treadmill. Users are asked to perform several activities during walking in order to generate changes in their levels of attention. Signals registered are processed and analyzed to extract their features. Several classifiers have been tested using these features as input. First investigations show a success rate of 65,25% for the classification of four attention levels.

Keywords: Attention levels, Brain-Machine Interface, Rehabilitation

1 INTRODUCTION

Nowadays, there are people who suffer from several motor diseases that affect their daily life. When an illness prevents a person from moving their muscles, tasks, otherwise easy to perform, become a hard challenge to accomplish. Brain-Machine Interfaces (BMI) allow the communication between humans and machines using several electrophysiological signals like electro-ocular (EOG) signals produced by the movement of the eyes or electroencephalographic (EEG) signals produced in the brain [1]. These interfaces are focusing more and more each day on helping people suffering from disabilities. BMI systems provide a new way of interaction between a person and their surroundings [2, 3]. BMI systems can be classified as either invasive and non-invasive depending on the methods used to register the brain signals. Non-invasive technologies are more extended than invasive technologies because they do not bring up ethical questions and neither have the risk associated with the occurrence of medical complications during surgeries to place electrodes inside the scalp. Non-invasive BMI systems are used to treat and help people with different degrees of disabilities from severe motor limitation, like Locked-in Syndrome and Spinal Cord Injuries [4], or minor treatable motor injuries like those produced on accidents that can be reversed through rehabilitation [5, 6].

Workshop Proceedings of IAS-13
13th Intl. Conf. on Intelligent Autonomous Systems
Padova (Italy) July 15-19, 2014
ISBN 978-88-95872-06-3 pp. 470-473

This research is part of the BioMot project - Smart Wearable Robots with Bioinspired Sensory-Motor Skills (Grant Agreement number IFP7-ICT- 2013-10-611695), which main goal is to develop a wearable robot for rehabilitation tasks that uses EEG information in order to improve the rehabilitation results on patients. This paper presents an experimental environment designed to measure EEG signals from users during gait. Through this environment, several levels of attention are stimulated on the user in order to evaluate how the attention mechanism affects the gait of a person. When the gait becomes more natural for the patient, the attention put on the gait is reduced. For that reason, measuring the level of attention provide useful information about the enhancement in the rehabilitation, allowing the rehabilitation system to adapt the rehabilitation process depending on that attention level. First tests have been performed by healthy users providing results clearly above chance levels for the classification of 4 different attention levels during walking.

2 MATERIAL AND METHODS

2.1 Setup

EEG register equipment is carried by the user in a backpack to provide he/she freedom of movement during the gait. This equipment is connected to a computer where the data are stored. A treadmill is used to simulate a constant gait. A screen is placed in front of the user to provide visual stimulation to generate different levels of attention.

2.2 Register and Processing

Signals are registered with 2 commercial amplifiers g.USBamp from g.Tec with the g.GAMMAcap which has active electrodes to reduce signal/noise ratio. The acquisition of EEG signals is done using 32 electrodes placed over the scalp with the following distribution: FZ, FC5, FC3, FC1, FCz, FC2, FC4, FC6, C5, C3, C1, Cz, C2, C4, C6, CP5, CP3, CP1, CPz, CP2, CP4, CP6, P3, P1, Pz, P2, P4, PO7, PO3, POz, PO4 and PO8 according to the International System 10/10 with a monoauricular reference in the right earlobe and ground in AFz. A sampling frequency of 1200 Hz has been used. A bandpass filter from 0.5 to 100 Hz has been applied. Also, a 50 Hz Notch filter to remove the power line interference is used. The time signal is divided into 1000 ms windows with a 500 ms overlap between windows. On each window a three-nearest neighbors Laplacian filter is applied. The spectrum of the signals is computed using the Welch method as in [7]. One feature per electrode is obtained as the addition of all frequencies from 8 to 40 hz. The complete features vector (32 features) is used as input for several classifiers listed as follows: Support Vector Machine (SVM), K-Nearest Neighbor(Knn), Naive Bayes(NB), Linear Discriminant Analysis classifier(LDA) and Quadratic Discriminant Analysis(QDA). The efficiency of each classifier has been tested with a cross validation between sessions.

Workshop Proceedings of IAS-13
13th Intl. Conf. on Intelligent Autonomous Systems
Padova (Italy) July 15-19, 2014
ISBN 978-88-95872-06-3 pp. 470-473

2.3 Experimental Procedure

The system has been tested with 4 healthy users, all of them right-handed with ages between 23 and 31 (27,5 ± 3.32). After preparing all the equipment, the user is asked to start walking on the treadmill with a constant velocity of 2 km/h and 0 degrees of inclination. First task is walking normally, looking at the front without any distractions. This task is going to be classified as standard attention level. During the second task, the screen shows mathematical operations that the user should mentally solve. On the third task a short video is shown on the screen. These two tasks simulate a low attention level over the gait. On the last task, the user is asked to walk following several marks planted on the treadmill. These marks are not perfectly adapted to the normal gait of the user and force he/she to increase his/her attention level on the gait. A whole session is composed of 8 runs with 20-30 seconds between runs. A graphical explanation of a session is shown on figure 1.

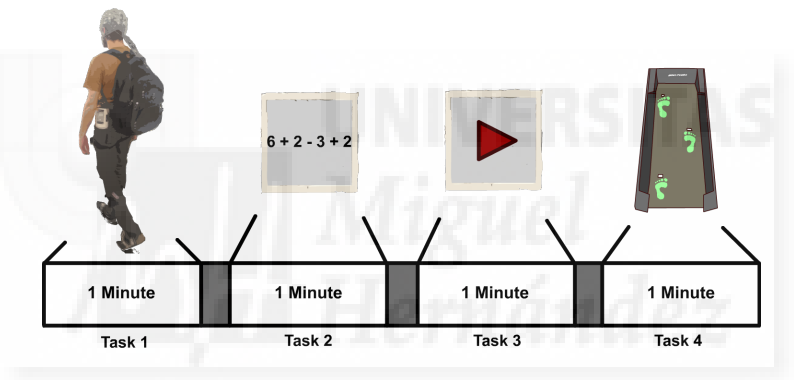

Fig. 1. Time spent during a run. Task 1: Normal walk. Task 2: Perform mathematical operations. Task 3: Watch video. Task 4: Steps in the marks planted on the treadmill. Between tasks, a few seconds are waited used by the user while the task performed changes.

3 RESULTS

Results obtained are represented in table 1. Each user has performed two sessions in order to compare how results differ between session. The model has been created with the runs of each session and the results have been validated with a 8-fold cross validation. LDA classifier provides the best results in both sessions for all users. The other classifiers efficiency also remains constant between users which is an evidence of stable behavior of the signals for each task. The correct rate mean value for the best classifier (LDA) for every user and session is 65,25% which is significantly above the chance level of for 4-task classification (25%).

Workshop Proceedings of IAS-13
13th Intl. Conf. on Intelligent Autonomous Systems
Padova (Italy) July 15-19, 2014
ISBN 978-88-95872-06-3 pp. 470-473

Table 1. Classification results for 4 users. Correct classification rate for 4 tasks are shown for five different classifiers

	User A		User B		User C		User D	
Classifier	Session 1	Session 2	Session 1	Session 2	Session 1	Session 2	Session 1	Session 2
SVM	43,88%	54,15%	54,28%	55,23%	66,68%	65,65%	59,80%	54,52%
KNN	40,34%	45,30%	53,81%	49,84%	57,77%	55,33%	53,34%	47,22%
NB	30,51%	40,94%	40,52%	32,51%	55,46%	56,70%	54,36%	26,05%
LDA	50,32%	54,99%	69,07%	62,63%	70,80%	67,88%	64,84%	57,98%
QDA	37,26%	46,38%	46,74%	42,96%	64,71%	60,16%	55,59%	52,13%

4 CONCLUSIONS

The results obtained on this research show that there is a detectable pattern on the signals registered from the scalp of healthy users who walk over a treadmill while experiencing different levels of attention. Results obtained are also preliminary, only different classifiers have been tested and compared on this research. On future investigations all frequencies ,from 1 to 100 hz, are going to be analyzed to find the frequency range that provides the best results. In the future, tests will be also done with real patients.

References

1. J. R. Wolpaw, N. Birbaumer, W. J. Heetderks, D. 1. McFarland, P. H. Peckham, G. Schalk, E. Donchin, L. A. Quatrano, c. J. Robinson, and T. M. Vaughan, "Brain-computer interface technology: A review of the first international meeting," IEEE Transactions on Rehabilitation Engineering, vol. 8, no. 2, pp. 164-173, June 2000.
2. M. Velliste, S. Perel, M. C. Spalding, A. S. Whitford, and A. B. Schwartz, Cortical control of a prosthetic arm for self-feeding, Nature, vol. 453, pp. 10981101, June 19, 2008.
3. F. Galan, M. Nuttin, E. Lew, P. W. Ferrez, G. Vanacker, J. Philips, and R. M. Jdel, A brain-actuated wheelchair: Asynchronous and noninvasive Brain-computer interfaces for continuous control of robots, Clin. Neurophysiol., vol. 119, pp. 21592169, Sept. 2008.
4. Jacome, D.E. and Morilla-Pastor, D. (1990) Unreactive EEG: pattern in locked-in syndrome. Clin. Electroencephalogr., 21: 3136.
5. N. Birbaumer and L.G. Cohen, Brain-Computer Interfaces: Communication and Restoration of Movement in Paralysis, J. Physiology, pp. 621-636, Mar. 2007
6. G. Mller-Putz and G. Pfurtscheller, Control of an Electrical Prosthesis with an SSVEP-Based BCI, IEEE Trans. Biomedical Eng. pp. 361-364, Jan. 2008.
7. E. Hortal, D. Planelles, A. Ubeda, A.Costa and J.M. Azorin, "Brain-Machine Interface System to Differentiate between Five Mental Tasks", System Conference 2014, to be publised.

UNIVERSITAS
Miguel
Hernández